

Investigation of mechanisms for restricting the activity of cyclic AMP- dependent protein kinase

Ryan Andrew Walker-Gray
Submission for the degree of PhD

Department of Neuroscience Pharmacology & Physiology
University College London
Gower Street, London
WC1E 6BT

I, Ryan Andrew Walker-Gray, confirm that this work presented in this thesis is my own, and where information has been taken from other sources it has been properly referenced.

Abstract

Cyclic AMP (cAMP) is an ancient second messenger that is essential for many cellular processes including synaptic plasticity and control of heart rate and contractility. Cyclic AMP-dependent protein kinase (PKA) is the major intracellular receptor for cAMP. PKA consists of dimeric regulatory (R) subunits that bind and inhibit catalytic (C) subunits. PKA is activated upon binding of cAMP to the R subunits, which leads to the release of C subunits, and phosphorylation of intracellular protein substrates. An enduring challenge in cAMP research is to understand how PKA activity is directed to specific substrates, as the C subunits exhibit only limited substrate specificity *in vitro*. Elevations of cAMP are controlled in both space and time in the cell. This is achieved by the co-localization of enzymes for both the synthesis (cyclases) and breakdown (phosphodiesterases) of cAMP. Anchoring proteins are also essential for directing PKA to substrates in their immediate vicinity. However, a mechanism is yet to be established to explain how the activity of the C subunit of PKA is restrained following its dissociation from R subunits.

This thesis details three parallel investigations that apply novel approaches with the shared aim of understanding how C subunit restraint is achieved. First, using quantitative immunoblotting in conjunction with purified PKA subunits, I investigated PKA subunit stoichiometry, finding that PKA R subunits typically outnumber C subunits by ~15-fold. Second, I developed a novel approach for monitoring R subunit isoform-specific association with C subunits in cells, with temporal precision. Comparative experiments using this approach and measurements with a fluorescent

reporter of PKA activity show that only a small portion of C subunits need be dissociated to achieve high PKA activity. Third, I applied and developed a novel cross-linking coupled to mass spectrometry (XL-MS) protocol for analysis of the structure of PKA complexes. Insights include the likely orientation of PKA complexes that contain type II R (RII) subunits towards the membrane, and identification of a possible conformational change in PKA upon binding an anchoring protein. Together these experiments illuminate several aspects of PKA to show how the activity of this critical signalling enzyme is restrained within cells.

Acknowledgments

I would like to thank Dr Matthew Gold for guidance during the project.

I would like to thank fellow Gold Lab members Neha Patel and Jamila Nayob for their comradery, and extend special thanks to Dr Florian Stengel of the University of Konstanz for his collaboration on this project as well as Stuart Martin for help re-purposing the plate reader for FRET recordings with HEK293T cells and Kanchan Chaggar for assistance with HEK293T cell culture.

Additionally, this project would not have been possible without the technical expertise of Tony Langford.

I wish to express gratitude for the contributions of Professor Kees Jalink (Netherlands Cancer Institute) for the gift of the T-Epac-VV sensor; Professor Jin Zhang (Johns Hopkins University School of Medicine) for the gift of the AKAR4 sensor and Professor Ron Hay (University of Dundee) for the auxotrophic *E. coli* strain.

For their assistance on this project, I would like to thank Professor Annette Dolphin, Ivan Kadurin, Otto Mayer, Wendy Pratt, Dr Joseph Tebbs-Warner, Dr Marisol Sampedro, Dr Duncan Laverty, the UCL Biosciences Stores staff, Tina Bashford, as well express my undying gratitude to the Salinas lab and the UCL Biosciences IT department.

I would also like to personally thank Ruth Walker-Gray, Timothy Gray, Megan Walker-Gray, Ryan Russell, Dr Sean Sweeney, Jason James, SSG Benjamin Applebaum, Timothy Beaudet, Anthony Valentino, Andrew Boddorff, Calvin Johnson, Annahita Lagevardi, Michael Sibley, Dr Jonathan Wilson, Dr Abhishek Sharma, Dr Samih Fourali, Dr Rosemary Anderson, and Joana Assis Manuel, as well as the entire staff of the Print Room Café.

Table of Contents

Abstract.....	3
Acknowledgments	5
Table of Contents	6
List of tables	11
List of figures	13
Abbreviations	16
Chapter 1. Introduction	18
1.1 Major discoveries in the cAMP second messenger signalling cascade	18
1.1.1 Early studies of protein phosphoregulation led to the discovery of cAMP	18
1.1.2 The discovery of phosphodiesterases.....	21
1.1.3 The discovery of adenylyl cyclase	21
1.1.4 The discovery of cyclic-AMP dependent protein kinase.....	22
1.1.5 Completing the canonical G-protein coupled receptor signalling cascade	23
1.2 Biochemical Discoveries of cAMP Compartmentalization	26
1.2.1 Discovery and localization of type I and type II PKA	26
1.2.2 Different hormones that elevate cAMP may exhibit different effects on PKA phosphorylation.....	27
1.2.3 The isoform-specific activation of PKA	30
1.2.4 Outstanding questions concerning PKA in compartmentalised cAMP signalling .	31
1.3 PKA subunit classification and function	33
1.3.1 PKA in synaptic plasticity	35
1.3.2 PKA-mediated control of heart rate and contractility	36
1.3.3 PKA in the kidney	37
1.3.4 PKA in disease	38
1.4 General insights into protein kinase function from studies of PKA	40
1.4.1 AGC family kinases	40
1.4.2 Insights from the first PKA structures	42
1.4.3 Catalytic mechanism of the kinase domain	43
1.4.4 Organization of the kinase domain.....	44
1.4.5 The role of disordered regions.....	46
1.5 Localisation synthesis and breakdown of cAMP	47

1.5.1 Localisation of phosphodiesterases	47
1.5.2 Localisation of adenylyl cyclases.....	48
1.6 Anchoring of PKA R subunits	50
1.6.1 The discovery of AKAPs.....	51
1.6.2 Molecular basis of AKAP – PKA interactions.....	52
1.6.3 AKAP-derived sequences for investigating PKA anchoring.....	53
1.6.4 Multivalent AKAP complexes	53
1.7 Recent Ideas for explaining C subunit restraint	55
1.7.1 Are catalytic subunits released upon activation?	55
1.7.2 Myristoylation of C subunits	57
1.7.3 RI buffering hypothesis	58
1.8 Recent technologies for investigating cAMP signalling	59
1.8.1 FRET-based sensors of cAMP concentration	60
1.8.2 FRET-based sensors of PKA activity	63
1.8.3 Crosslinking coupled to mass spectrometry (XL-MS).....	65
1.9 Project Aims	68
Chapter 2. Materials and Methods.....	70
2.1 Basic molecular biology techniques	70
2.1.1 Production of chemically competent <i>E. coli</i>	70
2.1.2 Bacterial transformation.....	70
2.1.3 <i>E. coli</i> culture.....	71
2.1.4 M9 minimal media	71
2.1.5 Expression and purification of glutathione-S-transferase (GST) tagged fusion proteins.....	72
2.1.6 Determination of protein concentration by bicinchoninic acid (BCA) Assay.....	80
2.1.7 Determination of protein concentration by absorbance at 280 nm (A280).....	80
2.2 Techniques in support of PKA subunit stoichiometry determination.....	81
2.2.1 Dissection.....	81
2.2.2 Protein extraction from tissue samples.....	82
2.2.3 Synaptosome-rich fraction preparation.....	83
2.2.4 HEK293T cell counting.....	85
2.2.5 Antibody calibration in ImageJ.....	86
2.3 Mammalian cell-based methods.....	90
2.3.1 HEK293T cell culture	90

2.3.2 Properties of NHS-diazirine.....	91
2.3.3 NHS-diazirine crosslinking with HEK293T cells	93
2.3.4 R subunit selective precipitation.....	94
2.4 Crosslinking coupled to mass Spectrometry (XL-MS)	95
2.4.1 XL-MS Sample preparation	96
2.4.2 Crosslinked peptide separation & identification by MS	97
2.4.3 MS data analysis using xQuest/Prophet	98
2.4.4 Quantitative XL-MS (qXL-MS)	103
2.5 Live cell FRET measurements using Mithras LB 940 plate reader.....	104
2.5.1 Plate reader set up.....	105
2.5.2 HEK293T cell transfection & attachment procedure	105
2.5.3 Drug preparation.....	106
2.5.4 Specific run parameters: β -adrenoceptor deactivation experiment	106
2.5.5 Specific run parameters: isoprenaline titration experiment	109
2.5.6 Data processing.....	109
2.5.7 Comparison of plate reader approach to single cell recording methods	110
Chapter 3. Quantification of PKA subunit stoichiometry in cell and tissue	
preparations.....	111
3.1 Anti- C, RI, RIIα, and RIIβ antibodies are suitable for quantitative immunoblotting	
.....	111
3.2 Selection and preparation of specimens for subunit quantification	114
3.2.1 Tissue and organ samples	114
3.2.2 Protein extraction from cell and tissue samples.....	118
3.2.3 Establishing a quantitative immunoblotting procedure	121
3.2.4 Determination of PKA subunit stoichiometries	124
3.2.5 PKA R subunits generally outnumber C subunits by ~15-fold	128
3.2.6 PKA subunit copy numbers per HEK293T cell support continued use of this cell line as a model for localized cAMP signaling	131
3.3 Summary & implications for PKA catalytic subunit restraint	132
Chapter 4. Investigation of the synchronization of PKA R-C subunit interactions	
with PKA activity in live cells.....	134
4.1 Establishing an approach for analysing R-C subunit interactions in cells with	
temporal precision	135

4.1.1 NHS-diazirine was selected for crosslinking assay	135
4.1.2 Development of the PKA R subunit isoform-specific pull down procedure	135
4.1.3 Calibration of UV exposure time	140
4.2 C subunits are released from R subunits upon PKA activation.....	142
4.3 Comparison of PKA activity to R-C subunit dissociation with different levels of β-adrenoceptor activation	147
4.4 C subunits do not preferentially associate with RI subunits immediately after cAMP signal termination	150
4.5 Conclusions from PKA activity investigations	152
Chapter 5. Application of crosslinking coupled to mass spectrometry (XL-MS) to investigate PKA architecture	154
5.1 Sample preparation	155
5.2 Overview of XLMS data	157
5.3 XLMS analysis of RII-C holoenzymes	158
5.4 XLMS analysis of RI-C holoenzyme.....	160
5.5 Architecture of RII β -C β complex in relation to AKAP18 α	164
5.6 Development of XL-MS using isotopically-labelled oligomeric proteins.....	171
5.6.1 Expression of isotopically-labelled test protein (glutathione S-transferase).....	171
5.6.2 Preparation of purified light-heavy GST dimers	173
5.6.3 XL-MS identification of cross-dimer interlinked peptides	176
5.7 Conclusions from XL-MS experiments.....	180
Chapter 6. Discussion.....	182
6.1 Implications of PKA subunit stoichiometries	182
6.2 Insights from light-activated crosslinking experiments	184
6.3 Future opportunities for exploiting the light-activated crosslinking/R subunit-selective pull down approach	186
6.4 Insights into structure and function of PKA from XL-MS measurements.....	187
6.5 Outlook for homo-oligomeric XL-MS.....	190
6.6 Modelling the diffusion and collision rate of C and R subunits at the membrane.	190
6.7 An integrated model for C subunit restraint.....	196

Chapter 7. References.....	198
Supplementary data	226

List of tables

1. Introduction.....	18
2. Materials and Methods.....	70
Table 2.1 Expression conditions of purified proteins.....	73
Table 2.2 Synaptosome rich fraction recovery	85
Table 2.3 Rat PKA subunit characteristics.	90
Table 2.4 Human PKA subunit characteristics	90
Table 2.5 Filters used in conjunction with Berthold Mithras LB 940 plate reader.	105
Table 2.6 Plate layout for β -adrenoceptor deactivation experiment.....	107
Table 2.7 Plate layout for isoprenaline titration experiment.	109
Chapter 3. Quantification of PKA subunit stoichiometry in cell and tissue preparations.....	111
Table 3.1 PKA antibodies used in immunoblotting.	112
Table 3.2 Mass of organs following dissection.	116
Table 3.3 HEK293T cell lysate quantification.....	118
Table 3.4 Protein concentrations of organ homogenates	121
Table 3.5 Relative subunit copy number normalized to PKA-C subunit	128
Chapter 4. Investigation of the synchronization of PKA R-C subunit interactions with PKA activity in live cells.....	134
Table 4.1 Regulatory subunit binding peptide sequences.....	136
Chapter 5. Application of crosslinking coupled to mass spectrometry (XL-MS) to investigate PKA architecture	154
Table 5.1 Numbers of crosslinked peptides detected in PKA samples	157
Table 5.2 Interlinks detected between AKAP18 α and RII β -C β	164
Table 5.3 Crosslinks in RII β -C β affected by association with AKAP18 α	166
Chapter 6. Discussion.....	182
Chapter 7. References.....	198

Supplementary table 1. Raw XL-MS data for RIIβ-Cβ crosslinking	226
Supplementary table 2. Raw XL-MS data for RIIβ-Cβ-AKAP18α crosslinking.....	233
Supplementary table 3. Raw data for XL-MS of RIβ-Cβ crosslinking	237
Supplementary table 4. Raw data for qXL-MS crosslinking of RIIβ-Cβ-AKAP18	243
Supplementary table 5. Raw data for XL-MS for light/heavy GST crosslinking.....	245

List of figures

Chapter 1. Introduction	18
Figure 1.1 The GPCR signalling cascade.....	25
Figure 1.2 Topology of PKA subunits RI α , RI β , RII α , and RII β	34
Figure 1.3 Inactive and active conformations of the PKA type I (RI) and type II (RII) holoenzyme	35
Figure 1.4 The conserved regions of AGC class kinases.....	41
Figure 1.5 AGC class bilobal arrangement and ATP binding cleft.....	43
Figure 1.6 C- and R- spines coordinate kinase domain conformation.	45
Figure 1.7 Comparison of AKAP binding to RI and RII D/D domains	52
Figure 1.8 FRET transfer efficiency.....	60
Figure 1.9 Schematic of a generic FRET/Epac-based cAMP sensor	62
Chapter 2. Materials and Methods.....	70
Figure 2.1 PKA C subunit purification	76
Figure 2.2 PKA RI subunit purification.	77
Figure 2.3 PKA RII subunit and AKAP18 α purification.....	78
Figure 2.4 Purifications of baits for isoform-specific R subunit pull down.	79
Figure 2.5 Immunoblot quantitation workflow.	88
Figure 2.6 NHS-Diazirine crosslinking.....	92
Figure 2.7 Generalized overview of XL-MS.....	95
Figure 2.8 Workflow of XL-MS processing.....	100
Figure 2.9 XL-MS MS2 ion spectrum	101
Figure 2.10 xQuest/Prophet output parameters	103
Figure 2.11 Plate reader parameters for β -adrenoceptor deactivation experiment ...	108
Chapter 3. Quantification of PKA subunit stoichiometry in cell and tissue preparations.....	111
Figure 3.1 Purified protein cross reactivity blots.	114
Figure 3.2 Pilot experiments to determine standard curve range.	123

Figure 3.3 HEK293T and rat organ PKA subunit immunoblots and quantifications.....	125
Figure 3.4 HEK293T and Rat organ PKA subunit low concentration immunoblots and quantifications	126
Figure 3.5 Tissue specific PKA subunit isoform quantification.....	127
Figure 3.6 PKA R subunit copy numbers normalized to C subunit	129
Figure 3.7 Relative concentrations of PKA subunits by tissue type in terms of copy number	130
Figure 3.8 PKA subunit copy number per cell.....	131
Chapter 4. Investigation of the synchronization of PKA R-C subunit interactions with PKA activity in live cells.....	134
Figure 4.1 RI precipitation pilot experiment	138
Figure 4.2 RII pull down pilot experiment.....	139
Figure 4.3 R-C complex association detected by light-induced crosslinking & isoform-specific R subunit pull down.	140
Figure 4.4 Crosslinking time point assay.	142
Figure 4.5 Effect of isoprenaline on RII-C association determined by light-induced crosslinking.	145
Figure 4.6 Effect of isoprenaline on RI-C association determined by light-induced crosslinking.	146
Figure 4.7 R subunit specific coprecipitation of C subunits isoprenaline titration.	148
Figure 4.8 Isoprenaline induced PKA activity.	149
Figure 4.9 R-subunit specific pull down of propranolol treated HEK293T lysate	152
Chapter 5. Application of crosslinking coupled to mass spectrometry (XL-MS) to investigate PKA architecture	154
Figure 5.1 DSS crosslinking of PKA complexes.....	156
Figure 5.2 Distribution of crosslinking distances	158
Figure 5.3 XL-MS analysis of C β -RII β holoenzyme	159
Figure 5.4 Location of the docking and dimerization domain in the C β -RII β holoenzyme	160

Figure 5.5 Challenges in crosslink assignment in C β -RI β complex.....	161
Figure 5.6 Primary sequence comparisons of R subunit isoform N-termini.....	162
Figure 5.7 Primary sequence comparisons of RII subunit isoform R subunit CBDs	163
Figure 5.8 Interlinking sites between AKAP18 α and RII β -C β	165
Figure 5.9 Visualization qXL-MS of PKA C β -RII β with or without AKAP18 α	168
Figure 5.10 C subunit myristoylation site	170
Figure 5.11 Lys/Arg auxotrophic bacteria growth curves	173
Figure 5.12 Preparation of purified light-heavy GST dimers.....	175
Figure 5.13. Homotypic GST interlinks	177
Figure 5.14 Additional cross-dimeric interlinks observed in light-heavy GST sample .	178
Figure 5.15 Aberrant crosslink from light-heavy dataset.	179
Figure 5.16 DSS crosslinking sites detected within the light-heavy GST dataset plotted on the GST crystal structure.	180
Chapter 6. Discussion.....	182
Figure 6.1 FKBP dimerization	189
Chapter 7. References.....	198

Abbreviations

AKAP	cAMP dependent protein kinase anchoring protein
AKAR	A kinase activity reporter
AMPA	α -amino-3-hydroxy-5-methyl-4-isoxazolepropionic acid
amu	atomic mass unit
BCA	bicinchoninic acid
BSA	Bovine serum albumin
C subunit	Catalytic subunit
CBD	cAMP binding domain
CID	collision induced dissociation
CNG	cyclic nucleotide gated
D/D	Docking and dimerization domain
DMEM	Dulbecco's modified eagle medium
DMSO	Dimethyl sulfoxide
DSS	disuccinimidyl suberate
DTT	1,4-Dithiothreitol
EDTA	Ethylenediaminetetraacetic acid
EPAC	exchange protein directly activated by cAMP
ESI	electrospray ionization
FDR	false discovery rate
FHA1	forkhead-associated domain 1
FKBP	FK506 binding protein
FICRhr	fluorescein C subunit and rhodamine R subunit
FRET	Forster resonance energy transfer
FSB	Frozen storage buffer
GPCR	G protein coupled receptor
GST	glutathione s-transferase
HEPES	4-(2-Hydroxyethyl)piperazine-1-ethanesulfonic acid
HRP	Horseradish peroxidase
HRV 3C	Human rhinovirus 3C protease
IB	immunoblot
IPTG	Isopropyl β -D-1-thiogalactopyranoside

kDa	kilodaltons
LB	Lysogeny broth
LC-MS/MS	Liquid chromatography tandem mass spectrometry
LSP	Local spatial pattern alignment
LTD	Long term depression
LTP	Long term potentiation
MS	mass spectrometry
MS/MS	tandem mass spectrometry
NHS	N-hydrozysuccinimide
NHS-Diazirine	succinimidyl 4,4'-azipentanoate
Ni-NTA	Nickel nitrilotriacetic acid agarose
OD ₆₀₀	Optical density at 600 nm
PBS	Phosphate buffered saline
PKA	cAMP dependent protein kinase (protein kinase A)
PKI	Protein kinase inhibitor
PLB	Phospholamban
q-value	false discovery rate of quantitative crosslinking
qXL-MS	quantitative crosslinking mass spectrometry
R subunit	regulatory subunit
RIAD	RI anchoring disruptor
RIPA	Radioimmunoprecipitation assay
SILAC	stable isotope labelling by amino acids in cell culture
SOB	Super optimal broth
SPR	Surface plasmogen resonance
TCEP	tris(2-carboxyethyl)phosphine
TIC	total ion current
TnC	Thrombin C
TnI	Thrombin I
Tris	tris(hydroxymethyl)aminomethane
uID	unique crosslink ID
XL-MS	Crosslinking couple to mass spectrometry

Chapter 1. Introduction

1.1 Major discoveries in the cAMP second messenger signalling cascade

Much of the knowledge of second messenger systems, as well as study of their constituent parts, including kinases, phosphodiesterases, and cyclases has come from research into the cAMP signalling cascade as it relates to PKA. Here I will detail the discoveries that underlie the current state of research in the field, as well as some of the recent methodological developments that are continuing to drive advancement. In the context of this background, I will also outline the goals I hoped to accomplish with this project.

1.1.1 Early studies of protein phosphoregulation led to the discovery of cAMP

cAMP is now understood to be a second messenger molecule that is essential for the transduction of chemical signals from outside the cell into a range of biochemical modulations inside the cell, as part of the G-protein coupled receptor (GPCR) cascade. Continuing research across many disciplines is actively elucidating in greater detail the downstream effects of cAMP activation, as well as the functional consequences of the modulation of cAMP signalling.

The study of the biological effects of cAMP is generally considered to have started in the mid-1950s, though it can trace its origins to even earlier work. Earl Sutherland, who won the Nobel Prize in Physiology or Medicine in 1971 for the discovery of cAMP, started his work in the lab of Carl and Gerty Cori, who themselves won a Nobel Prize in 1947 for work on glycogen phosphorylase (Houssay, 1956; Kresge, Simoni, & Hill, 2005a). Sutherland and his

co-workers showed that the incubation of an enzyme from liver tissue that deactivated glycogen phosphorylase resulted in an increase in free phosphate in the system (Sutherland & Wosilait, 1955; Wosilait & Sutherland, 1956). Experiments using radiolabelled substrates further showed that the phosphate was released from glycogen phosphorylase directly (Wosilait & Sutherland, 1956). Based on this result Rall, Sutherland and Wosilait hypothesized that the reactivation of glycogen phosphorylase would require the incorporation of phosphate (Rall, Sutherland, & Wosilait, 1956). This was supported when the authors showed that radiolabelled phosphate that was incorporated into glycogen phosphorylase in conjunction with its activation by epinephrine. They further showed that phosphatase removed this radiolabelling, showing that reversible, enzymatically mediated phosphorylation was key for the control of glycogen phosphorylase activity (Rall, Sutherland, & Wosilait, 1956).

Working contemporaneously with Sutherland, Fischer and Krebs showed that the activation of glycogen phosphorylase in rabbit skeletal muscle required ATP, as well as a divalent cation (Fischer & Krebs, 1955). They hypothesized that the conversion was catalysed by an enzyme, reliant on the fact that in muscle extract that was treated and cleared at low pH, the addition of a divalent cation and ATP could not induce phosphorylase activation. However, adding the precipitated fraction to back into the supernatant resulted in the activation of phosphorylase. They purified the enzyme present in the supernatant, and showed that it was capable of activating glycogen phosphorylase by phosphorylation, this enzyme was deemed phosphorylase kinase (Fischer & Krebs, 1955).

Similarly, Rall, Sutherland and Berthet showed that epinephrine and glucagon activated glycogen phosphorylase in an ATP and Mg^{2+} dependent manner when applied to liver cell lysate (Rall, Sutherland, & Berthet, 1957). However, when the lysate was centrifuged to

remove the particulate fraction, the hormone-mediated response was lost. The authors found that this activity could be restored by adding pelleted material to the supernatant. This led to experimentation with washed particulate fractions of centrifuged homogenate. Pelleted cellular material was incubated with hormones, magnesium, and ATP, following which the mixture was boiled to denature any active enzymes, and further centrifuged. The resulting supernatant was mixed with the non-hormone-responsive supernatant of untreated homogenate. An increase in activation of glycogen phosphorylase proportional to the amount of boiled supernatant added was then observed. When the same process was carried out in the absence of hormones in the initial liver homogenate treatment, there was no increase in glycogen phosphorylase activation.

From these experiments, the authors inferred the presence of a previously unidentified active factor resulting from the treatment of pelleted liver homogenate with hormones. This factor was found to be heat stable, and was purified by ion exchange chromatography. The application of this purified factor, which the authors showed to contain adenine, ribose, and phosphate in a 1:1:1 ratio, resulted in raised glycogen phosphorylase activation in liver homogenate supernatant (Rall, Sutherland, & Berthet, 1957). Further analysis of the active factor, by identification of breakdown products, showed the molecule to be identical to a product of barium hydroxide digest of ATP, which yielded a molecule which would later be classified 3',5'-cyclic adenosine monophosphate or cAMP (Cook, Lipkin, & Markham, 1957; Lipkin, Cook, & Markam, 1959; Sutherland & Rall, 1957). Rall and Sutherland showed using radiolabelled molecules that cAMP was a product of the cyclization of ATP. These results also indicated that the previously observed increased formation of active glycogen phosphorylase as the result of the application of glucagon and epinephrine was the result of indirect activation of an unknown mechanism, rather than direct action on phosphorylase

(Rall & Sutherland, 1958). In this way, a burst of activity in the late 1950s established many key features of cAMP signalling.

1.1.2 The discovery of phosphodiesterases

The first indication of a control mechanism for cAMP concentration was noted by Rall and Sutherland, who showed that a component of brain homogenate hydrolyses cAMP into 5'-AMP (Rall & Sutherland, 1958). Building on this observation, Drummond and Perrott-Yee described an active factor of tissue extract that was capable of hydrolyzing cAMP, was precipitated by sulfate, and required the addition of $MgCl_2$ for activity (Drummond & Perrott-Yee, 1961; Sutherland & Rall, 1958; Sutherland & Rall, 1960). This work was further supported by Butcher and Sutherland who, noting that the enzyme breaks an ester bond to turn 3',5'-cyclic monophosphate into 5'-AMP, called the enzyme phosphodiesterase (Butcher & Sutherland, 1962). They also showed that phosphodiesterases were present in sufficient intracellular quantities to have a significant effect on physiological cAMP concentrations.

1.1.3 The discovery of adenylyl cyclase

With the downstream target of cAMP, and an enzyme responsible for its hydrolysis established, Sutherland, Rall, and a number of co-workers announced their preliminary investigation into the enzymatic system catalysing the formation of cAMP in a series of four papers in which they named the enzyme adenylyl cyclase (Klainer et al., 1962; Murad et al., 1962; Sutherland, Rall, & Menon, 1962; Rall & Sutherland, 1962). Sutherland, Rall, and Menon described the localization of adenylyl cyclase as particulate fraction associated, and independent of mitochondria, noting specifically the high likelihood of membrane association, which was later confirmed by Sutherland and Davoren (Davoren & Sutherland, 1963; Sutherland, Rall, & Menon, 1962). In the second paper, Rall and Sutherland showed,

through the use of ATP with radiolabelling on different phosphates, that cAMP was produced by the cleavage of the γ and β phosphates from ATP which then created pyrophosphate (1962). In the remaining papers, the authors tested the effects of hormones on the production of cAMP, showing that several, including epinephrine, norepinephrine and isoprenaline increased cAMP production in a variety of tissues (Murad et al. 1962; Klainer et al., 1962).

1.1.4 The discovery of cyclic-AMP dependent protein kinase

The search for another protein constituent of the cAMP signaling cascade was driven by suggestions that phosphorylase kinase was not activated directly by cAMP (Delange et al., 1968; Krebs, Graves, & Fischer, 1959). In 1968 Walsh, Perkins, and Krebs reported the discovery of such a protein, which could be purified from rabbit skeletal muscle and was found to transfer the γ -phosphate of γ -³²P-ATP to the target proteins casein or protamine. This reaction was found to be completely dependent on cAMP to progress, and was not stimulated by a range of other nucleotides. The protein was then shown to activate phosphorylase kinase by phosphorylation, again in a completely cAMP dependant manner. The authors noted that the likely source of phosphorylase kinase activation observed in earlier purifications was likely due to trace contamination from the original purification of phosphorylase kinase, citing the previously published dependence of phosphorylase kinase activation on cAMP, and similar K_m values for the reported activation of phosphorylase kinase, thought to be by autophosphorylation (Delange et al., 1968; Walsh, Perkins, & Krebs, 1968)

Walsh, Perkins, and Krebs offered the theory that this new protein might be the missing step between the production of cAMP by adenylyl cyclase and the activation of phosphorylase kinase, and offered that if this relationship were correct the new protein should be called

phosphorylase kinase kinase later becoming known as cAMP-dependent protein kinase (PKA).

1.1.5 Completing the canonical G-protein coupled receptor signalling cascade

With the main components of the intracellular cAMP signalling cascade identified, the focus now turned to understanding how the application of extracellular agonists was capable of modulating intracellular processes (Beavo & Brunton, 2002). The first molecular studies in this vein expanded upon the known properties of adenylyl cyclase activation.

In a series of studies which showed that a combination of hormones that were known to bind at different sites did not increase cAMP concentration beyond the single-hormone maximum, another molecularly discreet recognition component was discovered (Birnbaumer et al., 1969; Rodbell et al., 1971).

It was shown that the activation of adenylyl cyclase by glucagon following high temperature incubation was dependent on the presence of guanyl nucleotides, even in instances where the maximum amount of glucagon was bound to the membrane, indicating a relationship between glucagon and guanyl nucleotides (Rodbell et al., 1971). The authors also used a biosynthetically generated non-hydrolyzable analog of ATP, Gpp(NH)p, to show that GTP was necessary for glucagon to induce adenylyl cyclase activation (Rodbell et al., 1971; Rodbell, 1994).

Rodbell, Lin and Salomon further showed in a liver cell membrane system that there was a lag in activation of adenylyl cyclase following the application of glucagon in the absence of added GTP. This lag was ameliorated if GTP was added to the system. Equally, treatment of the system with glucagon for an incubation period before ATP based substrates were added

also abolished the lag. GTP added without glucagon did not increase adenylyl cyclase activity (Rodbell, Lin, & Salomon, 1974). These experiments cemented the understanding of GTP as a transducer in the activation of adenylyl cyclase (Rodbell, 1994).

The discovery of the G protein hinged upon the use of mutant cell lines to deduce the role of each component in the cascade. Most important was the use of a cell line, now known as $\bar{S}49$, which was shown to bind hormones, but could not produce cAMP, leading to the assumption that it was deficient in AC (Insel et al., 1976; Tatsuya Haga, Ross, Anderson, & Gilman, 1977). However the combination of extracts from this cell line, as well extract from others that were deficient in β adrenergic receptors did not reconstitute a working system, though extract from wild type cells with heat deactivated AC could restore function. From this, Ross and Gilman suggested the existence of an as yet uncharacterized protein in the adenylyl cyclase system, which is activated by fluoride ions and Gpp(NH)p, and suggested that it might be a guanine nucleotide binding protein (Ross & Gilman, 1977). This was further supported by work that showed the AC and receptor were not colocalized (Haga, Haga, & Gilman, 1977; Limbird & Lefkowitz, 1977). The thermostabile portion of this system would prove to be the G-protein, and it would prove that the $\bar{S}49$ cells contained functional AC, but were deficient in the G-protein (Howlett & Gilman, 1980).

Northup and colleagues were the first to successfully purify the regulatory component, now known as the G protein, of the adenylyl cyclase system. Their separation indicated three distinct proteins of 52, 45 and 35 kilodaltons, the first two of which would prove to be splice variants of $G_{s\alpha}$, while the third is the β subunit (Gilman, 1995; Northup et al., 1980).

The aforementioned studies combine to form the framework of the general dynamics of the GPCR signalling cascade as it is understood today. An extracellular hormone binds to the GPCR, which spans the membrane, and allows GTP to replace GDP in the heterotrimeric

$G\alpha:G\beta\gamma$ assembly (McCudden et al., 2005). The dissociated $G\alpha$ subunit then binds to AC, activating it and enabling the generation of cAMP from ATP. The released cAMP then binds to a range of downstream effectors, including PKA (**Figure 1.1**).

The understanding of GPCRs and their signalling cascade would later expand greatly. There are now more than 800 known human GPCRs, which play major roles in processes from cardiovascular activity to neuronal activation (Katritch, Cherezov, & Stevens, 2013). The understood complexity of the regulation of GPCRs has also advanced since this time. The discovery of β -arrestins, which block the reactivation of deactivated GPCRs is one way in which the intricacies of GPCR activity is beginning to be understood.

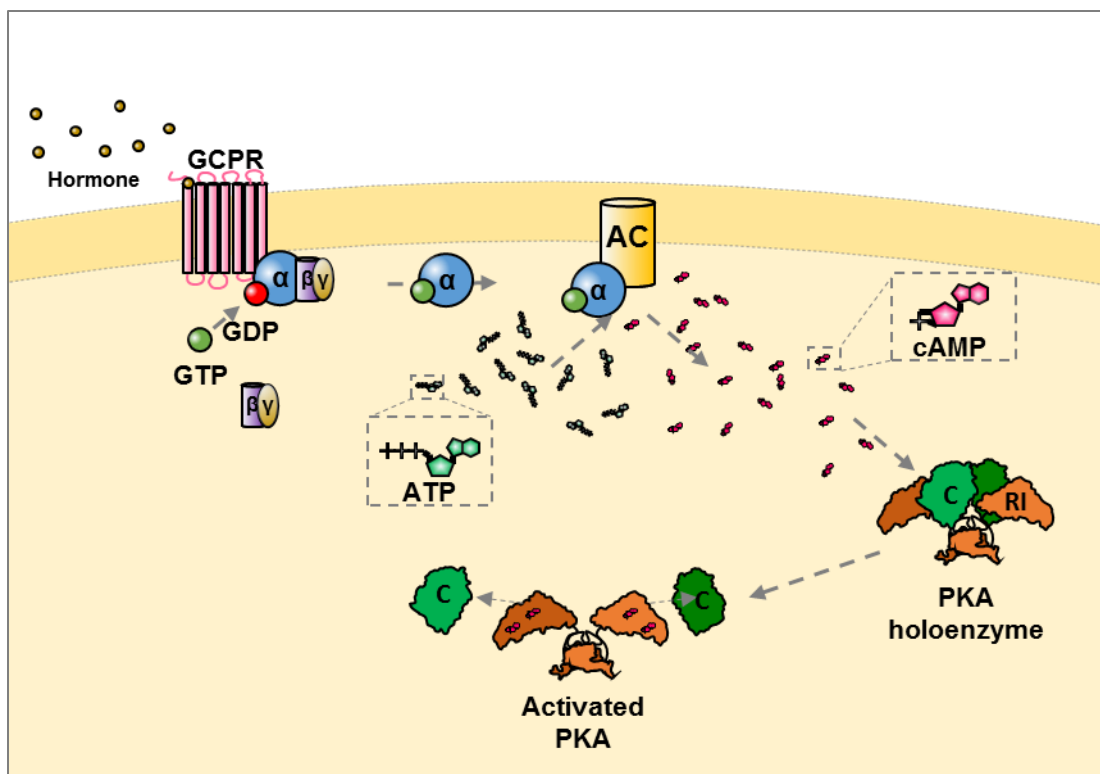


Figure 1.1 The GPCR signalling cascade. An extracellular hormone binds to the GPCR, stimulating the exchange of GDP for GTP and activating the G protein. The $G\alpha$ subunit of the G protein activates AC, which begins producing cAMP from ATP. cAMP then diffuses to activate PKA, inducing the dissociation of the C subunit.

1.2 Biochemical Discoveries of cAMP Compartmentalization

In the late 1970s, with the major functional pieces of the GCPR cascade elucidated, researchers started to detail how these components interacted with one another to impart spatiotemporally specific control within the cell.

1.2.1 Discovery and localization of type I and type II PKA

Corbin, Keely and Park discovered that PKA purified from adipose tissue or from heart tissue exhibited differing dissociation kinetics (1975). Spurred by this finding, the authors identified two different PKA isoform peaks by ion exchange chromatography (Corbin, Keely, & Park, 1975). It was subsequently discovered that both isoforms were also present within the same tissues (Corbin & Keely, 1977).

The first study to characterize spatial separation of regulatory subunit isoforms was carried out by Corbin and co-workers in 1977. The authors noted that previous studies on PKA localization had reported populations of PKA associated with both the particulate fraction and the soluble fraction of homogenized tissue following low speed centrifugation, but their differences had not been explored further (Corbin et al., 1977). Based on this, Corbin and colleagues spun rat heart homogenate at low speeds and then used ion exchange chromatography to characterize the localization of the PKA isoforms. After applying the pellet or supernatant to a DEAE-cellulose column, the two distinct peaks that were produced as the result of increasing NaCl concentration were dubbed PKA type I and II. The characteristics of these PKA isoforms matched with those isolated from the separate tissues in their 1975 study (Corbin et al., 1975). Importantly, the authors also showed that the concentration of type II holoenzyme in the particulate fraction was not altered when exogenous purified RII protein was added to the homogenate as a competitor binding, indicating that the association between the holoenzyme and the particulate fraction is the

result of a specific anchoring mechanism (1977). These findings are consistent with later discoveries about the primarily membrane associated anchoring of RII subunits, and the cytosolic positioning of RI subunits (Gold et al., 2013; Gold et al., 2006; Skålhegg et al., 1994).

1.2.2 Different hormones that elevate cAMP may exhibit different effects on PKA phosphorylation

The functional consequences of PKA isoform specificity were first seen by Corbin and co-workers, who used a radiometric cAMP binding assay, in conjunction with PKA activity assays based on the phosphorylation of histidine, to demonstrate that the application of epinephrine, a G-coupled protein receptor agonist, to whole hearts caused an increase in activation of particulate bound cAMP and a corresponding increase in soluble fraction phosphorylation, presumably induced by the release of catalytic (C) subunits from particulate-associated RII subunits into the soluble fraction. With these findings, Corbin et al. suggested for the first time that the cAMP mediated response of PKA to a hormone might be regulated by the association of specific isoform of regulatory subunit with a specific compartment of the cell.

In 1977 Stanley Keely published his observations on the differences in cAMP concentration, protein kinase activity, and phosphorylase activation in response to the perfusion of rat hearts with prostaglandin E₁ (PGE₁) or epinephrine. Keely found that cAMP concentration and protein kinase activity rose in response to both hormones. However, phosphorylase activation, which requires phosphorylation by PKA, increased only when epinephrine was applied. He also showed that the addition of both hormones together caused a greater cumulative increase in PKA activity, but phosphorylase activation increased only to the level seen with epinephrine alone. These findings indicated that each hormone had a separate pool of kinase on which it acted, and importantly that lack of phosphorylase increase seen

PGE1 was not due to any inhibitory activity of the hormone. This marked the observation of differential downstream activity as the result of the activation of protein kinase, and would become a keystone discovery to the field of cAMP signalling, laying the groundwork for the study of cAMP compartmentalization that was to come.

Two years later Keely expanded upon this work by characterizing the effects elicited by the application of varying concentrations of PGE1 and epinephrine on cAMP concentration, PKA activation, glycogen phosphorylase activity, and contractile force in perfused rat hearts (Keely, 1979). Keely reiterated his 1977 findings, pertaining to PKA activity and glycogen phosphorylase activation, and he also showed that epinephrine increased heart contractility while, PGE1 failed to produce this change, though both had activated PKA. Keely further showed that PGE1 did not inhibit epinephrine activation of glycogen phosphorylase or heart contractile force by applying it in conjunction with cAMP. Based on these findings, Keely offered two hypotheses. The first, that the hormones might be acting on different cell types in the heart tissue, was based on the observation that the activation of PKA was not increased by the addition of PGE1 at maximum concentrations of epinephrine. Keely postulated that both cell types were acted upon by epinephrine, while PGE1 only caused responses in a smaller subset. Importantly, he also suggested that the same results could be achieved if the hormones acted upon spatially separated pools of PKA within the same cell (Keely, 1979). Citing his previous work (Corbin and Keely, 1977; Corbin et al., 1977) Keely noted that the differential activation of PKA pools might be connected to differences in the activation of type I and type II PKA, and their localization at the membrane and in the cytosol of the cell (Keely 1979).

This work was then built upon by Hayes and colleagues, who studied the effects of the β -adrenergic receptor agonist isoprenaline, as well as PGE1 on cAMP concentration, PKA

activity, and the phosphorylation states of phosphorylase b kinase and glycogen synthase (1979). Isoprenaline was chosen over the previously used epinephrine, which activates both β and α receptors, due to its selectivity for β -adrenergic receptors (Hayes et al., 1979).

Hayes and co-workers observed the expected effects of isoprenaline, an increase in phosphorylase kinase activation, a decrease in glycogen synthase activity, and increased pressure in the heart ventricle. However, only an increase in cAMP concentration and an increase in PKA activity were observed following the application of PGE1. Even when the concentration of each hormone was adjusted to produce similar cAMP concentration, downstream effects were not seen with PGE1 application. This indicated that the activation of PKA by cAMP was not solely sufficient to cause downstream activity of phosphorylase kinase and glycogen synthase (Brunton, Hayes, & Mayer, 1979). The authors also noted that the effects of isoprenaline and PGE1 are additive, and there is no increase in the concentration of cAMP when both are applied to whole hearts in comparison to isoprenaline alone, suggesting that the differences in downstream activation do not stem from the hormones acting on separate cell populations (Hayes et al., 1979). A subsequent study carried out by Hayes and co-workers using 85% homogenous cultured cardiomyocytes recapitulated these findings and furthered the finding that different cell populations are not responsible for differential responses to PGE1 and isoprenaline (Hayes et al., 1982)

To augment this work, Brunton Hayes and Mayer examined the effects of PGE1 and isoprenaline on troponin I activation in the heart (1979). Troponin is a protein that helps control relaxation and contraction in muscles, the dynamics of which are regulated by phosphorylation. Though the manner in which PKA interacts with troponin I to cause increased heart contractility was not clear at the time, it is now known that PKA phosphorylates serine residues in the inhibitory subunit of troponin in an N-terminal domain

that is present only in the cardiac muscle isoform, which results in decreased sensitivity to Ca^{2+} , and leads to an increased rate of contraction and release cycling (Layland, Solaro, & Shah, 2005). Brunton, Hayes and Mayer found that similarly to the previous results, the application of both PGE1 and isoprenaline raised the levels of cAMP and PKA activation, while only isoprenaline activation produced troponin I phosphorylation and increased heart valve pressure. These findings further supported the idea that a secondary mechanism controls the downstream effectors of PKA, beyond the simple cAMP concentration of a tissue.

1.2.3 The isoform-specific activation of PKA

Building on the earlier work presented here, Hayes, Brunton, and Mayer attempted to elucidate the mechanism by which different downstream effects are created by hormones which cause similar rises in cAMP concentration, noting that the difference very likely arises from timing and localization dependent relationships of the receptor, cAMP, PKA and the substrate (1980). They investigated the possibility that it is activation of the separate particulate RII and soluble RI populations of regulatory subunits that causes differences in downstream activation of PKA phosphorylation targets. To further support the idea of different intracellular PKA pools, the authors examined the effects of isoprenaline and PGE1 on the primarily type II PKA in the particulate fraction of heart tissue (1980). They found that isoprenaline, PGE1, or a combination of the two led to an increase in PKA activity in the soluble fraction of cell homogenate, however only isoprenaline or isoprenaline with PGE1 led to the activation of phosphorylase. In addition to which, this condition also led to a decrease of the PKA activity associated with the particulate fraction, which the authors hypothesized was caused by the dissociation of the catalytic subunit from its anchored regulatory subunit. PGE1, in contrast, did not change the localization of PKA activity. Considering these findings, Hayes, Brunton, and Mayer hypothesized that the cause of the

differential effects of PGE1 and isoprenaline is the spatial separation of PKA pools activated by each hormone (1980).

Buxton and Brunton also focused on measuring the hormone-induced changes in the glycogen metabolism cascade in homogenous cell populations (1983). Using rabbit heart myocyte suspensions, Buxton and Brunton found an increase over heart homogenate in both cAMP levels and PKA activation with PGE1 and isoprenaline, indicating that PKA is also localized in myocytes. The authors also found that the application of isoprenaline raised the level of cAMP and demonstrated a corresponding decrease in total particulate PKA activity, presumably owing to the release of the catalytic subunit into the soluble fraction. In contrast, PGE1 increased cAMP concentration in the soluble fraction alone, and did not cause a shift in PKA activity away from the particulate fraction, indicating activation of only soluble-fraction PKA.

From these experiments, it was determined that β -adrenergic receptor agonists as well as PGE1 cause increased intracellular cAMP concentration when applied to tissue and cell samples. However, only β -adrenergic receptor agonists lead to the downstream phosphorylation of substrates. The mechanism by which these processes are separated is still not fully understood.

1.2.4 Outstanding questions concerning PKA in compartmentalised cAMP signalling

Despite the advances that have been made in the understanding of the cAMP second messenger system, the field awaits a satisfactory mechanism to explain how PKA C subunits are restricted following their dissociation from R subunits. This problem was encapsulated by Ted Rall, the co-discoverer of cAMP, in his opening remarks of the 1974 Second International Conference on cAMP

“Attention now is focused on cAMP-‘dependent’ protein kinases and their substrates...As I hear more about membrane-bound protein kinases, the ‘autophosphorylation’ of regulatory subunits, and the impact of ‘substrate’ and ‘nonsubstrate’ proteins on the properties of protein kinases in the days ahead, a picture of pre-existing multimolecular complexes may begin to emerge. Either these complexes are part of a membrane matrix whose properties might be changed by combination with cAMP with or without protein phosphorylation, or these complexes may become associated with other cellular components as a consequence of interaction with cAMP, again with or without phosphorylation of the ‘initial’ or ‘final’ complexes. In any event some conceptualization must emerge to replace the unsatisfying picture of the catalytic subunit of protein kinase swimming about, happily phosphorylating a variety of cellular constituents whether they need it or not.”

This problem outlined by Ted Rall over forty years ago was the focus of my doctoral studies. In the remainder of my introduction, I first review the state of our current understanding of the physiological roles of PKA in a selection of biological processes (**Section 1.3**). I next explore the functional organization and mechanistic properties of the PKA subunits, as they pertain to both catalysis and regulation of the catalytic subunit, and how the dynamics of the subunits contribute to their biological function (**Section 1.4**). I will then turn to the best understood mechanisms by which the control of spatial and temporal localization of PKA activation by cAMP generates diverse function in subcellular regions, in regards to cAMP hydrolysis and selective anchoring (**Sections 1.5 & 1.6**). Having established more established aspects of PKA form and function, in **section 1.7** I cover emergent ideas for restraining C subunits following activation, including post-translational modification, and the potential for the translocation of active C subunits to inactive R subunits. I will then detail the

methodological advances that are enabling advances in the field, with a special emphasis on the techniques used in this study (**Section 1.8**). Finally, having outlined the state of the field, I will define the further contributions I hope to make to it, by enumerating the aims of the project (**Section 1.9**).

1.3 PKA subunit classification and function

PKA consists of complexes of catalytic (C) and regulatory (R) subunits that can assemble into tetramers formed of two regulatory subunits and two catalytic subunits. The PKA 'holoenzyme' is considered to be a complex of 2 R subunits in complex with 2 C subunits. The foundation of the PKA holoenzyme is a pair of isoform-matched regulatory subunits that form a constitutive homodimer (Bruystens et al., 2014). There are two types of regulatory subunit, type I and type II (RI and RII), which are differentiated from each other by the nature of their binding to the C subunit. While C subunit binding to RII subunits relies on phosphorylation of the serine within the inhibitor site, RI has a pseudo-inhibitor site in which the phosphorylatable serine in the N-terminal linker region is replaced with an alanine residue in RI α or a glycine residue in RI β (Kim, Xuong, & Taylor, 2005). Due to the pseudo-inhibitor site, RI subunits require MgATP for binding to C subunits, with affinity between the subunits in the presence of MgATP at a K_d of below 1 nM, and in the absence of MgATP at a K_d of 125 nM (Herberg & Taylor, 1993). Each of the two regulatory types is further divided into two isoforms, to make four functionally nonredundant regulatory subunits (RI α , RI β , RII α , RII β).

The R subunit isoforms of PKA share the same general structure (**Figure 1.2**). The N-terminus contains a docking and dimerization (D/D) domain that organizes into a four helix X-bundle (Newlon et al., 1999, described further below). The D/D is followed by a linker region, which is the least conserved region between R subunit isoforms. Within this disordered N-terminal linker is the five residue inhibitor site, which binds to the C subunit active site cleft upon formation of the holoenzyme (Taylor et al., 2012). The N-terminal linker is followed in primary sequence by two highly conserved cAMP binding domains, A and B (CNB-A, CNB-B), which are joined by a short helix (Bruystens et al., 2014).

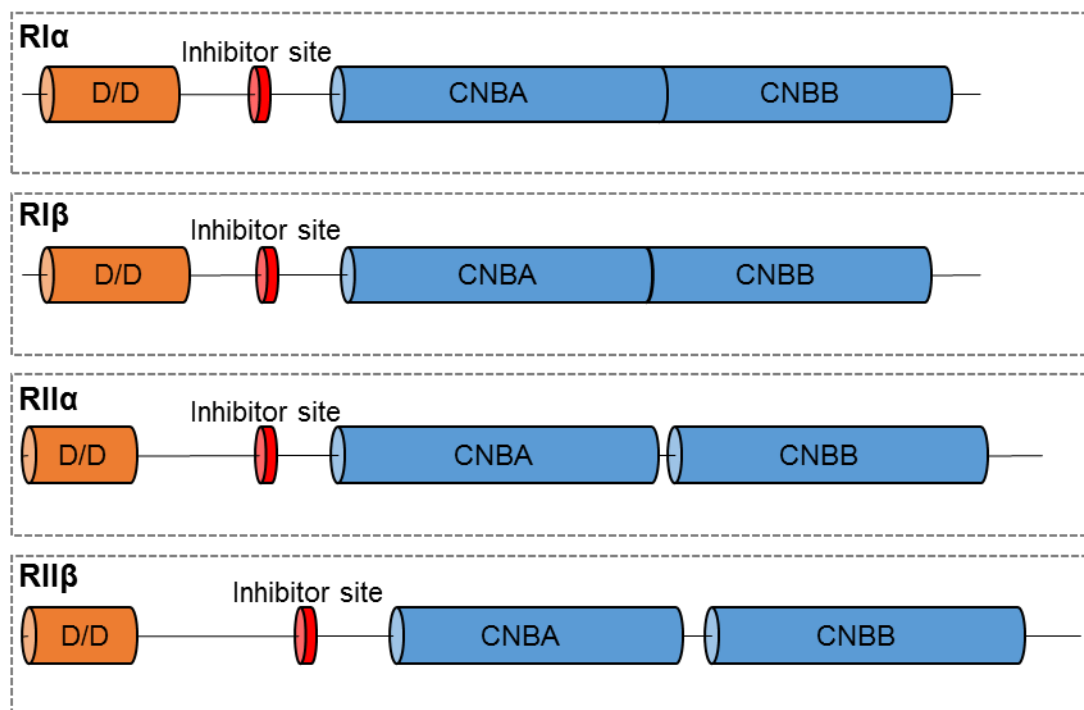


Figure 1.2 Topology of PKA subunits RI α , RI β , RII α , and RII β . Each of the R subunit isoforms features an N-terminal D/D domain (orange) followed by a linker region which contains a five residue inhibitor site (red) that binds to the C subunit. The N-terminal linker is followed in primary sequence by two highly conserved cAMP binding domains, A and B (CNB-A, CNB-B, blue).

The CNBs contain phosphate binding cassettes, whose overall structure is highly conserved throughout evolutionary history. The CNBs binds to the phosphate of cAMP via an arginine residue (Berman et al., 2005; Kornev, Taylor, & Ten Eyck, 2008). The two CNBs show

cooperativity in their binding of cAMP, in RI α CNB-B was shown to have 15 nM affinity for cAMP, while CNB-A exhibited 60 nM binding affinity, with a Hill Coefficient of 1.6 (Herberg et al., 1994). The crystallization of the RI α homodimer also showed that in addition to cooperative binding between CNBs of a single R subunit, there is cross-communication between the protomers in the R subunit dimer with regards to sensing the binding of cAMP at CNB-B (Bruystens et al., 2014). It is the binding of the second cAMP molecule which induces the conformational change that results in the release of the now active C subunit (Figure 1.3).

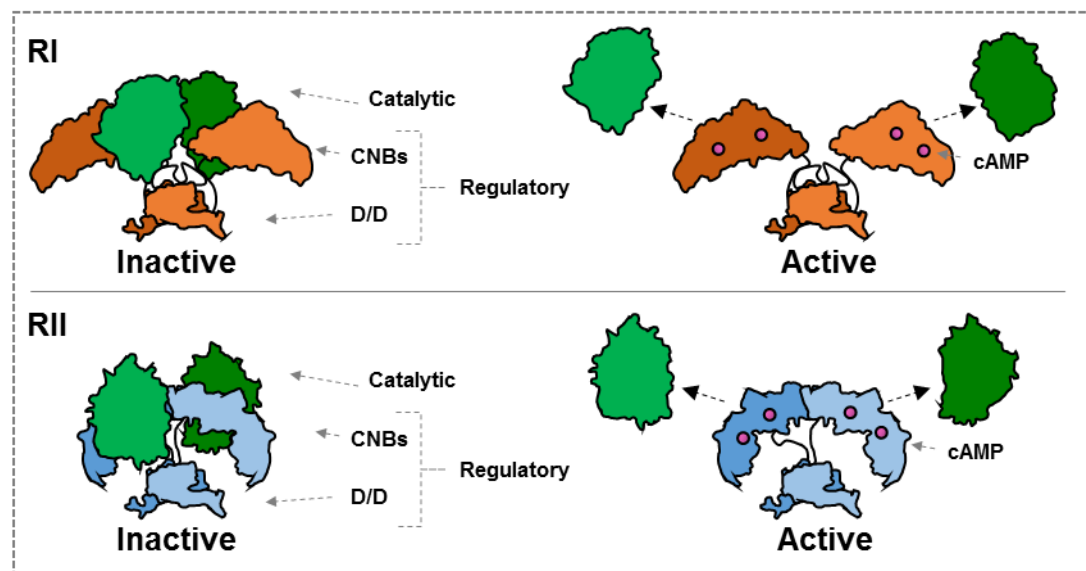


Figure 1.3 Inactive and active conformations of the PKA type I (RI) and type II (RII) holoenzyme. In the absence of cAMP two C subunits are bound to the R subunit homodimer, which is formed by association at the D/D. Following the binding of a cAMP molecule to each of the two CNBs in each of the R subunits, a conformational change is induced, resulting in the release of the now active C subunit (Taylor et al., 2012).

1.3.1 PKA in synaptic plasticity

The roles of PKA in the brain are too numerous to list, however amongst the best-studied are the function of PKA in the modulation of synaptic strength by long-term potentiation (LTP) and long-term depression (LTD). In excitatory glutamatergic synapses (the most prevalent class in the human brain), control of Na⁺ influx through AMPA-type glutamate receptors is

fundamental to synaptic plasticity. PKA plays a key role by phosphorylating a key amino acid – Ser845 in the AMPAR subunit GluR1. PKA phosphorylation of this amino acid is essential to LTD in the Schaffer collateral pathway of the CA1 region of the hippocampus (Kameyama et al., 1998). When PKA activity is inhibited, LTD cannot be reversed (Lee et al., 2000). It has further been shown that the PKA is co-localized with AMPA receptors at the post synaptic density via the anchoring protein AKAP79 (also known as AKAP150), which directs basal phosphorylation of Ser845, effectively priming the synapse for LTD (Gomez et al., 2002; Tavalin et al., 2002; Snyder et al., 2005).

In contrast to the post-synaptic LTP and LTD generally studied in the CA1 region, the mossy fibers of the CA3 region are a common system to observe the related phenomenon of pre-synaptic LTP and LTD, which are generally induced by modulated neurotransmitter release (Bliss & Collingridge, 2013; Nicoll & Schmitz, 2005). The earliest indication of the role of PKA in presynaptic LTP was the observation that the application of forskolin, which raises cAMP levels by activating adenylyl cyclase, leads to increased neurotransmitter release in mossy fibers (Huang, Li, & Kandel, 1994; Weisskopf et al., 1994). This was supported by the observation that inhibition of PKA reduces LTP (Y. Y. Huang et al., 1995, 1994). The PKA substrates underlying presynaptic LTP in mossy fiber synapses are currently unknown.

1.3.2 PKA-mediated control of heart rate and contractility

PKA is an essential part of the chain of events that transduces electrical excitation of the myocytes, in turn regulating cardiac contractility (Bers, 2002). The chief mediator of cardiac transduction is Ca^{2+} , which is raised intracellularly by a combination of entry through depolarization-activated Ca^{2+} channels and release from the sarcoplasmic reticulum through ryanodine receptors. The intracellular Ca^{2+} then binds to the myofilament protein troponin

C (TnC) to begin the mechanical process of contraction (Bers, 2002). In order for contraction to occur, the Ca^{2+} must be removed from the cell. In the absence of phosphorylation, the protein phospholamban (PLB) inhibits the activity of the sarcoplasmic reticulum Ca^{2+} pump, reducing the rate at which Ca^{2+} is removed from the intracellular space following its release (Li et al., 2000). The phosphorylation of phospholamban by PKA removes its inhibitory effect on the pump, increasing the rate at which Ca^{2+} is transported, thereby contributing to an increase in relaxation rate (Kranias, 1985; Tada et al., 1983).

PKA also phosphorylates troponin I (TnI), which in turn decreases the Ca^{2+} affinity of the associated protein troponin C, increasing the off rate of Ca^{2+} binding, which also contributes to an increased rate of cardiac cycling (L. Li et al., 2000; Robertson et al., 1982; Solaro, Moir, & Perry, 1976). The combination of increased rate of Ca^{2+} reuptake, and dissociation of Ca^{2+} from the myofilament leads to an increase in rate cardiac cycling (Bers, 2002).

1.3.3 PKA in the kidney

Water reabsorption in the renal collecting duct is a key homeostatic mechanism, and variable control of its regulation is essential to adjust the process to the hydration needs of the body. An important mechanism that determines the rate of reabsorption is cell surface expression of the water channel aquaporin 2 (AQP2) the trafficking of which is mediated by the GPCR cascade. Binding of the hormone arginine-vasopressin to the transmembrane vasopressin receptor (V2) initiates the GPCR signalling cascade (Valenti et al., 2005) (**Figure 1.1**). The resulting increase in cAMP concentration activates PKA, which phosphorylates Ser256 of AQP2, initiating the translocation of the phosphorylated channel to the cell surface from intracellular vesicles (Fushimi, Sasaki, & Marumo, 1997; Katsura, Gustafson, Ausiello, &

Brown, 1997). PKA is localized to these vesicles by the longest splice variant of AKAP18, AKAP18 δ (Henn et al., 2004; Stefan et al., 2007).

1.3.4 PKA in disease

The unregulated activation of AGC family kinases has been observed in a range of diseases (Pearce, Komander, & Alessi, 2010). There is evidence indicating that the loss of regulation of kinases is a contributing factor to tumorigenesis in cancer, as well as insulin insensitivity in diabetes (reviewed in Pearce et al., 2010). In addition to the kinase activity in these diseases, AGC substrates are involved in a multitude of other disorders, including Alzheimer's disease, schizophrenia and Huntington's disease. In addition to this, there are two known PKA specific disorders: Carney complex (CNC) and acrodysostosis.

First characterized in 1985, CNC is an autosomal dominant disorder that manifests in a number of symptoms including, myxomas, endocrine tumours, and schwannomas which generally arise in teens or young adults (Stratakis, Salpea, & Margarita, 2015). The typical outwardly presenting symptom is the formation of lentigines, discoloured brown or black patches on the skin. The greatest pathological risk to CNC sufferers is the formation of cardiac myxomas, which can occur in one or more heart chambers, leading to obstruction and occasionally heart failure (Stratakis et al., 2015).

The primary mutation underlying CNC was discovered in 2000 by Kirschner and colleagues, who observed the loss of one copy of a gene on chromosome 17. Noting the similarity of CNC symptoms to that McCune-Albright syndrome, in which AC is constitutively active, the authors investigated the possibility that CNC is a result of a mutation in the *PRKAR1A* gene, which encodes PKA R α . Sequencing of the gene in CNC patients uncovered a variety of mutations, in addition to which, it was shown that the tumour tissue of CNC sufferers had

lower basal PKA activity, but greater PKA activity following cAMP application (Kirschner et al., 2000).

The sequencing of CNC patient genes has revealed more than 100 different *PRKAR1A* (Horvath et al., 2010), and in a 2009 study, mutations to this gene were present in 73% of the patients (CNC1) (Bertherat et al., 2009). Most of these mutations, do not result in the expression of mutant protein, as cellular R elements degraded the mutant mRNA, however a subset of patients express mutant protein (Bertherat et al., 2009; Horvath et al., 2010). The remaining patients did not have mutations to the gene (CNC2). Subtle phenotypic differences in the manifestation of the disorder were also observed in the CNC2 patients, leading the authors to speculate that this disease subtype might be due to a deficiency relating to molecules relating to PKA RI, rather than the protein itself (Bertherat et al., 2009).

Recently, another mutation in *PRKAR1A* mutation was discovered, which is associated with a condition known as acrodysostosis, which causes skeletal deformation. Analysis of patients with the condition indicated the presence of a nonsense mutation at R1 α Arg368 leading to disruption of the CNB B domain, which effectively de-couples the CBN A and B domains, abolishing the cooperative dynamics of their cAMP binding (Linglart et al., 2011). As a result of the lowered affinity of PKA for cAMP, the patients exhibit hormone resistance. Patients with a similarly presenting mutation in the gene encoding phosphodiesterase 4D do not exhibit this hormone resistance (Linglart et al., 2012). The severe pathological consequences of PKA mutations observed in CNC and acrodysostosis demonstrate the critical role played by PKA in different parts of the body.

1.4 General insights into protein kinase function from studies of PKA

1.4.1 AGC family kinases

Protein kinases account for approximately 1.7% of human genes, coding for more than 500 recognized kinases, which are split into 9 evolutionarily conserved groups (Manning et al., 2002). The AGC group of highly conserved serine/threonine kinases, was named for its the three most highly researched members at the time of its characterization: cAMP-dependent protein kinase (PKA), cGMP-dependent protein kinase (PKG), and protein kinase C (PKC) (Hanks & Hunter, 1995; Manning et al., 2002). This group is now understood to contain 60 kinases, including many well studied kinases like phosphoinositide-dependent kinase-1 (PDK1), Akt, ribosomal S6 kinase (S6K), and G protein-coupled receptor kinase (GRK) (Anjum & Blenis, 2008; Pearce et al., 2010). The PKA C subunit has served as a prototype for understanding the structure and function of AGC protein kinases, and for protein kinases in general.

The defining characteristic of the AGC group is a conserved kinase core of 250-300 residues, which has been shown to fold into a conserved conformation of 12 sub-domains in all of structures determined to date (Pearce et al., 2010; Taylor & Kornev, 2011). The majority of protein kinases including all AGC kinases fold with a bilobal arrangement with a smaller amino terminal lobe (N-lobe) and a larger carboxy terminal lobe (C-lobe) (Pearce et al., 2010). The two lobes form the C cleft that binds ATP for γ -phosphate transfer during phosphorylation. It is because of the highly conserved core that work on the PKA C subunit has been highly transferable to other AGC kinases. The PKA C subunit provided the first crystal structure of an ACG kinase, and allowed the conserved sub-domains of the class to be three-dimensionally mapped (Knighton et al., 1991).

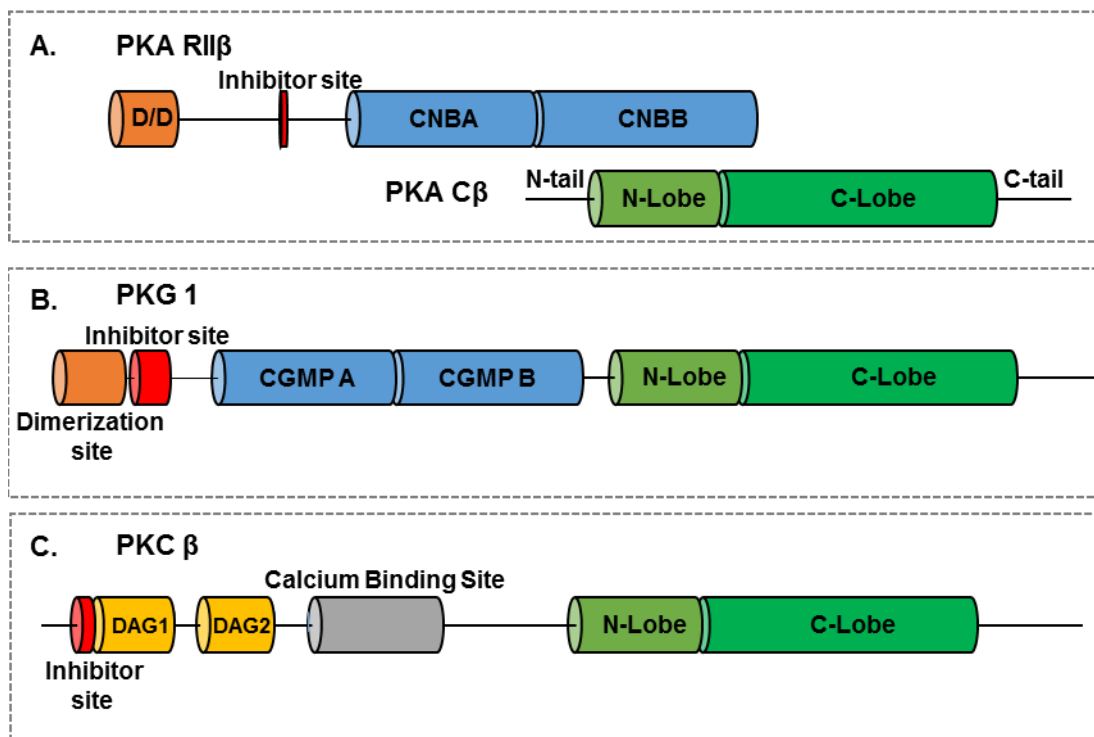


Figure 1.4 The conserved regions of AGC class kinases. The key characteristic of the AGC class of kinases is the conserved bilobal catalytic core (green), which is divided into an N-lobe and C-lobe, the cleft between which binds ATP for phosphorylation. **A.** The PKA holoenzyme forms a holoenzyme of four subunits, which consists of two R (RII β shown) and two C subunits (C β shown). The inhibitor site (red) which binds the inactive C subunit is on a separate polypeptide, which changes conformation following the binding of cAMP and releases the active C subunit. The D/D, which is the site of R dimer formation and association with scaffolding proteins is also in the R subunit (Cheng, Phelps, & Taylor, 2001; Taylor et al., 2012). **B.** In contrast, PKG regulatory and catalytic domains are contained in the same polypeptide, with the binding of cGMP causing the release of the inhibitor site from the catalytic domain, but not the catalytic domain from the regulatory domain (Pearce et al., 2010). Similarly to PKA, the dimerization of PKG is controlled by a leucine zipper dimerization domain at the N-terminus of the regulatory domain (Richie-Jannetta, Francis, & Corbin, 2003). **C.** In contrast to the PKA and PKG, PKC is activated by Ca²⁺ and/or diacylglycerol dependent on isoform. PKC β presented here requires both, though not all members of the family do (Webb, Hirst, & Giembycz, 2000). Accession numbers: PKA RII β : NP_001308911.1 PKA C β : NP_001157671.1, PKG 1: Q13976, PKC- β : P05771.

The prototypical members, PKA, PKG, and PKC, highlight both a number of similarities and differences within the class. While all of members have the same conserved kinase core, the elements both N- and C-terminal of the core can vary. Both PKA (**Figure 1.4 A**) and PKG (**Figure 1.4 B**) are cyclic nucleotide-dependent kinases, which are activated by cAMP and cyclic guanosine monophosphate (cGMP) respectively. In both cases, the binding of the cyclic nucleotide causes the dissociation of the inhibitor site, resulting in catalytic activity of the kinase domain (Pearce, Komander & Alessi, 2010). However, the regulatory domain of

PKA is a separate subunit from the catalytic domain, while the regulatory and catalytic domains of PKG are contained in same polypeptide (Pearce et al., 2010; Taylor et al., 2012). Similarly in both PKA and PKG, the regulatory domains are also the site of subunit binding, however the PKA subunit binds via the four helix docking and dimerization domain, while PKG is bound by leucine zippers (Richie-Jannetta et al., 2003). The cofactors with which kinases associate are one way in which control of the activation of the kinase domain of AGC kinases is imparted. The PKC β isoform show in **figure 1.4 C** requires Ca^{2+} and diacylglycerol as cofactors for activation, while others rely on other small molecules (Akt), phosphorylation (S6K), or are constitutively active (PDK1) (Pearce et al., 2010; Webb et al., 2000).

1.4.2 Insights from the first PKA structures

The PKA C subunit was the first AGC class catalytic subunit to be crystalized, revealing the kinase core that has served as the model for the entire class of enzymes. In 1991 Knighton and colleagues published a paramount paper in the field of PKA structural research, first x-ray diffraction crystal structure of the C subunit of PKA (Knighton et al., 1991). This structure brought to light the three dimensional significance of the many conserved regions of the protein kinase family. The authors found that the protein existed in a bilobal arrangement with the cleft between the smaller amino-terminal N-lobe, and the larger carboxy-terminal C-lobe in part occupied by the inhibitor peptide. This cleft was identified as the catalytic site of the molecule (**Figure Intro 1.5 A**). Throughout the protein kinase superfamily it is the residues around this cleft that are most highly conserved (Taylor et al., 2012). The N-lobe is the primary binding site for ATP, which causes a conformational change that links the lobes, without ATP the lobes are minimally connected (Johnson & Lewis, 2001). The authors also recognized the significance of many of the conserved catalytic core amino acids identified by

Hanks, Quinn and Hunter including the glycine-rich loop and the catalytic loop (Figure 1.5 B) (1988).

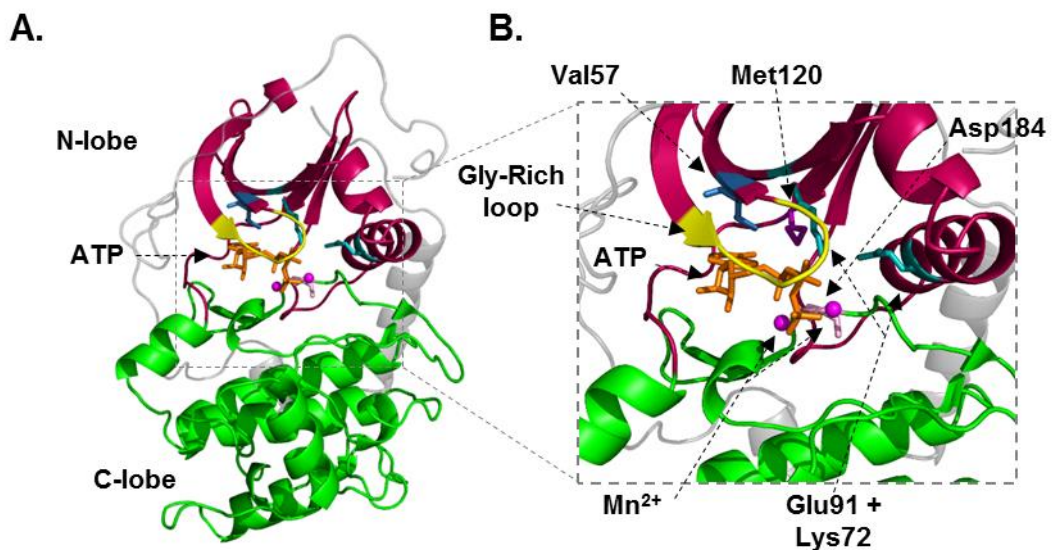


Figure 1.5 AGC class bilobal arrangement and ATP binding cleft. **A.** The defining characteristic of the ACG class is its conserved kinase core, which takes a bilobal conformation, with a small N-terminal N-lobe (dark pink), and a larger C-terminal C-lobe (green). The ATP binding cleft is formed between the two lobes (orange). **B.** The residues involved in phosphate transfer are highly conserved throughout the class. The naming conventions used here are from the PKA Catalytic subunit. The glycine rich loop (yellow) helps to orient the ATP molecule for transfer. The ATP molecule is further anchored by Val57 (blue). Met120 sterically limits access to the binding site by blocking larger molecules from entering (purple). Asp184 interacts with the Mn²⁺ ions, and is thought to help offset their charge (pink). The salt bridge formed between Glu91 and Lys 72 interacts helps to allosterically direct conformational shifts in the kinase core following the binding of ATP (teal). PDB: 1ATP (Zheng et al., 1993).

1.4.3 Catalytic mechanism of the kinase domain

The PKA catalytic subunit has been shown to phosphorylate more than 150 substrates, by the binding and transfer of the gamma phosphate of ATP to the target serine or threonine (Kemp, Graves, Benjamini, & Krebs, 1977; Neuberger, Schneider, & Eisenhaber, 2007). While the most common recognition sequence for substrates is the Arg-Arg-X-**Ser/Thr** motif, X-Arg-X-**Ser/Thr** and X-Arg-Arg-**Ser/Thr** substrates have also been identified (Kemp et al., 1977; Kemp & Pearson, 1990; Songyang et al., 1994). Indications from the ATP-bound crystal structure as well as a transitional state mimics show that the glycine rich loop (GxGxxG) associates with the γ -phosphate of ATP, helping to orient it for nucleophilic attack (Figure 1.5

B, yellow) (Madhusudan et al. 2002; Taylor & Kornev, 2011). The ATP molecule is further anchored by a valine residue following the loop (Val57), which makes a hydrophobic contact (**Figure 1.5 B**, blue) (Taylor and Kornev, 2012). The salt bridge formed between Glu91 and Lys72 in the closed conformation of the active loop couples the phosphates of the bound ATP to the C-helix of the N-lobe, which in turn coordinates many parts of the protein (**Figure 1.5 B**, teal) (Johnson et al., 2001; Taylor and Kornev 2012). ATP is also positioned in part by C-lobe residues. Asp184, which is highly conserved throughout the kinase superfamily, interacts with the Mg²⁺, which is thought to position the γ -phosphate for transfer, and which offsets the strongly negative charge of the phosphates (**Figure 1.5B**, pink) (Adams, 2001; Herberg et al., 1999; Johnson & Lewis, 2001).

1.4.4 Organization of the kinase domain

Analysis of the kinase domain by local spatial pattern (LSP) alignment, which compares protein sequences by assessing their position in space as opposed to sequence in relation to other residues, revealed a further level of organization that allows underlies communication throughout the molecule (Kornev et al., 2006; Kornev & Taylor, 2010). The C subunit is organized into two motifs called “spines” that are composed of non-contiguous hydrophobic residues (**Figure 1.6**). These spines coordinate the molecule by anchoring the structural elements to an α F-helix (**Figure 1.6**, yellow), and come into formation or disassemble based on the activation state of the subunit (Kornev and Taylor, 2010). The regulatory spine (R-spine) was discovered by comparing the surface residues of 23 active ser/thr kinase crystal structures, revealing a sequence of four highly conserved non-consecutive hydrophobic residues that link the two lobes and an aspartic acid on the α F-helix in the active conformation, but are not aligned in the inactive conformation (Kornev et al., 2006; Kornev and Taylor 2010). The assembly of the R-spine depends on the orientation of the active loop

(PKA residues 191-197), and typically forms following active loop phosphorylation (PKA Thr197) (Kornev, Taylor, & Ten Eyck, 2008; Taylor & Kornev, 2011; Taylor et al., 2013).

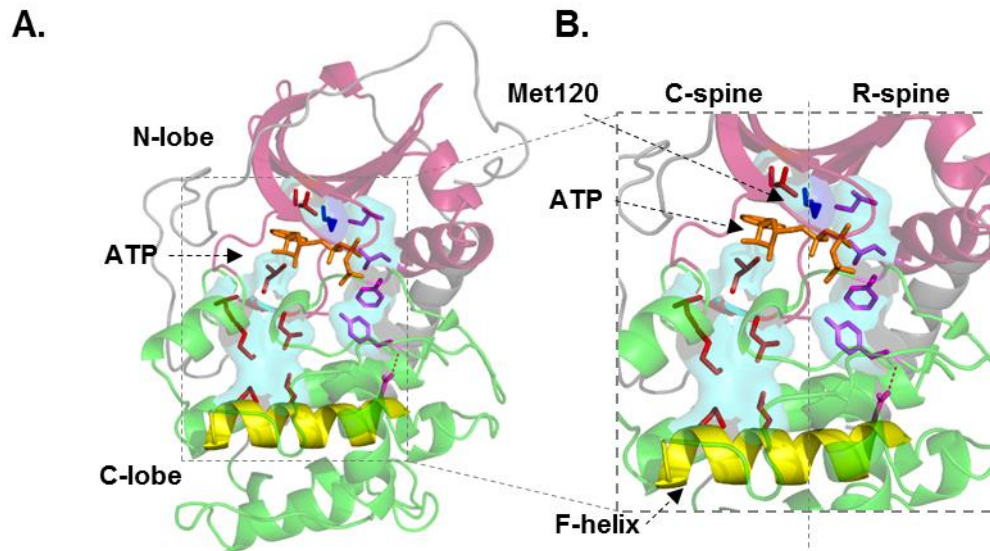


Figure 1.6 C- and R- spines coordinate kinase domain conformation. **A.** The discovery of the spatially aligned C-spine (red) and R-spine (blue) revealed a means of allosteric coordination between the N- and C- lobes of the kinase domain in response to ATP binding. **B.** The two coordinated spines coordinate the molecule by association with the F-helix (yellow). PDB: 1ATP (Zheng et al., 1993).

When the same principles of LSP alignment were applied to all of the residues in ser/thr kinases, a second spine, the catalytic spine (C-spine) was discovered that stretches across molecule and contacts the adenine moiety of bound ATP, coordinating the nucleotide binding and throughout the entire molecule via the α F-helix, meaning that ATP binding drives the coordination of the N and C lobes (Kornev, Taylor, and Eyck, 2008; Kornev and Taylor, 2010). With the recognition of the existence of these hydrophobic spines, it became clear that the hydrophobic F-helix in the conserved catalytic core is responsible for the overall coordination of the molecule as a whole (Taylor and Kornev, 2011). Between the two spines lies the “gatekeeper” residue (**Figure 1.6 B**, Met120, blue), the identity of which controls the binding pocket. The large methionine residue present in PKA means that only ATP can bind, though experimental evidence has shown that mutations in this position allow other larger nucleotides to bind (Taylor and Kornev, 2011). The C subunit has a C-terminal tail, called the

C-linker that contains two ATP binding residues, in addition to which the C-linker spans both N-and C-lobes (Taylor et al., 2012).

1.4.5 The role of disordered regions

While the allosteric interactions of folded domains have been extensively studied, there is relatively little information about the functional consequences of interactions involving disordered linker regions (Akimoto et al., 2013). Understanding of the R subunit linker function is limited in part due to its absence from crystal structures (Akimoto et al., 2013). Crystallization studies generally use RI α mutants from which the unstable linker and D/D domain have been removed in order to ensure stability (Bruystens et al., 2014). However, the deletion of these portions eliminates the cooperativity of cAMP binding between the CNBA and CNBB domains as shown affinity studies using a 1-91 deletion of RI (Herberg, Dostmann, Zorn, Davis, & Taylor, 1994). This is strong evidence for allostery between the two binding domains mediated by the N-terminal linker, which is absent from the traditional crystallographic studies. In the only tetrameric RII holoenzyme structures published to date, the N-linker, including the docking and dimerization domain is entirely absent from the electron density, and its position in relation to the rest of the holoenzyme has only been inferred from crystal packing. The functionally important RI α (99-118) linker is missing from crystal structures used to study the transitional states of R subunit activation (Akimoto et al., 2013; P. Zhang et al., 2012).

However investigations have begun into the role linker regions may play in enzymatic dynamics. The first holoenzyme structure to visualize a major portion of the N-terminal disordered region of the RI subunit showed that the linker region binds to a hydrophobic pocket on the opposing C subunit, creating a tetramer out of two homodimers, and dictating the shape of the holoenzyme which differs greatly between isoforms, despite their high

degree of sequence identity outside of the N-terminal region (Zhang et al., 2012). In 2013, Akimoto and colleagues showed, using NMR and thermodynamic modelling, that the interaction of the disordered linker region of RI α (99-118) helps to dictate the binding affinity of the C subunit in the transitional stage of holoenzyme activation and deactivation. This is accomplished by controlling the position of the CBD and increasing C subunit binding affinity for the holoenzyme conformation in the absence of cAMP (Akimoto et al., 2013). These examples indicate that, though poorly characterized, the disordered regions of the PKA holoenzyme are integral to the holoenzyme formation and function.

1.5 Localisation synthesis and breakdown of cAMP

1.5.1 Localisation of phosphodiesterases

The preceding sections have described how the PKA C subunit has some inherent substrate specificity; and how RI and RII subunits are able to inhibit the C subunit in the absence of cAMP. I now also appreciate that cAMP signals are spatially and temporally restricted in cells by the concerted action of cyclases and phosphodiesterases. Phosphodiesterases (PDEs) are enzymes that hydrolyse the cyclic nucleotides cAMP and cGMP into 5'AMP and 5'GMP. These enzymes are the longest recognized mechanism of termination of the cAMP signalling cascade, and are key regulators of the cyclic nucleotide second messenger cascade (T. Rall & Sutherland, 1958). The localization, concentration, and dynamics of PDEs delineate the temporal and spatial limits of cAMP activity. The binding of PDEs in specific subcellular locations helps to shape the cAMP concentration of these domains. Though there is much ambiguity surrounding the sub-cellular distribution of cAMP, there are strong indications that PDEs are integral to the maintenance of local cAMP concentration gradients. In FRET

studies, it was shown that the application of the PDE inhibitor IBMX ceased the formation of cAMP gradients (Zaccolo & Pozzan, 2002).

There are 11 classes of PDEs, each with distinct characteristics in terms of affinity for cyclic nucleotides, allosteric control, and localization, encompassing more than 50 mammalian proteins (Keravis & Lugnier, 2012). Of these, three classes are specific to cAMP, PDEs 4, 7, and 8, and an additional five can hydrolyze both cAMP and cGMP, PDEs 1, 2, 3, 10, and 11 (Conti & Beavo, 2007). The first crystal structure of the catalytic domain of a PDE was that of PDE4B (Xu et al., 2000). This data, combined with the structures that have followed, revealed a highly conserved binding pocket that contains 11 residues common to all PDEs (Conti & Beavo, 2007). Within this binding pocket is a glutamine residue which binds to the purine ring of cAMP or cGMP, and is believed to impart cyclic nucleotide specificity to the PDE through its orientation (Conti & Beavo, 2007). The position of this glutamine is held in a fixed conformation in cAMP or cGMP specific PDEs, while in dual specificity PDEs it has rotational freedom allowing the binding of either cyclic nucleotide (Conti & Beavo, 2007). The localization and functional specificity of PDEs is largely dictated by domains that fall outside of this region, generally at the N-terminal of the enzyme (Maurice et al., 2014). PDEs may also be part of multivalent complexes that include other cAMP dependent molecules, like PKA, and determinants of localization. Some examples include the colocalization of PDE4 to the plasma membrane by complexes containing AKAP3, and AKAP150, AKAP18, and AKAP79 (reviewed in Maurice et al., 2014).

1.5.2 Localisation of adenylyl cyclases

Another manner in which specificity of activation is imparted in the GCRP signalling cascade is through the differential expression, activation and localization of AC. Though there are

many mechanisms by which AC activity is controlled, G-protein subunit binding, PKC phosphorylation and PKA phosphorylation, the most analogous to our research is the colocalization of ACs with their interacting molecules.

All nine types of membrane associated ACs associate with AKAPs (Cooper & Tabbasum, 2014). Coprecipitation experiments using labelled forms of AC5 and AC6 in cell lines showed their association with AKAP79 (Bauman et al., 2006). It was further reported that cells coexpressing AKAP79 and ACV demonstrated significantly reduced cAMP production as compared to those expressing ACV alone, indicating the role of colocalization of AKAP79 in the deactivation of ACV. In a series of experiments, it was shown that the interruption of PKA anchoring to AKAP79, by either the addition of inhibitory binding peptides or mutation of the binding site, eliminated the reduction in AC activity typically seen following the activation of PKA. This revealed that the mechanism underlying the deactivation of ACV when coexpressed with AKAP79 is the colocalization of PKA, which directs the inhibition of AC by phosphorylation (Bauman et al., 2006; Chen et al., 1997; Iwami et al., 1995).

AKAP79 also serves other functions in coordinating the regulation of AC downstream of the muscarinic cholinergic receptor. It has been shown recently that not only does AKAP79 colocalize AC2 and its activating kinase PKC, it also binds PDE4, which breaks down cAMP produced by the AC, as well as PKA, which activates PDE4 (Shen & Cooper, 2013).

Additionally, the membrane associated AKAP9 splice variant, Yotiao illustrates the diversity of interactions an AKAP can have with AC isoforms. Yotiao has been shown to associate with AC1, 2, 3, and 9 in rat heart and brain tissue (Piggott, Bauman, Scott, & Dessauer, 2008). However, the effect Yotiao has across different ACs is striking, AC 2 is fully inhibited by Yotiao, while AC3 bound to the AKAP requires forskolin application in addition to the typically

sufficient $G_{\alpha s}$. In contrast, AC 1 and 9 are localized by not inhibited by Yotiao, indicating that it acts as a scaffolding mechanism for these ACs (Piggott et al., 2008). In support of this, Yotiao has been shown to localize with the slow delayed rectifier current potassium channel (I_{ks}) in cardiac tissue, which requires phosphorylation for activity, in addition to binding PKA, PDE4, and protein phosphatase 1, creating a localized regulatory domain controlling I_{ks} activation (Y. Li, Chen, Kass, & Dessauer, 2012).

1.6 Anchoring of PKA R subunits

While it has been shown that the subcellular localization of PKA is essential to the regulation of a wide range of processes effected by PKA activation, PKA R subunits have only two broad types divided into two isoforms each. This spatial specificity imparted by only four R subunit isoforms through their association with a class of proteins known as A kinase anchoring proteins (AKAPs). AKAPs act in conjunction with R subunits to convey a high degree of specificity to the positioning of PKA within the cell, which in turn imparts spatiotemporal control to the exposure of R subunits to cAMP, and ultimately the activation of C subunits.

To date there have been more than fifty AKAPs characterized (reviewed in Welch, Jones and Scott, 2010), which all share a characteristic helical domain that binds to the D/D domain found in the R subunits. AKAPs are the key structural protein in coordinating PKA activity by localization, and have been shown to direct PKA to the cytoskeleton, plasma membrane, postsynaptic density, nuclear envelope, sarcoplasmic reticulum, mitochondria, endoplasmic reticulum, centrosome, golgi, plasma membrane, microfilaments, vesicles and nuclear matrix among others (Welch, Jones, & Scott, 2010).

1.6.1 The discovery of AKAPs

The first AKAP was discovered in 1981 by Vallee, DiBartolomeis and Theurkauf, who had previously observed that mild digestion of the projection region of microtubule associated protein 2 (MAP2), a phosphorylation target for PKA, did not reduce the phosphorylation of the projection, leading the authors to suspect that PKA might be directly associated with this portion of the protein (Vallee, DiBartolomeis, & Theurkauf, 1981). Through a series of fractionation and kinase assay experiments, Vallee, DiBartolomeis and Theurkauf showed that a kinase cofractionated with MAP. The authors went on to show that this kinase was activated by cAMP, and inhibited by PKA specific protein kinase inhibitor peptide (PKI). In a further study, Theurkauf and Vallee went on to show using photoaffinity cAMP analogues that the cAMP binding protein corresponded in size to the phosphorylated and dephosphorylated RII subunit, while there was no detection of the RI subunit (1982). The authors then used a microtubule preparation to show that upon addition of cAMP, the active portion of the kinase could be completely separated from the cAMP binding portion, which was still associated with MAP2. Through this series of experiments, it was shown that MAP2 binds directly to PKA, and that binding takes place on the R subunit, and persists even after the dissociation of the C subunit, outlining the basics of the AKAP field (Vallee, DiBartolomeis and Theurkauf, 1981; Theurkauf and Vallee, 1982). Similarly AKAP75, another prototypical AKAP, was first identified due to its cofractionation with the RII subunit (Sarkar, Erlichman, & Rubin, 1984). Many further AKAPs were discovered by Far-western blotting using the N-terminal region of the R subunits as a probe, expression cloning, and yeast two-hybrid analysis (Welch, Jones and Scott, 2010).

While most RII is anchored by AKAPs to structures within the cell, the majority of RI is cytosolic (Skålhegg et al., 1994). All early studies identified only RII-binding AKAPs, however, in 1997, the first AKAP with the ability to bind to both RI and RII subunits D-AKAP-1, was

discovered by yeast two-hybrid analysis (Huang et al., 1997a). This category would expand to include other dual specificity AKAPs, D-AKAP2 (Huang et al., 1997), PAP7 (Li et al., 2001), AKAP220 (Reinton et al., 2000), merlin (Gronholm et al., 2003) and ezrin (Ruppelt et al., 2007). In the last decade, a number of RI-selective AKAPs have also been identified. These include PAP7 and ezrin (Jarnæss et al., 2008), and SKIP1, which contains two anchoring sites for RI subunits (Kovanich et al., 2010; Means et al., 2012).

1.6.2 Molecular basis of AKAP – PKA interactions

The basis of interactions between PKA R subunits and AKAPs have been extensively investigated by a combination of NMR and x-ray crystallography for both RII-AKAP interactions (Newlon et al., 2001; Gold et al., 2006; Kinderman et al., 2006; Götz et al., 2016) and RI-AKAP interactions (Banky et al., 2003; Sarma et al., 2010). The D/D domains of both RI and RII fold up into similar four-helical X-type bundles against which the amphipathic AKAP anchoring helix packs at an approximately 45° angle (**Figure 1.7**).

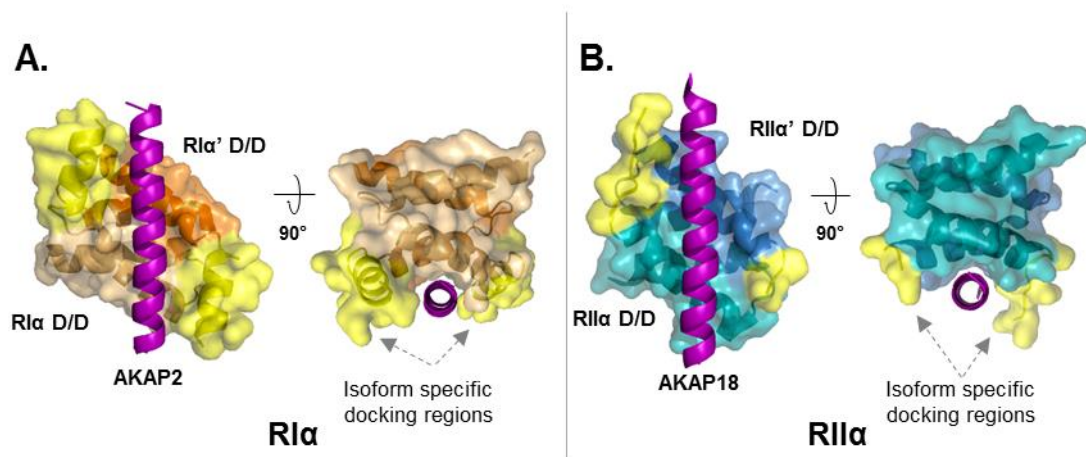


Figure 1.7 Comparison of AKAP binding to RI and RII D/D domains. **A.** RI α D/D domain bound to AKAP2 peptide. The amphipathic helix of AKAP2 (purple) is shown bound to the x-type bundle forming region of the N-terminus of RI known as the D/D domain. The helix formed by the N-terminal domain forms the isoform specific docking region (yellow), which creates the deep hydrophobic cleft that is characteristic of RI (Banky et al., 2003). (PDB: 3IM4, Sarma et al, 2010) **B.** RII α docking and dimerization domain bound to AKAP18. The amphipathic helix of AKAP18 is shown binding to the docking and dimerization domain of RII α . The N-terminal of RII α does not form helices, creating a shallower binding groove compared to the cleft of RI. The differences in RI and RII structure allow the preferential binding of AKAPs to one or the other isoform, and have been capitalized upon to create high-affinity synthetic binding peptides. PDB: 3IM4 (Sarma et al., 2010), 4ZP3 (Götz et al., 2016)

The most notable difference between binding of RI-selective compared to RII-selective AKAPs is that their-selective AKAPs engage with an additional relatively deep cleft created by an additional N-terminal helical region, which is known as the isoform specific docking region in RI (**Figure 1.7 A**; Banky et al., 2003). Presently, there are no structures of full-length AKAPs in complex with any fragment of PKA R subunits. The closest is a recent structure of the shortest variants of AKAP18 (AKAP18a) in complex with RII subunits. This structure shows that the anchoring helix in AKAP18 engages RII over a span of approximately 20 amino acids, which was a helical turn more than expected prior to this structural investigation (Gotz et al., 2016).

1.6.3 AKAP-derived sequences for investigating PKA anchoring

Anchoring disruptor peptides derived from AKAP anchoring helices have proved to be useful reagents for investigating PKA anchoring. Typically, short helical peptides (~18 amino acids) are rendered cell permeable by stearamide. Their application to cells enables the contribution of PKA anchoring to a given cellular process to be assessed. For example, the necessity of PKA anchoring for maintaining lens transparency was demonstrated using this approach (Gold et al., 2012). A number of synthetic peptides derived from endogenous AKAP sequences have followed (reviewed by Patel & Gold, 2013). The most recent generation includes two synthetic helical sequences: the highly RII-specific peptide Super-AKAP-is (Gold et al., 2006), and the highly RI-selective peptide RIAD (Carlson et al., 2006). I exploited the latter of these peptides during my doctoral studies (**Chapter 4**).

1.6.4 Multivalent AKAP complexes

In addition to binding PKA, AKAPs serve as binding sites for many other proteins, organizing functionally important colocalization of proteins by the formation of multivalent complexes.

This protein coordination has been shown to be a feature of almost all AKAPs (Welch, Jones and Scott, 2010). One of the best characterized examples of this is AKAP79, which is located predominantly on the plasma membrane of neurons and cardiomyocytes, has been shown to bind to PKA and the serine/threonine phosphatase calcineurin (CaN) as well as protein kinase C (PKC), placing them in position to respond to second messenger signals (Coghlan et al., 1995; Dell'Acqua et al., 1998; Klauck et al., 1996). The constituents of this AKAP79, PKA, PKC, and CaN complex have been shown to play a role in a wide variety of cellular activities. They act in the downregulation of cAMP by phosphorylation of adenylyl cyclase and β -adrenergic receptors (Bauman et al., 2006; Fraser et al., 2000). It has also been shown that AKAP79 based localization of PKC regulates some Ca^{2+} channels (Oliveria, Dell'Acqua, & Sather, 2007), as well as some potassium channels (Gao et al., 1997) and synaptic glutamate receptors (Colledge et al., 2000; Hoshi, Langeberg, & Scott, 2005; Tavalin et al., 2002), among many other functions.

Other examples include AKAP250 (gravin), which has been shown to associate with PKA, β_2 -adrenergic receptors, and PKC, localizing them to the plasma membrane (reviewed in Malbon, Tao, & Wang, 2004), and AKAP-Lbc binds protein kinase, guanine nucleotide exchange factor, and GTPase rho, coordinating their activity in a variety of functions (reviewed in Welch, Jones and Scott, 2010). Also, mAKAP was found to bind to the RyR2 ryanodine receptor Ca^{2+} release channel found in the sarcoplasmic reticulum of cardiac muscle in a complex consisting of mAKAP, RyR2 PKA, FKBP12.6, and phosphatases PP1 and PP2A (Marx et al., 2000; reviewed in Michel & Scott, 2002).

These discoveries have made it clear that the complexity and specificity of PKA localization is controlled by the multiplicity of AKAPs with which it associates, effectively conveying a diverse range of function to the relatively limited number of R subunit isoforms.

1.7 Recent Ideas for explaining C subunit restraint

Although many intricacies of cAMP signalling are understood, including the coordinated localisation and timing of PKA R subunits, phosphodiesterase and cyclases by anchoring proteins, our understanding of local cAMP signalling is still incomplete: it is still unclear how C subunits are restrained once they are released – what is the mechanism to prevent them from *“swimming about, happily phosphorylating a variety of cellular constituents whether they need it or not.”* (Rall, 1975)? In recent years, a number of new ideas and novel aspects of PKA have emerged that may be helpful for a complete understanding of local cAMP signalling. In this section, I consider two new theories to explain how the activity of C subunits is restrained, and describe recent insights into the myristoylation of C subunits, which may be important for determining movements of free C subunits in cells.

1.7.1 Are catalytic subunits released upon activation?

One of the theories as to how the activity of C subunits are restrained following their activation by cAMP discards the idea that dissociation is necessary for C activity, and instead focuses on the idea that activated PKA holoenzymes retain their association, and rely upon the flexible linker region spanning from the D/D to the CBD in the R subunit to define a sphere in which the kinase acts (Smith et al., 2013). One of the factors that led Smith and colleagues to question the canonical observation that C subunits dissociate from R subunits following cAMP binding, was the observation that binding affinity of cAMP for PKA R subunits is below 10 nM for both binding sites A and B in both Type I and Type II, while the association constant is 1, as well as the relatively low rate of cAMP hydrolysis by phosphodiesterases (Pope et al., 2008). The fast on time and slow off time led the authors to question how the activity of

the C subunit could be controlled with temporal and spatial accuracy if it was unable to re-bind these activated R subunits on a short time scale.

Smith and colleagues performed electron microscopy of negatively stained particles on AKAP18 coupled holoenzymes consisting of 2C α -2R11 α -AKAP18 γ . From this data, a model was constructed that placed the C subunit and the majority of the RI subunit at the end of the flexible linker region, allowing a range of conformations of the C-R assemblies in relation to the D/D. The authors suggested that the mechanistic justification for this disordered region was to allow the C subunit to orient itself in relation to a substrate within the reach of the linker arm, allowing phosphorylation of local substrates in the absence of cAMP activation (Smith et al., 2013).

Smith and colleagues investigated whether the association of the holoenzyme with the AKAP precluded the dissociation of the C subunit even in the presence of cAMP. To do so, the authors used a co-precipitation assay in which HEK293 cells were transfected with AKAP18 γ and R11 α constructs, which were then treated with 1 μ M isoprenaline or vehicle, resulting pull downs indicated that for all constructs and in all conditions, C subunits were recovered by the coprecipitation. The authors interpreted this to indicate an enduring association of the C and R subunits, even following the elevation of cAMP induced by the activation of the β -adrenergic signalling cascade by isoprenaline. In order for this to be true, they reasoned, the C subunit must be retained by the R subunit even when cAMP is bound. However, there were a number of procedural shortcomings apparent in the study that led us to question these conclusions, which will be discussed in **chapter 4.2**.

1.7.2 Myristoylation of C subunits

In eukaryotic cells, the N-terminus of the C subunit is post-translationally myristoylated. Myristoylation is the process by which the lipid myristoyl group is covalently bound to the N-terminal glycine of the C subunit by N-myristoyltransferase (Gaffarogullari et al., 2011). The N-terminus of the C subunit (residues 1-39) falls outside of the conserved region of AGC kinases, and differs between PKA isoforms (Bastidas et al., 2012). There is a body of work supporting the idea that RII subunits drive C subunit association with the membrane via conformational changes which alter the orientation of the myristoylated N-terminus.

Two studies in particular have attempted to quantify changes in the conformation of the myristoylated C subunit N-terminus. Gangal and colleagues studied membrane association of fluorescein maleimide-labelled C subunits (+/- myristoylation) with Texas red labelled-liposomes using FRET (Gangal et al., 1999). In the absence of R subunits, myristoylated C showed a modest increase of liposomal binding over non-myristoylated C. The combined addition of C subunit myristoylation and RII, but not RI, increased C subunit association with the membrane by 340% compared to the un-modified C subunit (Gangal et al., 1999). By comparison, the increase in membrane association resulting from the myristoylation of the C subunit alone was only 64%. NMR showed that RII binding greatly decreased the stability of the myristoylated C N-lobe, which is likely to be fundamental to its ability to induce membrane insertion of the myristoylated N-terminus of the C subunit (Gangal et al., 1999). Gaffarogullari and colleagues have also applied NMR to investigate C subunit myristoylation, and propose a two-state model in which the C subunit either adopts a 'myr-in' or 'myr-out' conformation (2012). These states are augmented by two transitional states in which the N-terminal is extruded from the C subunit and inserted into the membrane (Gaffarogullari et al., 2012). The authors predicted that the N-terminus assumes the myr-in conformation in

the absence of membranes, while the myr-out conformation is induced by the presence of membranes, possibly encouraging lipid binding by allowing the myristoyl group and the chain of basic residues at the N terminus to interact with the membrane (Gaffarogullari et al., 2012). Membrane association could potentially limit the movement of free C subunits within the cell to the two dimensional plane of the membrane, increasing the likelihood that contact would be made with membrane-associated RII subunits, and also maintain largely separate pools of C subunits for type I and type II R subunits.

1.7.3 RI buffering hypothesis

An alternate hypothesis that I was keen to test during my doctoral research was that C subunits may switch between RI and RII subunits during the on-set and off-set of cAMP signalling. According to this model, in the basal state, C subunits would associate predominantly with RII subunits with an excess of unoccupied RI subunits residing in the cytosol. The RI subunits would bind to C subunits following their release from anchored RII subunits following cAMP elevation. The position of RI subunits at a greater distance from the presumed highest concentrations of cAMP compared to RII might enable to satisfy this C subunit 'buffering' function. I aimed to test this hypothesis by monitoring the association of C subunits with both RI and RII during the activation and de-activation of cAMP signalling in HEK293T cells. One of the foundations to this model was that R subunits exist in an excess to C subunit – determining the stoichiometries of PKA subunits was accordingly also an aim of my doctoral research.

1.8 Recent technologies for investigating cAMP signalling

Forster resonance energy transfer (FRET)-based probes of cAMP concentration and PKA activity have transformed our understanding of localized cAMP signalling. In **Section 1.8.1**, the theoretical basis of FRET sensors is introduced, before sensors of cAMP concentration (**Section 1.8.1**) and PKA activity (**Section 1.8.2**) are described in the following sections. In **Section 1.8.3**, crosslinking coupled to mass spectrometry (XL-MS) is introduced, which is an emerging structural technique that promises to be powerful for investigating the structure of signalling complexes involving PKA.

1.8.1 Theoretical basis of FRET sensors

FRET relies upon the non-radiative energy transfer of energy applied a donor molecule that is then imparted upon an acceptor molecule, which in turn produces radiation. In biological systems this usually takes the form of two fluorescent molecules known as fluorophores. In these cases the donor molecule is excited by a specific wavelength of light, a portion of the energy of which is transferred to the acceptor fluorophore, which in turn radiates that energy as a different, separately measurable wavelength. However, this energy transfer only occurs over very short distances, due to the increased likelihood that donor energy will be lost as the distance increases. The simplified transfer efficiency of resonance energy transfer for complex systems in which the angular dependence of energy transfer is not considered can be expressed as:

$$\Phi_T = \frac{1}{1+(R/R_0)^6}$$

In which R is the distance between the donor and acceptor, and R_0 is the distance between the donor and acceptor at which the probability of transfer between the two is equal to the likelihood of spontaneous emission by the donor, that is when the FRET emissions are 50% of maximal (**Figure 1.8**) (Andrews, 2009; Piston & Kremers, 2007). It is also because of this

sixth power, that the distance between chromophores is the main determining factor of FRET intensity (Piston and Kremers, 2007). FRET offers much greater precision in determining molecular interactions than colocalization as measured by immunofluorescence microscopy, as the acceptor donor interaction occurs over a nanometer scale, while the resolution of colocalization is hundreds of nanometers wide (Piston and Kremers, 2007).

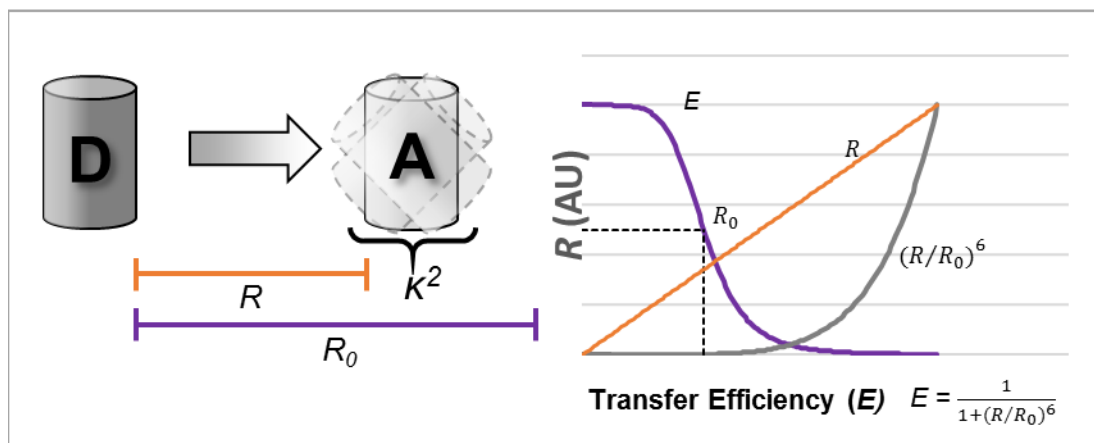


Figure 1.8 FRET transfer efficiency. A. The transfer of energy between donor and acceptor chromophores is dependent upon the distance between them (R), the distance as which the transfer is 50% of its maximum (R_0) and the orientation of the chromophores (κ^2). In biological systems the rotation of the chromophores is assumed to be free, and the κ^2 is not considered.

1.8.1 FRET-based sensors of cAMP concentration

The first studies of cAMP concentration using FRET relied upon microinjection of fluorescently labelled PKA R and C subunits (Adams et al., 1991). The first probe - fluorescein C subunit and rhodamine R subunit (FICRhR) – was applied to demonstrate through imaging the existence of cAMP functional compartmentalization in cells (Backskai et al., 1993). They demonstrated this by injecting FICRhR into *Aplysia* sensory neurons in culture and applying serotonin, which produced a gradient of FICRhR activation spreading from the distal processes of the cell and decreasing with proximity to the cell body. Though FICRhR was useful as the first tool to help researchers visualize the movement of cAMP and PKA subunits through the cell, its enzymatic activity and binding dynamics reduced its usefulness in

measuring cellular phenomenon. As Rich and Karpen examined in their 2002 meta-analysis of publications relying on FICRhR measurements, both the temporal and spatial results could be misleading. First, using reported PKA affinity for cAMP and observed dissociation rates, the authors showed that the rate of holoenzyme reassociation is too slow for capturing real-time oscillations in cAMP concentration, using modelling to show that while the system can discriminate changes over a 0.02 Hz (50 s) time scale, the dynamics fail to show oscillations of the physiologically relevant frequency of 2 Hz (5 s) (Thomas C. Rich & Karpen, 2002). Furthermore, as a high concentration of FICRhR is needed to overcome the effects of the labelled subunits associating with endogenous PKA, the FICRhR concentration is high enough to significantly alter cellular cAMP dynamics. At the experimentally typical FICRhR concentration of 2 μ M the authors showed that the buffering caused by the addition of FICRhR altered the dynamics of the rise in cAMP concentration (Rich & Karpen, 2002). In addition to which, the enzymatic activity of activated FICRhR could cause additional phosphorylation that is not characteristic of typical cellular functions.

A significant step forward in FRET-based cAMP sensors was made by Zaccolo and co-workers, who developed a genetically encoded PKA construct tagged with GFP-based donor and acceptor proteins on the RI and C subunits respectively (Zaccolo et al., 2000). This system had the advantage of not requiring the purification, labelling and injection of the FICRhR sensor. A second generation PKA-based FRET reporter was applied in myocytes to demonstrate that β -adrenergic stimulation caused by norepinephrine resulted in reduction of FRET ratios observed at Z-lines but less so in the cytosol (Zaccolo & Pozzan, 2002), and later to show that PDE4 is primarily responsible for the reduction in cAMP concentrations in the cell (Mongillo et al., 2004).

The identification of exchange proteins directly activated by cAMP (Epacs, de Rooij et al., 1998; Kawasaki et al., 1998) has more recently enabled the development of a new generation of FRET-based cAMP probes based on Epac1 and Epac2 (Nikolaev et al., 2004; DiPilato et al., 2004, Ponsioen et al., 2004). The mechanism of a generic Epac-based FRET sensor for cAMP concentration is shown in **Figure 1.9**. In the case of perhaps the most efficient Epac-based cAMP sensors - ^TEpac^{vv} – the GFP variants cerulean fulfils the role of donor and citrine the role of acceptor (Klarenbeek et al., 2011; Li et al., 2015). Elevation in cAMP results in a decrease in FRET between the two GFP variants (**Figure 1.9B**). Epac-based probes possess a number of advantages in comparison to PKA-based sensors: they exhibit higher FRET efficiency, have higher temporal resolution, and since they are unimolecular they are no concerns regarding balancing the expression levels of donor and acceptor proteins. Furthermore, if PKA-based signalling pathways are the focus of investigation, then there are fewer concern regarding potential complications from interaction between the sensors and endogenous PKA subunits.

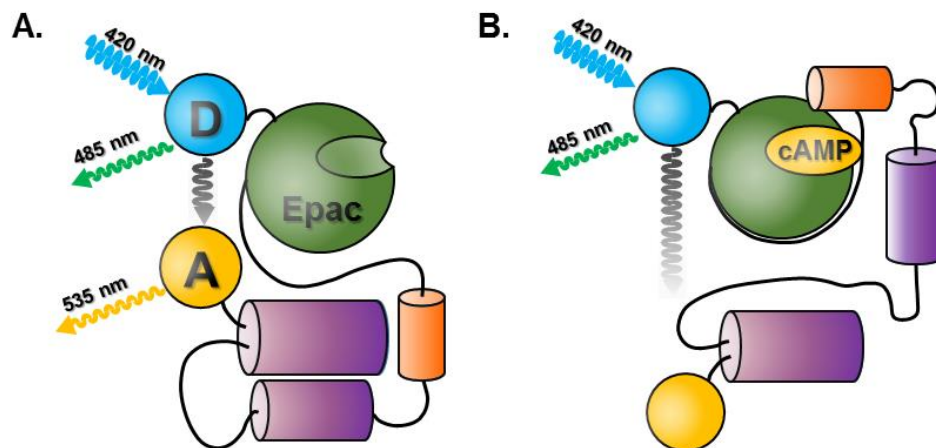


Figure 1.9 Schematic of a generic FRET/Epac-based cAMP sensor **A.** In its unbound state, the donor and acceptor are within transmission range of each other. **B.** In response to cAMP binding, a conformational change is induced which increases the distance between the donor and acceptor, decreasing the ratio of 535/485 emission.

One final class of cAMP sensor, that was not exploited during my doctoral studies are sensors based on cyclic nucleotide-gated channels (Rich et al., 2000; Fagan et al., 2001). The first example of this approach exploited rat CNG2 expression in human embryonic kidney-293 (HEK-293) cells (Rich et al., 2000). CNG2 mutations A C460W/E583M double CNG2 mutant, which has improved cAMP specificity and sensitivity compared to wild-type (Rich et al., 2001), was used as a sensor to reveal that both G protein coupled receptor kinases and PKA stimulate PDE degradation of cAMP following β 2-AR stimulation of HEK-293 cells (Xin et al., 2008). These sensors are commonly applied in combination with the Ca^{2+} dye Fura-2, which enables measurement of cAMP by proxy through imaging of Ca^{2+} influx rather than measuring CNGC currents by electrophysiology (Fagan et al., 2001; Rich et al. 2001; Willoughby et al., 2006).

1.8.2 FRET-based sensors of PKA activity

A number of reporters have also been developed for monitoring PKA activity in cells. Zhang and colleagues created the first A-kinase activity reporter (AKAR) (2001). They took advantage of the protein 14-3-3 τ , which binds to a motif containing phosphoserine, by incorporating a PKA substrate/14-3-3 τ binding sequence at the end of a flexible linker region separating it from the 14-3-3 τ protein. The authors used the modified kemptide sequence LRRASLP as a substrate for PKA, the phosphorylation of which created a target for 14-3-3 τ . They also fused the fluorophores enhanced cyan fluorescent protein, and citrine to the N and C terminals respectively. This organization yielded a four part chimeric protein in which phosphorylation of the modified kemptide sequence results in the binding of 14-3-3 τ , which in turn brings the fluorophores close enough together to produce a measurable FRET signal. In their initial investigations, Zhang and co-workers were able to show that anchoring PKA to the reporter by fusion with an anchoring sequence greatly increased PKA phosphorylation of

the reporter, thereby demonstrating the importance of PKA anchoring in cells (Zhang et al., 2001).

The major drawback of the previously described AKAR1 based on a 14-3-3 phosphoserine-binding domain is the lack of reversibility of its binding, which limits its usefulness to observe cellularly relevant dephosphorylation of substrates (Zhang et al., 2005). A reporter with improved reversibility, AKAR2, was therefore developed that incorporates the weaker binding forkhead-associated domain 1 (FHA1) in place of 14-3-3 (Zhang et al., 2005). The authors went on to show that in cells expressing AKAR2 following prolonged exposure to insulin, the speed of the FRET response of the reporter in response to isoprenaline was delayed. They also showed that chronic insulin treatment decreased the phosphorylation of nuclear CREB protein, which plays a role in controlling gene expression, in response to isoprenaline. The authors showed a decrease in association between RII β subunits and β_2 -adrenergic receptors in response to insulin treatment. Neither of these results were seen in response to forskolin or caged cAMP. These findings showed the ability of a hormone to disrupt the interactions between PKA and its downstream effectors by altering its subcellular position. The latest AKAR sensor, AKAR4, utilises cerulean and venus as the donor and acceptor (Depry et al., 2011, **Figure 1.10**). Depry and co-workers fused AKAR4 to different

membrane targeting sequences to demonstrate that there is high resting PKA activity in cholesterol-rich regions of the cell membrane (Depry et al., 2011).

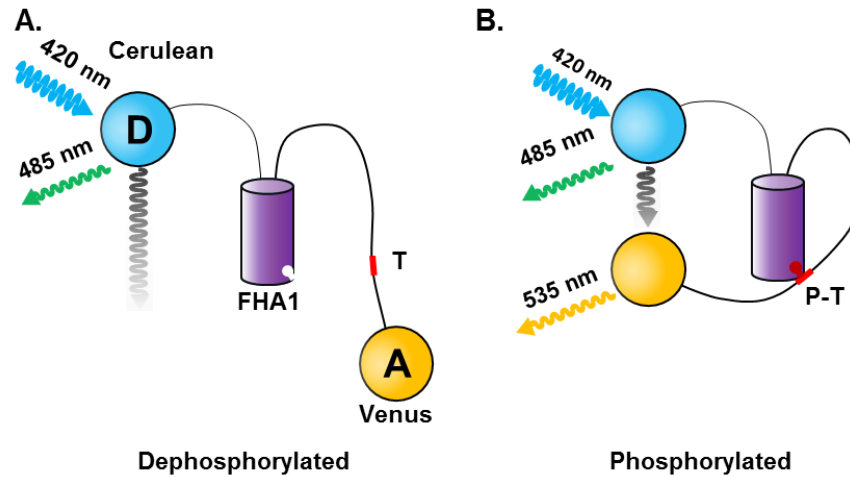


Figure 1.10 Schematic of the phosphorylation induced activation of AKAR4. **A.** AKAR4 is built around the FHA1 domain, which binds phosphothreonines, but with low enough affinity to allow unbinding by dephosphorylation. The region linking the FHA1 domain and the acceptor molecule contains a PKA threonine phosphorylation site. When AKAR4 is not phosphorylated, the Venus acceptor molecule (A) is out of range of FRET transfer from the Cerulean donor molecule (D). **B.** Upon phosphorylation, the phosphothreonine (P-T) is bound by the FHA1 domain, bringing the acceptor molecule within range of the donor, and increasing the ratio of 535 nm to 485 nm emission.

1.8.3 Crosslinking coupled to mass spectrometry (XL-MS)

Within structural biology, a number of techniques are available for interrogating protein structure. High resolution (typically 1.5-3 Å) approaches include X-ray crystallography and nuclear magnetic resonance (NMR) spectroscopy, whereas electron microscopy (EM), and small angle scattering (SAXS) are suitable for analysing larger structures at intermediate levels of resolution (4-20 Å). However, each of these techniques individually suffers from limitations. X-ray crystallography is unmatched for its resolution but achieving protein crystallisation can sometimes present an insurmountable hurdle. In addition the conformation observed in the crystal represents a single fixed view of the protein (Putnam et al, 2007) that may be physiologically inaccurate since crystal contacts can bias protein conformations in ways that are not observed in nature. The influence of crystal packing is

particularly pronounced on the protein surface and in flexible regions (Eyal et al., 2005). NMR is limited the proteins up to ~ 50 kD; EM and particularly cryo-EM are coming into their own with the advent of improvements in structural supports (reviewed in Russo & Passmore, 2016). Nevertheless, it can be challenging to locate protein domains within EM maps garnered through single particle averaging EM, and the process is not so well suited to structural analysis of more transient protein complexes. Crosslinking coupled to mass spectrometry (XL-MS) is a rapidly developing structural method that complements these more established structural methods.

In XL-MS, chemical crosslinking of protein side-chains, followed by protease digestion and identification of crosslinked peptides by peptide mass fingerprinting MS enables identification of side-chains that are close to one another in three-dimensional space. Both links within proteins (intra-links) and between different proteins (inter-links) contain useful structural information. The key strengths of XL-MS is that it allows protein interactions to be examined in their native conformations, and also particularly lends itself to the variability of association of disordered regions. Due to the ability of the method to capture multiple interactions, many associations of a flexible region can be captured in a single experiment. Another advantage of XL-MS is the reduced sample purity required as compared to crystallography (Leitner, 2016). Additionally, there are no size constraints on the complexes that can be analyzed, which is greatly advantageous when examining proteins that form multimeric complexes and allows the orientation of large subunits to be measured in relation to one another (Lietner et al., 2015; Leitner, 2016). However, the usefulness of XL-MS is limited by the large radius over which DSS can bind, resulting in relatively low spatial resolution, and by the relative scarcity of crosslinks (Leitner, Walzthoeni and Aebersold, 2014). As a result, XL-MS is not used as a stand-alone method for structural investigation. Instead XL-MS has been successfully combined with other structural methods including

crystallography, electron microscopy, and NMR, to elucidate structures, particularly those with flexible regions, in an approach known as integrative structural biology (Faini, Stengel, & Abersold 2016; Erzberger et al., 2014).

The majority of biological molecules contain regions of limited secondary structure, which are inherently movable in solution. These sequences are known as intrinsically disordered regions (IDRs) and pose a challenge for crystallographers, as their motion is incompatible with crystallization. At best, these regions produce areas of structural models with low resolution, while often they are missing from the electron density, or preclude the crystallization of the molecule entirely (Radivojac et al., 2004). The manifestation of this problem was illustrated by Le Gall and colleagues who showed that roughly 40% of a representative sample of structures from the RCSB protein data bank (PDB) contained regions of low resolution or ambiguity due to IDRs (Berman et al., 2000; Le Gall et al., 2007). During my doctoral studies, I took advantage of the unique advantages of XL-MS in undertaking the first major application of XL-MS to study the structure of PKA complexes. XL-MS is also described with more technical detail in **chapter 2.4**.

1.9 Project Aims

In light of the established research in the field, as well as the methods of investigation available to us, I have three main goals of the project. These aims were designed to fill major gaps in the current understanding of PKA restriction

Aim I. Quantify PKA subunits in terms of copy number and stoichiometric ratios.

The lack of information about the relative copy numbers of PKA subunits present in cells and tissues limits how I consider binding and release of PKA C subunits from RI and RII subunits. These investigations are detailed in **chapter 3**.

Aim II. Determine how C subunits associate with RI and RII in real time during activation and deactivation of cAMP signalling using a novel light-activated crosslinking approach.

The association of C subunits with specific R subunit isoforms determines both localization and activation dynamics of PKA. However, there is no existing method to monitor RI-C and RII-C subunit interactions in cells with temporal precision. **Chapter 4** sets out the development and application of a novel method to achieve this for the first time.

Aim III. Develop and apply crosslinking coupled to mass spectrometry (XL-MS) to investigate the quaternary structure of PKA complexes

XL-MS is an emerging structural technique that is well suited to investigating the quaternary structure of large protein assemblies such as PKA. **Chapter 5** describes experiments aimed at understanding how PKA subunits are oriented relative to one another and with respect to anchoring proteins. I also aimed to develop a novel

approach that relies upon isotopic labelling for identifying homo-oligomeric interlinks using XL-MS, which is described in this chapter.

Chapter 2. Materials and Methods

2.1 Basic molecular biology techniques

2.1.1 Production of chemically competent *E. coli*

To render *E. coli* BL21 (DE3) cells competent, four overnight cultures were grown in 100 mL of super optimal broth (SOB) (8.6 mM NaCl, 20 g/L tryptone, 5 g/L yeast extract, 2.5 mM KCl, 10 mM MgCl₂) in 1 L Erlenmeyer flasks at 18°C with shaking at 200 rpm. Four different concentrations of cells were set up by adding 50 µL, 150 µL, 500 µL or 1000 µL of starter culture at an OD₆₀₀ of 0.6 to each flask. Cells with an OD₆₀₀ between 0.3 and 0.5 were used to make competent cells. 1 mL of culture was cooled on ice for 15 minutes, then pelleted by centrifugation at 2,000 x *g* for 10 minutes. Cells were then resuspended in 24 mL of ice cold frozen storage buffer (FSB) (10 mM potassium acetate pH 7.5, 45 mM MnCl₂, 10 mM CaCl₂, 100 mM KCl, and 10% glycerol w/v) and incubated on ice for 15 minutes. The cells were then pelleted by centrifugation at 2,000 x *g* for 10 minutes, following which they were resuspended in 8 mL of ice cold FSB. Following this, 280 µL of filter sterilized DMSO was added and the mixture was incubated on ice for 5 minutes before another 280 µL of DMSO was added. Cells were incubated a further 5 minutes on ice before they were split into 60 µL aliquots in sterile 2 mL centrifuge tubes and flash frozen in a dry ice ethanol bath. Competent cells were stored at -80°C until use.

2.1.2 Bacterial transformation

DNA constructs were transformed into competent cells by heat shock. 100 ng of plasmid DNA was combined with 50 µL of competent cells in 1.5 mL microcentrifuge tubes, and incubated on ice for 30 minutes. Cells were then heat shocked in a 42°C water bath for 30 seconds, after which they were transferred to ice for 2 minutes. 200 µL of SOB was added

to the cells, which were incubated for 1 hour at 37°C with shaking at 200 rpm. Cells were then spread on agar plates supplemented with the appropriate antibiotic, and incubated overnight at 37°C.

2.1.3 *E. coli* culture

Recombinant protein constructs were grown in *E. coli* BL21 (DE3) cells line unless otherwise stated. All *E. coli* cultures were grown in LB (10 g/L tryptone, 5 g/L yeast extract, 5 g/L NaCl) with the exception of M9 minimal media cultures (described in section 2.1.4). Cultures were grown in 6 x 800 mL volumes in 2 L flasks. The LB was augmented with the appropriate antibiotic for the plasmid (ampicillin 370 µM; kanamycin 100 µM). Cultures were inoculated with saturated starter culture. In the initial instance, single colonies were picked from plates following transformation of competent cells and grown in LB overnight to make the starter. In subsequent iterations, glycerol stocks were scraped into LB to make overnight starter cultures.

Glycerol stocks were made by taking 500 µL of culture at OD₆₀₀ and combining it with 60% filter sterilized glycerol in a microcentrifuge tube, to give a final concentration of 30% glycerol. The stocks were then snap frozen in liquid nitrogen and stored at -80°C for future use. Cultures were induced at OD₆₀₀ ~ 0.5 by the addition of 375 µM isopropyl β-D-1-thiogalactopyranoside (IPTG). Cultures were then incubated overnight at 18°C.

2.1.4 M9 minimal media

Each construct used for experiments with heavy lysine and arginine isotopes was transformed into *E. coli* BL21 (DE3) ΔArg/Lys cells that are auxotrophic for arginine and lysine. Cell transformed with each protein construct were grown in M9 minimal media (25 mM Na₂HPO₄, 25 mM KH₂PO₄, 50 mM NH₄Cl, 5 mM Na₂SO₄, supplemented with 1 mM MgSO₄,

0.1 mM CaCl₂, and 0.2% glucose) to an OD₆₀₀ of between 0.5 and 0.9 before induction by the addition of IPTG to a final concentration of 1 mM.

2.1.5 Expression and purification of glutathione-S-transferase (GST) tagged fusion proteins

GST tagged constructs (C β , RI α , RI β , RII α , RII β , AKAP18, AKAP79 c93, RIAD), and the poly-histidine tagged construct (C α) were transformed into *E. coli* BL21 (DE3) cells, and cultured in 1.6-4.8 L total volumes as described above. Recombinant protein expression was induced at an OD₆₀₀ of 0.5-1.0 with the addition of 375 μ M IPTG (**Table 2.1**). Expression was then allowed to progress at 20°C overnight. Following this incubation, cells were pelleted by centrifugation for 10 minutes at 12, 250 x *g* in a fixed angle rotor (Beckman JLA 8.100). Pellets were then washed by resuspension in PBS, transferred to 50 mL conical tubes, and spun for a further 20 minutes at 3, 220 x *g* in a swing bucket rotor (Eppendorf A-4-81) before being snap frozen in liquid nitrogen. Pellets were stored at -80°C prior to processing. Thawed pellets were resuspended in 50 mL of glutathione sepharose lysis buffer (30 mM HEPES pH 7.5, 500 mM NaCl, 2 mM DTT, 0.5 mM EDTA, and 1 mM benzamidine). Benzamidine was included in the buffer as a protease inhibitor, and EDTA was included as a chelator to reduce enzymatic activity by sequestering cofactors. Some purifications were augmented with 10 % glycerol w/v to increase solubility (Gräslund et al., 2008). 0.01 mg lysozyme was added to the lysis buffer, and the cell lysate was sonicated at 20 kHz, for 2x30 second intervals, between which it was incubated on ice. The lysate was then incubated on a rolling mixer for 30 minutes at 4°C. Following incubation, the lysate was transferred to 50 mL polypropylene tubes (ThermoFisher) and spun at 31,360 x *g* for 30 minutes (**Table 2.1**). The clarified supernatant was then transferred to a 50 mL conical tube and the pellet was discarded.

Construct	Plasmid	Time to OD ₆₀₀	OD ₆₀₀ at Induction	Affinity beads	Glycerol
AKAP18 α	pGEX-6p-1	2 hours 45 minutes	0.7	Glutathione sepharose	10%
AKAP79 c93	pGEX-6p-1	3 hours 30 minutes	0.55	Glutathione sepharose	-
PKA C α	pET28m	4 hours	0.6	Ni-NTA	-
PKA C β	pGEX-6p-1	3 hours 50 minutes	0.8	Glutathione sepharose	10%
PKA RI β	pGEX-6p-1	2 hours 25 minutes	0.6	Glutathione sepharose	-
PKA RI α	pGEX-6p-1	2 hours 25 minutes	0.65	Glutathione sepharose	-
PKA RI β	pGEX-6p-1	2 hours 45 minutes	0.8	Glutathione sepharose	10%
PKA RI α	pGEX-6p-1	2 hours 30 minutes	0.7	Glutathione sepharose	10%
Short RIAD	pGEX-6p-1	2 hours 50 minutes	0.9	Glutathione sepharose	-

Table 2.1 Expression conditions of purified proteins

Constructs in the pGEX-6p-1 plasmid possess a GST tag, and the supernatant from these cells was incubated with glutathione sepharose 4B (GE Healthcare Life Sciences). Binding of these constructs to glutathione sepharose was found to be slow, and the incubation was allowed to proceed for at least 3 hours. Following incubation, the mixture was spun at 350 x *g* for 5 minutes to pellet the bound proteins and sepharose. The beads were washed by resuspension and another 5 minute spin at 350 x *g*, before they were transferred to an 8-mL drip column with a 90 μ M filter (Evergreen Scientific). Once in the drip column, the beads were washed with three column volumes of glutathione sepharose lysis buffer.

Two separate methods of elution were used depending on the whether a GST-tagged or untagged final construct was being produced. When the GST tag was desired in the final construct, proteins were eluted from the beads with 2 mL of 15 mM L-glutathione (Sigma), which competes with the GST tag for glutathione sepharose binding sites. The beads were incubated with L-glutathione for 1 hour on ice. When untagged proteins were being produced, the GST tag was cleaved using 60 μ g of human rhinovirus 3C (HRV 3C) protease in 2 mL of glutathione sepharose buffer. In this case, the bound proteins were incubated with the protease overnight at 4°C before elution leaving most of the GST bound to the bead, and allowing the rest to be separated by size exclusion.

Constructs made using the pET28 plasmid backbone contain a tag consisting of 6 histidine residues. Histidine interacts strongly with transition metals, which allows affinity purification of tagged proteins by interaction with immobilized metals. For this, I used nickel-nitrilotriacetic acid (Ni-NTA) agarose (Qiagen), which consists of immobilized Ni^{2+} ions in a matrix, which orients them for interaction with histidine residues (Bornhorst & Falke, 2000). The association of this matrix with agarose allows the material to be recovered. The binding step was carried out in batch mode in 50 mL conical centrifuge tubes for 1 hour in slightly basic buffer (30 mM Tris pH 8.0, 500 mM NaCl, 10 mM Imidazole, 1 mM benzamidine). His-tagged protein elution was performed by adding 20 mL buffer containing 300 mM imidazole (chemically identical to the histidine side-chain) for competitive exclusion. The elution buffer also had a lower pH to encourage protonation of the histidine and subsequent dissociation from the Ni^{2+} -NTA (30 mM Tris pH 7.0, 500 mM NaCl, 300 mM imidazole, 1 mM benzamidine).

All proteins were purified by size exclusion chromatography using an 80 mL Superdex 200 column (GE Healthcare Life Sciences), which combines a dextran and agarose in a matrix optimized for the purification of 10-600 kDa proteins. An ÄKTA fast protein liquid chromatography system operated by Unicorn control software (GE Healthcare Life Sciences) was used to conduct the purification. The concentration of protein in eluted fractions was preliminarily evaluated by absorbance at 280 nm (A_{280}), which is primarily caused by tryptophan and tyrosine residues, as measured by an inline UV detector (**Figures 2.1-2.4**, panels A & C). The Superdex-200 column was equilibrated with at least 1.5 column volumes of 20 mM HEPES pH 7.5, 200 mM NaCl whereby a steady baseline was reached. Following column equilibration, proteins were loaded in a 2 mL injection loop, and automatically loaded onto the column by passing 5 mL of purification buffer through the loop. All proteins

were purified in 20 mM HEPES pH 7.5, 200 mM NaCl, with or without 2 mM DTT and 1 mM EDTA. Eluent was captured in 2 mL fractions by an automatic fraction collector, and the protein purity of the fractions was assessed by SDS-PAGE and subsequent Coomassie staining.

Both PKA C subunit isoforms were purified for quantitative immunoblotting experiments (**Figure 2.1**), with C β used further for XL-MS analysis. C α was purified via a polyhistidine tag, using Ni-NTA agarose. C β was expressed with a GST tag, allowing for purification using glutathione sepharose. The GST tag was subsequently cleaved by HRV 3C. Initial measurement by A₂₈₀ produced a single peak for each construct (**Figure 2.1 A & C**), the purity of which was evaluated by Coomassie staining of SDS PAGE gels (**Figure 2.1 B & D**). Both constructs were found to be of suitable purity for experiments. In each case, the fractions within the dashed boxes were combined for use.

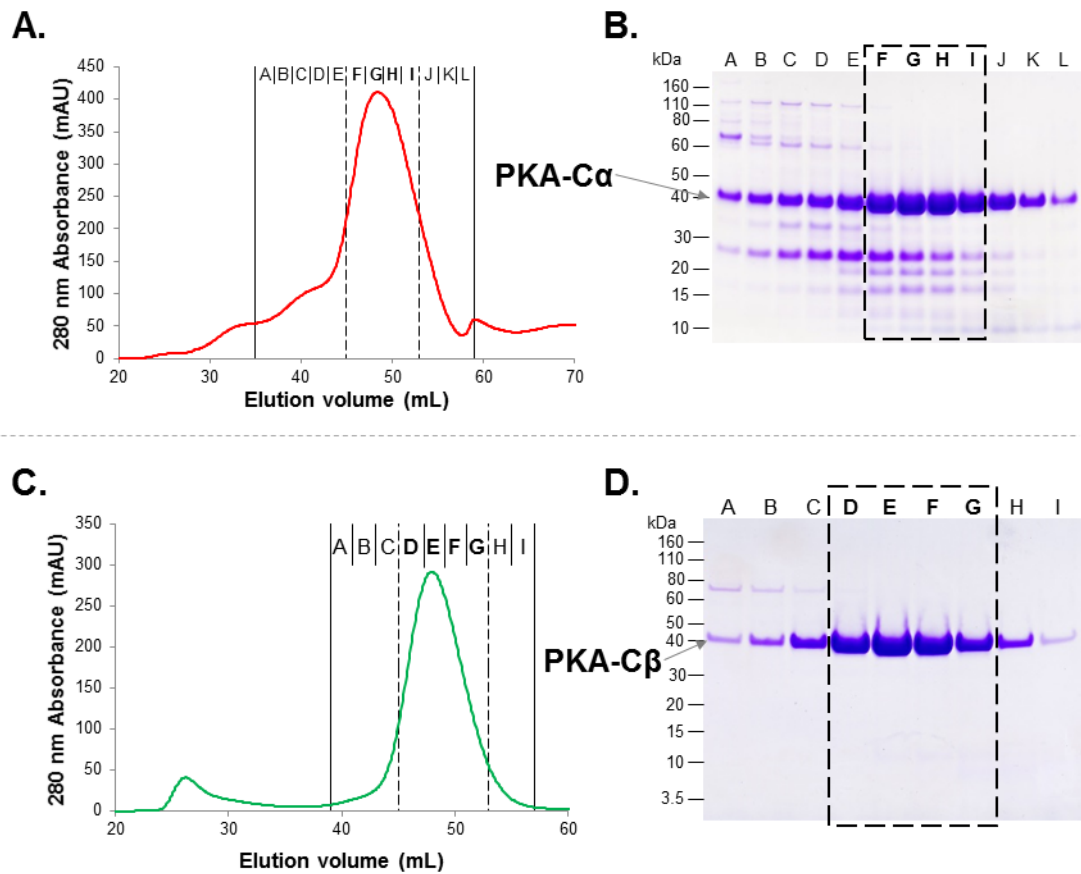


Figure 2.1 PKA C subunit purification. **A.** An 8 histidine tagged PKA C α subunit construct was expressed in *E. coli*, and enriched by Ni-NTA agarose association. The protein was purified by size exclusion chromatography using an 80 mL Superdex 70 column, and eluent was collected in 2 mL fractions. **B.** The purity of the size exclusion fractions was assessed by SDS-PAGE. The presence of a band at approximately 40 kDa indicates the purification of PKA C α . Fractions F, G, H, and I were combined for further experiments. **C.** GST tagged PKA C β subunit construct was expressed in *E. coli* and enriched by association with glutathione sepharose. The protein was purified by size exclusion chromatography as described above. **D.** The presence of a band at approximately 40 kDa indicates the successful purification of the subunit.

PKA R1 α and R1 β were both purified using glutathione sepharose affinity (**Figure 2.2**). Both were used as protein standards in quantitative immunoblotting, and R1 β was further used for XL-MS. The A₂₈₀ of both subunits showed single peaks. The signal in the void volume of the purified R1 β subunit was much larger than any other subunits (**Figure 2.2C**), however the Coomassie staining did not uncover a significant degree of contamination (**Figure 2.2D**). The R1 α subunit had a much smaller void (**Figure 2.2A**), and also exhibited high purity (**Figure 2.2**

B)

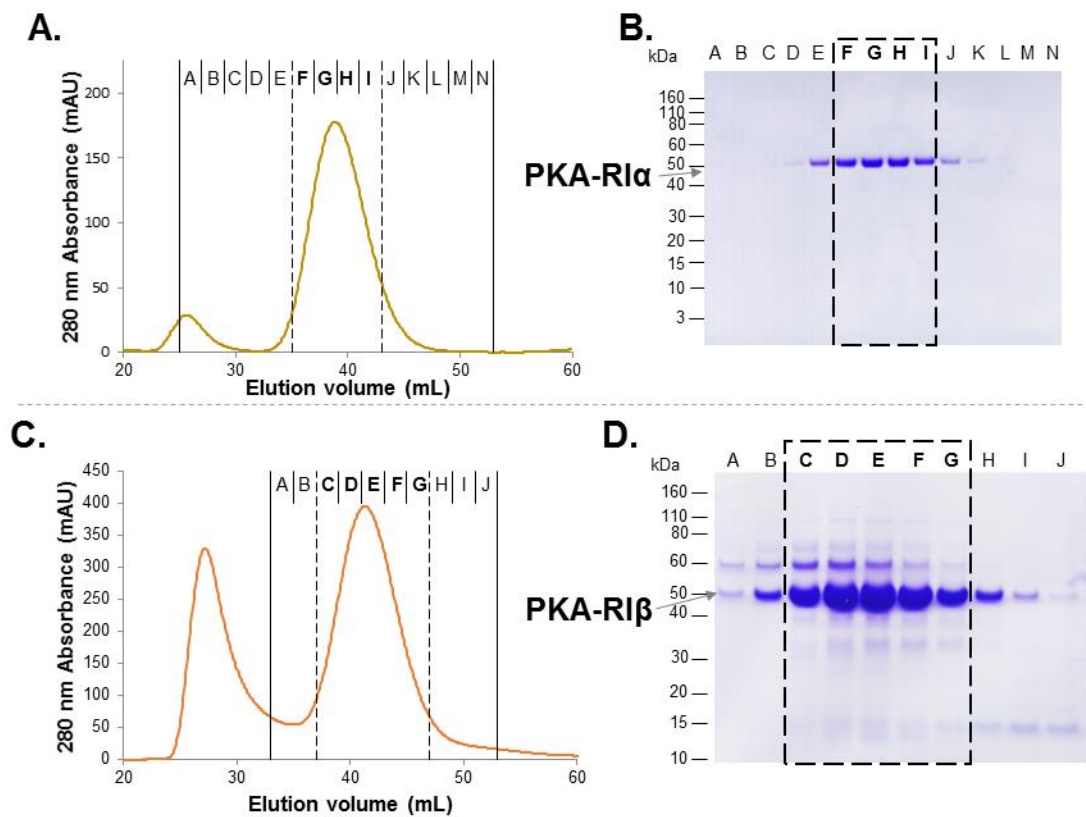


Figure 2.2 PKA RI subunit purification. GST tagged PKA RI α (**A, B**) and RI β (**C, D**) subunit constructs was expressed in *E. coli* and enriched by association with glutathione sepharose. The protein was purified by size exclusion chromatography using an 80 mL Superdex 70 column, and eluent was collected in 2 mL fractions. The elution of proteins from the column was measured by A280 using an in-line UV sensor (**A, C**). The purity of the size exclusion fractions was assessed by SDS-PAGE, which were relatively free of contaminants. (**B, D**). **B.** The presence of a band at approximately 43 kDa indicates the purification of PKA RI α . Fractions F, G, H, and I were combined for further experiments. **D.** The presence of a band at approximately 40 kDa indicates the successful purification of PKA RI β . Fractions C, D, E, F, and G were combined for further experiments.

RII subunits were purified for use as protein standards in quantitative immunoblotting experiments, and RII β and AKAP18 α were used for XL-MS, and all were purified by affinity to glutathione sepharose (**Figure 2.3**). RII α and RII β constructs showed somewhat broader peaks than the other constructs in the A₂₈₀ trace (**Figure 2.3 A & C**), however there was little contamination present in the Coomassie stained gels (**Figure 2.3 B & D**).

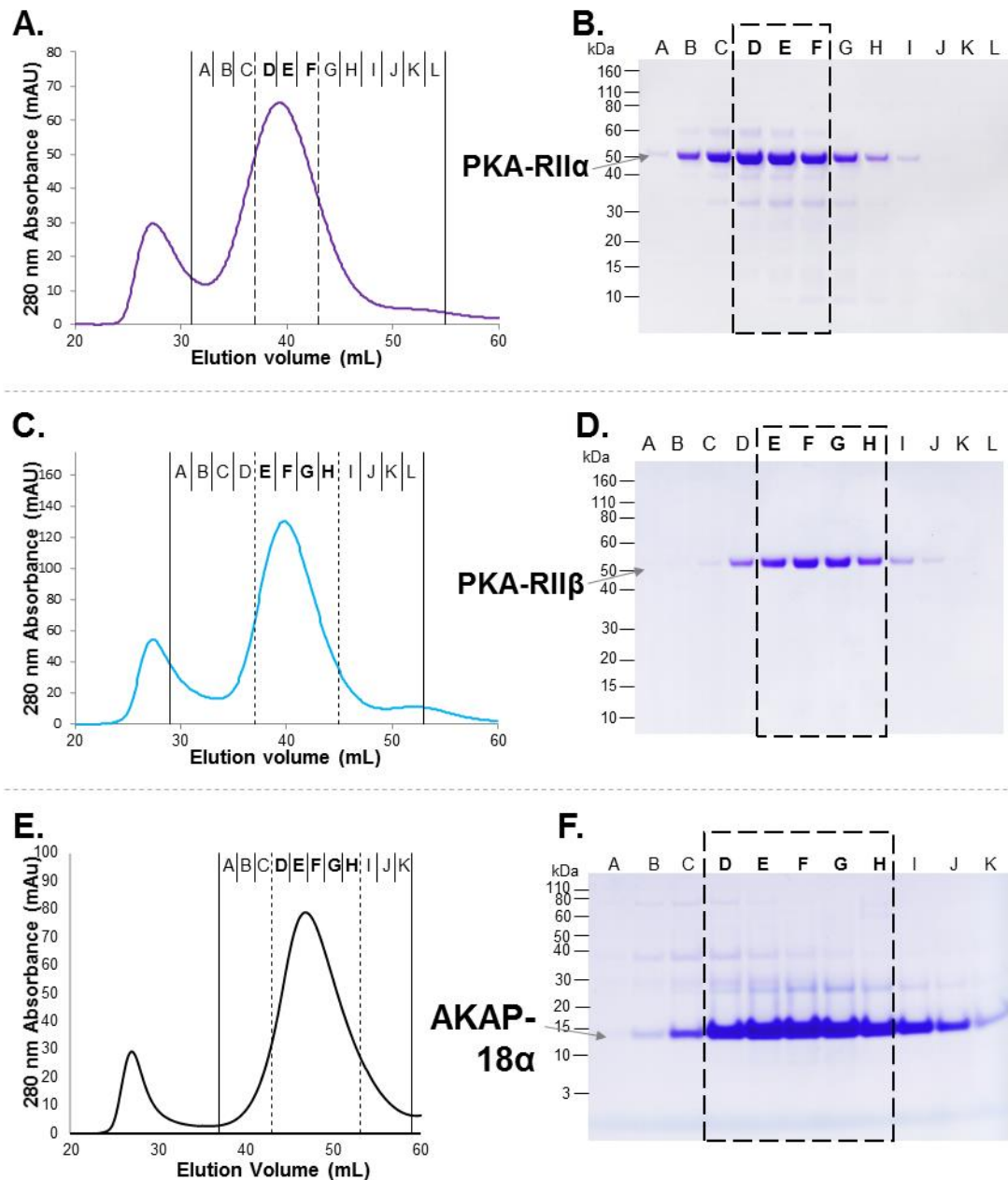


Figure 2.3 PKA RII subunit and AKAP18 α purification. GST tagged PKA RII α (A, B), RII β (C, D) subunit constructs as well as AKAP18 α were expressed in *E. coli* and enriched by association with glutathione sepharose. The protein was purified by size exclusion chromatography using an 80 mL Superdex 70 column, and eluent was collected in 2 mL fractions. The elution of proteins from the column was measured by A280 using an in-line UV sensor (A, C, E). The purity of the size exclusion fractions was assessed by SDS-PAGE, which showed relatively little contaminant staining (B, D, F). **B.** The presence of a band at approximately 46 kDa indicates the purification of PKA RII α . Fractions D, E, and F were combined for further experiments. **D.** The presence of a band at approximately 46 kDa indicates the successful purification of PKA RII β . Fractions E, F, G, and H were combined and used for experiments. **F.** The presence of a band at approximately 15 kDa indicates the successful purification of AKAP18 α . Fractions D, E, F, G and H were combined for further use.

The baits used in the R subunit specific pull downs were also purified by glutathione sepharose affinity, however the GST tag was not removed in this case (**Figure 2.4**). Instead, the purified GST-fusion proteins were eluted by competition using 15 mM L-glutathione. The very small size of the GST-RIAD peptide allowed very high expression as measured by A₂₈₀ (**Figure 2.4A**), and very high purity (**Figure 2.4B**). GST-AKAP79 c93 also showed high expression (**Figure 2.4C**), however there was slightly more contamination was apparent upon Coomassie staining (**Figure 2.4D**).

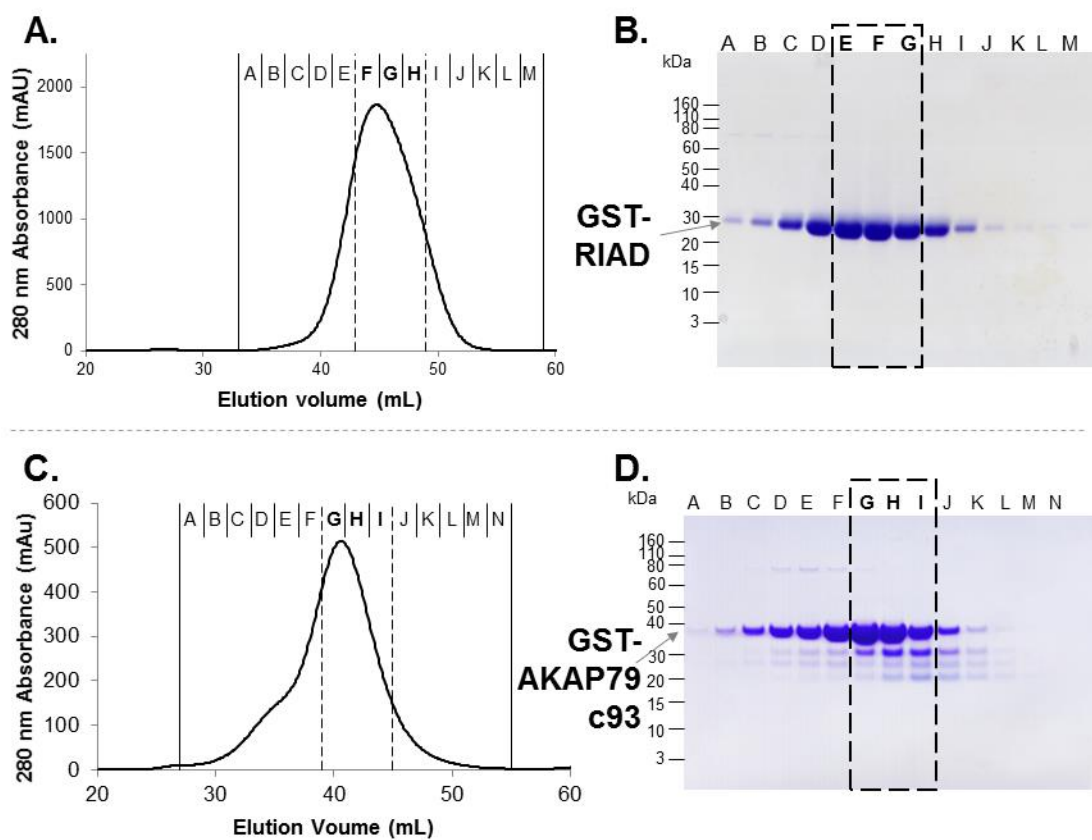


Figure 2.4 Purifications of baits for isoform-specific R subunit pull down. GST tagged RIAD (**A, B**) and AKAP79 c93 were expressed in *E. coli* and enriched by association with glutathione sepharose. The protein was purified by size exclusion chromatography using an 80 mL Superdex 70 column, and eluent was collected in 2 mL fractions. The elution of proteins from the column was measured by A₂₈₀ using an in-line UV sensor (**A, C**). The purity of the size exclusion fractions was assessed by SDS-PAGE., which showed relatively little contaminant staining (**B, D**). **B.** The presence of a band at approximately 30 kDa indicates the purification of GST-tagged RIAD. Fractions E, F and G were combined for further experiments. **D.** The presence of a band at approximately 37 kDa indicates the successful purification of GST-tagged AKAP79 c93. Fractions G H, and were combined for further use.

2.1.6 Determination of protein concentration by bicinchoninic acid (BCA) Assay

Protein concentrations were principally determined using the colorimetric BCA assay for protein quantification (Novagen). This approach was taken to establish reference protein standard concentrations in quantitative immunoblotting experiments. Protein solutions containing bovine serum albumin (BSA) were made by serial dilution at concentrations of 0 mg/mL, 62.5 mg/mL, 125 mg/mL, 250 mg/mL, 500 mg/mL, and 1000 mg/mL. 25 μ L of the solutions, either protein standard or test conditions, were first added to 96 well plates, before 200 μ L of the 1:200 mixture of cupric sulfate to bicinchoninic acid was added. Two sets of standards were used, one prepared immediately before the addition of the experimental conditions, and one immediately after. The results of these two curves were averaged. BCA reaction containing plates were covered in PVC film and incubated at 37°C for 30 minutes. Results were then read at 570 nm on an ELx800 microplate reader (BioTek Instruments). Results of the protein standards were then used to generate a standard curve. Only experimental values that fell on between the uppermost and lowermost values of the curve were used, in cases in which the experimental concentration was above this value, further dilutions were made and the assay was run again. If the experimental concentration was below the lowest value, additional material was added in further assays.

2.1.7 Determination of protein concentration by absorbance at 280 nm (A280)

The amino acids tyrosine and tryptophan, and to some extent cysteine absorb light with at 280 nm. This absorption is proportional to the concentration of these residues in a solution, and can be estimated for a given protein using the formula:

$$\epsilon = (nW \times 5500) + (nY \times 1490) + (nC \times 125)$$

in which ϵ is the calculated molar extinction coefficient for a protein (Thermo Scientific, 2013). I used the ExpASy protparam tool to calculate the extinction coefficient (Gasteiger

et al., 2005). The concentration of protein in a solution can then be calculated using this measure in the formula:

$$c = A_{\lambda} \epsilon L$$

In which A_{λ} is the absorbance at 280 nm, and L is the path length of the measurement (Ahmed, 2005). The measurement and subsequent calculation was performed by a NanoDrop 2000c (Thermo Scientific) spectrophotometer. A280 values were used as a belt-and-braces measure to confirm the accuracy of protein concentrations obtained by the BCA method.

2.2 Techniques in support of PKA subunit stoichiometry determination

2.2.1 Dissection

Male, four-week-old, Sprague-Dawley rats were euthanized by cervical dislocation carried out in the UCL Biological Services Unit. Immediately following which, the animals were placed on ice. Cortex, cerebellum, heart, tibialis anterior muscle, lung, liver, and kidney were excised, washed in cold PBS, and transferred to pre-weighed 50 mL conical centrifugation tubes containing 10 mL of PBS. Brain tissue was removed by first cutting the skin of the neck with surgical scissors, after which the skin was cut at the midline of the head from the neck to the nose, and peeled back to reveal the skull. The skull was cut with small scissors, with a single incision stretching from the base of the skull to the nasal bone. The skull flaps resulting from this incision were prized up and broken away from the skull. Using curved forceps the brain was then removed from the open skull. Once out of the skull, the brain was washed several times in ice cold PBS to lessen blood carry over. The cerebellum and cortex were then cut away and further processed separately from each other.

The internal organs were removed through a ventral incision in the skin, continuing through the rib cage. The heart was removed first, followed by the lungs, liver, and finally kidneys. Care was taken to remove the entire organ, while removing as much of the membranes and connective tissues as possible. All organs were washed several times in PBS. The tibialis anterior muscle was removed through an incision in the skin of the leg made with a razor blade. The muscle was cut free at either end of the tibia, and as much of the muscle as possible was removed while avoiding tendons. All tissue was removed from the animal and processed within 30 minutes. Following dissection PBS was aspirated from the organs, which were transferred to dry 10 cm tissue culture dishes for weighing.

2.2.2 Protein extraction from tissue samples

PBS was aspirated from the organs, and they were weighed, and resuspended in 10 mg/ml of modified radioimmunoprecipitation (RIPA) Buffer (30 mM HEPES pH 7.5, 150 mM NaCl, 0.5 mM EDTA, 1 mM benzamide, 1% Igepal CA-630 w/v, and 0.25% sodium deoxycholate w/v). The organs were transferred to 10 cm plates on ice and roughly chopped with a straight disposable razor blade. The chopped organ suspension was then transferred into a 50 mL conical centrifuge tube using a disposable Pasteur pipette. Rough suspensions were then processed at 9,500 rpm with a Di 25 Basic rotor/stator homogenizer (Yellowline) for 2 x 30 second increments, between which they were returned to ice to prevent over heating the samples. A 1 mL portion of the resulting homogenate was taken and transferred into a 1.5 mL microcentrifuge tube. This homogenate was then sonicated for 30 seconds at 20 KHz and was then spun at 21, 130 x *g* for 1 hour at 4 °C. The resulting supernatant was removed from the pellet and transferred to a clean 1.5 mL microcentrifuge tube, before it was flash frozen in liquid nitrogen for storage. A 100 µL sample of all homogenates was saved for protein concentration analysis by BCA assay (**Table 3.4**)

2.2.3 Synaptosome-rich fraction preparation

For synaptosome enrichment, I adapted a protocol for the purification of synaptosomes published by Dunkley, Jarvie and Robinson (2008). Four-week-old male Sprague-Dawley rats were killed by cervical dislocation. Rats were immediately placed on ice until dissection could take place. Brains were excised in whole from the skull and rinsed several times in ice cold sucrose EDTA buffer (0.32 M sucrose, 1 mM EDTA, 5 mM HEPES pH 7.4) to lessen blood contamination. The cortex was then separated from the rest of the brain, and placed in a pre-weighed 50 mL conical centrifuge tube with approximately 20 mL of sucrose EDTA buffer. The mass of the tube containing the buffer and brain region was then weighed to determine the mass of the cortex. Following this, a 10 cm tissue culture dish was prepared on ice with 3.5 mL of sucrose EDTA buffer. The cortex was removed from the centrifuge tube using forceps and transferred into the dish, and it was rapidly chopped using a straight razor blade. The coarsely chopped tissue and buffer was then drawn up using a disposable Pasteur pipette and placed in a 7 mL Dounce homogenizer (Wheaton) on ice. The tissue was ground with 5 strokes of the tight insert, followed by 5 strokes of the loose insert. A sample of 100 μ L of the homogenate was kept for BCA assay. The remaining homogenate was transferred into a 15 mL conical centrifuge tube, and spun at 1,000 $\times g$ at the average radius of the tube for 10 minutes at 4°C. Following centrifugation, 3 mL of the supernatant, termed here the synaptosome-rich fraction, was removed while being careful not to disturb the loose pellet, which was subsequently discarded.

The shearing action of the Dounce homogenizer causes the synapses to be gently torn away from the cell body, but allows the membrane to re-close around the synapse, creating a membrane bound structure known as a synaptosome. However, in an effort to reduce processing time and increase total yield, I did not purify the synaptosomes to completion.

Our procedure stopped at the first supernatant fraction 'S1', termed here the synaptosome-rich fraction, so called as this preparation does not isolate synaptosomes, rather it removes the bulk of nuclei and cellular debris resulting from the lysis of the cortical tissue (Dunkley, Jarvie and Robinson, 2008). The preparation of the synaptosome rich fraction did not include any detergent, rather solubilization occurred as the result of LDS application during denaturing for electrophoresis.

The protein content of the synaptosome-rich fraction was assessed by BCA assay, and the average concentration was found to be $8.83 \text{ mg/ml} \pm 0.478$ with an average percent recovery of $2.85\% \pm 0.193$ of the original mass of the organ ($n=4$, **Table 2.2**). Though the homogenate protein concentrations are very similar between the synaptosome-rich fraction and the cortex, the procedure for preparation differed, as 3.5 mL of buffer per cortex were used to prepare the synaptosome rich fraction, while 10 mL of buffer per gram of cortex was used to prepare cortical lysate. This means that the per starting mass yield of the cortical lysate was two to three times higher than that of the synaptosome rich fraction ranging from 7.8% to 10.4% of the total organ mass. It is important to note that these percent recovery figures are presented as a comparison between the two tissue preparation methods, and are measures of the concentration of only the protein yield following homogenization as compared to the total wet weight of the tissue, a measure which includes all of non-protein components as well. These numbers are consistent with enrichment of synaptosomes from cortex using the Dounce homogenisation method.

Cortex weight (mg)	Syn. Rich Fraction Concentration (mg/ml)	Recovery (mg)	Recovery (%)
1060	9.85	34.5	3.25
1080	9.26	32.4	3.00
1140	7.62	26.7	2.34
1070	8.59	30.1	2.81
1088 ± 18.0	8.83 ± 0.479	30.9 ± 1.68	2.85 ± 0.194

Table 2.2 Synaptosome rich fraction recovery. The cortex was removed from four animals, following which it was subjected to homogenization by gentle mechanical shearing in order to create membrane encapsulated synapses, which were then crudely purified by centrifugation in isotonic buffer. Average recovery of the synaptosomes from cortical tissue was 2.85% ± 0.193 (n=4).

2.2.4 HEK293T cell counting

HEK293T cells were grown on 75 cm² as described in **section 2.3.1**. After DMEM aspiration, cells were resuspended in 10 mL PBS and transferred to 15 mL conical centrifuge tubes. Cells were subsequently spun at 1, 200 x g at 22°C. The cells were washed and resuspended in 10 mL of PBS for cell counting. Approximately 100 µL of suspension was applied to the edge of the cover slip on an Improved Neubauer pattern haemocytometer, which was then placed on an inverted microscope for counting using a 10X magnification objective. This count was extrapolated to give the number of cells in the total of suspension. The cells were then lysed in approximately 700 µL of lysis buffer (30 mM HEPES pH 7.5, 150 mM NaCl, 1 mM DTT, 0.5 mM EDTA, 1 mM benzamidine, 1% Igepal CA-630 w/v, and 0.25% sodium deoxycholate w/v), sonicated for 30 seconds at 20 MHz, and the lysate was centrifuged for 1 hour at 21, 130 x g at 4°C. Following centrifugation, the supernatant was collected, and the volume noted down. Using the volume of lysate and the number of cells in each starting pellet, the number of lysed cells contained in a single microliter of cell suspension was calculated.

The main drawback of haemocytometer count is related to the subjectivity of the counts. I attempted to lessen this concern by only counting those cells that were within the quadrant, or that were touching the rightmost or bottom line. Those touching the leftmost or top line

in any part were excluded from the count. Systems exist which use either electrical resistance or flow cytometry to count all or a more significant portion of the cells within a culture while allowing the cells to remain viable. Though the sophisticated equipment required for these methods was not available to us at this time, these more accurate cell counting approaches may be able to be employed in the future. The final measurement of cell numbers were expressed in terms cells/ μL lysate, as calculated by dividing the total number of cells from the culture by the final lysis volume. As unknown volumes can be difficult to measure with a micropipetter without introducing inaccuracy, the volume was determined by weighing the final lysate, and using the measured density of the lysis buffer to determine the final volume. This method also kept variation very low in the final cells/ μL lysate calculation, with only 1.78% standard error.

2.2.5 Antibody calibration in ImageJ

In order to accurately determine the quantity of different PKA subunits in protein extracts, I applied quantitative immunoblotting. The goal of this approach was to establish the relationship between signal and protein quantity for each anti-PKA subunit antibody using its purified cognate protein. This could then serve as a reference curve to determine the amount of protein in different protein extracts. Densitometry was applied in order to numerically quantify the signal from our western blots using the built-in gel analysis tools in ImageJ (Schneider, Rasband, & Eliceiri, 2012). Quantification was performed using .gel format image files output by an ImageQuant (GE Healthcare Life Sciences) that utilizes a highly sensitive charge-coupled device detector. A worked example for determining the relationship of pixel density to protein concentration for purified RII α , using PKA RII α antibody is shown in **figure 2.5**. First, each lane is designated by demarcation with a rectangular selection box (**Figure 2.5A**, yellow boxes) taking care to include the entirety of

the band in the box, as well as a portion of the rest of the lane sufficient to establish a baseline pixel density in order to carry background corrections. The size of this selection area is maintained throughout the analysis to allow direct comparison between the measurements. Following demarcation of all of the lanes to be quantified, each lane were plotted as a function of density of pixels in comparison to distance along the lane by the built-in ImageJ utility (**Figure 2.5A**). The form of the curve enables assignment of appropriate upper and lower boundaries in 'y' (**Figure 2.5B**). For example, in the example shown in **figure 2.5B**, the background is denoted by red stars and the baseline is in blue. This approach also allows for unwanted off target signal to be excluded, the trace of which is represented here by red hashed lines.

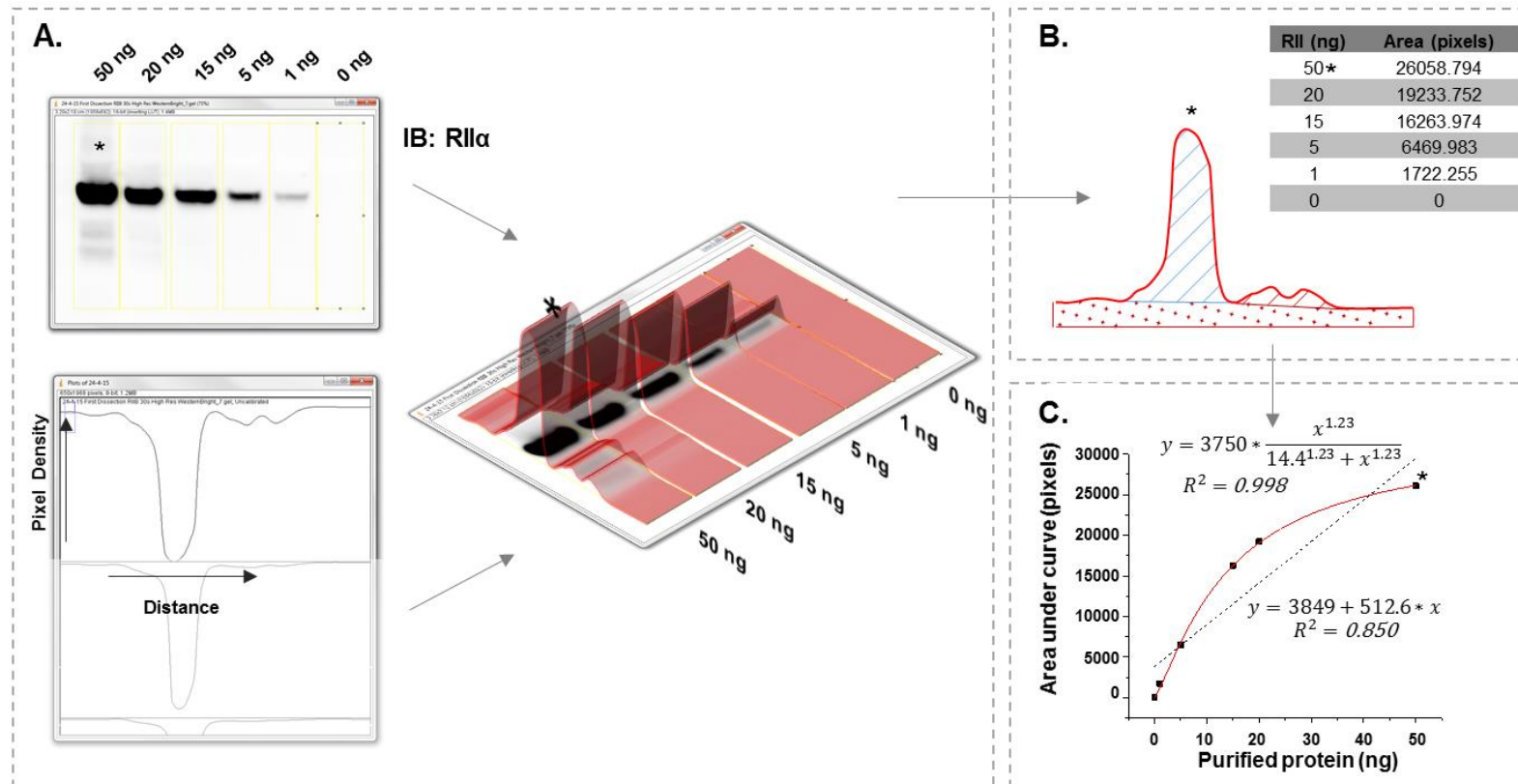


Figure 2.5 Immunoblot quantitation workflow. Worked example of ImageJ quantification for RII α . In this example, the protein sample of highest concentration (50 ng) bears an asterisk so that it can more easily be traced throughout the process. **A.** First, a rectangular quantification area is selected to include both the band of interest and background regions of each lane. Equal sized boxes are then used to quantify all lanes. **B.** Pixel density is plotted against distance to create a curve indicating the position and intensity of the protein band. The area under the curve is then quantified using the selection tool in ImageJ. A baseline (blue) is included to remove background intensity (red stars). In addition, protein bands of lower or higher mass (red hashed lines) are excluded. **C.** Plot of pixel density against protein concentration. Curve fitting against a series of protein concentration standards enables the relationship between pixel density and protein concentration to be accurately determined using a Hill function in the curve-fitting program ORIGIN. For comparison, a linear fit is also illustrated demonstrating that fitting with a Hill function ($R^2 = 0.998$) is much superior to the best linear fit ($R^2=0.850$).

This method of quantification has distinct advantages over the often used “block” method of quantification, in which a box is placed over the band of interest, and the mean gray pixel density of the entire area measured, before the same box is moved to another portion of the membrane to take a background measurement. In the block method, the location of the background box placement can introduce a great deal of variability to the measurement, especially if there is no clear area of membrane immediately adjacent to the band of interest. Additionally, if there are off target bands present, as is the case in our 50 ng lane, they can be difficult to exclude while maintaining a consistent box size and sampling the entire band of interest.

Following determination of the pixel density for each band, these numbers are plotted against protein concentration to enable determination of the relationships between the two. I found that the most accurate fits were obtained using the following Hill function equation:

$$x = \left(\frac{\frac{y}{V_{max}} * k^n}{1 - \frac{y}{V_{max}}} \right)^{-n}$$

where y = pixel density, x = protein quantity

The variables V_{max} , k , and n were fitted by iterative rounds of least-squares refinement using ORIGIN. Origin software uses the Levenberg-Marquardt algorithm of least squares fitting to produce the output that minimizes the difference between the theoretical curve and the experimental data. The accuracy of the fit to the experimental data is provided as a chi-square measurement. In the worked example in **figure 3.4** across even a small range of protein concentrations, linear fitting yields a high error (dashed line, $R^2 = 0.850$). In comparison, fitting to the Hill function which takes into account cooperative antibody

binding and signal saturation, the fit is much improved (red line, $R^2 = 0.999$). The copy number of proteins per μg wet volume was determined using the molecular weights listed in **table 2.3** for rat tissues, and those listed in **table 2.4** for HEK293T cells.

Species	Subunit	Isoform	Accession Number	Molecular Weight (amu)	Single Copy Mass (ng)
Rat	PKA-C	C α	NP_001094392.1	40605.6	6.74E-11
		C β	NP_001071113.1	40707.8	6.76E-11
Rat	PKA-RI	RI α	NP_037313.1	43094.9	7.16E-11
		RI β	NP_001028851.2	40238.5	6.68E-11
Rat	PKA-RII	RII α	NP_062137.1	45540.2	7.56E-11
		RII β	NP_001025191.1	46122.9	7.66E-11

Table 2.3 Rat PKA subunit characteristics. For the quantification of proteins in rat tissue lysates, reported PKA subunit molecular weights were used as follows. Accession number identify the specific proteins in the NCBI database.

Species	Subunit	Isoform	Accession Number	Molecular Weight (amu)	Single Copy Mass (ng)
Human	PKA-C	C α	NP_002721.1	40589.6	6.74E-11
		C β	NP_891993.1	46235.9	7.68E-11
Human	PKA-RI	RI α	NP_001265362.1	43393.1	7.21E-11
		RI β	NP_001158233.1	43072.9	7.15E-11
Human	PKA-RII	RII α	NP_004148.1	45518.4	7.56E-11
		RII β	NP_002727.2	46302	7.69E-11

Table 2.4 Human PKA subunit characteristics. For the quantification of proteins in HEK293T cell lysates, reported PKA subunit molecular weights were used as follows. Accession number identify the specific proteins in the NCBI database.

2.3 Mammalian cell-based methods

2.3.1 HEK293T cell culture

All experiments using cell lines were carried out with HEK293T cells grown in Dulbecco's modified eagle media (DMEM) (Gibco™) supplemented with 100 units/ml penicillin, 100 $\mu\text{g}/\text{ml}$ streptomycin, 10% fetal bovine serum, and 2 mM glutaMAX (Gibco), at 37°C in 5% CO_2 . For routine passaging, cells were grown in 75 cm^2 culture area Nunc™ Cell Culture Treated EasyFlasks (Thermo Scientific), and split at a ratio of 1:6 from 80% confluence. These cells

were further prepared for stoichiometry, FRET population assays, or NHS-diazirine crosslinking as described below.

2.3.2 Properties of NHS-diazirine

The heterobifunctional crosslinker NHS-diazirine terminates at one end in N-hydroxysuccinimide. Upon exposure to a primary amine, the NHS moiety is displaced, forming an amide bond (**Figure 2.6**). This reaction is spontaneous and occurs as soon as the molecules come in contact. One of the key factors to the development of the method was the ability of the crosslinker to cross membranes. This meant that the experiments could be carried out in whole cells, preserving the endogenous structure and chemical interactions which I was trying to capture. NHS-diazirine solutions are made immediately before use, as the half-life of the NHS moiety is on the scale of minutes to hours, due to spontaneous hydrolysis in solution (Hermanson, 2013).

The second functional portion of the NHS-diazirine molecule, the diazirine ring, forms covalent bonds on exposure to UV radiation. Upon irradiation at ~350 nm, molecular nitrogen is dissociated, leaving a reactive carbene (Preston & Wilson, 2013). The carbene then forms a covalent bond with the nearest molecule, usually by insertion into C-H or N-H bonds (Kresge, Simoni, & Hill, 2005b; Wong & Jameson, 2012). The use of reagents activated outside of the visible spectrum helps to limit off target activation by ambient lighting. It is also important that the activation wavelength of the diazirine group is above 300 nm, in order to minimize absorption that can cause protein degradation (Blencol & Hayes, 2005; Brunner, Senn, & Richards, 1980).

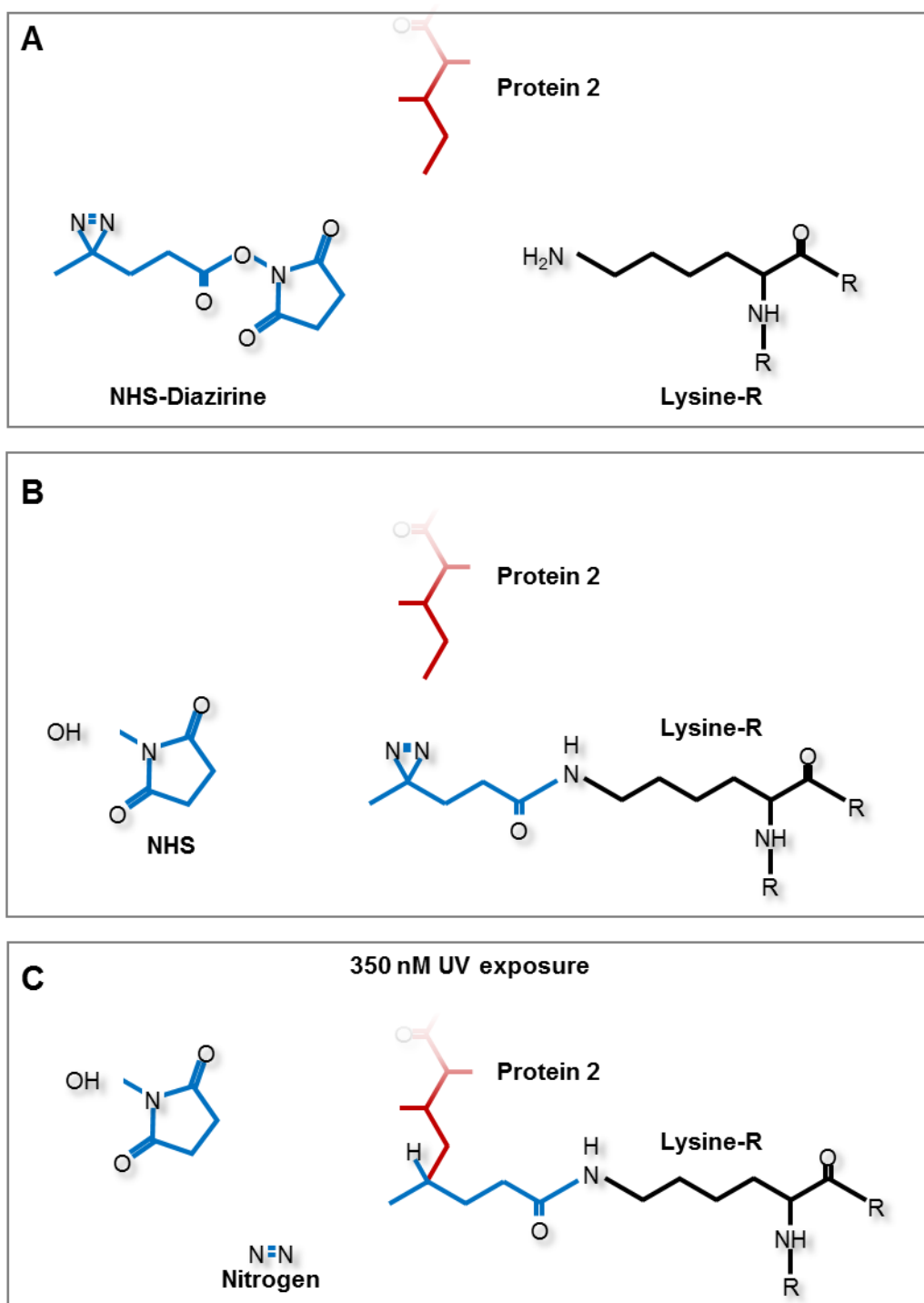


Figure 2.6 NHS-Diazirine crosslinking. **A.** An amide bond is formed by displacement of the NHS moiety upon exposure to a primary amine. **B.** Once the amide bond is formed, the NHS-diazirine is primed for binding to a second protein. **C.** Upon 350 nm UV radiation the nitrogen dissociates from the NHS ring, leaving a reactive carbene, which in turn forms covalent bonds with the nearest molecule, usually by insertion between C-H or N-H bonds.

2.3.3 NHS-diazirine crosslinking with HEK293T cells

Human embryonic HEK293T cells were grown as previously described to approximately 80% confluence. Cells from 175 cm² or 350 cm² of total cell culture area were resuspended in Gibco™ Dulbecco's Modified Eagle Medium (DMEM) (Thermo Scientific), transferred to a 50 mL conical centrifuge tube, and pelleted centrifuged for four minutes. All cell centrifugation steps were performed at 1, 200 x *g* at 22°C. The supernatant was aspirated from the pellet, which was washed by resuspension in 10 mL of phosphate buffered saline (PBS) (Sigma), and transferred to a 15 mL conical centrifuge tube. A second wash was performed immediately following this step. The resulting pellet was then resuspended in 10 mL of 1 mM succinimidyl 4,4'-azipentanoate NHS-Diazirine (Thermo Scientific) in PBS with 10% dimethyl sulfoxide (DMSO) (Sigma Aldrich). The cell suspension was incubated at room temperature in the presence of 1 mM NHS-Diazirine on a roller mixer for 30 minutes before 1 M tris(hydroxymethyl)aminomethane (Tris) pH 7.4 was added to quench the remaining reactive NHS moieties. The cells were pelleted and the NHS-Diazirine solution was removed, before they were again washed with 10 mL PBS. In experiments in which hormones were applied to the cells, it was at this stage that the cells were resuspended in experimental solutions, before a further incubation at room temperature on the rolling mixer. Following incubation, cells were transferred to a 60 cm² tissue culture dish (Sigma), which was kept on ice. The lid was removed from the plate along with the ice it was immediately placed under a 100 watt 365 nm UV light source (UVP) at a distance of approximately 10 mm from the lens of the lamp to the surface of the plate. Illumination lasted typically for 5 minutes, after which the cells were again transferred into a 15 mL conical centrifuge tube and pelleted as before. The supernatant was removed and the cells were washed in 10 mL PBS. The PBS was aspirated from the pellet, which was then lysed in 1 mL 1% Igepal CA-630 CA-630 (Sigma) w/v, 20 mM HEPES pH 7.5, 200 mM NaCl, 2 mM DTT, 1 mM EDTA and 0.05% TWEEN 20 (Sigma) w/v, and in some cases 0.25% sodium deoxycholate, and transferred to a 1.5 mL microcentrifuge tube.

The cells were incubated in lysis buffer at 4°C on a rotating mixer for 20 minutes to 1 hour before they were sonicated and cellular debris was pelleted at 21,100 $\times g$ at 4°C for 1 hour. The supernatant was removed from the pellet and transferred to a new 1.5 mL microcentrifuge tube.

3.3.4 R subunit selective precipitation

In preparation for pull downs, 30 μg of purified GST-fusion protein, either GST-RIAD or GST-AKAP79 c93, were preloaded onto 30 μL of Fast-Flow Glutathione Sepharose 4B (GE Healthcare Life Sciences) in a total volume of 500 μL of 20 mM HEPES pH 7.5, 200 mM NaCl, 2 mM DTT, 1 mM EDTA and 0.05% TWEEN 20 (Sigma) w/v by incubation on a rotating mixer for 2 hours. Following this binding period, the unbound protein was removed by a series of four washes in 20 mM HEPES pH 7.5, 200 mM NaCl, 2 mM DTT, 1 mM EDTA and 0.05% TWEEN 20 (Sigma) w/v. The loaded beads were then transferred to a 15 mL conical centrifuge tube, and the total volume was brought up to 4.5 mL with wash buffer, in order to dilute the sodium deoxycholate from the wash buffer during the pull down step.

Supernatant from the crosslinked HEK293T cells was then added to the mixture, which was subsequently incubated overnight on a rolling mixer at 4°C. The beads were then spun down at 1200 $\times g$ for 3 minutes before the supernatant was removed. The beads were then resuspended in 1 mL of 20 mM HEPES pH 7.5, 200 mM NaCl, 2 mM DTT, 1 mM EDTA and 0.05% TWEEN 20 (Sigma) w/v with 100 μM -1mM cAMP to remove non-covalently bound C subunit, and transferred to a 1.5 mL microcentrifuge tube. Beads were washed four additional times in this buffer, following which the buffer was removed, and the glutathione sepharose was treated with 1X NuPage LDS Sample Buffer (Thermo) and heated to 85°C for 10 minutes to release the protein. Variations on this basic procedure were incorporated into some experiments, as specified in **chapter 4**.

2.4 Crosslinking coupled to mass Spectrometry (XL-MS)

XL-MS is a structural method that uses chemical crosslinking of protein residues and subsequent digestion and identification of peptide sequences by tandem MS to determine the spatial orientation of protein regions in relation to each other, both within a single protein or subunit (intra-link) and between different proteins or subunits (inter-links). The key strengths of XL-MS are that it allows protein interactions to be examined in their native conformations, and it enables structural analysis of disordered regions. The generalized workflow of XL-MS consists of purification of the protein sample of interest, followed by chemical crosslinking, enzymatic digestion into peptides, and finally identification of crosslinked peptides by tandem MS (**Figure 2.7**).

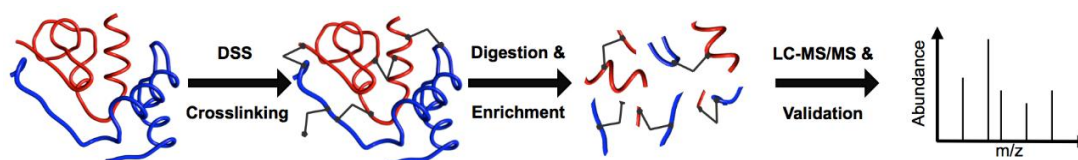


Figure 2.7 Generalized overview of XL-MS. Proteins are crosslinked by DSS in order to lock in their conformation. Following this, the protein mixture is enzymatically digested to create peptides, which are subsequently analysed by liquid chromatography and tandem mass spectrometry.

I utilized the chemical crosslinker disuccinimidyl suberate (DSS), which consists of a homobifunctional arrangement of two N-hydrozysuccinimide (NHS) esters on either side of an eight-carbon spacer arm, is used to form spontaneous crosslinks. The NHS esters can react with free amines on lysine side-chains and the protein N-terminus to form covalent amide bonds. The greatest possible distance between the $C\alpha$ atoms of two DSS-linkable residues is $\sim 35 \text{ \AA}$, factoring in the 24 \AA combined length of the crosslinker, the reach of lysine side chains, and the inherent flexibility of protein in solution (Leitner et al., 2014). The NHS-moiety of DSS hydrolyses quickly in aqueous solutions, so solutions must be made shortly before use to prevent loss of activity (Leitner et al., 2010).

Purification, mixing, and crosslinking of the proteins were handled in our lab, as was crosslink mapping and analysis. Digestion, enrichment, LC-MS/MS and initial processing by xQuest/xProphet/xTract was carried out by our collaborator, Florian Stengel at the University of Konstanz. Analysis of data output by xQuest/xProphet/xTract was performed collaboratively.

2.4.1 XL-MS Sample preparation

To assist identification of crosslinked peptides by tandem MS/MS, I applied an isotopically-labelled form of DSS, in which the 12 hydrogen atoms of the linker arm are replaced with deuterium, resulting in a 12.075 Da mass shift. Crosslinking was performed with a 1:1 mix of DSS-H₁₂ and DSS-D₁₂. The different masses of the heavy and light crosslinkers appear as a mass shifted doublet on the spectrum which assists in their assignment (Leitner et al., 2014; Seebacher et al., 2006).

In general crosslinking reactions were performed using 100 µg protein in 100 µL total volume. Mixtures were incubated at 30°C for 10 minutes with mixing at 500 rpm prior to the initiation of the crosslinking reaction by the addition of 0.5 mM DSS (1:1 molar ratio of DSS_{H12}:DSS_{D12} purchased from Creative Molecules). The crosslinking reaction was allowed to progress for 30 minutes at 30°C with shaking at 500 rpm, and was then quenched by the addition of 50 mM ammonium bicarbonate. The reaction mixtures were then snap frozen and sent to Florian Stengel for qXL-MS analysis.

Prior to analysis on the spectrometer, crosslinked samples were treated with a urea/tris(2-carboxyethyl)phosphine (TCEP) solution to reduce disulphide bonds, then free cysteines were alkylated with iodoacetimide. Protein was subsequently digested with trypsin, which

cuts at the C-terminus of arginine or lysine residues, excluding those that have been crosslinked (Leitner et al., 2014). This trypsinized peptide mixture was then treated with formic acid to inhibit trypsin activity. The digested peptides are separated from the solution and retained by a solid phase extraction system. The eluted peptides were separated by size exclusion chromatography and collected in 50-100 μ L fractions, which were individually processed on the spectrometer.

2.4.2 Crosslinked peptide separation & identification by MS

Peptides samples were sequenced using tandem MS. First, charge was imparted on the digested peptides by electrospray ionization (ESI). This process is essential to the identification of peptides by MS, as it is what is called “soft ionization”, which means that there is little transfer of excess energy to the target peptide, charging the peptides without causing fragmentation (Banerjee & Mazumdar, 2012; Fenn et al., 1989). In ESI, the peptides are suspended in a carrier solution containing a polar solvent, and then forced through the tip of a capillary, which is maintained at high voltage. This results in the transformation of the liquid into electrospray droplets, which evaporate, eventually releasing the peptides, which have now acquired the charge of the droplets (Banerjee & Mazumdar, 2012). Samples processed as part of this investigation were ionized using a nanospray ionization system, which creates smaller droplets than conventional systems, and allows a smaller amount of material to be processed in the course of an experiment (Banerjee & Mazumdar, 2012; Rinner et al., 2008). During our investigations, peptides were analyzed using an Orbitrap spectrometer (ThermoFisher Scientific), which measures oscillations of ions as they orbits a central electrode (Leitner et al., 2014) to determine mass to charge ratios thus enabling very accurate mass measurements (Leitner et al., 2014; Makarov, 2000).

The charged peptides progress from the first MS phase (MS1) to the second MS phase (MS2), in which the peptides are further fragmented by collision induced dissociation (CID). In this process, the ionized peptide is bombarded with a neutral gas, the additional energy of which causes the peptide to break apart in a predictable pattern, generally between the residues of the peptide, producing fragments with mass differences that can be analyzed in relation to one another to determine the peptide sequence (Biemann, 1990). The peptide linkages are broken in a manner that produces both a charged peptide, the mass to charge ratio of which is further analyzed, and a neutral peptide, which is lost. The individual properties of peptide residues, as well as post-translational modifications, dictate the position and value of the charge, but either C- or N-terminally charged ions can be formed from a peptide, depending of the conditions of the bonds (Biemann, 1990). The data resulting from these two charge forms is then combined to produce greater coverage of the peptide sequence.

2.4.3 MS data analysis using xQuest/Prophet

The data output from the LC-MS/MS was next processed by xQuest/Prophet software to identify crosslinked peptides. Peptides that were linked by DSS-D₁₂ and the equivalent peptides linked with DSS-H₁₂ were processed by MS2 separately from one another, but matched by the software on the basis of the isotopic shift (Rinner et al., 2008). When the MS2 data from the two DSS species are compared to one another, there is a population of peaks that are the same, resulting from the generation of an ion that does not include the crosslinker, and a population that has the characteristic 12.075 Da shift (**Figure 2.8A**).

In a pre-processing step, the software compiled a library of theoretical peptides based on the enzymes and proteins used in the experiment, in order to carry out comparison. However, the number of theoretical spectra that need be produced would increase exponentially if every crosslinked peptide possibility had to be included, which would also

exponentially increase the number of theoretical spectra to which the experimental data would have to be compared. Instead, the software compared the spectra produced by a peptides of the same identity, which exhibited the characteristic 12.075 Da shift during MS1 analysis. The software then compiled a combined spectrum from both the DSS-H₁₂ and DSS-D₁₂ linked peptides consisting of only those peaks that appeared at exactly the same mass during MS2 analysis, without the 12.075 Da shift. These peaks, which showed no shift, indicated the portion of the peptide that did not contain the linker. These peaks, which both spectra share, are known as common links (**Figure 2.8B**).

The common-peak spectra were subsequently compared to the software-generated index of theoretical peptides to find the closest matches. The stringency of this step was kept low, as crosslinked ions make up the bulk of the data generated by MS2, leaving relatively few common peaks out of which to form the spectra (Rinner et al., 2008, supplementary discussion). Full theoretical spectra, this time with the more computing-intensive full range of crosslinking combinations, were then generated for these selected, size-matched potential crosslinks (**Figure 2.8C**). This analysis populated a list with potential peptide matches from the theoretical peptide library in which even a single peak was matched to the experimental spectrum. These common-link spectra contained data from both peptides present in the crosslinked precursor, so potential peptide matches from the theoretical library were then paired in such a way that their combined mass was equal to the mass of the intact crosslinked peptide, which was measured in the first MS1 step (**Figure 2.8D**). The correctness of the peptide matches was then evaluated by the software (**Figure 2.8E**).

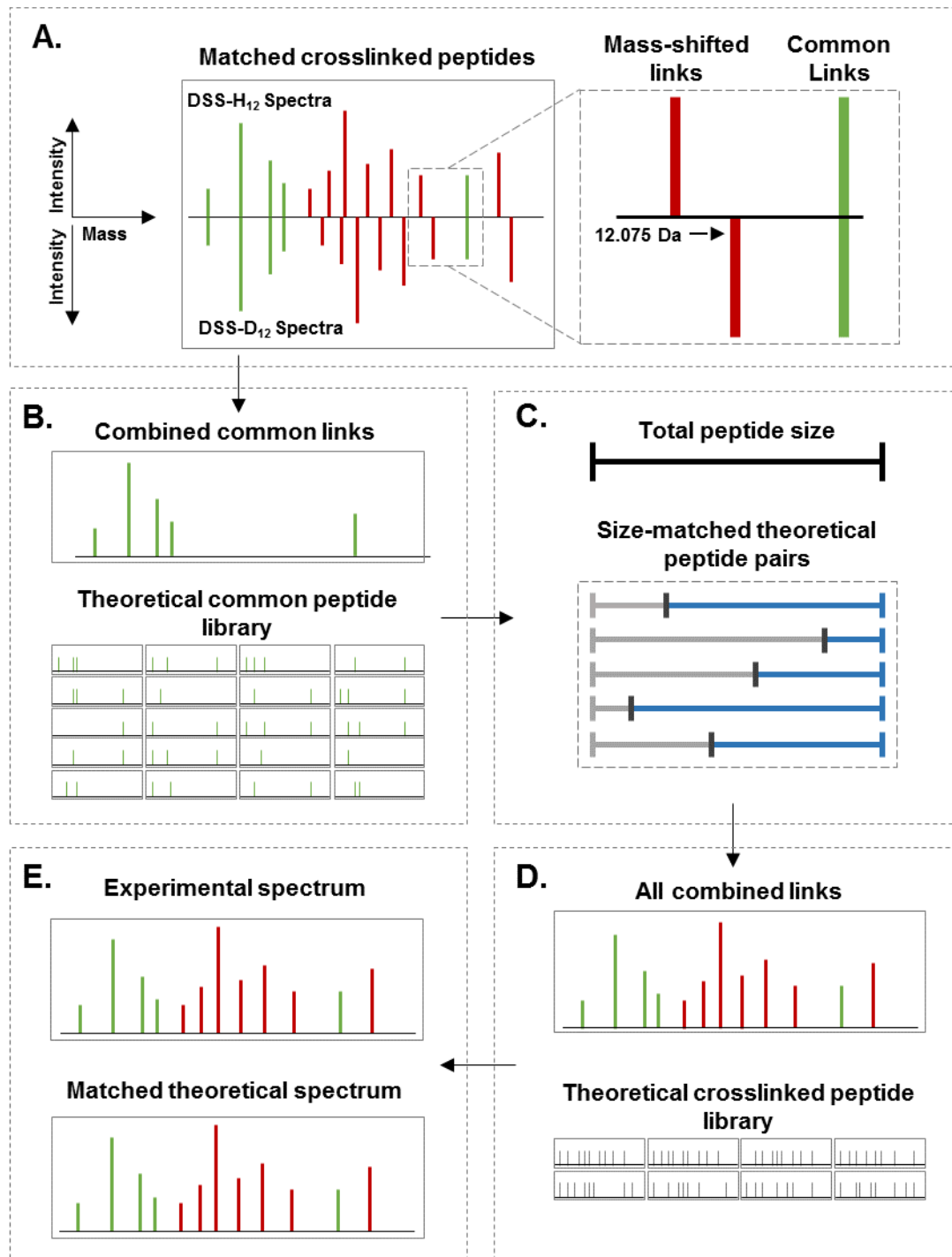


Figure 2.8 Workflow of XL-MS processing. **A.** DSS-H₁₂ and DSS-D₁₂ crosslinked peptides are matched to each other using MS1 to identify the 12.075 Da shift in their mass. When the MS2 data for each peptide is compared, some of the collision dissociated ions exhibit the 12.075 Da shift between the two DSS conditions, while some have exactly the same mass. These shifted peaks (red) are ions that contain the crosslinker when analyzed by MS2, while the peaks that do not exhibit a shift are ions that did not contain the crosslinker during MS2 analysis (green). These peaks are known as common links. **B.** The software generates a library of theoretical links based on the protein and digestion enzyme parameters of the experiment. The spectra containing only the common links is then searched against this library. The stringency of this search is very low, and matches of even a single peak are retained. **C.** These newly identified potential links are then processed to produce a library of theoretical crosslinked spectra, which contains the software predicted ion spectra of all combinations of peptides identified in the first library search. **D.** The potentially matched ion spectra are combined with so that

only pairs that match the mass of the original experimental peptide are retained. **E**. The ion spectra of the peptide pairs with the same cumulative mass as the original peptide are searched to produce the best match. The quality of this match is then assessed by a series of statistical measures.

A typical MS2 spectrum is shown in **figure 2.9**. Collision-induced dissociation (CID) breaks apart the initial peptide such that it is possible to sequence the crosslinked peptide on the basis of differences in mass as single amino acids are lost from the peptide termini. In **figure 2.9**, fragments containing DSS crosslinker are shown in red, whereas common ions are shown in green.

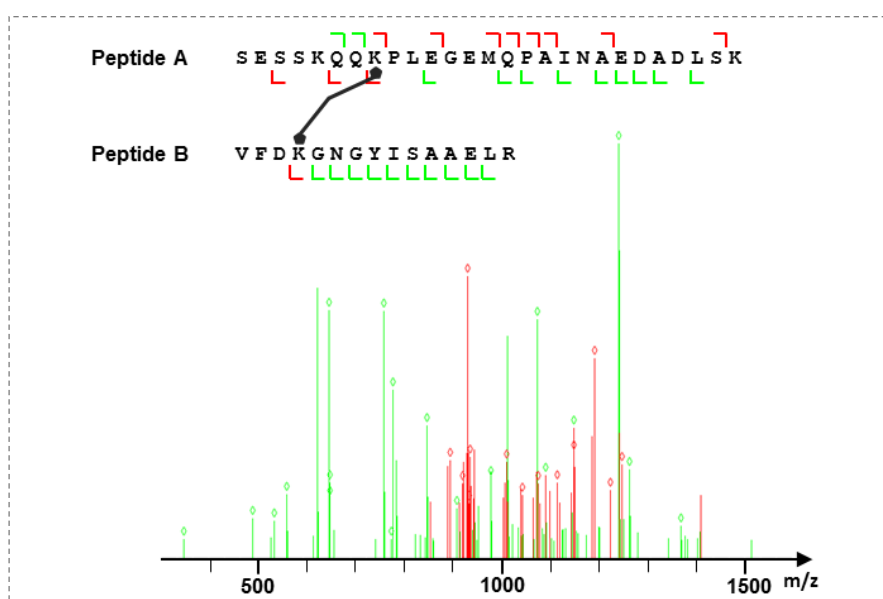


Figure 2.9 XL-MS MS2 ion spectrum. An MS2 spectrum is shown for an example crosslinked peptide. Fragments containing crosslinker are shown in red; common ions are in green.

The xQuest/xProphet pipeline outputs a number of scoring parameters, shown in **figure 2.10**, to evaluate the validity of crosslinking matches (Walzthoeni et al., 2012). The strongest indication of match fit is the MatchOdds parameter, which is calculated by taking the negative log of the probability that the peak matches generated by the software are a random fit, factoring in the theoretical number of ions, the number of matches, and the mass accuracy. The software also determines the closeness of fit between the experimental ion spectrum and the predicted ion spectrum of the crosslinked peptides as compared to the

second best match, which are output as the `xcorrx`, and `xcorrb` parameters for crosslinked and common peaks respectively (MacCoss, Wu, & Yates, 2002).

A correction to overcome an observed bias of early versions of the software pipeline to accept assignments of peptide identity in which one peptide is correctly identified and the other is erroneously assigned, the weighted total ion current (wTIC), is also evaluated (Walzthoeni et al., 2012). The wTIC scoring parameter uses the amino acid length of each peptide, the length of the total crosslinked unit, and the dissociation pattern of the peptide to rule out crosslink matches in which only one peptide is matched. The intensity sum score (`intsum`) measure is the total of the normalized intensities of the peaks in the crosslinked spectrum (Walzthoeni et al., 2012). In order to optimize the separation between the true and false positive hits, the authors used linear discriminant analysis on a population of known true-positive and false-positive links, and determined a measurement single measurement (`Id-score`), which combines `MatchOdds`, `intsum`, `xcorrb`, wTIC and `xcorrx` into a single weighted measurement. ID scores greater than 25 are considered to be strong candidates.

`xProphet` also estimates false discover rate based on individual calculations of FDR for mono and loop links, intraprotein crosslinks, and interprotein crosslinks. This is accomplished using a target-decoy strategy in which the library of candidate peptides populated by `xQuest` is combined with generated decoy peptides and the number of false discoveries within the linked dataset is estimated based on the number of returned links that contain at least one decoy sequence. The selection criteria can be tuned to provide links that fall within a specified FDR percentage (Walzthoeni et al., 2012).

Id	AbsPos1	AbsPos2	MatchOdds	Cross correlational scores		WTIC	intsum	Combined weighted score	
				Xcorr _x	Xcorr _b			Total intensity of all peaks	
								Id-Score	FDR
IAYSKDFETLK- IKGLVQPTR-a5-b2	113	11	11.41	0.25	0.35	0.1	337	38.03	0

Negative log of match probability Weighted total ion current False discovery rate

Figure 2.10 xQuest/Prophet output parameters. These values are representative of the processed information produced for each crosslink in a dataset, combining information from MS¹ analysis, as well as processed MS² data as generated by the xQuest/xProphet pipeline.

2.4.4 Quantitative XL-MS (qXL-MS)

Standard XL-MS datasets include a quantitative measure of detection intensity within the ion chromatogram for each peptide that is dependent upon the abundance of a given crosslink. The usefulness of this parameter is limited when considered in isolation, but fluctuations in intensity can then be used to evaluate how spatial relationships, both between and within proteins, change in response to factors such as inclusion of additional proteins or molecules. However, this information has only been utilized in a small number of studies, and analysis was carried out by manual extraction of the data these few cases (Walzthoeni et al., 2015). While the quantification of protein abundance in a sample by MS has been widely used, applying the same concepts to XL-MS introduces new challenges. The presence of the same crosslinked lysines within peptides of varying digested lengths, or of different charge states complicates the quantification of their abundance. Comparison problems are further exacerbated by the characteristically low presence of crosslinks among peptides, and the common use of enrichment methods to specifically identify crosslinked peptides.

In order to overcome these problems, and facilitate the use of qXL-MS, Walzthoeni and colleagues have developed a software package, xTract, which quantifies and compares XL-MS data (2015). xTract uses the crosslinked spectrum matches from the xQuest/xProphet pipeline that conform to the user defined FDR cutoff, and appends the precursor information from the MS1 scan, including the precursor retention time and intensity. At this point, a library of decoy extracted ion chromatographs is populated for later use in determining the false discovery rate (q-value) of the quantified peptides. This is performed by mutating the n^{th} amino acid in each of the peptides, where n is repeated for the number of residues in the peptide, according to a defined exchange table to create decoys which differ only in mass, but not retention time of the peptide (Walzthoeni et al., 2015). The information is searched based on a reference peptide spectrum match, to identify MS¹ scans within a specified retention time and mass to charge tolerance, from which an isotope peak group, corresponding to a single peptide, is defined. The suitability of this fit is then assessed by the program and output as a score from zero to one, with higher scores indicating a lower chance of a random match. The area under the curves of the matched isotopes within one peak group is calculated to give a total intensity of the observed isotope. Statistical analysis of the peak groups is then carried out by mProphet. The results of this analysis are then compared between the reference set and the experimental set, yielding a measurement of change of intensity between the two states which is expressed as a \log_2 change of the ratio between the reference and experimental samples, and a probability score yielding from a t-test for all the comparisons between the groups.

2.5 Live cell FRET measurements using Mithras LB 940 plate reader

2.5.1 Plate reader set up.

Fluorescence-based recordings of cAMP concentration and PKA activity were performed using a Mithras LB 940 plate-reader (Berthold Technologies) controlled by a computer running Mikrowin 2000 software. The plate reader was equipped with emission and excitation filters (**Table 2.5**) compatible with measurements using the reporters AKAR4 (Depry, Allen, & Zhang, 2011) and ^TEpac^{VV} (Klarenbeek et al., 2011).

Center Wavelength (nm)	Full-width at half maximum (nm)	Transmission (%)	Application	Berthold part number
420	10	50	Excitation	39452
485	14	60	Emission	40271
535	25	60	Emission	40273

Table 2.5 Filters used in conjunction with Berthold Mithras LB 940 plate reader.

2.5.2 HEK293T cell transfection & attachment procedure

Recordings were performed using transfected HEK293T cells attached to 96-well plates. Cells were cultured in DMEM (Gibco, E2693) supplemented with GlutaMAX (Gibco, P4417-100TAB), Penicillin/Streptomycin (Gibco, 15140-122), and 10 % fetal bovine serum (Gibco, 10270). Cells were transfected at 60 % confluence with control or reporter DNA in 6-well plates. Each well was transfected by first mixing 1 µg vector DNA with 4 µg Fugene 6 (Promega, E2693) in serum-free DMEM and then applying the mixture after 15 minutes to each well. Two days after transfection, HEK293T cells were resuspended in 3 mL supplemented DMEM, and replated at 100 µL cells/well in 96-well black-walled plates (Molecular Probes, M33089) that had been coated overnight with poly-L-lysine (Sigma, P6282).

2.5.3 Drug preparation

Propranolol hydrochloride (Sigma P0884, MW 295.8; 2.9 mg/10 mL for 1 mM), and isoprenaline hydrochloride (Sigma I5627, MW 247.72; 2.5 mg/10 mL for 1 mM) were prepared immediately prior to experiments by dissolving in PBS to produce 1 mM stock solutions. Isoprenaline was added to wells at the appropriate concentration at 10 μ L/well using a 12-channel BioHit e300 in multi-dispense mode. The Mithras LB 940 pump was primed with 100 μ M propranolol to enable injection of 10 μ L propranolol per well (final concentration: 10 μ M).

2.5.4 Specific run parameters: β -adrenoceptor deactivation experiment

To perform this experiment, HEK293T cells were laid out in the pattern depicted in **table 2.6**. In each experiment, either AKAR4 or ^TEpac^{vv} was used as the FRET reporter. DMEM was aspirated from the wells immediately before the experiment and replaced with enough PBS to lead to final volumes of 100 μ L after addition of additives. All subsequent steps were performed at room temperature (22 °C).

Well number	Isoprenaline added	Propranolol added	Transfected with:
A1	Yes	Yes	pcDNA3.1 control
A2	Yes	Yes	FRET Reporter*
A3	Yes		pcDNA3.1 control
A4	Yes		FRET Reporter
A5	Yes	Yes	pcDNA3.1 control
A6	Yes	Yes	FRET Reporter
A7			pcDNA3.1 control
A8			FRET Reporter
A9		Yes	pcDNA3.1 control
A10		Yes	FRET Reporter
A11			pcDNA3.1 control
A12			FRET Reporter
B1		Yes	pcDNA3.1 control
B2		Yes	FRET Reporter
B3			pcDNA3.1 control
B4			FRET Reporter
B5		Yes	pcDNA3.1 control
B6		Yes	FRET Reporter
B7	Yes		pcDNA3.1 control
B8	Yes		FRET Reporter
B9	Yes	Yes	pcDNA3.1 control
B10	Yes	Yes	FRET Reporter
B11	Yes		pcDNA3.1 control
B12	Yes		FRET Reporter

Table 2.6 Plate layout for β -adrenoceptor deactivation experiment. This experiment was performed using HEK293T cells transfected with either AKAR4 or $T^{\text{Epac}}^{\text{VV}}$ as the FRET reporter.

The plate was first read with no additives to determine baseline ratios for 535/485 nm emission following excitation at 420 nm (2 measurements per well). Next, the multi-channel pipette was used to rapidly apply 10 μL of 1.5 μM isoprenaline (final concentration: 150 nM) to wells A1-A6 and B7-B12. After four minutes, the protocol depicted in **figure 2.11** was initiated.

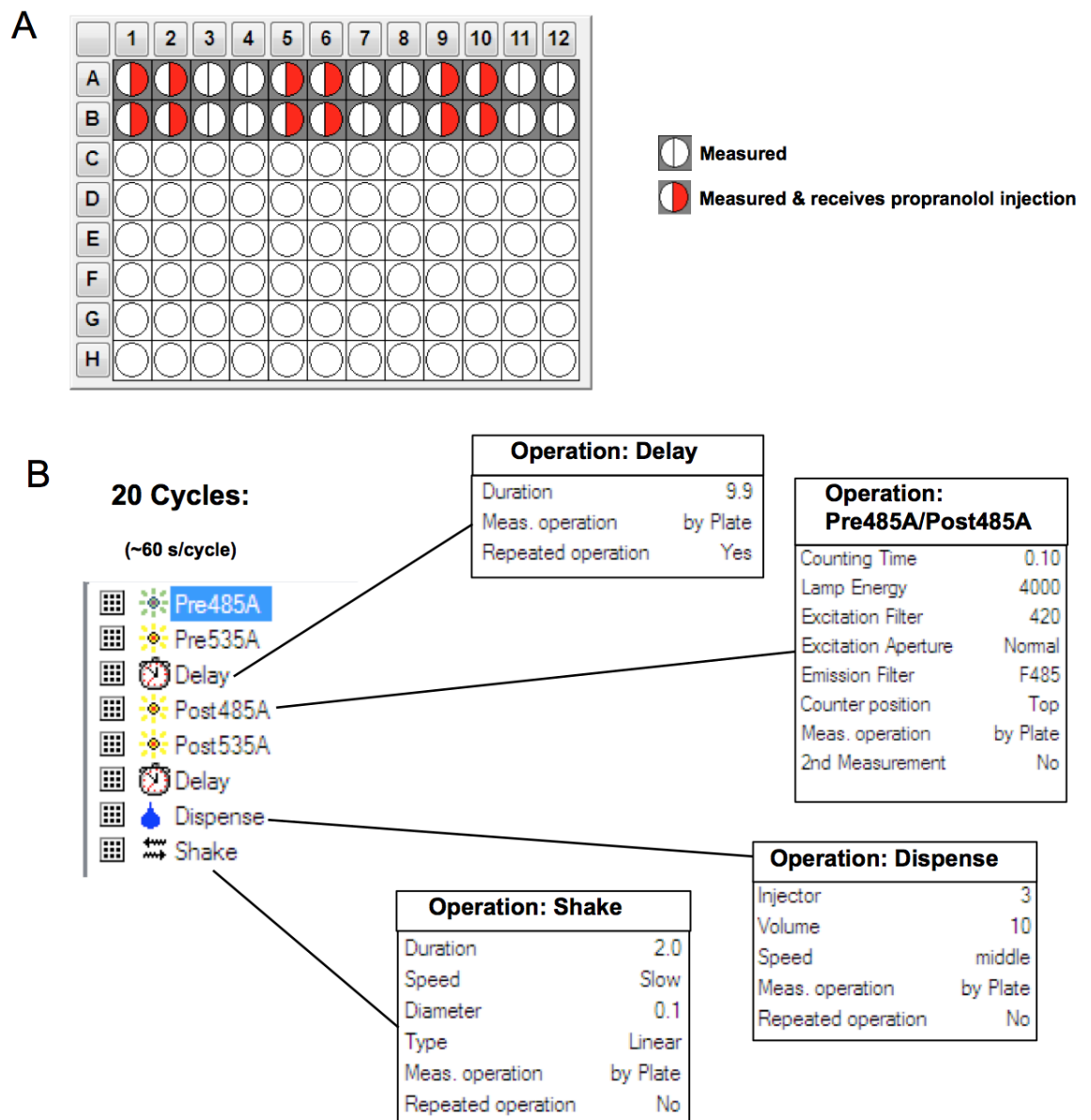


Figure 2.11 Plate reader parameters for β -adrenoceptor deactivation experiment.

The program performs 20 cycles of recordings such that 40 total 535/485 emission ratios are collected at ~ 30 seconds intervals. After the first two recordings, the plate reader is programmed to inject 10 μL of 100 μM propranolol into wells A1-2, A5-6, A9-10, B1-2, B5-6 and B9-10. Addition of propranolol thus occurs five mins after addition of isoprenaline, which is the same timing as experiments using NHS-Diazirine crosslinking (**Chapter 4**).

2.5.5 Specific run parameters: isoprenaline titration experiment

In this case, HEK293T cells transfected with either AKAR4 or control DNA were laid out in the pattern depicted in **table 2.6**.

Iso (nM)	0	0.01	0.03	0.1	0.2	0.5	1	2	5	10	100	1000
Row A	AKAR4											
Row B	AKAR4											
Row C	pcDNA	pcDNA	pcDNA	pcDNA	-	-	-	-	-	-	-	-

Table 2.7 Plate layout for isoprenaline titration experiment.

Cells were switched into 90 μ L PBS 3 days after transfection. After two baseline 535/485 ratio measurements per well, different concentrations of isoprenaline were rapidly added to each well as indicated in **table 2.7** (top row) using the multi-channel pipette in multi-dispense mode. A brief shake (2 s, slow speed, 0.1 cm diameter, orbital, by plate) was included prior to the first data point after addition of isoprenaline. Recordings began immediately after shaking such that the first data point fell 30 seconds after addition of isoprenaline and continued at \sim 30 seconds intervals for a further 20 mins.

2.5.6 Data processing

Data processing was performed using Microsoft Excel. Background emission at 485 and 535 nm was subtracted using data recorded in cells transfected with control DNA. Changes in FRET ratio were calculated on a per well basis. 535/485 FRET ratio changes were then averaged across replicates of the same condition collected in different wells. Replicates were collected on different weeks using new transfected cell and drug preparations.

2.5.7 Comparison of plate reader approach to single cell recording methods

There are advantages and disadvantages to performing measurements using AKAR4/^TEpac^{VM} in 96-well plates in comparison to the more common method of measuring single cells with a light microscope equipped with lasers and filters for FRET measurements (Depry et al., 2011). Recording plates enables the experimenter to trial many variables in parallel, as exemplified by our recordings with 12 different concentrations of isoprenaline. Since recordings are on the population level, well-to-well variations are relatively small in comparison to single cell differences. Conversely, our sampling frequency (one recording per 30 s) is very slow in comparison to microscopic methods. Furthermore, there is a lag of ~ 8 seconds between each 535 nm and 485 nm emission measurement. In addition, some subtleties including single cell oscillations in cAMP/PKA activity will be averaged out at the population level. The experiments conducted during this project were therefore tailored to exploit the advantages of the plate reader and do not require high temporal resolution.

Chapter 3. Quantification of PKA subunit stoichiometry in cell and tissue preparations

The exact molar excess of PKA R subunits to C subunits is a key factor in understanding how PKA C is restrained following its release from the R subunit. Remarkably, to our knowledge, there are no published attempts to accurately determine PKA subunit copy number in different biological preparations using modern techniques. In order to address this problem, I took advantage of a range of commercially-available antibodies (BD Biosciences). I applied these in conjunction with purified PKA subunits to establish a quantitative immunoblotting protocol. After validating the specificity and dynamic range of the selected antibodies, and developing a densitometric analysis procedure, I systematically quantified C, RI and RII subunit expression across a range of organs and cell types. The ratios of R to C subunits that I determined have important implications for the interactions of the subunits following activation.

3.1 Anti- C, RI, RII α , and RII β antibodies are suitable for quantitative immunoblotting

Before undertaking subunit quantification in tissue homogenates, I performed preliminary experiments to assess the specificity of different antibodies that might be useful in the study. Preliminary immunoblots (IBs) were performed against purified PKA subunit isoforms C α , C β , RI α , RI β , RII α , and RII β . Each protein was purified by glutathione affinity and size exclusion chromatography, following overexpression in bacteria (**Methods 2.1.5**). The use of purified proteins for immunoblotting enabled the assessment of isoform-specificity, and enabled accurate protein concentration measurements of protein standards by BCA assay. As the antibodies demonstrated varying degrees of sensitivity (**Table 3.1**), the amount of protein

loaded was tuned to fall within the dynamic range of each. Accordingly, the amount of protein loaded for each isoform-specific immunoblot varied, but the same amount of each PKA subunit isoform was used within each antibody test. 3 ng of each purified subunit were loaded to test the specificity of PKA C antibody; 100 ng for anti-Pan RI and anti-RI α ; and 30 ng for anti-RII α and anti-RII β (**Table 3.1**). The loading mixture for each lane contained 1.3 μ g BSA to decrease non-specific binding. In all cases, primary antibodies were used in conjunction with goat anti-mouse IgG (H+L) poly-horseradish peroxidase (HRP) secondary antibody (ThermoFischer Scientific). This immunoglobulin, which is coupled to multiple copies of HRP, was found to produce the strongest and most reliable chemiluminescence of tested antibodies, when incubated with SuperSignal™ West Dura (ThermoFisher) HRP substrate.

Primary Antibody	Specificity	Sensitivity (ng)	Dilution	Product Number
PKA C	C α , C β	0.1 – 100	1:530	610981
anti-PKA[RI]	RI α , RI β	1 – 100	1:320	610166
anti-PKA[RI α]	RI α , RI β	-	1:320	610609
anti-PKA[RII α]	RII α	3 – 50	1:320	612243
anti-PKA[RII β]	RII β	3 – 50	1:320	610626

Table 3.1 PKA antibodies used in immunoblotting. Antibodies were tested by detection of purified protein to establish subunit specificity and sensitivity.

Pan-C antibody was found to be highly sensitive and selective for PKA C subunits (**Figure 3.1**, top panel lanes 1 & 2). This antibody was raised against purified human PKA C subunit α isoform residues 18-347 (accession numbers in **Table 2.4**). Sequence alignment using BLASTP indicates 94% sequence identity across residues 18-347 between the PKA C subunit isoforms α and β (Altschul, Gish, Miller, Myers, & Lipman, 1990). This information combined with the equivalent pixel density for C α and C β in our validation experiments indicates that

the Pan-C antibody does not preferentially bind to either C subunit. Ideally, the levels of PKA C α and C β could be established separately but no isoform specific antibodies are currently available. It may be possible to develop such an antibody in future by utilizing a peptide immunogen derived from the most divergent sequence spanning residues 30-45 of the C subunit.

Validation experiments using anti-R subunit antibodies produced more mixed results. Anti-R1 α antibody exhibited considerable cross-detection of R1 β isoform (**Figure 3.1**, fifth panel from top). Sequence alignment reveals 83% sequence identity between the two RI subunit isoforms across the residue range used in antibody production. Qualitative densitometry analysis shows some specificity for R1 α , with approximately 2.3-fold higher signal for R1 α compared to R1 β (**Figure 3.1**, lanes 3 & 4). Pan-RI antibody proved to be more reliable. This antibody was raised against the much shorter sequence, residues 285-351 of R1 α , which has 88% identity with the equivalent region of R1 β . In this case, the antibody performed as advertised, producing the same signal for purified R1 α as for R1 β (**Figure 3.1**, second panel from top, lanes 3 & 4).

In contrast to the poor specificity shown by the R1 α antibody, RII α and RII β -specific antibodies showed very little cross-reactivity. Immunoblotting (**Figure 3.1**, third and fourth panels from top, lanes 5 and 6) showed no off-target detection. These antibodies are evidently able to distinguish between the 66%-identical RII subunit isoforms. I therefore proceeded with Pan-C, Pan-RI and RII isoform-specific antibodies in subsequent analyses.

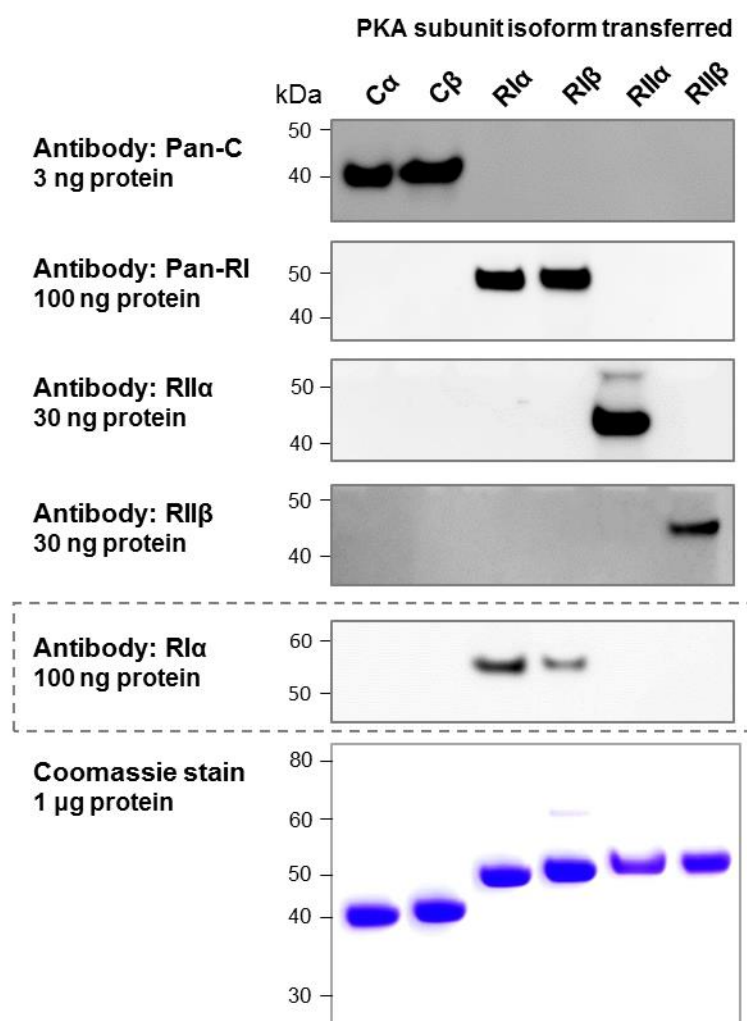


Figure 3.1 Purified protein cross reactivity blots. In order to verify the specificity of primary antibodies for each subunit or subunit isoform, a standardized quantity of each purified protein was transferred onto the same membrane. For PKA C and RI antibodies, the binding was confirmed to be equivalent across isoforms. For PKA RII isoform-specific antibodies no cross reactivity was detected. The antibody marketed to detect RI α in an isoform specific manner (dashed box) was found to have a high degree of cross reactivity with the RI β isoform, and was therefore excluded from subsequent quantitative experiments.

3.2 Selection and preparation of specimens for subunit quantification

3.2.1 Tissue and organ samples

There were a number of factors that influenced the decision to focus on organ and tissue samples prepared from Sprague Dawley rats for PKA subunit quantification. Rats are a widely

used model organism for studies of cAMP and PKA signalling. For example, studies of sympathetic nervous system control of heart contractility, and long-term changes in synaptic strength have utilized this model organism owing to its high genetic similarity to humans. Studies of synaptic plasticity typically utilize brain slices prepared from four-week-old rats: I also focused our quantitative experiments on four-week-old male rats. At this age, rats are large enough that dissection of organs and brain sub-regions is relatively simple.

I sought to compare PKA subunit stoichiometries over a range of different tissue types. Logistical considerations about the loading and quantification of a large number of samples meant that only a limited number of tissues could be included for subunit quantification, and careful consideration was given to their selection. I decided to focus on brain, heart, kidney, liver, lung and skeletal muscle. All of these preparations have been historically important in cAMP research. Heart tissue was used extensively to characterize the differences in downstream effects between β -adrenergic agonists and PGE1 and to inform the field of cAMP compartmentalization (Buxton & Brunton, 1983; Hayes et al., 1979; Keely, 1979; Mongillo et al., 2004; Zaccolo & Pozzan, 2002). cAMP research has also classically featured studies in liver dating back to the first work on the glycogen phosphorylase cascade including the first studies of glycogen physiology (Cori & Cori, 1928) and phosphorylase kinase (T. Rall et al., 1956). The use of liver tissue was instrumental in the studies leading to the discovery of cAMP (T. Rall et al., 1957; E. Sutherland & Rall, 1957). Lung tissue was selected due to the activation of the disease-relevant chloride channel, cystic fibrosis transmembrane conductance regulator (CFTR) by PKA (S. H. Cheng et al., 1991; Guggino & Stanton, 2006). Skeletal muscle has equally been a long-standing tissue of interest for PKA-related study. Glycogen phosphorylase was first crystallized from skeletal muscle, and muscle was the first tissue from which PKA was purified (Walsh et al., 1968). The earliest differentiation in the tissue specific expression of RI α , and RI β as well as RII α and RII β focused on the brain and

neurons, with the first identification of RI β and RII β as brain-specific isoform (Cadd & Mcknight, 1989; Clegg, Cadd, & McKnight, 1988).

Organs were extracted from eight different male, four-week-old rats. There was little variation between the weights of the organs from the dissected animals (**Table 3.2**). The use of consistent age and sex animals ensured a similar total weight, which contributed to the similarity of organ mass. The greatest variation in weight was seen in skeletal muscle (standard error = 13%). This reflects challenges in extracting skeletal muscle from membranes and connective tissue without losing some of the target tissue. However, tissue was collected in excess of the amount needed for the experiments, and homogeneity was considered a priority over total yield. The average weight of the cortex across the animals varied by only 3.4%, and only 2.12% for the cerebellum. All other tissues fell between skeletal muscle and cerebellum in terms of error. Though kidneys were extracted, weighed, and processed, they were not further quantified due to logistical limitations on the number of tissues that could be analyzed, as well as their physiological overlap with HEK293T cells.

Tissue	Average Mass (g)
Cortex	1.13 \pm 0.038
Cerebellum	0.28 \pm 0.006
Heart	0.57 \pm 0.042
Kidney	1.20 \pm 0.118
Liver	4.88 \pm 0.446
Lung	1.20 \pm 0.121
Skeletal muscle	0.48 \pm 0.064

Table 3.2 Mass of organs following dissection. Organs were removed from eight animals, and washed thoroughly in PBS, from which they were subsequently removed and weighed.

Studies of PKA and cAMP signaling in the brain have revealed that the mechanism for synaptic plasticity in cerebellar granule cells is quite different from that observed in typical

glutamatergic excitatory synapses in the rest of the brain: in cerebellar granule cells, long-term potentiation of synaptic strength is thought to be driven by a presynaptic cAMP/PKA-dependent mechanism. Therefore, I decided that it would be valuable to fractionate the brain into cortex and cerebellum. A major focus of the research community is the role of cAMP and PKA in regulating synaptic strength. I therefore additionally fractionated cortex to enrich synaptic material, in addition to the whole cortex lysate. This method was intended to give a better measure of the stoichiometry of PKA in the synapse, while excluding other tissues and tissue portions, like glia and myelinated membranes. The use of homogenization by calibrated mechanical shearing force followed by centrifugation is a well-established method of isolating nerve terminals and thereby enriching the proportion of synaptic protein in the resulting homogenate (Dunkley, Jarvie, and Robinson 2008).

I also decided to include protein extracted from the cell line HEK293T in our analysis. While the use of whole animals allowed us to determine the PKA subunit abundance and stoichiometry from a variety of tissues, the copy number calculations can be expressed only in terms of subunits per unit wet mass. Expanding our investigation to include cultured cells enabled us to easily and accurately determine the stoichiometry and subunit copy numbers per cell. The use of cultured cells also meant that the cell type was entirely homogenous. The HEK293T line is a very popular model cell line that has been widely utilized in studies of localized cAMP signalling (Ponsioen et al., 2004; Willoughby & Cooper, 2006; Willoughby et al., 2006). In addition, I also used this cell line for studies involving light-activated crosslinking and fluorescent reporters of PKA activity (**Chapter 4**), therefore the experiments in this chapter give some context to these recordings. Comparing PKA subunit ratios between HEK293T and rat organ/tissue preparation also helps to assess the physiological relevance of results in this cell line.

The number of cells in a total HEK293T cell culture volume following washes with PBS was estimated by using a haemocytometer to determine the cell count in 0.1 µl of culture, and multiplying by the total volume of the culture (see **chapter 2.2.4**). Cell cultures were then pelleted and lysed, and the total volume of the lysate was measured. The total number of cells was divided by the volume of lysate produced to determine the average number of lysed cell contents per µl of lysate (**Table 3.5**, columns 4 &5). This figure was used in PKA subunit quantification calculations going forward.

Replicate	Cells/0.1 ul	Cells/ml	Lysate Volume (ul)	Cells/ul Lysate
1	93.75	9.375 x 10 ⁵	727.6	12884.83
2	96.00	9.600 x 10 ⁵	769.3	12478.88
3	103.25	1.0325x 10 ⁶	759.2	13599.84
4	98.25	9.825 x 10 ⁵	753.8	13033.96

Table 3.3 HEK293T cell lysate quantification.

3.2.2 Protein extraction from cell and tissue samples

Following dissection, protein was extracted from specimens by mechanical homogenization and sonication in the presence of detergents. Our main aim in choosing the conditions of homogenization was to release as many of the PKA subunits as possible into the soluble fraction of the homogenate for quantification by immunoblotting.

The use of mechanical homogenization by rotor/stator homogenizer was chosen for its ability to process a relatively large mass of tissue quickly, and to produce a homogenous suspension of tissue. The consistent dispersal of the tissue was paramount. It was also essential to use a method rigorous enough to separate the tough connective tissues of organs like heart and lung. Course chopping of the tissue by hand prior to homogenization

was necessitated by the geometry of the homogenizer attachment. If tissues were left in pieces larger than the intake of the dispersal mechanism they were not drawn into the tool and instead left whole. The use of the rotor/stator also broke the tissues down to a great enough degree for sonication to act effectively. The mechanical rotor/stator was chosen over cryogenic grinding with liquid nitrogen and a mortar and pestle due to the number of tissues requiring processing, the volumes of those tissues, and the desire to retain the entirety of the sample in the lysate. Mortar and pestle grinding risks losing a portion of the sample in transfer of the particulate out of the apparatus, and as our calculations were based on the wet weight of the organ, any tissue loss would have introduced error. This was an especially important consideration with the smallest tissues like cerebellum, which would have been disproportionately affected. Similarly, this method was chosen over the more delicate Dounce homogenization, used for the production of the synaptosome fraction, for its greater ability to lyse cells. As identification of proteins in denaturing conditions was our ultimate use for these samples, it was not essential that protein binding be maintained, which allowed us to use more stringent solubilization methods.

Sonication, which causes cavitation of the samples resulting in a high degree of disruption to individual cells, was used following mechanical homogenization to further lyse the tissues, in order to ensure that the contents of the cells were released into the soluble fraction of the final homogenate. Efforts were made to reduce the denaturation of samples by performing sonication in short bursts, on ice, in a cold room at 4°C. The combination of rotor/stator homogenization with sonication yields greater protein solubilization than either method alone (Burden, 2012).

Finding an effective method of releasing R subunits from the membrane was one of the key hurdles in solubilisation. The association of the type II R subunit with the membrane has

been well characterized, with its colocalization with pelleted material following centrifugation being one of the defining characteristics that led to the discovery of specific localization of type I and II R subunits (Corbin et al., 1977). The anionic detergent sodium deoxycholate was chosen based on its ability to solubilize lipid membranes, while not causing a high degree of protein denaturation (M. N. Jones, 1999). As identification of proteins in denaturing conditions was our ultimate use for these samples, I could have used more stringent solubilisation methods, like higher concentrations or stronger surfactants. However, in an effort to maintain consistency between experiments to facilitate comparisons, I chose detergents that were compatible with subsequent pull down experiments (**Chapter 4**). Finally, homogenates were centrifuged at high speed to pellet the particulate material that was not solubilized by the homogenization method. This step was performed to remove the cellular debris that would have been incompatible with SDS-PAGE loading.

The results of protein extraction are shown in **table 3.3**. Tissues that showed the greatest standard error between animals were those with the most connective tissue (**Table 3.3**). The variations in total homogenate protein concentrations may have been in part due to the presence of this connective tissue, which would have contributed to the wet weight of the tissue while resisting solubilisation, increasing the amount of buffer used for the homogenization without significantly increasing the soluble protein concentration. The largest error (13.9%) was seen between lung tissues, which may have been further complicated by the inclusion of some of the trachea and bronchi. It is important to note that while I optimized the homogenization and solubilization conditions to best release PKA subunits, all of the quantification results that follow are presented with the caveat that they are dependent on the efficiency of this method.

Average Concentration (mg/ml)	
Cerebellum	6.680 ± 0.702
Cortex	8.520 ± 0.248
Heart	7.734 ± 0.708
Kidney	10.756 ± 0.495
Liver	13.503 ± 1.377
Lungs	8.209 ± 1.148
Skeletal muscle	5.710 ± 0.478
Synaptosome rich	8.832 ± 0.477

Table 3.4 Protein concentrations of organ homogenates. The table shows the concentration of protein extracted for different organs/fractions of four different animals. 1 mL/g of wet tissue weight to produce the homogenates. Protein concentrations were determined by BCA assay.

3.2.3 Establishing a quantitative immunoblotting procedure

Immunoblotting is typically considered a qualitative technique. When using chemiluminescent substrates to detect protein transferred to membranes, raw pixel density upon imaging does not necessarily relate linearly to protein concentration. However, advances in digital imaging technology, and the availability of highly purified PKA subunits meant that I could accurately determine the characteristics of different anti-PKA subunit antibodies, enabling the accurate quantitation of PKA subunit stoichiometries in our panel of cell and tissue extracts.

The variability inherent to immunoblotting means that quantitative comparison between immunoblots of separate nitrocellulose membranes is prone to error. I therefore developed an approach in which a reference standard series of the conjugate protein for each antibody is transferred alongside a series of experimental samples. However, before I could undertake this procedure, I first needed to establish the suitable dynamic ranges for each antibody. Our antibody calibration procedure is explained in detail in **methods 2.2.5**.

Preliminary experiments to determine suitable reference quantities of RI protein and cortical lysate using pan-RI antibody are shown in **figure 3.2**. In this case, ten different reference concentrations of purified RI were transferred alongside three different quantities of cortical lysate (**Figure 3.2A**). The relationship between pixel density and RI quantity was modeled using a Hill function (**Figure 3.2B**), which closely predicted pixel density with different concentrations of RI ($R^2=0.999$). For quantification of PKA subunit content in protein extracts, I selected sample volumes that fell within the near-linear portion of the calibration curve were chosen (1 μ L for cortical lysate in **Figure 3.2C**). Equivalent pilot experiments were performed with the full panel of antibodies (Pan-RI, Pan-C, anti-RII α , and anti-RII β) to determine appropriate PKA subunit reference quantities and sample loading volumes for each antibody and sample. These determinations allowed us to perform a quantitative analysis of PKA subunit stoichiometries across our full range of protein extracts.

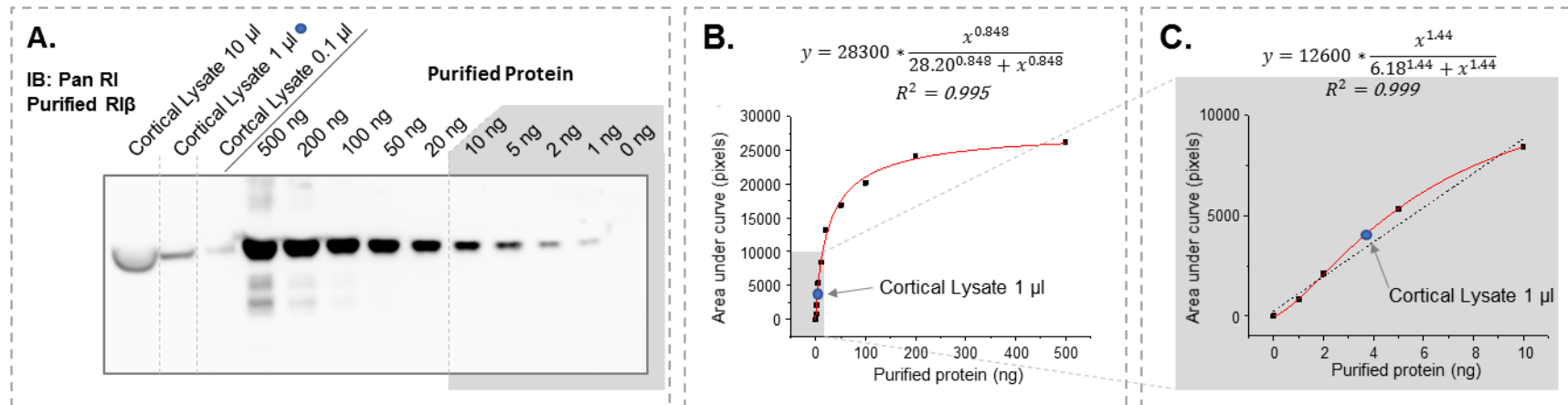


Figure 3.2 Pilot experiments to determine standard curve range. **A.** Serial dilutions of purified PKA subunits of known concentration over a large range were immunoblotted and subsequently quantified by densitometry in order to determine the most appropriate range for stoichiometric determinations. Both the dynamic range of the immunoblotting system and the maximum viable concentration of detergent in lysates were considered for the selection of ranges. **B.** Hill plot of the quantified immunoblot. **C.** The area shaded in gray represents the protein concentrations that were used going forward, which include points near the most viable organ lysate conditions.

3.2.4 Determination of PKA subunit stoichiometries

Having established suitable reference curves and loading volumes for our samples, I completed accurate quantitation of protein extracts from 8 different sources using 4 different anti-PKA antibodies, with four replicates for each sample (total = 128 data points). For each data point, protein extracts were initially loaded to fall within the detergent constraints outlined by pilot experiments. As the experiments progressed, input volumes were adjusted as necessary to ensure that samples fell within the optimal dynamic range of each antibody. As far as possible, all extracts were loaded in parallel (**Figure 3.3**), however, in some cases the differences in concentrations between tissues with the highest abundance of subunit and those with the lowest necessitated the use of two separate transfers (**Figure 3.4**). In all cases, the use of PKA subunit reference points ensured the comparability between results. After determining raw numbers for the protein concentration per μg extract, the numbers were adjusted to take into account the predicted size of the given PKA subunit (see molecular weights listed in **table 2.2** and **table 2.3** of methods). The final copy number per μg wet weight of the organ for each PKA subunit is listed in **figure 3.5**. C subunits are represented in green, combined RI subunits in orange, RII α in purple, and RII β in blue. Initial examination of the data revealed that despite the limited sample size ($n=4$), copy numbers were consistent from sample to sample as reflected by small standard deviations.

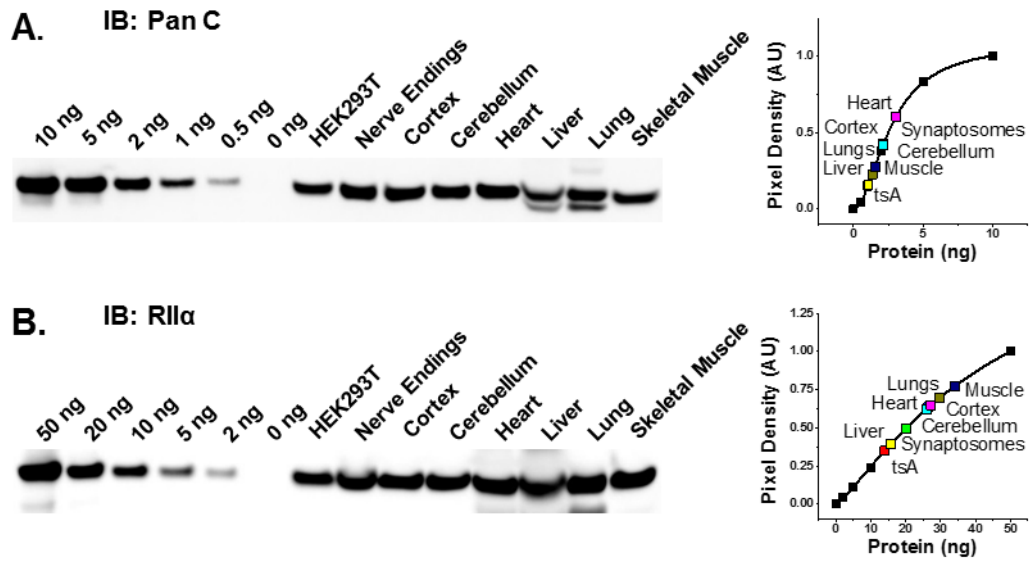


Figure 3.3 HEK293T and rat organ PKA subunit immunoblots and quantifications. A representative immunoblot is shown for **A.** PKA pan C and **B.** RII α type spanning the measured rat tissue lysates as well as HEK293T cells. Each blot contains a standard curve in order to control for variations inherent to the treatment and conditions each membrane experiences.

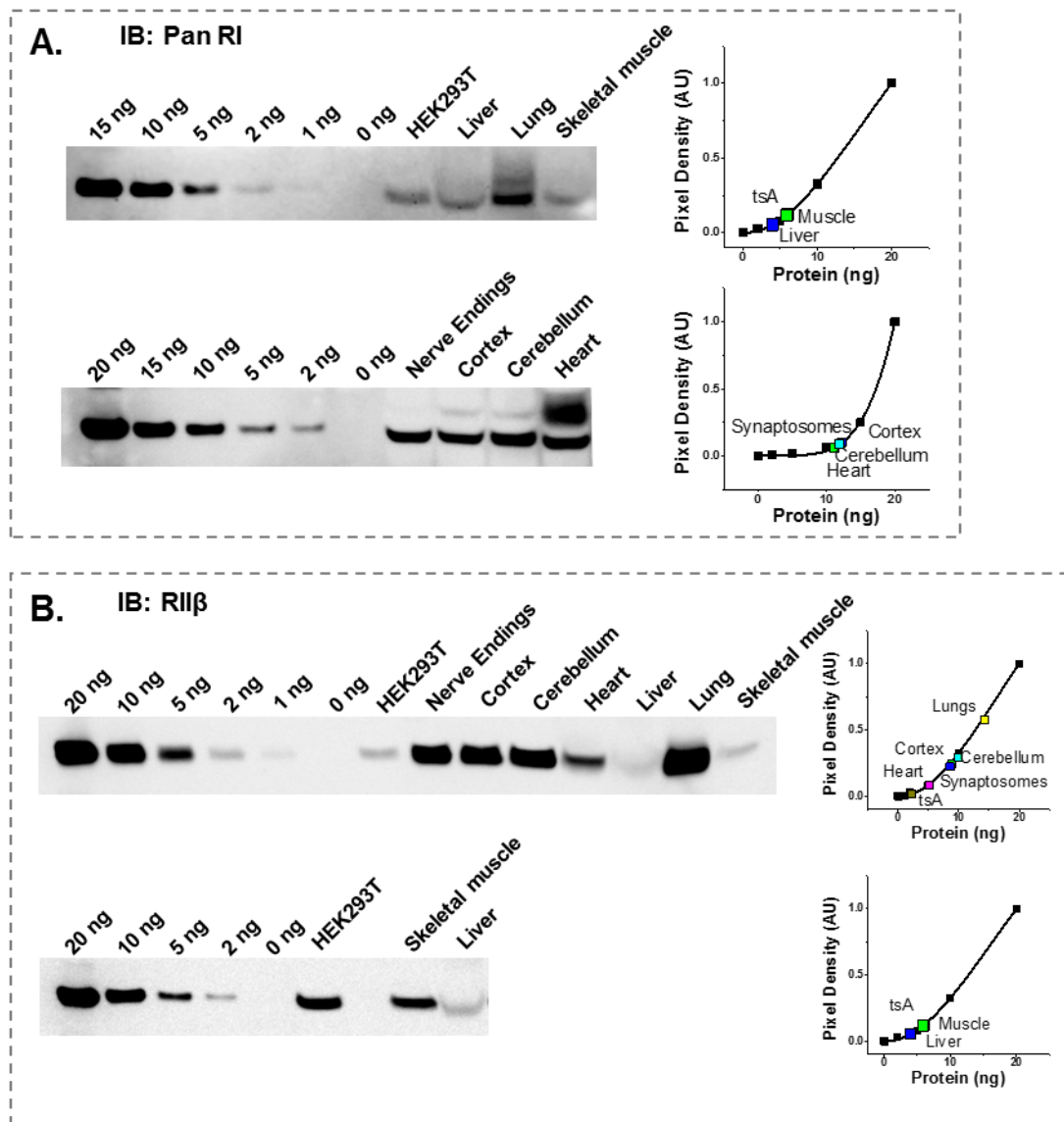


Figure 3.4 HEK293T and Rat organ PKA subunit low concentration immunoblots and quantifications. Immunoblots for subtypes **A.** Pan RI and **B.** were carried out in the same manner as figure 3.6, however, in some cases, the samples containing less protein were blotted separately from those containing higher levels of the subunit. Following quantification of the blots by densitometry, the subunit concentration of the lysates was determined by comparing them to the protein standard curves.

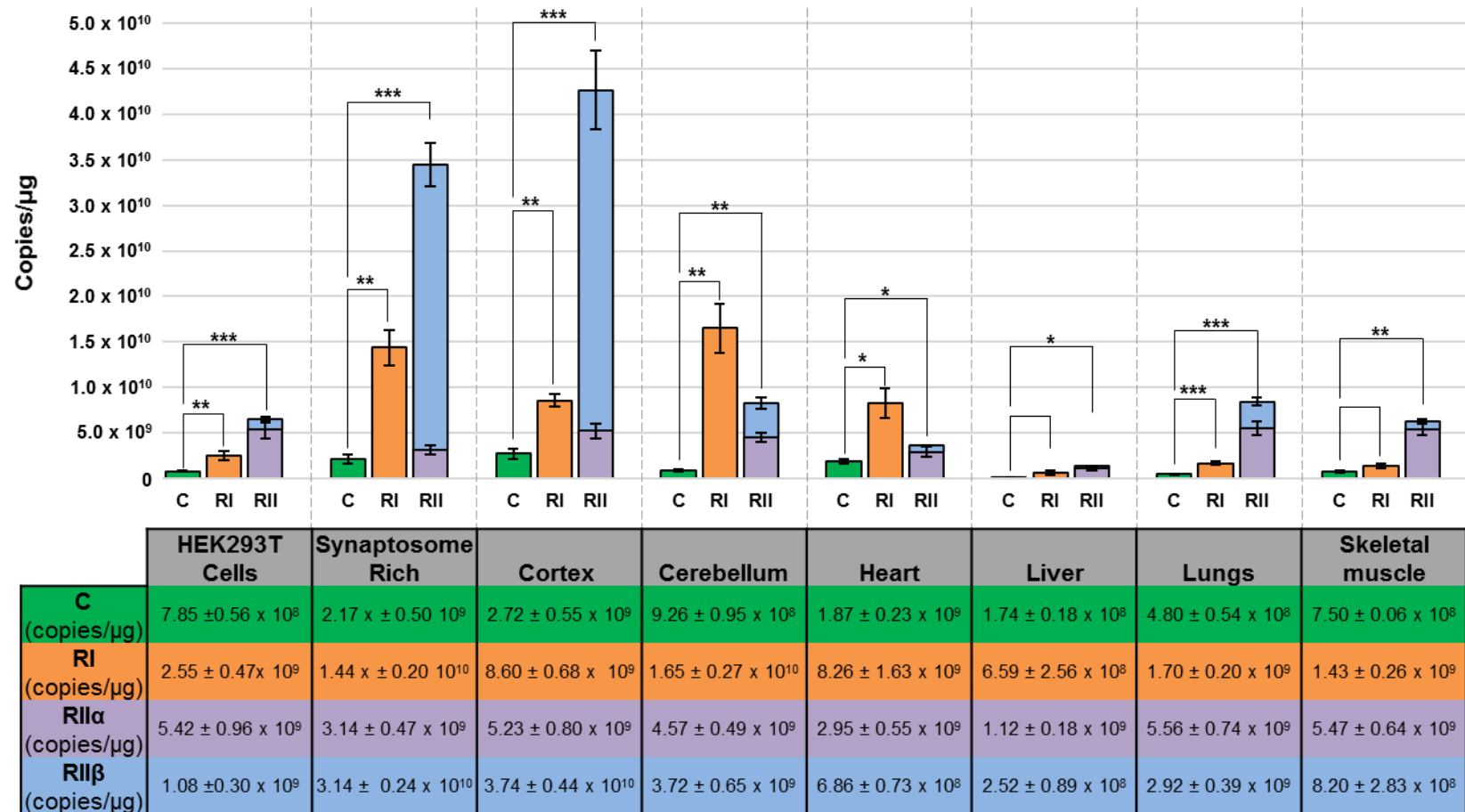


Figure 3.5 Tissue specific PKA subunit isoform quantification. Subunit numbers were calculated in terms of copies per μg wet weight of input tissue. (Error bars represent standard error n=4) Combined Cα and Cβ are shown in green, combined RIα and RIβ are shown in orange, RIIα is shown in purple, and RIIβ is shown in blue. These color conventions will be maintained throughout the document. (Student's t-test, **p* < 0.05, ***p* < 0.01, ****p* < 0.001, n=4).

3.2.5 PKA R subunits generally outnumber C subunits by ~15-fold

The most striking feature of the copy number/ μg extract distributions is that in every sample, PKA R subunits greatly outnumber C subunits. To our knowledge, this is the first concrete demonstration of this fundamental aspect of cAMP signalling. When the average copy numbers are compared by student's T-test, both RI and RII were separately found to outnumber C subunits with $p < 0.05$ in all samples with the sole exception of RI in liver (**Table 3.5**). The higher p value for the comparison in liver likely reflects higher standard errors for copy numbers in liver extracts rather than anything more meaningful.

	HEK293T	Syn. Rich	Cortex	Cere.	Heart	Liver	Lungs	Muscle
RI	4.13*	5.22**	2.78**	13.09**	3.15*	5.52	4.04**	2.44*
RII α	6.46***	1.45*	1.92**	4.94**	1.58**	6.44**	11.57**	7.29**
RII β	1.29***	14.44*	13.77**	4.02**	0.37**	1.81**	6.07**	1.54**
Total RII	7.75	15.89	15.69	8.96	1.95	8.25	17.65	8.83
Total R	11.88	21.11	18.47	22.05	5.1	13.77	21.69	11.27

Table 3.5 Relative subunit copy number normalized to PKA-C subunit. Copy numbers were calculated per μg by determining the concentration of protein in a known quantity of lysate by quantitative immunoblotting, and comparing this to the concentration of the lysate established by BCA assay. (Student's t-test, * $p < 0.05$, ** $p < 0.01$, *** $p < 0.001$, $n=4$).

The relative numbers of C to total R subunits are shown as column stacks in **Figure 3.6**. Across all eight samples, the total R subunit number is on average 15.7-fold higher than that of C subunits. The heart is an outlier with only a 5.1-fold excess of R to C subunits. The three brain samples, and lung sample show the highest relative excesses of R to C subunit, with HEK293T cells, liver and muscle exhibiting an intermediate R:C ratio.

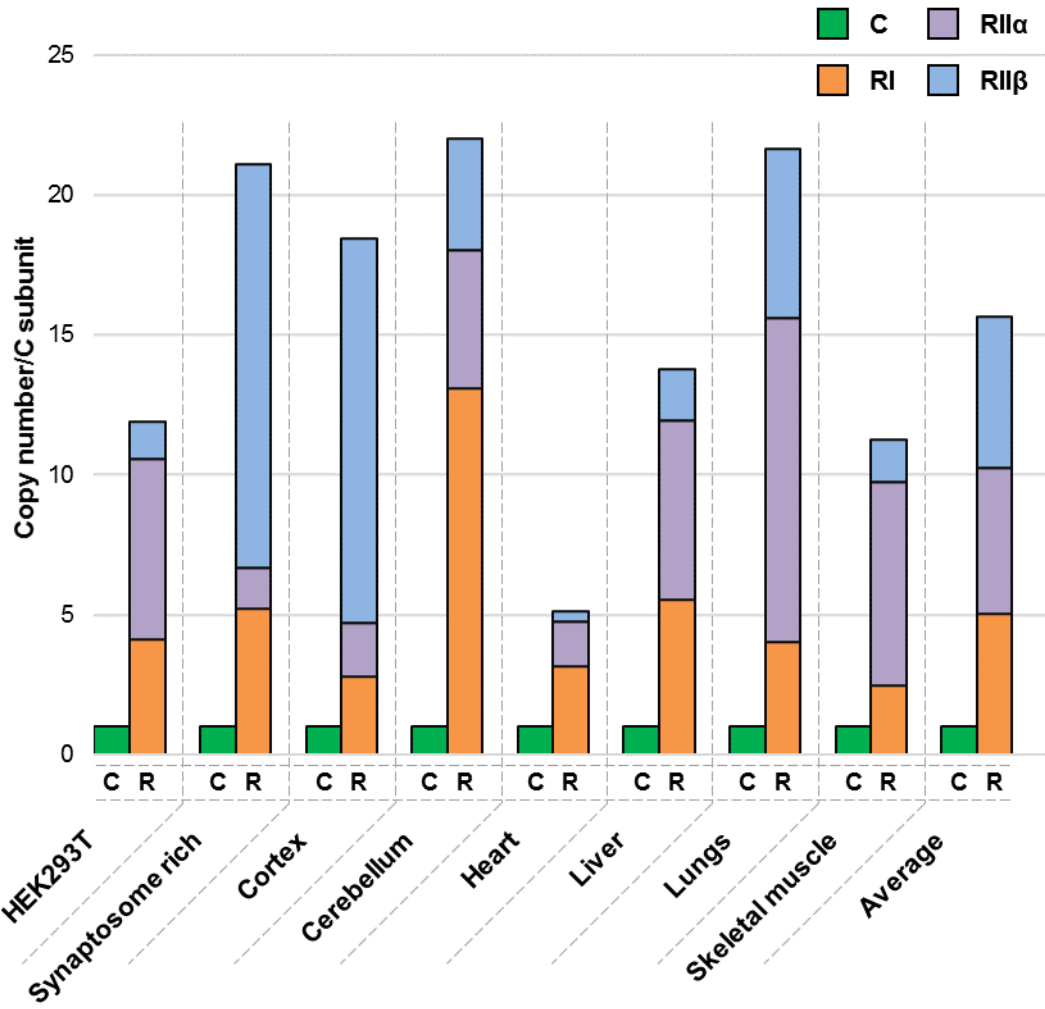


Figure 3.6 PKA R subunit copy numbers normalized to C subunit. In all tissues combined R subunits outnumbered the C subunit by no less than fivefold.

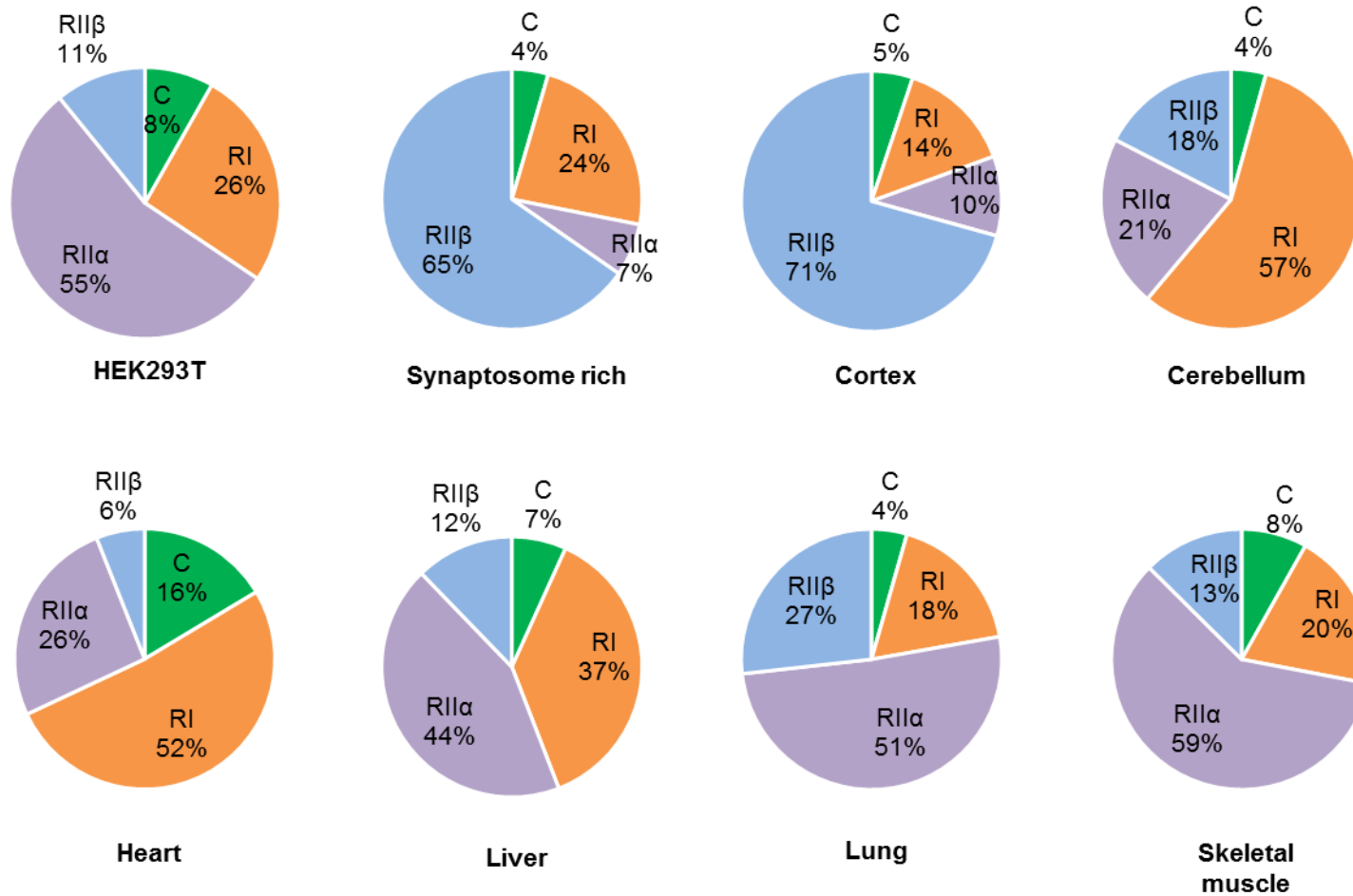


Figure 3.7 Relative concentrations of PKA subunits by tissue type in terms of copy number. The total PKA subunit copy number per unit concentration, or per cell in the case of HEK293T lysates, was totalled and expressed by PKA subunit type or isoform here in terms of relative percentages of total copies.

3.2.6 PKA subunit copy numbers per HEK293T cell support continued use of this cell line as a model for localized cAMP signaling

In the case of HEK293T cells, data from these investigations was referenced against calculations of protein extract per cell (**methods 2.2.4**) to output estimated copy numbers of each PKA subunits per HEK293T cell. The results of this additional analysis are shown in **figure 3.8**. This analysis indicates that there are approximately 229, 000 PKA C subunits per HEK293T cell. The full list of copy numbers per cell is shown in **figure 3.8 A**. Student t-testing again confirmed differences with $p < 0.001$ between C and RI, and C and RII subunits (**Figure 3.8 B**).

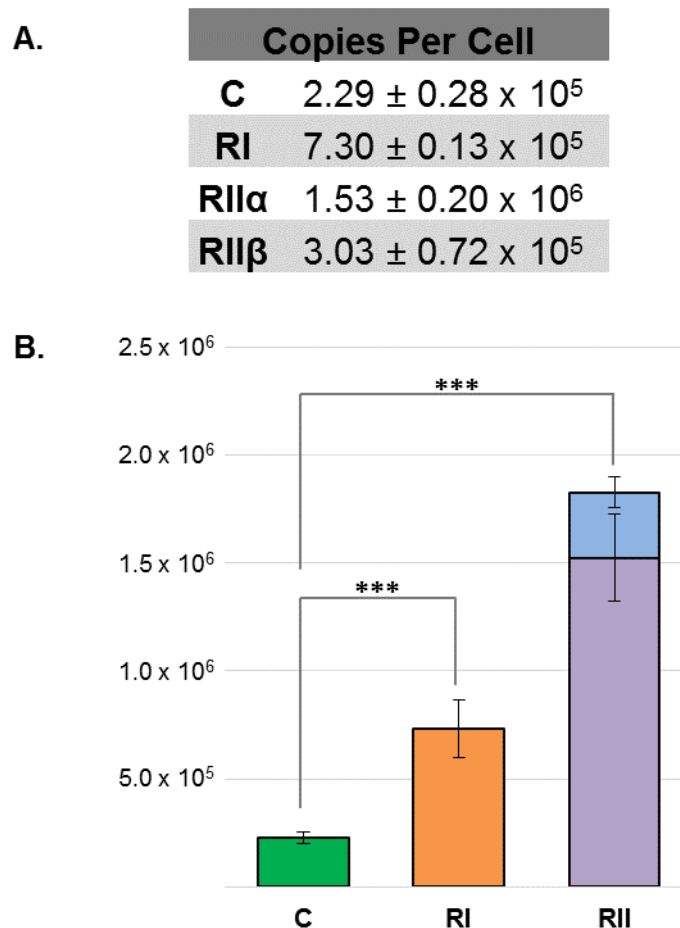


Figure 3.8 PKA subunit copy number per cell. A. Copy numbers were calculated per cell by determining the concentration of protein in a known quantity of lysate by quantitative immunoblotting, and comparing this to the known number of cells per unit lysate. **B.** The number of copies per cell in comparison to one another (Student's t-test, *** $p < 0.001$, $n=4$).

In HEK293T cells, the RII β isoform (3×10^5 /cell) is present at ~5-fold lower levels than the RII α isoform (1.5×10^6 /cell). The relatively higher level of the alpha isoform is seen across all tissues with the exception of brain cortex. This is consistent with previous observations that RII β is the predominant RII isoform in brain, although interestingly cerebellum exhibits a unique distribution of R subunits with an unusually high copy number of RI subunits and a balanced ratio of RII subunit isoforms. Overall, HEK293T cells contain a rather typical distribution of C and RII subunits, which supports their continued use as a model cell line for investigating local cAMP signalling mechanisms.

3.3 Summary & implications for PKA catalytic subunit restraint

This systematic determination of PKA subunit is the first of its type, and establishes that PKA R subunits are much in excess of C subunits. To my knowledge, there is one other documented attempt to quantitate the relative proportions of R and C subunits from the 1970s (Hofmann, Bechtel, & Krebs, 1977). In this study, the authors do not attempt to account for membrane-associated R subunits and reach the conclusions that the R:C ratio is about 1:1. As stated by the authors: *“The decision to limit the investigation to the soluble fraction of tissue homogenates was not meant to infer that the cyclic AMP-dependent protein kinase present in other fractions might not be important functionally, but only that its contribution to the total cellular concentration of enzyme subunits would be very small”*. I know that in the majority of tissues tested, excluding heart and cerebellum, RII subunits are more prevalent than RI.

It should be noted that there are potential limitations to the approach described in this chapter. Although quantitative immunoblotting is accurate, the numbers are dependent on

the efficiency of protein extraction from the different tissue samples. Specifically, the unusually low copy numbers of RII isoforms measured in heart extract may reflect the difficulty of homogenising tissue from this organ. Nevertheless, on balance I thought the best approach was to maintain a consistent extraction approach across all samples that would also be compatible with follow up experiments in HEK293T cells (**Chapter 5**). HEK293T cells proved to be an appropriate model system for further analysis as the overall ratio of R:C subunits, and the proportions of RI:RII α :RII β are in the middle range of the panel of extracts tested.

The finding that RI and particularly RII subunits are in large excess of C subunits has important implications for considering how C subunits may be restrained following their release. Importantly, this data indicates that a large unoccupied pool of R subunits resides in the cell that could potentially rapidly buffer C subunits released upon binding of cAMP to R-C complexes. In the next chapter I describe experiments that build on these observations by monitoring the associations of RI/RII and C subunits in HEK293T cells with temporal precision using a novel light-induced crosslinking method.

Chapter 4. Investigation of the synchronization of PKA R-C subunit interactions with PKA activity in live cells

The experiments in this section aimed to explore exactly when and to what extent PKA C subunits dissociate from R subunits upon activation of PKA. I was particularly interested to explore these ideas in light of the large excess of R to C subunits that established in the experiments laid out in **Chapter 3**. I was particularly interested to examine two hypotheses. First, I aimed to test the idea put forward by Smith and co-workers that C subunits do not dissociate from R subunits upon PKA activation (F. D. Smith et al., 2013). Second, I aimed to test a novel hypothesis that C subunits may be buffered by RI subunits following release from RII subunits.

To achieve these aims, I first established a new approach for measuring RI-C and RII-C association in cells with temporal precision (**Section 4.1**). The approach combines light-induced crosslinking in live cells with isoform-specific R subunit pull down using immobilised GST fusion sequences. I went on to apply this approach to investigate PKA subunit association during activation (**Section 4.2**) and deactivation (**Section 4.3**) of cAMP signalling in HEK293T cells.

4.1 Establishing an approach for analysing R-C subunit interactions in cells with temporal precision

4.1.1 NHS-diazirine was selected for crosslinking assay

The development of a time-resolved crosslinking assay centered on the properties of the amine-reactive, photolabile chemical crosslinker NHS-diazirine. It is this UV-induced diazirine crosslinking that confers temporal specificity to our protocol. Though photoinducible crosslinkers are available with a range of linker arms, the NHS-diazirine form I used has a length of 3.9 Å, meaning that only the closest interacting residues are bound to one another. I anticipated that NHS-Diazirine could crosslink R and C subunits when bound to one another, but not when dissociated upon cAMP stimulation. In this way I could use the crosslinker as a real-time read out of R-C subunit interactions in live cells.

4.1.2 Development of the PKA R subunit isoform-specific pull down procedure

In our initial experiments, I attempted to pull down C subunits following crosslinking as a prelude to comparing R-C crosslinking by immunoblotting following different cellular treatments. There is no suitable high affinity binding site in the C subunit that can be exploited for pull down, necessitating the use of a transiently expressed construct appended with an affinity tag. However, the N-terminus of the C subunit undergoes post-translational myristoylation when expressed in eukaryotic cells, which is important for its subcellular localization, making it unsuitable for the tag. While the C-terminus of subunit is not post-translationally modified, the final residue, a phenylalanine, is bound within a cleft of the protein. In order to create an exposed tag that does not de-stabilise the kinase domain, a poly-glycine region must be inserted at the C-terminus before the affinity tag. However, even if a construct could be developed that is suitable for affinity based pull downs, the

largest problem remains balancing the expression of the C subunit with endogenous subunits.

Facing these barriers, I instead developed a new approach using regulatory subunit binding sequences fused to immobilised GST to pull down R subunits. In this method, I utilized the inherent binding affinity of the D/D domain for AKAP-based peptides to capture R subunits, which were then probed for the presence of C subunits to indicate their association state at the time of UV illumination. The initial test panel of regulatory subunit binding peptides (**Table 4.1**) was chosen based on their reported binding affinity as well as our ability to produce them, and the best choices were determined empirically by pull down efficacy and selectivity.

Peptide	Sequence	Length	Species
AKAP18	MGQLCCFPFSRDEGKISEKNGGEPDDAELVR LSKRLVENAVLKAVQQYLEETQNKKNKPGEGS SVKTEAADQNGNDNENNRK	81	Human
AKAP79 C93	MEPIAIIITDTEISEFDVTKSKNVPKQFLISAENE QVGVFANDNGFEDRTSEQYETLLIETASSLVK NAIQLSIEQLVNEMASDDNKINLLQ	93	Human
AKAP-Lbc	DMKQVAQASIPAEESNATTVSTQAADVPTRA DSIEETATRIVEAVIRQVRASNALMAKVET	62	Mouse
D-AKAP2	KSFSDHGFYSPSSTLGDSPSVDDPLEYQAGL LVQNAIQQAIAEQVDKAEAHTSKEGSEQQE	61	Mouse
RIAD	LEQYANQLADQIIKEATEK	19	Engineered

Table 4.1 Regulatory subunit binding peptide sequences. The regulatory type II subunit specific binding peptides AKAP18, AKAP79 c93 and AKAP-Lbc were, as well as the dual specificity D-AKAP2 and the RI specific peptide RIAD were tested for affinity and specificity in precipitation experiments.

All peptides were expressed with a GST-tag, allowing their precipitation by association with glutathione sepharose. Peptides derived from RII-selective AKAP79, AKAP18 and AKAP-Lbc, as well as the RI-selective peptide RIAD, and the dual-selectivity AKAP D-AKAP2 were tested (**Table 4.1**). The AKAP79 c93 construct consists of the last 93 amino acids from the C-terminal of AKAP79, which includes the amphipathic RII-binding helix. The reported K_{Ds} of AKAP79 for

RII α and RII β are 0.5 nM and 4.5 nM respectively, while its affinity for RI is greater than 1 μ M as determined by surface plasmon resonance (SPR) (Herberg et al., 2000). An 81-residue peptide containing the binding helix of AKAP18 α was also produced. AKAP18 α binds RII with a reported K_d of 16.3 nM as determined using the ALPHA-screen binding assay (M.G. Gold et al., 2013). Finally, a 62 residue, RII-selective peptide from AKAP-Lbc was tested. The AKAP-Lbc derived peptide Ht31 was measured to have a K_d in the low nanomolar range RII, while RI α binding was so weak as to preclude measurement by SPR (Herberg et al., 2000). Due to the reduced affinity of naturally occurring anchoring molecules for RI, there was more limited selection of peptides suitable for RI selective binding. The engineered 19 residue RI selective peptide, RIAD, which exhibited a K_d of 1 nM for RI α while only showing a K_d of RII α 1760 nM using fluorescence polarization assays, was our most promising option (Carlson et al., 2006). The novel mammalian RI-selective AKAP, sphingosine kinase interacting protein (SKIP), discovered in 2010, was also considered, however it was not included due to low affinity for RI (Kovanich et al., 2010). As well as these regulatory subunit type selective AKAPs, the dual specificity D-AKAP2 was tested for its ability to bind RI. D-AKAP2 has been shown to bind the RI docking and dimerization domain of RI α with a K_d of 100 nM using the fluorescence anisotropy binding assay (Burns-Hamuro et al., 2005)

To test the R subunit pull down capabilities the GST fusion baits, 30 μ g of each GST-tagged construct was first incubated with glutathione sepharose, after which the beads were washed several times in buffer to remove any unbound baits. In the initial tests, R subunit precipitation was assessed using an equimolar mixture of recombinantly-expressed RI α and RII β subunits, totalling 10 μ g. The efficacy of the pull downs was assessed by immunoblotting against RI α (**Figure 4.1**) or RII β (**Figure 4.2**). As expected AKAP18 α , AKAP79 c93 and AKAP-Lbc exhibit very low RI pull down capability (**Figure 4.1** lanes 3-5), of a similar level to the GST negative control (**Figure 4.1** lane 2). While both AKAP2 and RIAD constructs bound RI (**Figure**

4.1 lanes 6 & 7), for its slightly higher signal, as well as RI selectivity, RIAD was chosen for tests moving forward.

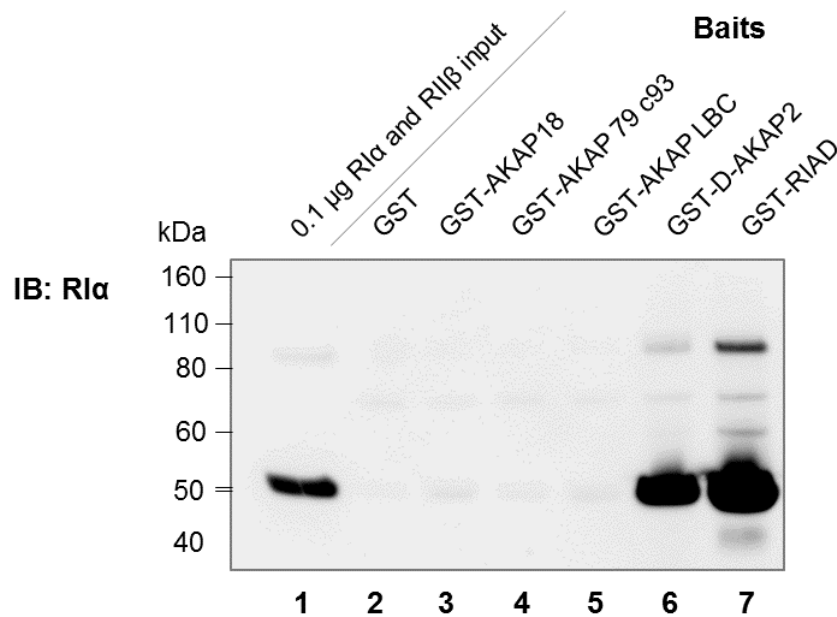


Figure 4.1 RI precipitation pilot experiment. Glutathione sepharose bound GST-tagged baits were incubated with a mixture of RI α and RII β subunits, and the eluted protein was immunoblotted against RI α . The results showed low background binding with the RII specific AKAP18, AKAP79 c93 and AKAP-Lbc peptides, while the dual specificity D-AKAP-2 and RI-specific RIAD exhibited strong binding.

RII β pull down using the different GST fusions is shown in **figure 4.2**. AKAP18, AKAP79 c93 and AKAP-Lbc were all found to effectively pull down RII (**Figure 4.2** lanes 3-5). Though some nonspecific binding to RIAD was observed, it was much lower than any of the RII-selective constructs (**Figure 4.2** lane 6). Ultimately, based on signal intensity, AKAP79 c93 was chosen for further tests (**Figure 4.2** lane 4).

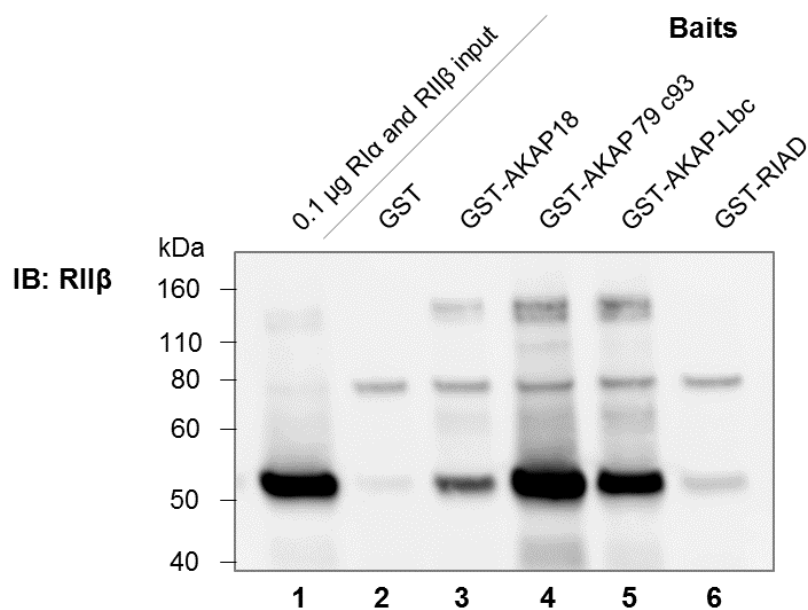


Figure 4.2 RII pull down pilot experiment. Glutathione sepharose bound GST-tagged baits were incubated with a mixture of RI α and RII β subunits, and the eluted protein was immunoblotted against RII β . The results showed binding with the RII specific AKAP18, AKAP79 c93 and AKAP-Lbc peptides, with the RI-specific RIAD showing low background binding.

The affinity and selectivity of these constructs was further tested using NHS-diazirine treated HEK293T cell lysate, which was either exposed to UV, or left unexposed. GST was used as a negative control for background binding (**Figure 4.3**, lanes 1 & 2). Both GST-fusions were found to only co-precipitate their specific R subunit target, regardless of crosslinking condition (**Figure 4.3** second and third panels). Importantly, the fusions also pulled down crosslinked 1R:1C complexes, with a band of approximately 85 kDa on the PKA C immunoblot corresponding to the C-R heterodimer present only in the UV exposed condition (**Figure 4.3**, IB:PKA-C). Without UV exposure, this band was absent. This result confirms that our approach can potentially be applied to monitor real-time association between RI-C and RII-C subunits.

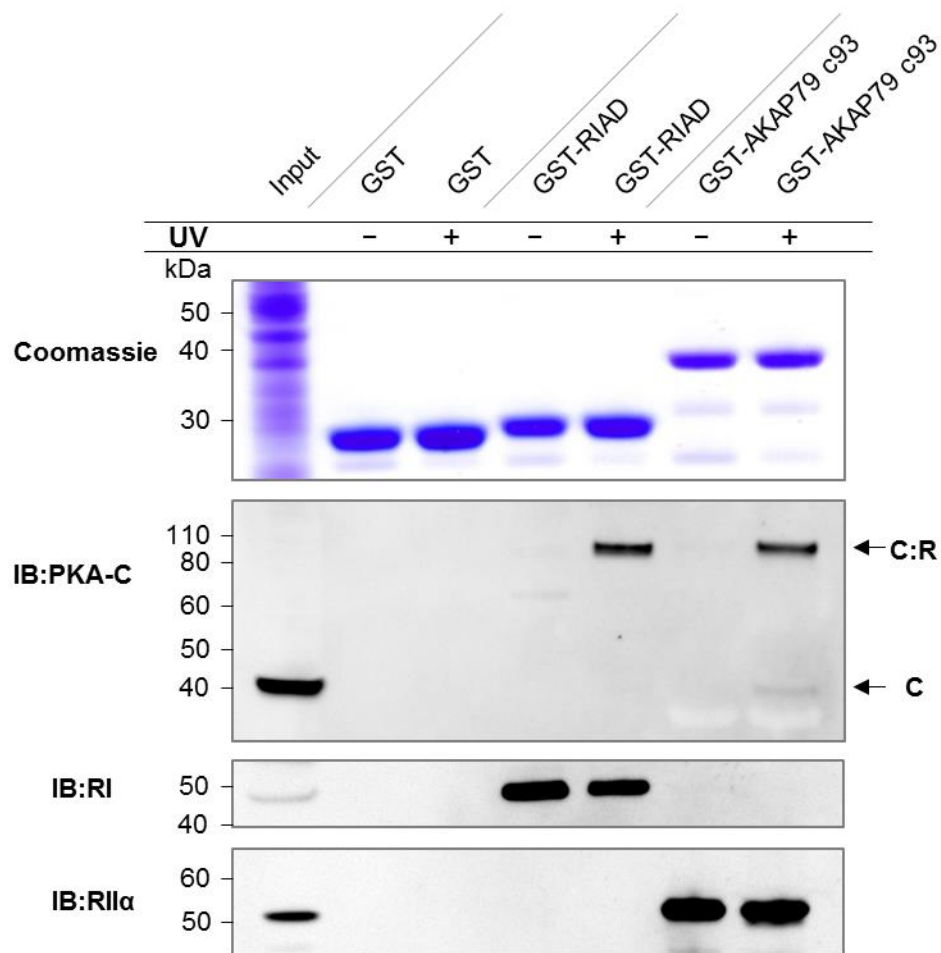


Figure 4.3 R-C complex association detected by light-induced crosslinking & isoform-specific R subunit pull down. The sensitivity and selectivity of the R subunit specific GST-tagged baits was confirmed by pull down using NHS-diazirine treated UV crosslinked or un-crosslinked HEK293T cell lysate. 30 μ g of each bait was loaded (Coomassie). The presence of bands at ~80 kDa in only the UV treated conditions when immunoblotted against the C subunit (IB:PKA-C) indicates that crosslinked subunits were selectively precipitated. The baits were shown to be selective, as GST-RIAD pulled down only RI subunits (IB: RI), while GST-AKAP79 c93 pulled down only RII subunits (IB: RII).

4.1.3 Calibration of UV exposure time

I was interested to determine how R-C crosslinking varied with UV exposure time. This would dictate the choice of time windows in subsequent experiments. While longer exposures time increases the rate of effective NHS-diazirine crosslinking, prolonged exposure to intense UV light will damage the cells. Furthermore, the temporal resolution of the assay is dependent

on the length of the UV exposure, with shorter exposures allowing us to better characterize temporal dynamics in the association of R and C subunits. To determine the optimal UV exposure length I undertook a time-course assay, in which NHS-Diazirine crosslinking experiments were carried out as previously described while sampling the duration of UV exposure at 0s, 5s, 30s, 120s and 600s (**Figure 4.4**). Densitometry was performed on the immunoblot, and the signal of the experimental bands was normalized to the input C subunit in each condition. The resulting ratios were compared and plotted as a function of time. Pull down of C subunits with both RI and RII specific baits resulted in stronger signals as the duration of UV exposure increased. Although the strongest signal was seen in samples exposed to UV radiation for 600 s, in subsequent experiments I crosslinked in 300 second time windows. This time point was determined to offer the best balance between signal-to-noise ratio and a short enough time window to be informative in experiments concerned with dynamic R-C interactions.

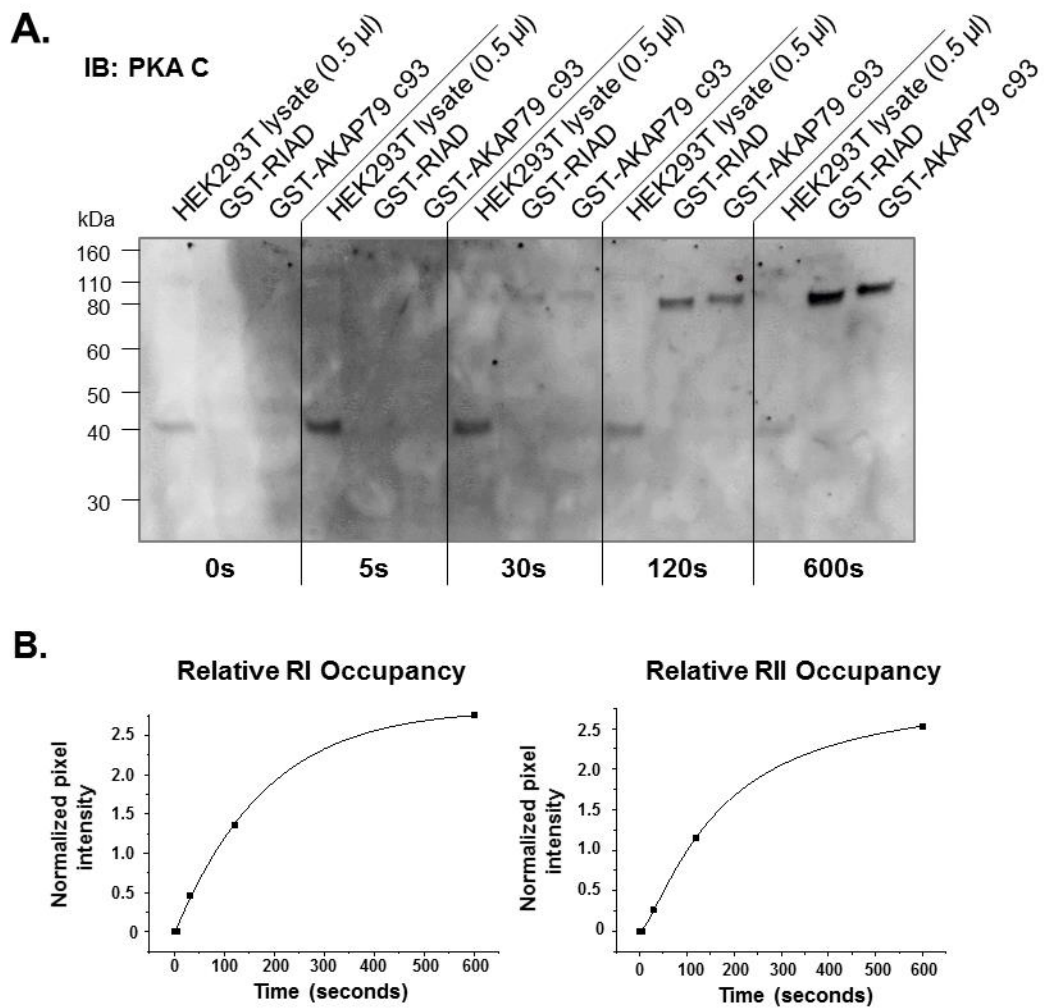


Figure 4.4 Crosslinking time point assay. NHS-diazirine treated HEK293T cells were exposed to UV illumination for 0s, 5s, 30s, 120s or 600s. Precipitation with subunit specific baits was then carried out as described above. The 120s and 600s illuminations were found to have signal intensity suitable for detection. The crosslinking window was set at 300s in length based on these findings.

4.2 C subunits are released from R subunits upon PKA activation

I first took advantage of this new approach to analyse an experiment performed by Smith and co-workers that was put forward as supporting the notion that R and C subunits do not

dissociate upon cAMP elevation (F. D. Smith et al., 2013). The authors immunoprecipitated RII subunits either with or without β -adrenergic receptor activation with isoprenaline, and immunoblotted against co-immunoprecipitated C subunit. Surprisingly, C subunit was found to co-immunoprecipitate with equal efficiency regardless of isoprenaline addition (see **Section 1.2**). I suspected that the result may have been an artefact resulting from re-association of RII and C subunits in the cell lysate during the antibody incubation for immunoprecipitation. Our new approach offered an opportunity to capture RII-C association with temporal resolution that would remove the possibility of reassociation during subsequent processing steps.

I exposed HEK293T cells to 1 μ M isoprenaline or vehicle for 5 minutes prior to lysis, as was done by Smith and colleagues. UV illumination was performed either prior or following cell lysis to test whether RII-C subunit reassociation had indeed occurred following cell lysis. Importantly, the buffer used to wash the beads following precipitation contained 1 μ M cAMP, releasing any C subunit that was not covalently attached to the regulatory subunit by NHS-diazirine crosslinking. I then used densitometry of PKA-C subunit immunoblotting to quantify the percent change between the isoprenaline and vehicle conditions. For the most direct comparison to the work carried out by Smith and co-workers, who used GFP tagged RII α for their pull downs, I analysed the coprecipitation of the C subunit with GST-AKAP79 c93, which is selective for RII subunits. Co-precipitated C subunits are visualized on the blot at \sim 90 kDa, which is the combined molecular weight of the C and regulatory subunit (**Figure 4.5 A**). This band is absent in the input condition without NHS-diazirine. Similarly to Smith and co-workers, I found that C subunits are associated with RII following Igepal CA-630/deoxycholate lysis, regardless of whether the cells have been treated with isoprenaline or not. This association rose slightly in the isoprenaline treated cells following lysis, with C subunit detected in the treated sample increasing by $27.28 \pm 2.62\%$ ($p < 0.01$, $n = 4$) (**Figure**

4.5 B, lanes 4 and 5). However, when crosslinking was carried out prior to lysis and in the presence of isoprenaline, there was a $-77.72 \pm 6.8\%$ ($p < 0.01$, $n = 4$) change in C subunit binding when compared to the vehicle treated condition that was illuminated prior to lysis (**Figure 4.5 A** lanes 2 and 3, **B**). When compared to one another, this change in association before or after lysis and incubation causes a 105% difference in immunoblot intensity, ($p < 0.001$, $n=4$). These changes are based on the comparison between the isoprenaline positive and negative conditions, and not between the pre- and post- lysis conditions, as the efficiency of the coprecipitation of the regulatory subunit varied greatly between the pre- and post- lysis replicates (**Figure 4.5 A**). This is potentially due to the preservation of endogenous anchoring associations of some regulatory subunits caused by the UV exposure while the cell structure was intact, which would in turn preclude the binding of our baits. Selectivity for the type II regulatory subunit is indicated by the absence of detection of RI by immunoblotting.

This result strongly indicates that the conclusion of Smith and co-workers, that the majority of the C subunit is still associated with the type II regulatory subunit in the presence of 1 μM isoprenaline, is based on an artefact introduced by the immunoprecipitation conditions used by the authors. In fact, 1 μM isoprenaline does lead to pronounced dissociation of C subunits from RII subunits.

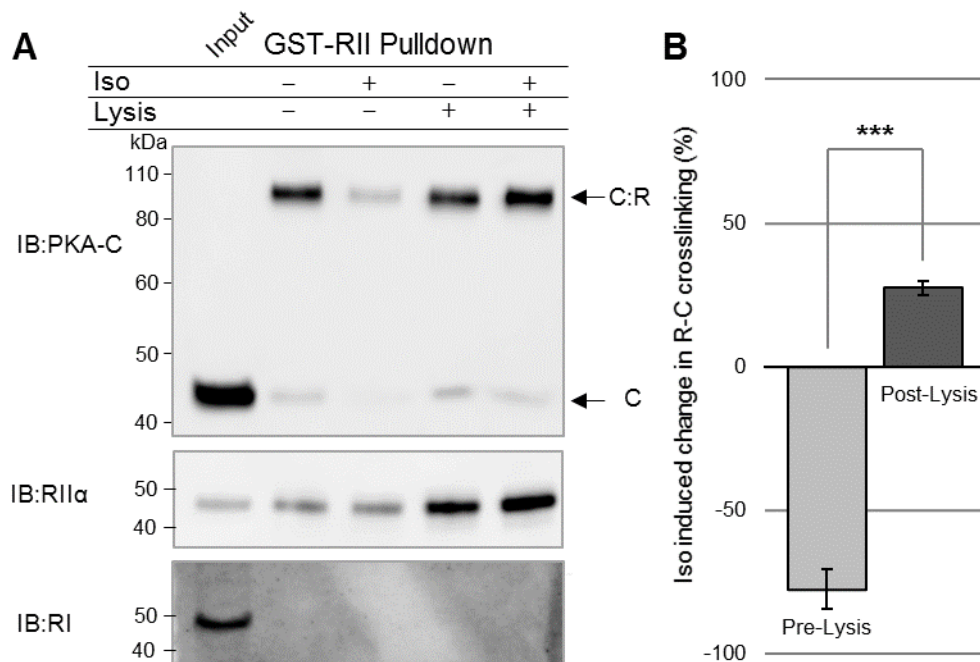


Figure 4.5 Effect of isoprenaline on RII-C association determined by light-induced crosslinking. A. HEK293T cells were incubated with 1 mM NHS-diazirine for 30 minutes. Following NHS-diazirine incubation, cells were treated with 1 M isoprenaline, or vehicle for 5 minutes. In pre-lysis illumination conditions (Lysis -, lanes 2 and 3), the cells were exposed to UV immediately, while in post lysis (Lysis +, lanes 4 and 5), lysate was incubated overnight before exposure to UV. **B.** UV treatment prior to lysis results in a decrease in subunit association of the isoprenaline treated condition of $77.72 \pm 6.8\%$ ($p < 0.01$, $n = 4$). When UV exposure follows lysis, there is a slight increase in subunit association of the isoprenaline treated condition, of $27.28 \pm 2.62\%$ ($p < 0.01$, $n = 4$).

I also analysed the association of C subunits to type I holoenzymes by RI selective pull down, which was not investigated by Smith and co-workers (**Figure 4.6**). In this case, there was a reduction in C subunit association following isoprenaline application in both the UV illumination conditions, before lysis, $-84.03 \pm 3.17\%$ ($n=4$, $p < 0.001$) and following lysis of $-62.68 \pm 4.75\%$ ($n=4$, $p < 0.001$). This uniform reduction, which contrasts that seen in the RII selective precipitation, may have stemmed from the hydrolysis of ATP in the lysate, which is required for type I holoenzyme binding, but not for type II. The reduction in C-RI association in the isoprenaline lysate may explain the slight increase in C-II association in the lysate.

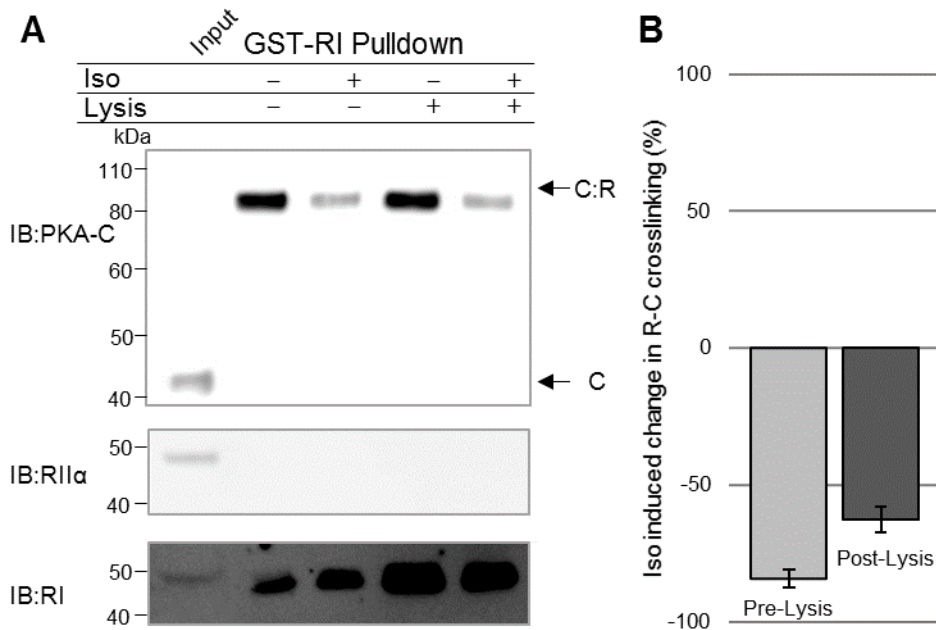


Figure 4.6 Effect of isoprenaline on RI-C association determined by light-induced crosslinking. A. HEK293T cells were incubated with 1 mM NHS-diazirine for 30 minutes. Following NHS-diazirine incubation, cells were treated with 1 μ M isoprenaline, or vehicle for 5 minutes. In pre-lysis illumination conditions (Lysis -, lanes 2 and 3), the cells were exposed to UV immediately, while in post lysis (Lysis +, lanes 4 and 5), lysate was incubated overnight before exposure to UV. **B** UV exposure both pre and post lysis exhibits a decrease subunit association for the isoprenaline treated condition $84.03 \pm 3.17\%$ ($n=4$, $p < 0.001$) and $62.68 \pm 4.75\%$ ($n=4$, $p < 0.001$) respectively. The difference between the reductions in both conditions is not statistically significant.

It is important to note that these quantifications represent only the relative change in immunoblot signal intensity, which is non-linear, and is dependent on many factors including the dynamic range of the antibody, the ECL, and the exposure time of the blot. Though the qualitative comparisons of relative increase or decrease within the experiment are relevant to the association state of the holoenzyme, they cannot be considered exact quantitative measures of R-C association.

4.3 Comparison of PKA activity to R-C subunit dissociation with different levels of β -adrenoceptor activation

On the basis of existing knowledge pertaining to RII cell membrane association and RI cytosolic localization, I hypothesized that the elevation of intracellular cAMP triggered by β -adrenoceptor agonists would induce the dissociation of type II holoenzymes at lower concentrations than type I. This change in association would manifest itself in our assay by a greater decrease in RII-C association than RI-C association following activation of the β -adrenergic receptors. In order to investigate this, I again turned to our regulatory subunit isoform-specific UV-induced crosslinking procedure. NHS-diazirine crosslinking and subsequent regulatory subunit specific precipitations were carried out as described above for the pre-lysis UV condition. Following NHS-diazirine incubation but prior to UV illumination, HEK293T cells in suspension were incubated with isoprenaline at concentrations ranging from 0-1000 nM for 5 minutes on a rolling mixer. Following this incubation, the cell suspension was transferred to a 10 cm dish and immediately UV illuminated for a further 5 minutes. Elution, immunoblotting, and quantification were carried out as described above.

Contrary to our expectations, our experiments did not detect an increased sensitivity to isoprenaline in RII-C association compared to RI-C association (**Figure 4.7 A**). Instead I saw a uniform decrease in association across the R subunit isoforms as the concentration of isoprenaline increased. I also assessed the dissociation dynamics of the holoenzyme, and found the half-maximal isoprenaline dose to be ~ 27 nM based on these experiments (**Figure 4.7 B**).

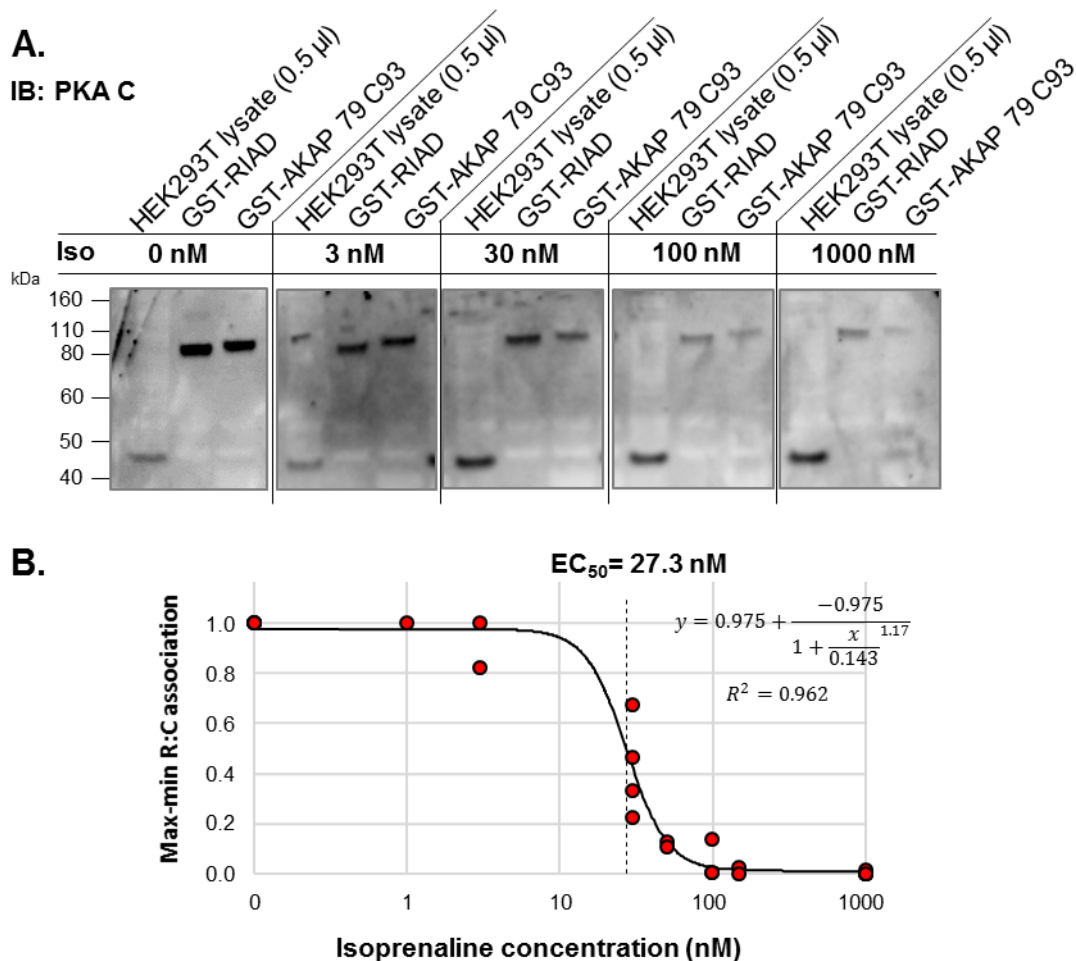


Figure 4.7 R subunit specific coprecipitation of C subunits isoprenaline titration. NHS-diazirine treated HEK293T cells were incubated with 0-1000 nM isoprenaline for 5 minutes, and subsequently UV illuminated for 5 minutes. Cells were then lysed and coprecipitate with R-subunit isoform specific baits. **A.** Representative blot of isoprenaline titration experiments. **B.** Logistic fit of normalized C-subunit association with both RI and RII subunits as calculated by fixing the maximum signal to 1, and the minimal signal to 0. From this combined data of 4 experiments the EC_{50} was determined to be 27.35 nM.

I was curious to determine how R-C subunit dissociation related to PKA activity following application of different concentrations of isoprenaline. To achieve this, I established a high-throughput plate reader assay that utilised the FRET-based PKA activity reporter AKAR4. AKAR4 combines the PKA phosphothreonine recognition site within the linker region of a fluorophore, with the phosphosubstrate binding FHA1 domain. Upon phosphorylation by PKA, the linker binds to the FHA1 domain, bringing the fluorophores within range of each

other (**Figure 1.10**). FRET ratios are then calculated by dividing emission intensity at a wavelength corresponding to FRET (535 nm filter) by fluorescent emission from the Cerulean donor (485 nm filter). The key advantage of the FHA1 domain (AKAR2-4) over the previously used 14-3-3 domain (AKAR1) is that its affinity for phosphothreonine is low enough to allow dephosphorylation (Zhang et al., 2005). This means that the calculated FRET ratio represents a measure of the instantaneous net phosphorylation and dephosphorylation, as opposed to the total phosphorylation activity.

HEK293T cells transiently expressing AKAR4 were distributed into 96-well plates. Baseline readings were taken at 420-485 and 420-535 nm. Subsequently, the wells were supplemented with 0 – 1000 nM isoprenaline, and further FRET measurements were collected at 30 second intervals for 20 minutes (n = 6, **Figure 4.8 A**).

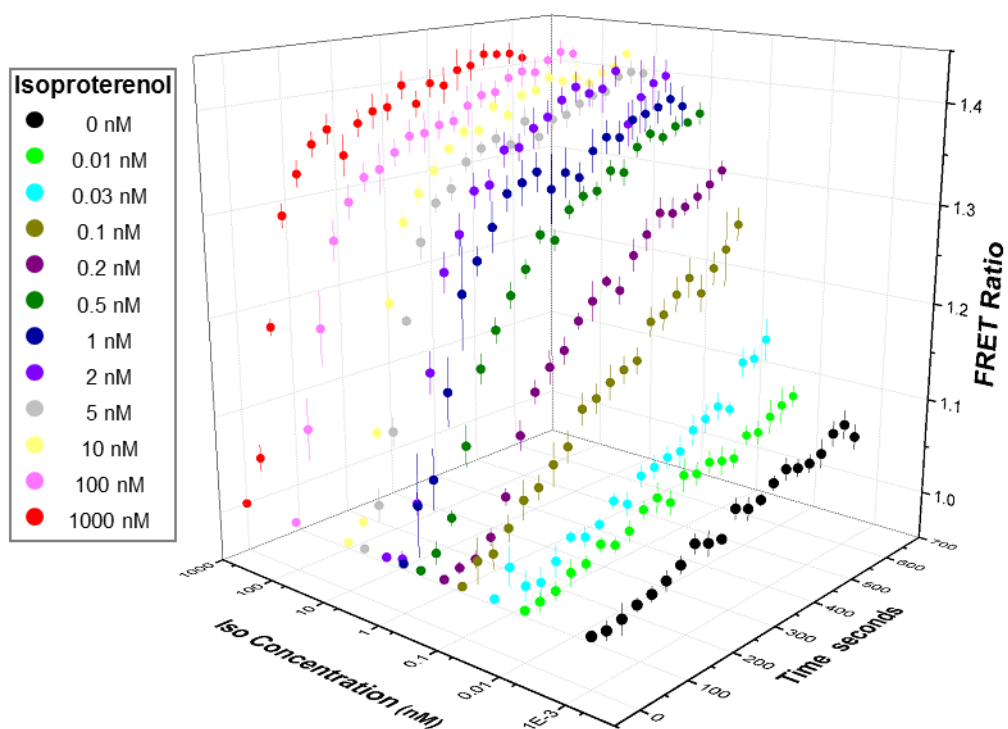


Figure 4.8 Isoprenaline induced PKA activity. A. HEK293T cells transiently expressing the FRET sensor AKAR4 were treated with isoprenaline concentrations from 0-1000 nM, and emission was measured approximately every 30 seconds for 10 minutes. FRET measurements are expressed as the ratio of the emission of the acceptor at 575 nm divided by the emission of the donor at 435 nm, normalized to the 0 time point emission ratio. Error bars represent standard error.

The isoprenaline concentration required for half-maximal PKA activation according to the AKAR4 reporter value was calculated for all time points from 2 minutes onwards as earlier measurements did not reach a minimum value. For all calculated points, the half-maximal fell below 0.5 nM.

However, while these results indicate the successful transfection, expression, and detection of the FRET reporter, proper controls were not performed. While a baseline was established before the experimental conditions were started, a maximum should have been determined for each measured well. Other authors have achieved this maximum through the application of the PDE inhibitor IBMX or the AC activator forskolin (DiPilato, Cheng, & Zhang, 2004; Herbst, Allen, & Zhang, 2011). The combination of which ensures the maximum concentration of cAMP in the cell is achieved, resulting in a measureable maximum value.

Using this maximum, a ratio of the experimental value to the dynamic range of the individual well, determined by subtracting the baseline measurement from the maximum measurement, should have been used to accurately characterize differences in intensity. Without this information, fluctuations in the cell population, transfection efficiency, protein expression, and cell surface adhesion of each individual well could all have drastically effected the results of the experiments.

4.4 C subunits do not preferentially associate with RI subunits immediately after cAMP signal termination

One of our aims in developing the NHS-diazirine/R subunit pull down approach was to test a novel hypothesis to explain how C subunits are restrained following their release from R subunits. The hypothesis was built on the knowledge that RII subunits are predominantly membrane-associated, and RI subunits cytosolic, and that β -adrenoceptor agonists are thought to elevate cAMP predominately in the vicinity of RII subunits. I hypothesised that C

subunits may associate with RI subunits after their release from anchored RII subunits following activation with β -adrenoceptor agonists such as isoprenaline. I applied our light-activated crosslinker/pull down approach, in tandem with further high-throughput FRET recordings, to test this hypothesis.

I treated HEK293T cells with 150 nM isoprenaline, followed 5 minutes later by 1 μ M propranolol, having pre-treated the cells with NHS-diazirine. After treatment with propranolol, different groups of cells were illuminated at 350 nM over 5 minutes time windows, either 0-5, 5-10, 10-15 minutes after propranolol addition. R subunit-specific pull down and immunoblotting were performed as before (**Figure 4.9**). I found no evidence of a preference for association with RI subunits compared to RII during the re-association phase. When crosslinking was induced between 5-10 minutes after propranolol addition both RI-C and RII-C crosslinking was up-regulated to a similar extent. When crosslinking was induced between 10-15 minutes after addition of propranolol, both RI-C and RII-C crosslinking had returned to their original levels prior to addition of isoprenaline.

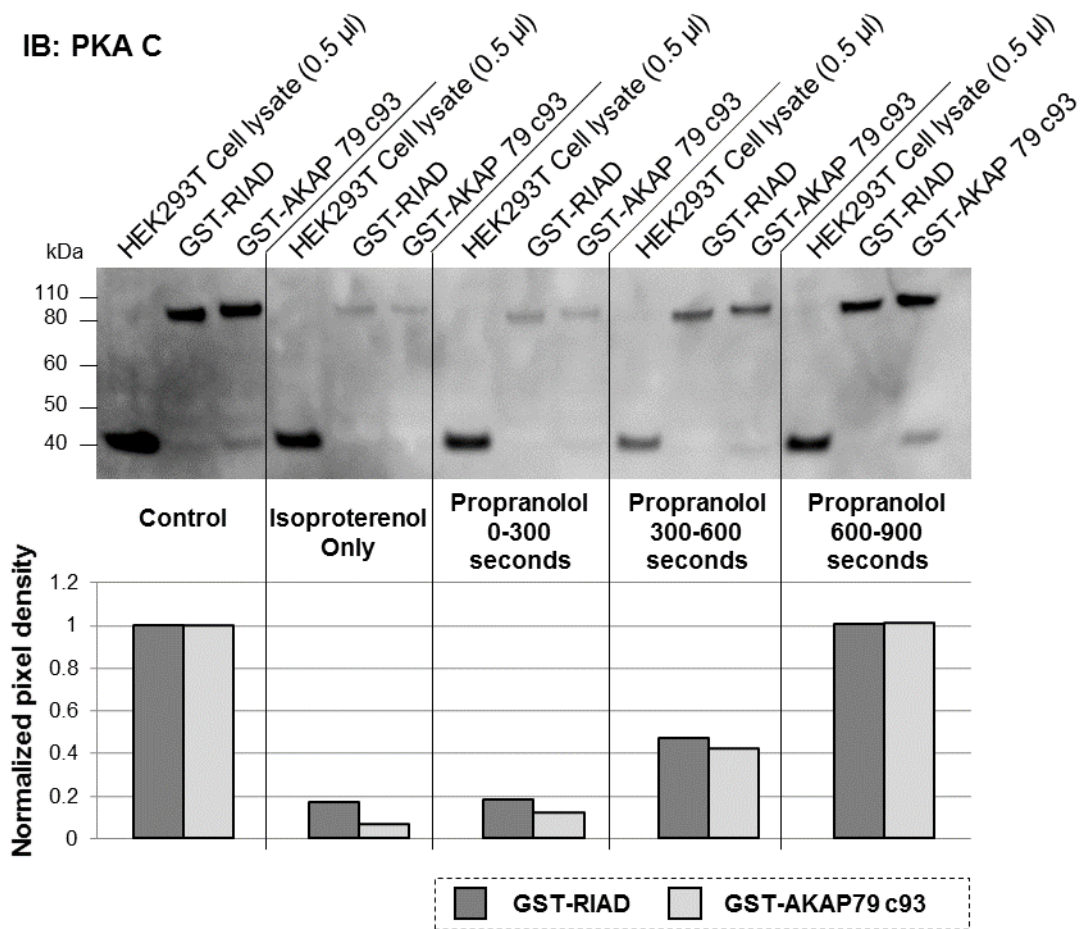


Figure 4.9 R-subunit specific pull down of propranolol treated HEK293T lysate. Reassociation of C subunits with regulatory subunits following deactivation of the β -adrenergic signalling cascade by propranolol was observed to result in equivalent isoform specific RI-C and RII-C association as seen in the absence of propranolol.

4.5 Conclusions from PKA activity investigations

I successfully developed an R subunit-specific pull down technique using D/D binding peptides, which was applied in conjunction with NHS-diazirine crosslinking. This method is the first to capture the association state of the C subunit under specific conditions. The somewhat unusual characteristic of PKA activation of the C subunit by dissociation from the R subunit, combined with the transient nature of the subunits means that this method is essential to understanding the dynamics of the regulation of C subunit activity. Having developed this method, I was able to show that the C subunit is indeed released from the R

subunit following application of a β -adrenoceptor agonist, and that this dissociation is reversed when signalling is terminated with the β -blocker propranolol. I also made the unexpected finding that substantial R-C subunit association is not required to yield high PKA activity. Our data suggest a mechanism in which short-lived free C subunit species shuttling between R subunits are sufficient to generate high PKA phosphorylation.

We also showed that contrary to the RI buffering hypothesis, the light-induced crosslinking method indicates that C subunits do not preferentially associate with RI subunits either during or following termination of cAMP signalling through β -adrenoceptors. This suggests that there may be a mechanism for restraining C subunits within the membrane following their release from anchored RII subunits. To investigate this idea, and other aspects of PKA quaternary structure, I turned to XL-MS as laid out in my final results chapter, **chapter 5**.

Chapter 5. Application of crosslinking coupled to mass spectrometry (XL-MS) to investigate PKA architecture

Calculation of PKA subunit stoichiometry in different tissues (**Chapter 3**) reveals that typically PKA RII subunits outnumber both C and RI subunits. Furthermore, monitoring of real-time association/dissociation of PKA C subunits from R subunits in HEK293T cells using light-activated crosslinking (**Chapter 4**) indicates that C subunits rapidly return to RII subunits following termination of cAMP signalling. My experiments in HEK293T cells are also consistent with C subunits predominantly reassociating with RII subunits rather than RI subunits prior to activation of cAMP signalling. I was interested to explore the structural basis of these properties using the novel technology for structural biology, crosslinking coupled to mass spectrometry (XL-MS).

XL-MS is a rapidly developing structural technique that is well suited to the investigation of large multi-protein complexes. I aimed to take advantage of XL-MS to address a number of outstanding questions concerning the structure of PKA including: how is the D/D domain of RII positioned relative to the CBD domains of RII and the PKA C subunit; how are RII-C complexes oriented relative to AKAP proteins and the membrane; and does association with AKAPs alter the conformation of RII-C complexes? In this chapter, I first describe how I prepared crosslinking samples (**Section 5.1**), before giving an overview of the datasets that I collected (**Section 5.2**). I describe structural insights garnered from XL-MS with RII-C complexes (**Section 5.3**), and RI-C complexes (**Section 5.4**). I also applied XL-MS to study RII-C associated with the prototypical AKAP, AKA18 α (**Section 5.5**), taking advantage of quantitative XL-MS to identify potential regions in RII-C that change conformation upon association with the AKAP. The study of PKA complexes is complicated by an inability to distinguish homo-dimeric interlinks from intralinks. Accordingly,

in the final section, I introduce a novel technical approach that I have developed that will be useful in future investigations of oligomeric proteins including PKA (**Section 5.6**).

5.1 Sample preparation

XL-MS experiments focused on isoforms of PKA subunits and AKAP18 α that predominate in the brain: RII β , RII β , C β , and AKAP18 α . All proteins were expressed in *E.coli* BL21 (DE3) and purified using glutathione sepharose and size exclusion chromatography (see **Methods 2.1.5** for details). Protein concentrations were determined by BCA assay, and verified by absorbance at 280 nm. 100 μ L mixes were assembled with proteins at the following concentrations: (1) 25 μ M C β + 25 μ M RII β ; (2) 25 μ M C β + 25 μ M RII β + 12.5 μ M AKAP18 α , and (3) 25 μ M C β + 25 μ M RII β . Each sample was incubated for 2 hours at 4 $^{\circ}$ C, before addition of 0.5 mM D₁₂/H₁₂-DSS. After incubation for 30 minutes at 30 $^{\circ}$ C, crosslinking reactions were terminated by addition of 5 μ L ammonium bicarbonate (1M). Each crosslinking sample was prepared in triplicate.

The effectiveness of crosslinking was assessed in each case by a combination of Coomassie staining, and western/far-western immunoblotting. **Figure 5.1** shows Coomassie-stained (**Figure 5.1 A**), anti-RII β IB (**Figure 5.1 B**), anti-Pan C IB (**Figure 5.1 C**), and far-western blotting using V5-tagged RII to detect AKAP18 α (**Figure 5.1 D**). In each panel, lanes 1 & 3 show samples prior to crosslinking, while lanes 2 & 4 contain protein loaded following 30 minutes incubation with DSS. In each panel, RII β -C β complexes are shown in lanes 1 & 2; RII β -C β -AKAP18 α complexes are shown in lanes 2 & 4. Across all of the detection methods, covalent DSS crosslinking is apparent by the appearance of polypeptides of higher molecular weight upon electrophoresis through the denaturing SDS-PAGE gel (**Figure 5.1**). In the Coomassie-stained gel, prior to crosslinking (lanes 1 & 3), RII, C and AKAP18 α migrate with apparent molecular weights of approximately 50, 40 and 12 kD, respectively. Upon crosslinking, prominent bands appear at \sim 100 and \sim 140 kD in the

RII-C sample, which likely correspond to crosslinked RII-RII and RII-RII-C species (Panel A, lane 2). For the RII-C-AKAP18 α sample, the crosslinked masses are shifted higher by ~ 10 kDa consistent with inclusion of AKAP18 α in these species (**Figure 5.1 A**, lane 4). The results of Anti-Pan C (**Figure 5.1 B**), anti-RI β (**Figure 5.1 C**) and far-western blotting with RII-V5 to detect AKAP18 α (**Figure 5.1 D**) are consistent with this assessment. For example, the $\sim 100/100$ kDa species stabilized by crosslinking is detected by anti-RI β antibody (**Figure 5.1C**, lanes 2 & 4) but not by anti-Pan C antibody (**Figure 5.1B**, lanes 2 & 4). Blotting with anti-Pan C antibody also revealed stabilisation of crosslinked 2RII-2C and 2RII-2C-AKAP18 α complexes at ~ 200 and ~ 210 kDa (**Figure 5.1B**, lanes 2 & 4) albeit at lower levels than the equivalent complexes containing a single copy of C subunit.

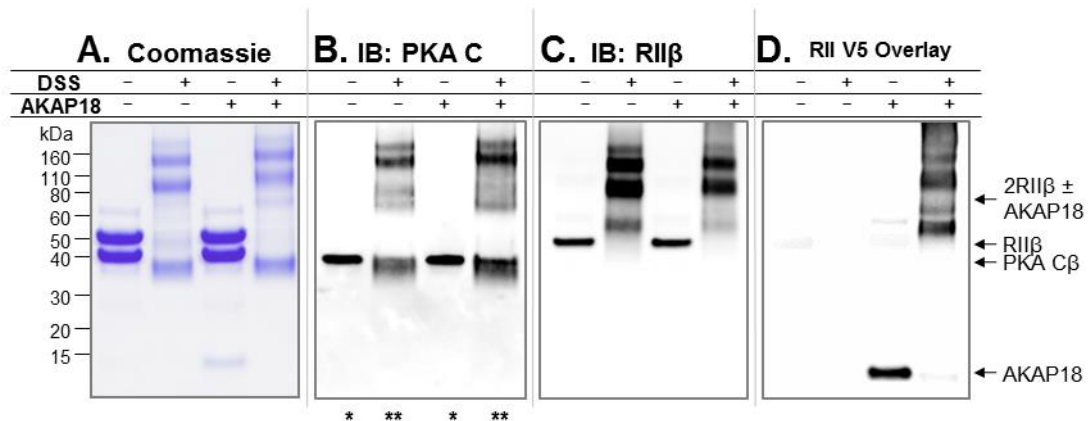


Figure 5.1 DSS crosslinking of PKA complexes. In all panels, lanes 1 and 2 correspond to equimolar mixtures of PKA C β and PKA RII β . Lanes 3 and 4 correspond to equimolar mixtures of PKA C β and PKA RII β with half the concentration of AKAP18 α . Samples in lanes 2 and 4 were run after DSS crosslinking. (A) Coomassie staining, 5 μ g protein (B) Anti-Pan C immunoblot *1.67 ng protein, ** 83 ng protein (C) Anti-RII β immunoblot, 50 ng protein (D) Far-western blot with RII α -V5 to detected AKAP18 α , 40 ng protein. The positions of monomeric, and crosslinked higher molecular weight species are indicated by arrows on the right-hand side. Anti-Pan C IB necessitated running 50-fold more (83 ng compared to 1.67 ng/lane) for the crosslinked samples (indicated by asterisks in lanes 2 & 4, panel B) since DSS crosslinking interfered by recognition using anti-Pan C antibody.

Having confirmed that addition of DSS to purified PKA complexes was leading to efficient crosslinking, I proceeded to analyse the samples using XL-MS.

5.2 Overview of XLMS data

Each sample was analyzed in technical duplicate such that 6 spectrometer runs were performed in total for each of the 3 PKA complexes analyzed (18 total runs). Once purification and crosslinking were completed, samples were processed using LC-MS/MS and peptides were identified using xQuest/xProphet software (see **Section 2.4.3**) by Florian Stengel at the University of Konstanz. I carried out crosslink analysis and position assignment using this data. Crosslinks with ID scores > 20 were included. **Table 5.1** summarises the number of intralinks (crosslinks within the same polypeptide), and interlinks (crosslinks between different polypeptides) detected in each of the three samples using these data quality cut offs.

Dataset	R-R intralinks	C-C intralinks	R-C interlinks	RII β -AKAP18 Interlinks	RII β -AKAP18 Interlinks	Total
RII β -C β	42 (26)	74 (21)	10 (5)	0	0	126 (52)
RII β -C β -AKAP18 α	20 (20)	50 (40)	3 (3)	1 (0)	1 (0)	75 (63)
RI β -C β	44 (44)	62 (60)	26 (4)	-	-	132 (108)

Table 5.1 Numbers of crosslinked peptides detected in PKA samples. The number of crosslinked peptides identified in the three PKA samples are listed, broken down into different classes. Numbers correspond to the number of crosslinks peptides detected with ID scores > 20. Peptides with both ID scores > 20, and false-discovery rates (FDRs) < 0.05 are shown in parentheses.

As an overall approximation of data quality, and also to understand typical crosslinking distances, I calculated distances between C α positions of crosslinked lysine pairs detected in this study when structural information was available (PDB IDs: 3TNP for RII-C; 4DIN for RI-C; 1Y6E for GST). This data should be considered with the important caveat that some interlinks between copies of the same protein may be erroneously assigned as intralinks – this is likely to be the case for distances > 40 Å; and the crystal structures may not represent true reflections of the

relative locations of paired lysines. Nevertheless, the distribution suggests that the most favorable distance for crosslinking is between ~ 10 - 25 Å (**Figure 5.2**).

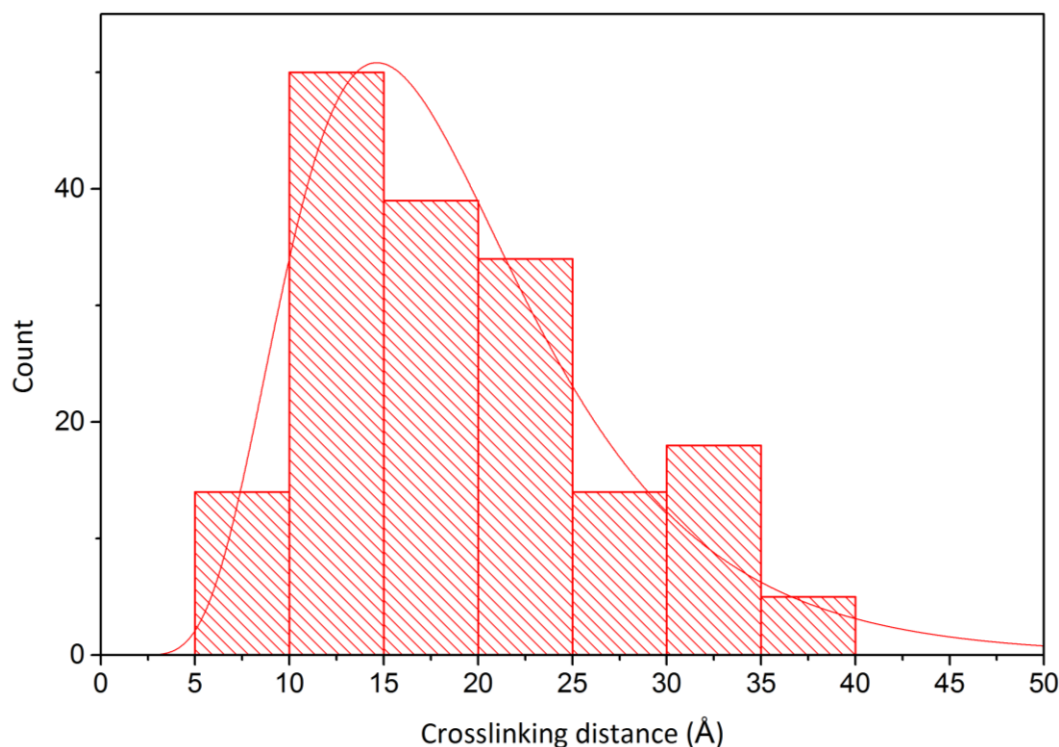


Figure 5.2 Distribution of crosslinking distances. Numbers of crosslinks are categorized in different classes depending on the separation of the $C\alpha$ positions of paired lysines with reference to crystal structures when such information was available. Crosslinks were omitted from this analysis where high-resolution structural information was unavailable.

5.3 XLMS analysis of RII-C holoenzymes

I first analyzed the $C\beta$ -RII β XL-MS dataset. Automated peptide identification from $C\beta$ -RII β sample spectra using the xQuest/xProphet pipeline yielded 126 crosslinks with an ID score above 20 (**Table 5.1, Supplementary table 1**). Mapping these crosslinks to the $C\alpha$ -RII β crystal structure (Zhang et al., 2012) provided matches for 102 of the 126 crosslinks (**Figure 5.3 A**). The remaining 24 links had either one or both partners in regions of PKA that were not visible in the electron density map. Where both lysines were modelled in the crystal structure, 84.4% of links fell within 30 Å. These calculations indicate that overall the crosslinks I observed are in agreement with the crystal structure.

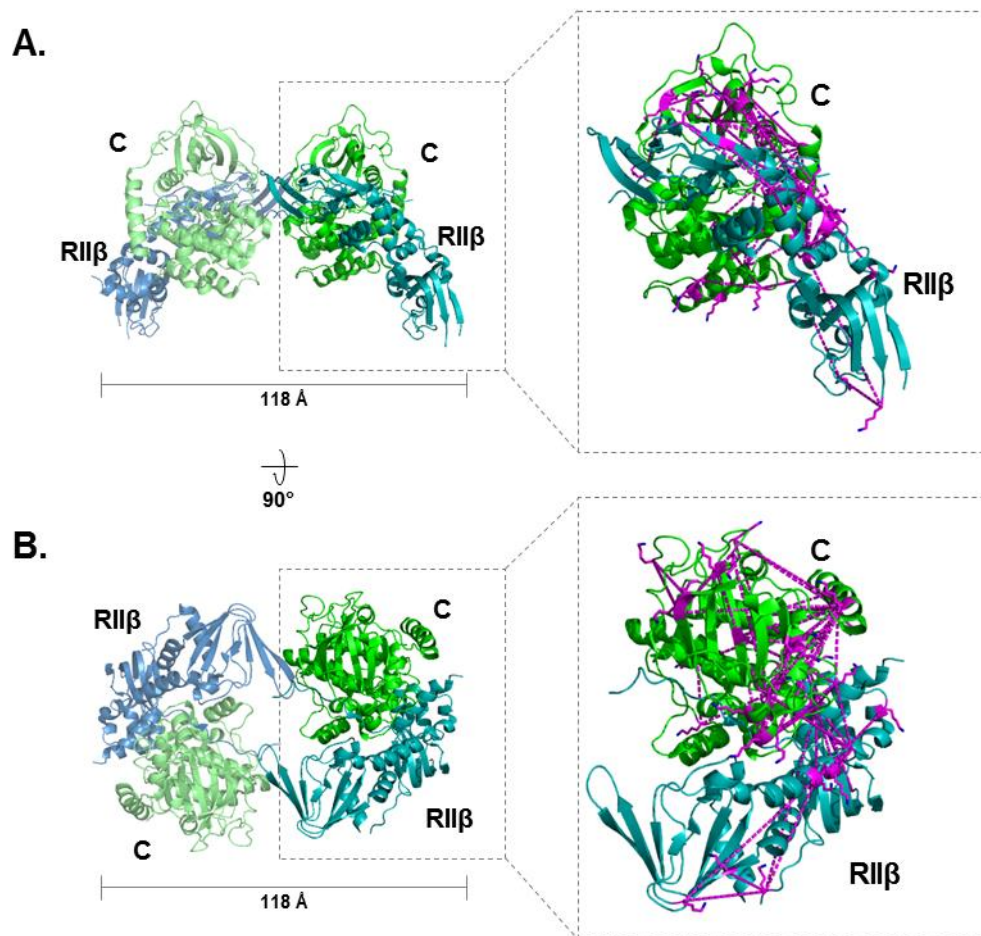


Figure 5.3 XL-MS analysis of C β -RII β holoenzyme. A. Location of the 102 crosslinked peptides (magenta) within the crystal structure (PDB ID 3TNP). B. Holoenzyme rotated through 90°.

The most important findings relate to crosslinks involving lysines that are missing from the crystal structure model (Taylor et al., 2013). In particular, 11 different peptides were detected corresponding to 9 different types of link with Lys44 in RII. Lys44(RII) is at the C-terminus of the second of two helices that folds into the bundle that constitutes the D/D domain. Due to the flexibility of the region linking the D/D domain and the first CBD of the RII subunit, amino acids N-terminal to the pseudosubstrate sequence of RII have never been resolved in the electron density of any crystal containing full-length RII subunits (Zhang et al., 2012). There are two conceivable positions for the D/D domain relative to the RII CBDs and C subunit on the basis of the position of Ile104 (the most N-terminal amino acid visible in electron density, PDB ID: 3TNP): either in the vicinity of the surface formed by the N-lobes of the C subunits (**Figure 5.4 A**, site A),

or near to the surface formed by the C subunit C-lobes on the opposite face of the complex (**Figure 5.4 A**, site B). I used spheres to represent the 30 Å potential binding radius around lysines that were detected as crosslinking partners of RIIβ Lys44 (**Figure 5.4 B**). Where these overlap is the likely location of Lys44 at the C-terminus of the RIIβ D/D. This analysis indicates that the RIIβ D/D is on the side of the complex next to the surface of the C subunit C-lobes (**Figure 5.4 A**, site B). This finding has functional ramifications, as it determines the orientation of RII-C complexes towards anchoring sites and by extension to the cell membrane.

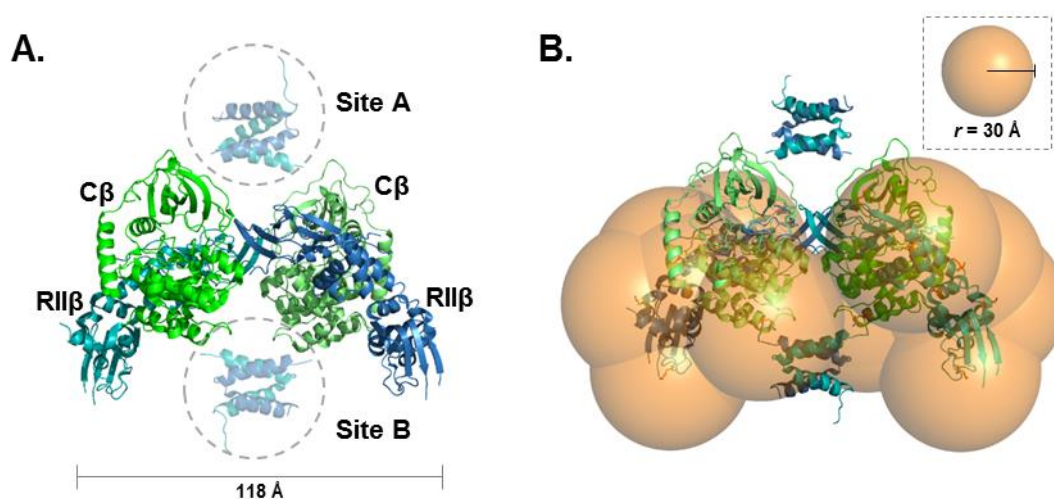


Figure 5.4 Location of the docking and dimerization domain in the C β -RII β holoenzyme. Though the crystal structure of the holoenzyme using full length constructs has been solved, the N-terminal flexible linker region is absent from the electron density raising questions about its positioning. **A.** The two potential positions of the D/D are shown within dotted circles. **B.** The data showing one crosslinking to the Lys44 in the D/D indicates that the D/D is positioned in the cleft between the R subunits. Spheres represent the 30 Å binding radius of the crosslinker.

5.4 XLMS analysis of RI-C holoenzyme

I next considered XL-MS data from crosslinked C β -RI β . XL-MS analysis of C β -RI β returned 92 crosslinks with an ID score above 20. Of these crosslinks only 53.2% fall within 30 Å when plotted on the published 2C-2RI tetrameric structure (Ilouz et al., 2012) (**Figure 5.5, Supplementary table 2**). However, the RI-C crystal structure indicates that there is potential for extensive homodimeric (RI-RI' or C-C') crosslinking in the RI-C tetramer. There is no way to distinguish

homodimeric interlinks from intralinks within the dataset. Of the observed crosslinks, 26 crosslinks have binding partners that are close enough in both the inter- and intra- heterodimer to be ambiguous (**Figure 5.5**). The prevalence of this problem in the RI rather than RII dataset likely arises from the finding that the RII β holoenzyme forms a ring with a cavity in the center, while RI β subunits make contact with one across the center of the holoenzyme (Ilouz et al., 2012; Taylor et al., 2012; Zhang et al., 2012). This problem highlights one of the key shortcomings of existing XL-MS methods, and is the focus of **section 5.6**. This ambiguity is illustrated in **figure 5.4**, in which the interlinks (magenta) and intralinks (teal) which stem from the same lysine residues and fall under 35Å are shown.

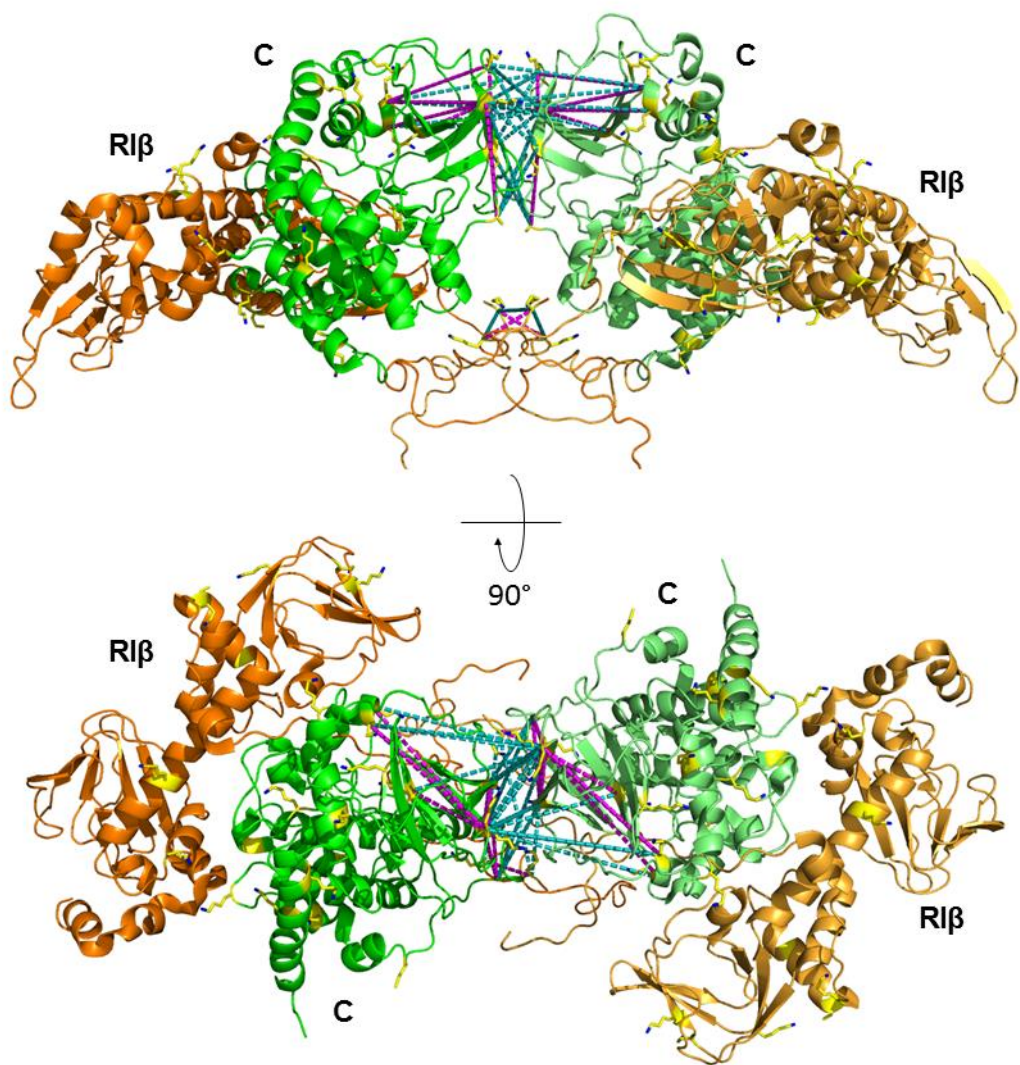


Figure 5.5 Challenges in crosslink assignment in C β -RI β complex. A. Using XI-MS, 92 crosslinks were identified with an ID score over 20 that span a distance of 35 Å. However, there is ambiguity as to the binding partners

of these links. Some binding partners fall within 35 Å of one another in all peptides, meaning they are both potential interlinks (teal) and intralinks (magenta), highlighting the problem posed by homomeric protein assemblies (PDB ID 4DIN).

Recent work carried out by the Taylor lab has shown that while the heterodimeric architecture of each C-R subunit pair is similar between all four R subunit isoforms, the final tetrameric structures differs substantially (Ilouz et al., 2012). The sequence and three-dimensional structure of the four R subunit isoforms are highly conserved throughout the two CBDs, especially between isoforms (Figure 5.6). However, there is much lower conservation of sequence between the N-terminal linker regions of the subunits (Figure 5.6; Ilouz et al., 2012). Though the pseudosubstrate sequences (Figure 5.6 B, red) share a similar sequence, differences in the way these highly variable and flexible N-terminal regions assemble explain how strikingly different quaternary structures can be assembled from the same basic building blocks.

A.

Percent Identity Matrix

	Human RI α	Human RI β	Human RII α	Human RII β
1: Human RI α	100.00	68.57	21.67	20.95
2: Human RI β	68.57	100.00	21.67	23.81
3: Human RII α	21.67	21.67	100.00	45.97
4: Human RII β	20.95	23.81	45.97	100.00

B.

R subunit D/D and N-linker

```

Human RI $\alpha$  (1-60) | MESGSTAASEEARSLRECELYVQKHNIQALLKDSIVQLCTARPERPMAFLREYFERLEKE
Human RI $\beta$  (1-60) | MASPPACPSEEDESLKGCELYVQLHGIQQVLKDCIVHLCISKPERPMKFLREHFERLEKE
Human RII $\alpha$  (1-43) | -----MSHIQI PPGLTELLQGYTVEVLRQQPPDLVEFAVEYFTRLREA
Human RII $\beta$  (1-42) | -----MSIEIPAGLTELLQGFTEVLRHQPADLLEFALQHFTRLQQE
                        :  :*  :  *.:  :*  : *  :*:  :*.
Human RI $\alpha$  (61-87) | EAKQIQNLQKAGTRTDSR-----EDE---I----SPPPP
Human RI $\beta$  (61-87) | ENRQILARQKSNSQSDSH-----DEE---V----SPTPP
Human RII $\alpha$  (44-87) | RAPASVLPAAATPRQSLGH-----PPPEPGPDRVA-----DAKGDSESEEDLE
Human RII $\beta$  (43-102) | NERKGTARFGHEGRWTGDLGAAAGGTPSKGVNFAEPEMQSDSEDEEEEEAAPADAGAFN
                        .      :  :  .
Human RI $\alpha$  (88-140) | NPVVKGRRRRGAISAEVYTEEDA--ASYVRKVI PKDYKTMAALAKAIEKNVLFSH
Human RI $\beta$  (88-140) | NPVVKARRRRGGVSAEVYTEEDA--VSYVRKVI PKDYKTMTALAKAISKNVLFSAH
Human RII $\alpha$  (88-140) | VPVPSRFNRVSVCAETYNPDEEEDTDPRVIHPKTDEQRCRLQEACKDILLF--
Human RII $\beta$  (103-140) | APVINRFTRRASVCAEAYNPDEEEDDAESRIHPKTDD-----
                        ** .  ** .:*.*. .:  :  *  : ** .

```

Figure 5.6 Primary sequence comparisons of R subunit isoform N-termini. A. Percent identity comparisons for the four R subunit isoforms. B. Sequence alignment of the R subunit isoforms. The inhibitor site is shown in red, docking and dimerization domain in orange.

5.5 Architecture of RII β -C β complex in relation to AKAP18 α

Our remaining experiments focused on understanding how a prototypical A-kinase anchoring protein (AKAP) interacts with the RII β -C β complex, and whether the anchoring protein has any effect on this PKA complex upon binding. I focused on the short isoform of AKAP18 α . Although only 81 amino acids in length, AKAP18 α possesses many typical AKAP properties that make it a suitable prototype for understanding PKA anchoring: it contains an amphipathic helix (amino acids 27-48, Götz et al., 2016) that binds with high affinity to PKA D/D domains (Fraser et al., 1998; Gray et al., 1998); it contains lipid modification sites in its first 6 amino acids that enable association with the membrane (Fraser et al., 1998); and it is involved in targeting PKA for regulation of voltage-gated ions channels (Tibbs et al., 1998). This shortest isoform of AKAP18 is highly expressed in the brain (Jones et al., 2012). I chose to focus on AKAP18 interactions with RII β -C β complex because the concertina-like structure of RII β -C β is more amenable to XL-MS than RI β -C β in which the both the R-R and C-C dimeric interfaces are larger (Ilouz et al., 2012). In addition, RII subunits are typically anchored to AKAPs unlike RI subunits for whom anchoring is considered exceptional (Means et al., 2011). XL-MS with purified RII β -C β -AKAP18 α complex led to the identification of two interlinks involving AKAP18 α with ID scores > 20 (**Table 5.2, Supplementary table 4**).

No.	Peptide Sequence	Site A	Site B	ID score
1	FGNL <u>K</u> NGVSDIK-ICE <u>K</u> DR-a5-b4	C β K286	AKAP18 α K19	24.44
2	AVQQYLEETQNKKQPGEENST <u>K</u> AEEGDR - <u>K</u> MYESFIESLPFLK-a22-b1	AKAP18 α K65	RII β K263	21.07

Table 5.2 Interlinks detected between AKAP18 α and RII β -C β .

Peptide '1' involves K19 of AKAP18 α , which lies between its N-terminal lipid attachment sites and its R subunit anchoring helix, which begins at amino acid 27. Peptide '2' links AKAP18 α K65 near to the anchoring protein's C-terminus (**Table 5.2**). As shown in **figure 5.8**, these crosslinking sites are consistent with the position of the D/D domain close to the C-termini of the C subunits,

and suggest that AKAP18 anchors PKA such that the N-terminus of the C subunit (which is myristoylated *in vivo*), is oriented towards the cell membrane.

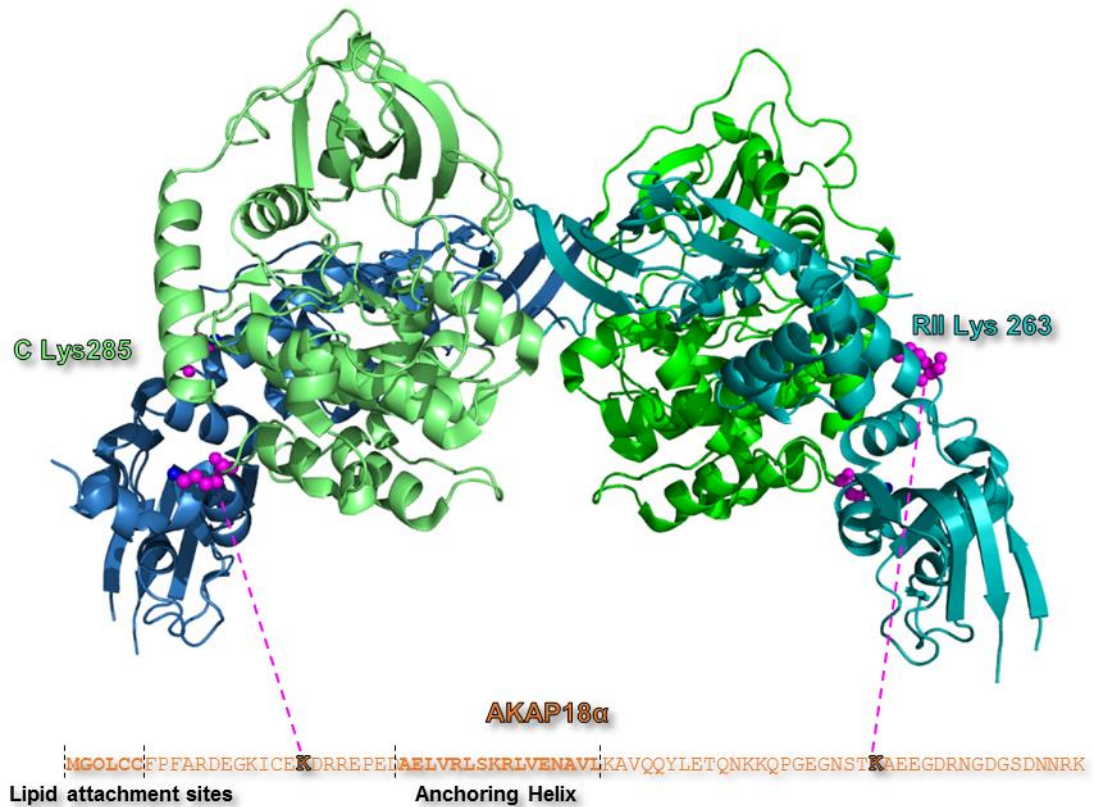


Figure 5.8 Interlinking sites between AKAP18 α and RII β -C β . Two interlinks were detected: their locations in the primary sequence of AKAP18 α and in the structure of RII β -C β are shown. PDB: 3TNP (Zhang et al., 2012).

5.6 Dynamics in RII β -C β structure upon binding AKAP18 α

I also took advantage of a novel technique, quantitative XL-MS (qXL-MS), to investigate whether association with AKAP18 α alters the conformation of the RII β -C β complex. Changes in the abundance of particular crosslinks may result from either alterations in the distance between lysines (which may indicate a conformational change), or steric blocking of particular crosslinking sites upon binding of an additional protein (which may reveal a protein binding site). To perform qXL-MS, I compared the intensities of peaks eluting for crosslinks between the RII β -C β and RII β -C β - AKAP18 α samples (n=3, each sample analysed in duplicate). The analysis was limited to

peptides that were identified and scored consistently over all samples, and that were not obscured by over-shadowing from other peaks. Overall, 45 different crosslinked lysine pairs were compared between the two samples. **Table 5.3** lists eight crosslinking sites whose abundance was found to change by a log₂-ratio of either > 0.65 or < -0.65, and with $p < 0.01$ (**Supplementary table 2**).

Dynamic Crosslink	Change upon addition of AKAP18 α	Ratio (+AKAP18/-AKAP18)	p value
RII β K285 - RII β K324	Decrease	0.186	1.32×10^{-9}
C β K267 - RII β K44	Decrease	0.345	2.58×10^{-3}
RII β K263 - RII β K44	Decrease	0.387	1.58×10^{-5}
RII β K285 - RII β K44	Decrease	0.424	1.3×10^{-6}
RII β K357 - RII β K44	Decrease	0.462	1.17×10^{-4}
C β 77 - C β 84	Increase	1.64	4.07×10^{-6}
C β 22 - C β 84	Increase	1.92	2.23×10^{-4}
C β 17 - C β 293	Increase	2.12	1.26×10^{-6}

Table 5.3 Crosslinks in RII β -C β affected by association with AKAP18 α . Crosslinks that exhibited abundance changes upon addition of AKAP18 α are listed, where $p < 0.01$, and where the log₂-ratio (+AKAP18/-AKAP18) was either > 0.65 or < -0.65. The full dataset included crosslinks whose abundance changed less markedly is listed in **supplementary table 1**.

Five of these most dynamic crosslinks were found to substantially decrease upon addition of AKAP18 α (**Table 5.3**). The greatest change in intensity occurs between RII β 285 and Lys333 (**Figure 5.9 A**, 5.4-fold decrease). These two lysines are located at either end of the CBD2. The four other decreasing links all involve linkages between Lys44 at the C-terminus of the D/D: three links to RII CBD2 (RII β Lys263, Lys285 & Lys357), and one to the C subunit C-lobe (C β Lys267). This pattern of down-regulated links is consistent with the position of the D/D proposed from the RII β -C β XL-MS dataset: in proximity to the CBD2 of RII and C subunit C-lobes. Association with AKAP18 α likely sterically blocks coupling between these crosslinking sites that either

involve the D/D or are close to the position of the D/D. A model of the PKA RII β -C β holoenzyme is shown in **figure 5.9** that was assembled by combining crystal structures of the 2C α -2RII β tetramer (PDB ID: 3TNP), the RII α D/D in complex with AKAP18 α (Götz et al., 2016, PDB ID: 4ZP3), and myristoylated C α subunit (Zheng et al., 1993, PDB ID: 1CMK). It should be noted that this representation is of the C α isoform, while our crosslinking experiments were carried out using the C β isoform. However, there is 93% sequence identity between the two isoforms. The last visible amino acid in the RII D/D (PDB ID 4ZP3) is Arg43, so the important crosslinking position Lys44 is modeled immediately C-terminal to this position (**Figure 5.9**).

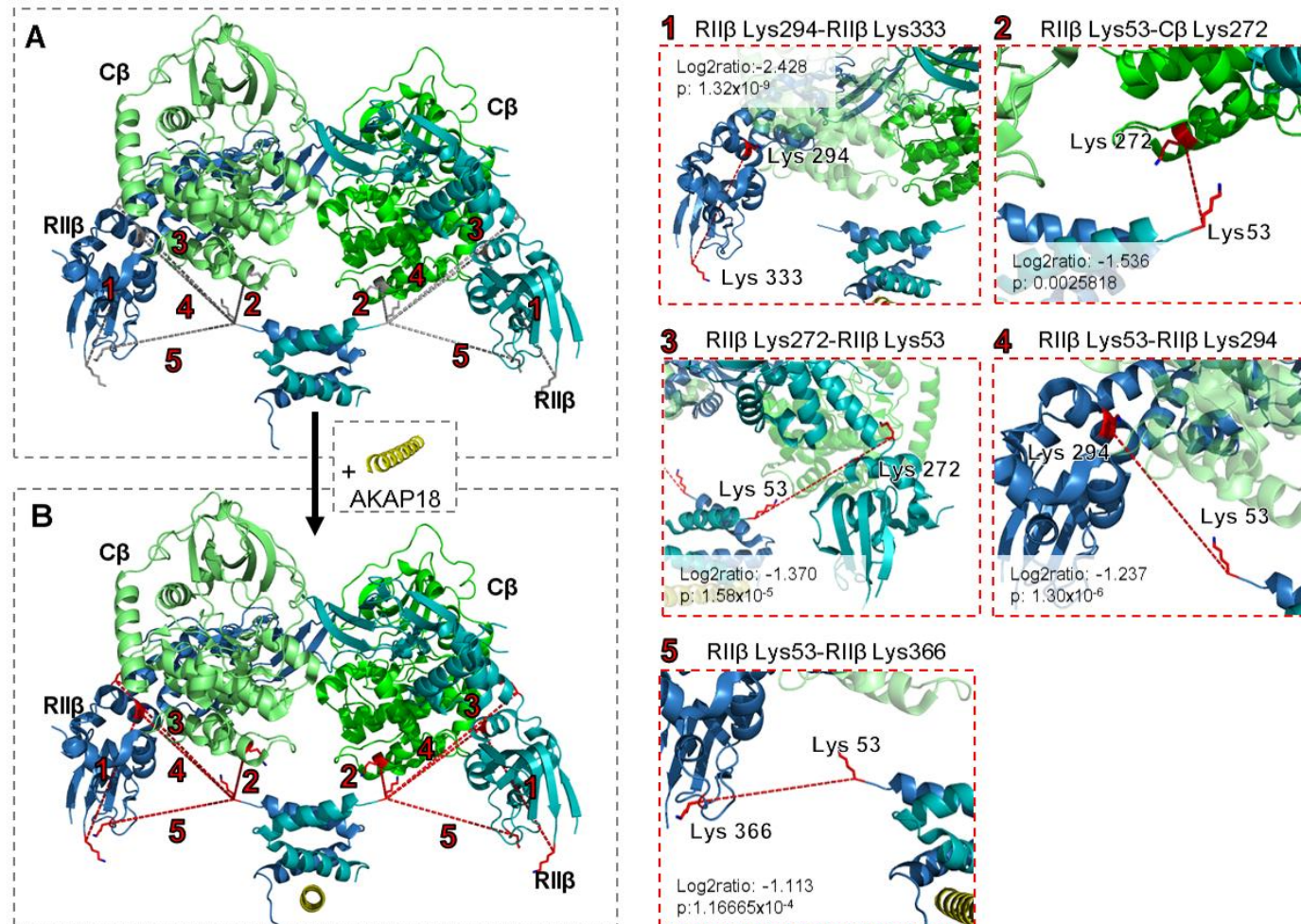


Figure 5.9 Visualization qXL-MS of PKA C β -RII β with or without AKAP18 α . **A.** The position of crosslinks before the addition of AKAP18. **B.** Crosslinks that decreased in intensity following the addition of AKAP18. All variable crosslinks identified by the xQuest/xProphet/xTract pipeline were manually verified by comparison against the crystal structure. Positions of the five significant crosslinks ($|\log_2\text{-ratio}| > 1$, $p < 0.01$) are indicated by a number corresponding to the close up at the right. The initial states of crosslinks are in the reference set are indicated in gray. II. Crosslinks that exhibited reduced intensity when complexed with AKAP18 α are shown in red (1-5).

Three crosslinks met the criteria for up-regulation upon the addition of AKAP18 α (**Table 5.3**). All three are C β subunit intralinks that reveal a structural rearrangement within the C subunit N-lobe upon addition of AKAP18 α . Two of the links (C β Lys22- Lys84 & Lys17- Lys293) involve linkages with the N-terminal helix, which is myristoylated *in vivo*. The myristoyl group binds to a hydrophobic pocket formed by nine residues from both lobes of the C subunit (**Figure 5.10**, myristoyl group shown in pink, binding pocket in purple) (Bastidas et al., 2012). The N-terminus of the C subunit (residues 1-39) falls outside of the conserved region of AGC kinases, and differs between PKA isoforms (**Figure 5.10**). As discussed in the introduction, Gaffarogullari and colleagues propose a two state model for the N-terminus: *myr-in* or *myr-out* on the basis of NMR using myristoylated and non-myristoylated C subunit (Gaffarogullari et al., 2011). The assumption is that the *myr-out* conformation supports C subunit association with the membrane through insertion of the myristoyl group into the lipid bilayer (Gaffarogullari et al., 2011). Our crosslinking analysis also shows that binding of an AKAP to the RII subunit induces dynamics within this same region, perhaps also inducing the *myr-out* conformation. This could further support targeting of the C subunit to the cell membrane. Our crosslinking data show that the D/D and AKAP18 membrane binding regions are located such that the N-terminus of the C subunit is oriented towards the membrane. It is possible that the AKAP further supports targeting of the C subunit to the membrane by stabilizing the *myr-out* conformation of the myristoylated N-terminal helix.

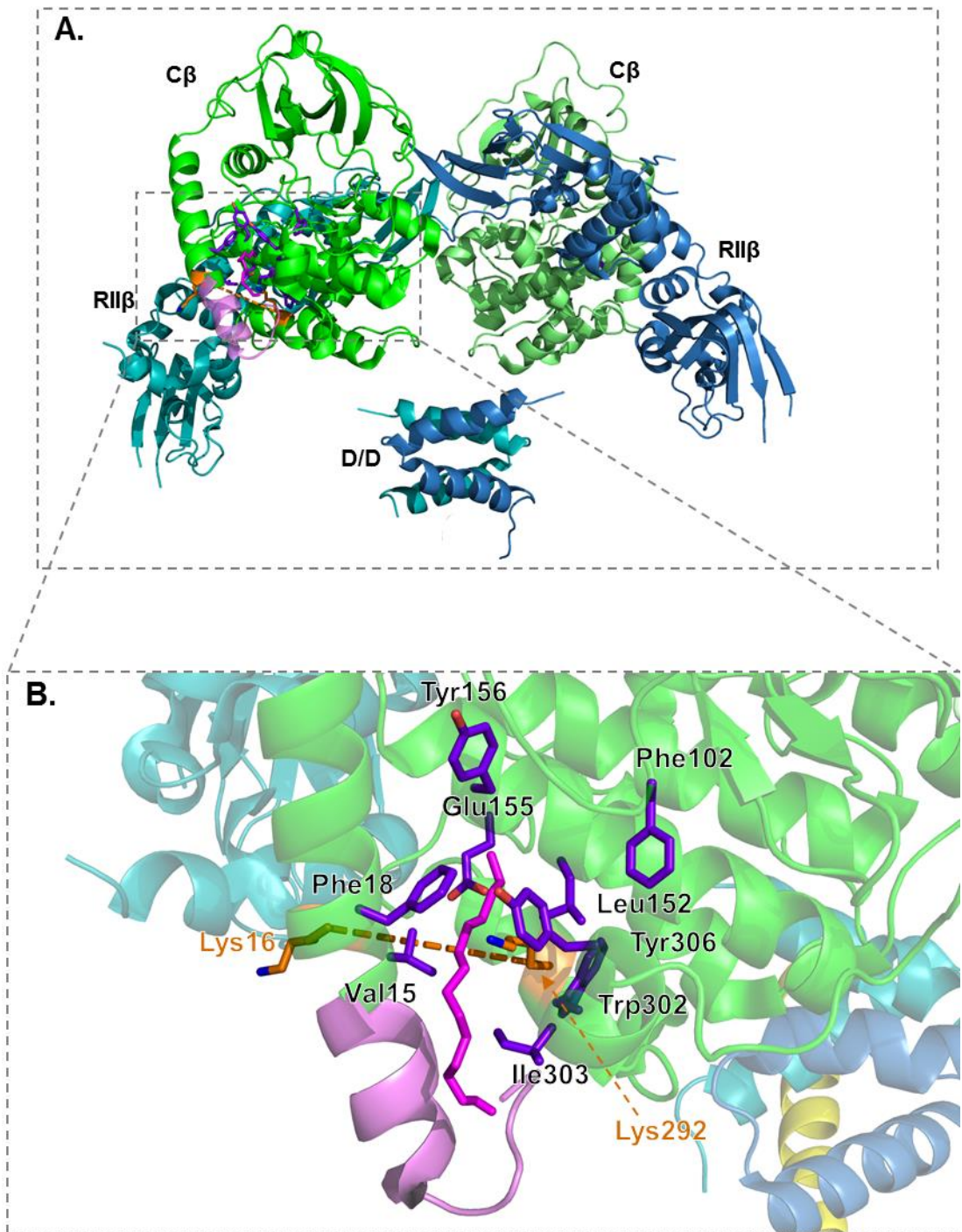


Figure 5.10 C subunit myristoylation site. **A.** Position of the myristoyl binding pocket in the C subunit in the PKA complex. **B.** The nine residues that make up the binding pocket contacts of the myristoylation binding pocket (purple), which span the N and C lobes of the C subunit are shown in contact with the myristoyl group of the N-terminus (pink). This representation combines the holoenzyme structure of the α -RII β holoenzyme crystal structure (PDB: 3TNP) with the 13 N-terminal residues and myristoyl group of the myristoylated α structure (PDB: 1CDK) as no holoenzyme crystal structure which contains the N-terminus has been solved. The crosslink between Lys16(C)-Lys292(C), which increases in intensity following AKAP18 α binding, is shown in orange.

5.6 Development of XL-MS using isotopically-labelled oligomeric proteins

One limitation of the XL-MS experiments with PKA was that I am unable to distinguish cross-dimer interlinks from intralinks within a heterodimer. For example, in the C β -RI β complex, it would be interesting to test whether trans-dimer C β -C β interlinks are consistent with the close apposition of the two C β protomers observed in the crystal structure (PDB ID 4DIN, Taylor et al., 2012). During the latter part of my doctoral studies, I developed and validated a novel approach that takes advantage of heavy amino acid isotopes. The approach builds on stable isotope labelling by amino acids in culture (SILAC; Ong, 2002), and a method for expressing proteins containing isotopically labelled lysine and arginine in bacteria (Matic et al., 2011). I took advantage of the heavy isotopes L-lysine (4,4,5,5-D₄, Cambridge Isotope Laboratories item number DLM-2640-PK), which is 4.025108 Da heavier than light L-lysine, and L-arginine (13C₆; 15N₄, Cambridge Isotope Laboratories item number CNLM-539-H-PK), which is 10.00826 Da heavier than light L-arginine. I focused on the protein glutathione S-transferase (GST) that forms constitutive dimers in establishing the approach. The following sections describe the procedure for expressing isotopically-labelled protein (**Section 5.6.1**), forming dimers of light and heavy GST (**Section 5.6.2**), and how MS identification of interlinks between light and heavy GST enable cross-dimeric interlinks to be distinguished from intralinks (**Section 5.6.3**).

5.6.1 Expression of isotopically-labelled test protein (glutathione S-transferase)

The first challenge was to establish a method for incorporating lysine and arginine into target proteins with the incorporation of heavy amino acids approaching 100%. To achieve this, I exploited an *E. coli* strain that is auxotrophic for lysine and arginine. This strain of auxotrophic *E. coli* was a gift of Ronald T. Hay of the Wellcome Trust Centre for Gene Regulation and Expression, College of Life Sciences, University of Dundee. This cell line, *E. coli* BL21 (DE3)

Δ Arg/Lys, was generated by knocking out the *lysA* and *argA* genes in the popular protein *E. coli* BL21 (DE3) expression strain (Matic et al., 2011). *LysA* encodes the enzyme diaminopimelate-decarboxylase, which decarboxylates the L-aspartate derived meso-diaminopimelate to create lysine (Hu et al., 2008), whereas *ArgA* encodes the enzyme N-acetylglutamate synthase, which acetylates L-glutamic acid in the first step of arginine synthesis (Marvil & Leisinger, 1977).

In order to validate our novel approach, I chose the constitutively homodimeric protein, glutathione-S-transferase (GST) as our test protein. I took advantage of the vector pGEX-6P-1 to express GST. The 26 kDa GST encoded by pGEX6P1 is from the parasitic flatworm *Schistosoma japonicum*, and has been widely adopted as an affinity tag for the purification of proteins by binding to immobilized glutathione (Harper & Speicher, 2011; Rufer et al., 2005; Smith & Johnson, 1988). *Schistosoma japonicum* is one of the three main species of schistosomes which infect humans, causing a condition known as schistosomiasis, in which the immune response to schistosome eggs causes the formation of granulomas which lead to extensive tissue damage and often death (Colley, et al., 2014; McTigue, Williams & Tainer, 1995). The preferred treatment for schistosomiasis is the administration of the small molecule drug praziquantel which has been shown to bind to schistosomal GST and interfere with transport mechanisms (Colley, et al., 2014; McTigue, Williams, & Tainer, 1995). This clinical importance, in tandem with its utility as an affinity tag, has led to a large supporting of body of research including crystal structures of GST that encouraged us to focus on this protein to validate the approach. Before proceeding to protein expression, purification and crosslinking, I first verified that the Δ Lys/Arg *E. coli* behaved as expected (**Figure 5.11**). The cells were rendered competent and transformed with pGEX-6P-1. An overnight culture of the cells in LB/ampicillin was used to inoculate M9 minimal media with different additives (**Figure 5.11**). Whereas cells with either no supplements (**Figure 5.11** red), lysine alone (yellow), or arginine alone (orange) were unable to grow, addition of both lysine and arginine enabled cell growth to approaching $OD_{600\text{ nm}} = 1$ (green). Having

confirmed that the transformed cells were unable to synthesize arginine and lysine from carbon sources in the media, I proceeded to protein production and crosslinking.

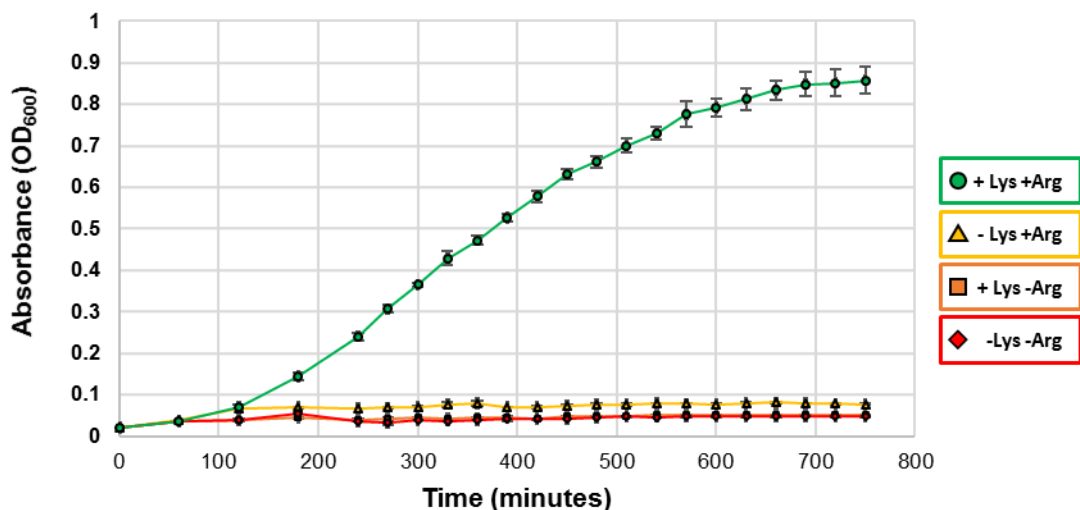


Figure 5.11 Lys/Arg auxotrophic bacteria growth curves. Growth curves are shown for Δ Lys/Arg auxotrophic BL21 (DE3) *E. coli* cells transformed with pGEX6P1. Cells were grown in M9 minimal media + ampicillin at 37°C with either no supplements (red), arginine (orange), lysine (yellow) or both arginine and lysine (green). As expected, only cells supplemented with both amino acids (green) were able to grow

5.6.2 Preparation of purified light-heavy GST dimers

E. coli BL21 (DE3) Δ Arg/Lys were used to express either light GST, using LB, or isotopically Lys/Arg-labelled GST (M9 minimal media supplemented with (4,4,5,5-D₄) L-lysine and (13C₆; 15N₄) L-arginine). Light (**Figure 5.12 A**) and heavy (**Figure 5.12 B**) GST were purified separately using the same approach: affinity to glutathione sepharose, followed by elution with 10 mM L-glutathione and size exclusion chromatography using a Superdex 200 column. GST binds to itself very tightly, so in order to generate mixed light/heavy dimers, I could not rely on spontaneous exchange between light-light and heavy-heavy dimers (Hornby et al., 2000). Previous work has shown that the application of the chaotropic agents urea or guanidine hydrochloride can dissociate the dimer (Hornby et al., 2000). I mixed light and heavy GST dimers in 6 M urea at 30°C for 30 minutes to induce dissociation into monomers (**Figure 5.12 C**) on the basis of these studies (Hornby et al., 2000). An all-light GST control was also included. Following urea dissociation, the urea concentration of the buffer was reduced by rounds of dilution and

centrifugal concentration to bring about dimerization including formation of mixed light-heavy dimers. Hornby and co-workers showed that the folded native dimer reforms below 4 M urea, and trace amounts of urea are compatible with MS/MS preparation and processing (Hornby et al., 2000). Finally, 100 µg aliquots of light GST and light/heavy were crosslinked in triplicate with D₁₂/H₁₂-DSS and processed as normal for analysis on the spectrometer.

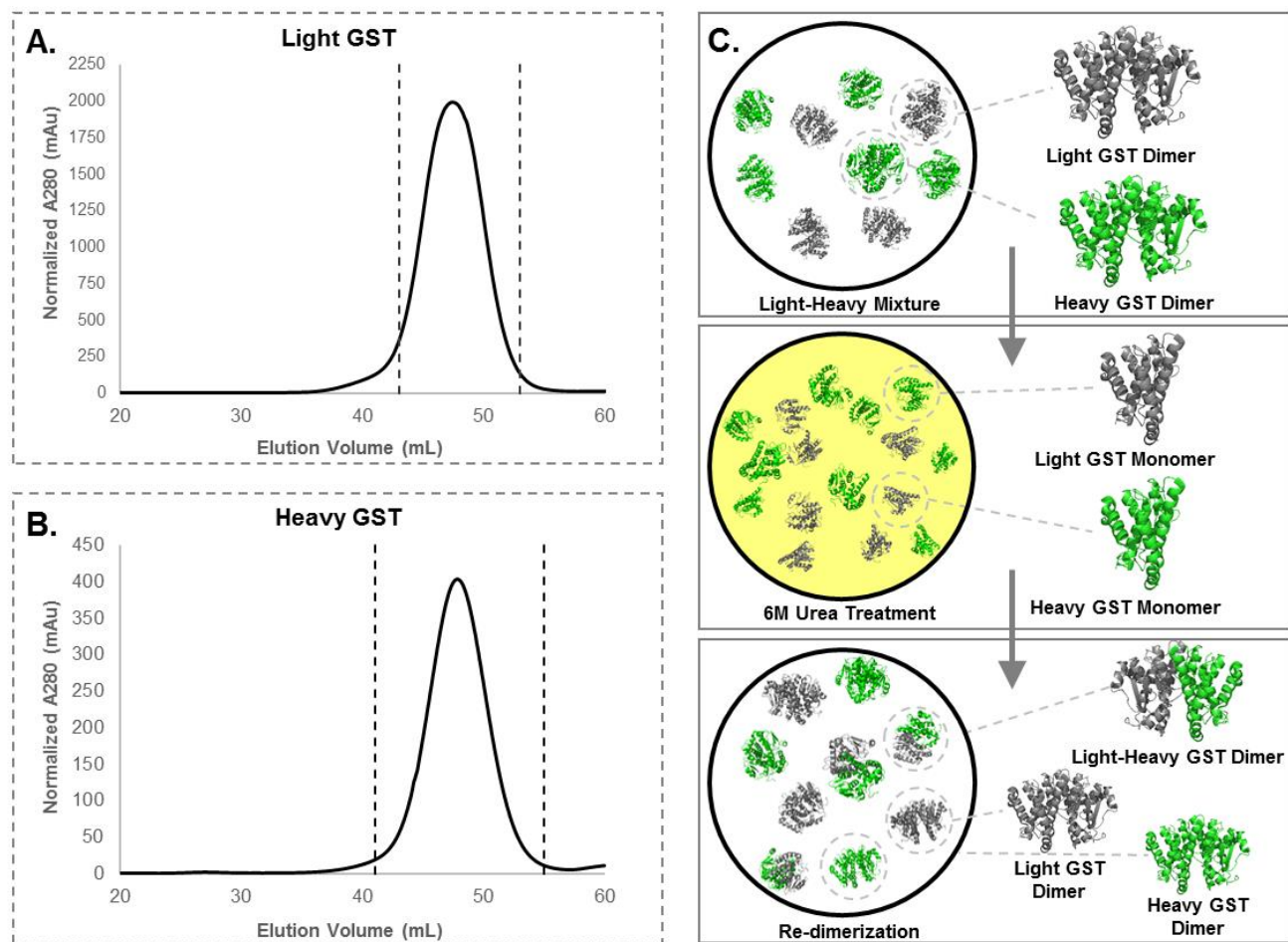


Figure 5.12 Preparation of purified light-heavy GST dimers. A.,B. GST constructs were grown in an arginine and lysine deficient auxotrophic *E. coli* BL21 (DE3) cell line in M9 minimal media augmented with either unlabelled arginine and lysine (light GST) or isotopically labelled L-lysine (4,4,5,5-D4) and L-arginine(13C6; 15N4) (heavy GST). The protein was then purified by affinity to glutathione sepharose, and separated by size exclusion. Dotted lines represent the material used for further experiments. C. Mixed heavy and light dimers were created by mixing single heavy and light dimers, which was incubated in 6M urea to induce dissociation. The urea concentration was then reduced by dilution, leading to the reassociation of dimers, some of which become mixed.

5.6.3 XL-MS identification of cross-dimer interlinked peptides

Two samples were analysed on the spectrometer: (i) urea-treated light GST (ii) urea-treated light/heavy GST. Each sample was analysed in technical duplicate such that 12 total spectrometer runs were carried out. Peptide matching was performed with two reference sequences: light GST, and an additional version of GST in which every lysine and arginine were assigned as heavyK and heavyR, respectively. *Schistosoma* GST contains 21 lysine residues accounting for 8.6% of the sequence.

I first inspected crosslinks identified in the light GST sample. Unexpectedly, two of the highest scoring links were homotypic crosslinks - links between two copies of the same lysine residue in GST. The links involved symmetrical crosslinking of Lys10-Lys10' (**Figure 5.13 A**) and Lys112-Lys112' (**Figure 5.13 B**). I measured distances between the C α coordinates of these paired lysines in the crystal structure of *Schistosoma japonicum* GST (Rufer et al., 2005; PDB ID 1Y6E). While the link between two copies of Lys112 conforms to the expected conditions of crosslinking, as it covers only 17Å between the two GST proteins, and is highly solvent accessible (**Figure 5.13 B**), the more highly scoring link between Lys10 in two proteins covers a distance of 34Å in the crystal structure (**Figure 5.13 A**). However, this may demonstrate the strength of the combined approach over crystallography in isolation, as Lys10 falls within a flexible linker region, and is likely not constrained in the manner indicated by the crystal structure.

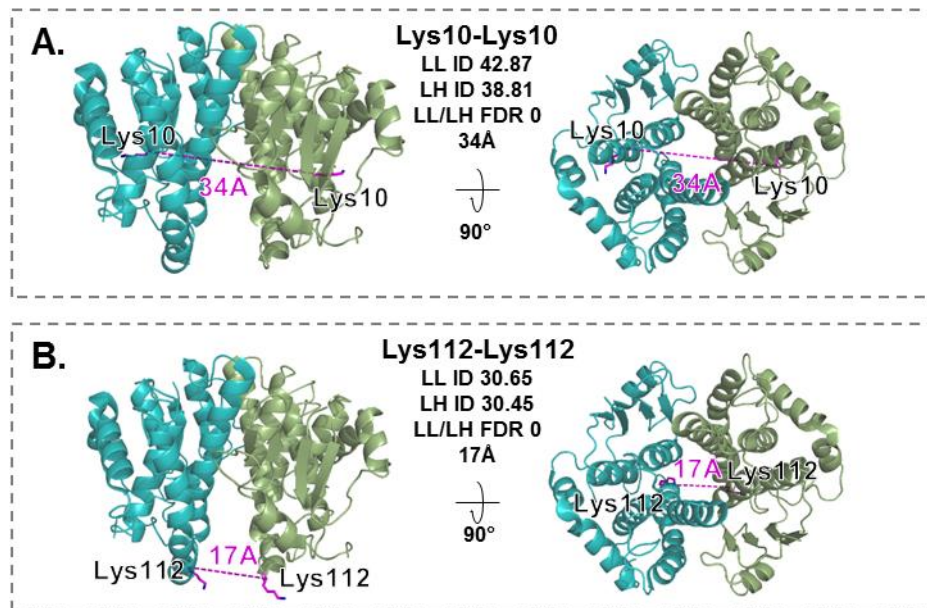


Figure 5.13. Homotypic GST interlinks. Two homotypic links were observed in the light-light dataset that were also present as interlinks in the light-heavy dataset. A. Lys10-Lys10 in the binding cleft of GST was linked in the light dataset with an ID of 42.87, and 38.81 in the light-heavy dataset (LL/LH FDR: 0). B. The homotypic link Lys112-112 was present in the light-light dataset with an ID score of 30.65, and 30.45 in the light-heavy dataset (LL/LH FDR: 0).

Besides the homotypic crosslinks in the light GST dataset, there is no way to distinguish which of the crosslinks detected are intralinks and which are cross-dimeric interlinks. With the light-heavy GST dataset, this distinction can be made. Out of a total of 36 crosslinks with an ID score > 20 and FDR < 0.05, 8 were determined to be interlinks between light and heavy peptides. This indicates that these 8 crosslinks involve separate GST polypeptides meaning they are dimeric links. Two of the links correspond to the homotypic links that were also identified in the light GST dataset. The highest scoring returned interlink Lys124-Lys10' (**Figure 5.13 A**) highlights the discriminatory value of our isotopic labelling approach. This same crosslink is also present with a high ID score in the light GST dataset but there is no way to distinguish whether it is an intralink or dimeric interlink in this dataset. In addition, a dimeric link between Lys86 and Lys10' was detected. Mapping these lysine positions within the crystal structure of dimeric GST (Rufner et al., 2005; PDB ID 1Y6E) reveals that both the Lys10-Lys124' (**Figure 5.14 A**) and Lys86-Lys10' (**Figure 5.14 B**) dimeric interlinks are

positioned with C α atoms separated by ~ 25 Å, which is within the most populated range of the distance distribution when crosslinking with DSS.

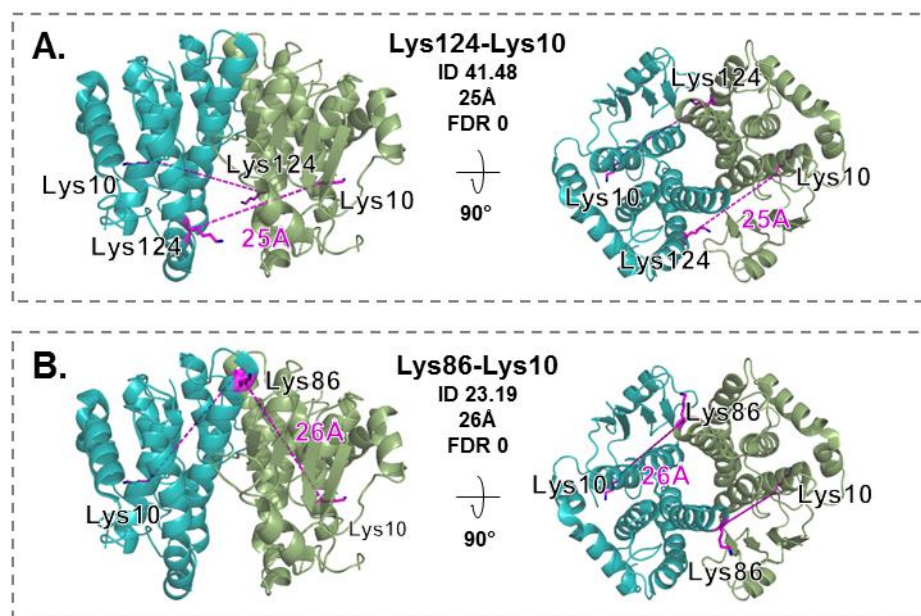


Figure 5.14 Additional cross-dimeric interlinks observed in light-heavy GST sample. **A.** The reported interlink with the highest ID score (41.48) spans the substrate binding cleft covering a distance of 25Å (FDR: 0). **B.** Interlink spanning 26Å between binding cleft Lys110 and Lys86 has an ID of 23.19 (FDR: 0). The homotypic links present in the light-light XL-MS dataset (**Figure 5.13**) are also strongly present in the heavy-light dataset.

The light-heavy GST dataset contains one interlink that is not consistent with the dimer conformation observed in the crystal structure (Rufer et al., 2005; PDB ID 1Y6E). Lys190-Lys193' (ID score 29.6), involves lysines which are situated with C α atoms separated by 59Å (**Figure 5.15**). It is inconceivable that DSS could span this distance, which is almost twice what is considered to be its maximum span. Lysine 190 was detected in crosslinks multiple times in both light and light-heavy GST datasets (**Supplementary table 5**), which suggests that it is highly accessible to DSS. The outlier interlink detected between Lys190 and Lys193' likely reflects a transient interaction between GST dimers (**Figure 5.15**).

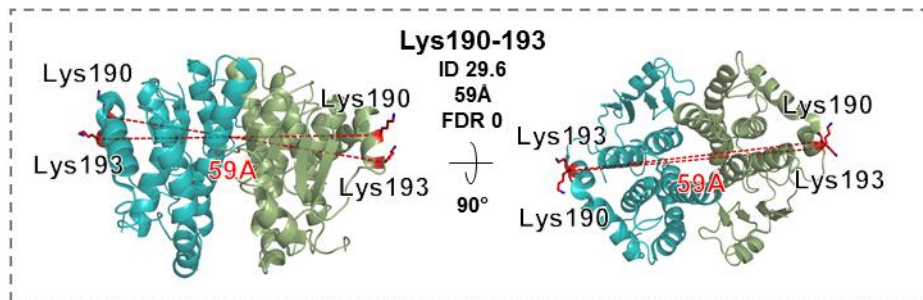


Figure 5.15 Aberrant crosslink from light-heavy dataset. A. The link between Lys190-Lys193 was present with a high ID score of 29.6, but the residues are 59Å from one another, almost double the length of the DSS crosslinker (FDR: 0). This was likely due to aggregation of GST in solution.

Overall, 33 out of a total of 34 intra- and inter-linking sites detected in the light-heavy GST dataset are consistent with the dimeric conformation of GST observed in the crystal structure (Rufer et al., 2005; PDB 1Y6E). This is clearly shown when the positions of all intra- (magenta) and inter- (orange) sites are highlighted in the GST dimer crystal structure (**Figure 5.16**).

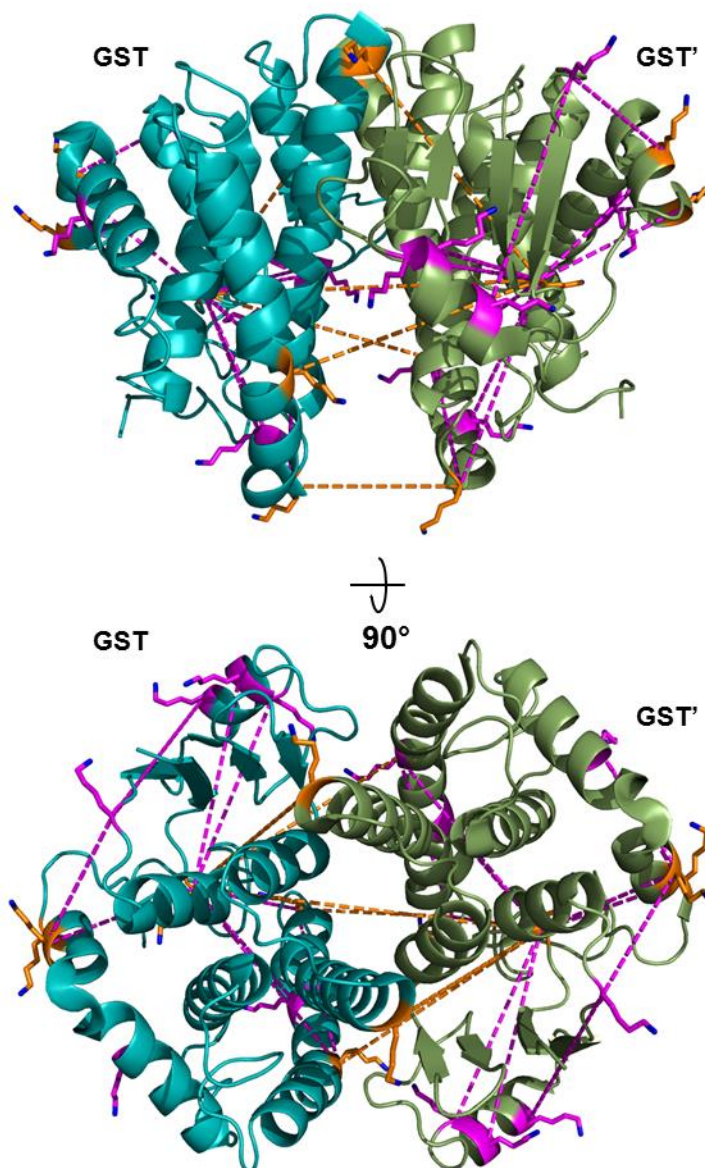


Figure 5.16 DSS crosslinking sites detected within the light-heavy GST dataset plotted on the GST crystal structure. Intralinks are shown in magenta, and interlinks are shown in orange. The α positions of lysine pairs for 33 of the 34 links detected fell within under 35 Å. One outlier crosslink (between lysines 190 and 193') is marked by asterisks.

5.7 Conclusions from XL-MS experiments

Overall, the experiments in this chapter represent the most extensive attempt to date to apply XL-MS to investigate PKA structure, and they have led to a number of novel insights. Notably, experiments with RII-C confirm the location of the RII D/D domain in relation to

other elements within the complex. Experiments with the RII-C-AKAP18 α complex show how RII-C is likely oriented towards the cell membrane, and qXL-MS reveals an unanticipated effect on RII-C structure in the vicinity of the C subunit myristoylation site upon association with the AKAP. Finally, I have successfully pioneered a novel approach for studying oligomeric interlinks that utilises isotopic K/R derivatives. This approach can be applied in the future to study oligomeric protein structures that include PKA.

Chapter 6. Discussion

The restraint of C subunit activity following PKA activation is essential to the control of phosphorylation in cells, as demonstrated by the deleterious physiological effects when this system malfunctions of this system in CNC and acrodysostosis. The findings of this project have advanced understanding of the molecular basis for controlling PKA activity in cells. I have successfully quantified PKA in terms of both copy number, and potentially of more functional importance, stoichiometric ratio, in a range of tissues (**Chapter 3**). These numbers have already changed the direction of our own studies, and will be useful to inform the models of PKA regulation developed across the field. The development of a method to determine C subunit association in an R subunit in a temporally specific manner enabled unprecedented insights into the dynamics of PKA association and dissociation than has previously been possible (**Chapter 4**). With the understanding that the function of macromolecules is predicated upon their structure. We have also used novel techniques to provide new structural insights to the conformation and interactions of PKA holoenzymes, including in complex with a prototypical anchoring protein (**Chapter 5**). Additionally, we have developed a new variant of XL-MS that may be applied to identify homo-meric interlinks within protein complexes. In the remainder of this chapter, I will discuss the implications of my results and consider where these experiments might lead.

6.1 Implications of PKA subunit stoichiometries

The copy number of PKA subunits per μg of wet protein weight might seem inconceivably large, however, recent estimates of protein copy number by cell volume puts these values into perspective. In brain cortex, which has the highest per mass copy number, the total number of copies of all PKA subunits was calculated at 5.33×10^9 per μg wet protein weight.

New mass spectrometry techniques have allowed the number of proteins copies per cell across mammalian, bacterial and yeast cells to be approximated, with low end estimates of 2×10^{15} per μL of cell lysate (Milo, 2013). If we roughly approximate the density of our cortical tissue to $1 \mu\text{g}/\mu\text{l}$, the most PKA subunits at their most prevalent only make up 0.0003% of the total protein copy number of the tissue.

Tissue-to-tissue stoichiometric comparisons reveal some interesting differences. The relatively high R:C ratio in the brain cortex and synaptosome-rich samples is commensurate with the idea that the excess of R subunit confers greater spatiotemporal control to the activation and deactivation of the C subunit,. The neurons of the cortex have been shown to be the location of many tightly spatiotemporally-controlled signaling events. The predominance of RII subunits in this tissue may also arise from the high surface area to volume ratio of the cells, providing more proportional opportunity for attachment than in other cells. The only tissues in which we saw a higher proportion of RI than RII were the heart and cerebellum. The observation that RI is especially prevalent in the heart is in agreement with the finding that CNC, which causes tumour growth that can lead to cardiac obstruction, reduces the RI activity in the tissues of patients. CNC suffers are also observed to suffer from schwannomas, tumours composed of the CNS glial tissue that myelinate neurons. The cerebellum-associated spinal nerve roots have been identified as a one of the most common locations for these tumours (Er et al., 2007). It is highly likely that the pathology seen in these tissues is related to the deregulation of the C subunit created by the reduced concentration of R subunits, which disproportionately effects the tissues in which RI is more abundant than RII.

In the future, it would be interesting to analyse PKA subunit stoichiometry of other tissues associated with *PKAR1A* disorders. The constituent activation of PKA has recently been

shown to increase the activity of osteocytes and osteoblasts stimulating bone growth (Kao et al., 2013), and the bone growth factor lactoferrin has been shown to stimulate PKA activation (Naot et al., 2005; Zhang et al., 2014). This is congruent with the pathology of acrodysostosis, in which RI is over-active due to a mutation that disrupts the cooperativity between the CBDs. CNC also characterized by lentigines, which densely pigmented regions of the skin. Melanin pigment is made in melanocytes, and direct inhibition of PKA has been shown to decrease the expression of melanogenic genes in hyperpigmentation disorders (Roh et al., 2013). It may be useful to characterize the relationship between the C and R subunits in these cell types, as we have done for the tissues used in this study, in order to better understand the role of association and dissociation of each R subunit, and how perturbations in the relationship may be treated.

Another important consideration from our stoichiometric calculations is that the majority of RII subunits will be unoccupied and therefore available dephosphorylation of their PKA autophosphorylation sites. Recent experiments have demonstrated that the phosphorylation state of the RII autophosphorylation site (p-Ser112) determines how rapidly C subunits associate with RII (Zhang et al., 2015). Our copy numbers indicate that most RII autophosphorylation sites will be accessible at any point in time, therefore cellular phosphatases could potentially prime the unoccupied RII population for rapid quenching of released C subunits in advance of cAMP elevation by extensively dephosphorylating p-RII subunits.

6.2 Insights from light-activated crosslinking experiments

Through the use of our novel R subunit specific pull down method we showed that contrary to previous reports (Smith et al., 2013), PKA C subunits dissociate from R subunits upon elevation of cAMP. However, we saw very little decrease in R-C association at the low

nanomolar isoprenaline concentrations that are sufficient to generate robust PKA activity as measured by the AKAR4 reporter. The most likely explanation for this phenomenon is that at the relatively low concentrations of cAMP generated by low nanomolar isoprenaline concentrations, only a small fraction of total C subunits are free at any one point in time. Instead, a small fraction of C subunits shuttle between R subunits in the context of a cell in which the majority of R subunits are unoccupied. We also hypothesized that the localization of the RI type subunit to the cytoplasm might be a mechanism to buffer the C subunits that were released from the type II holoenzyme. However, there was no observed translocation between the RI and RII subunits during either the on-set or off-set of cAMP signalling.

The light-activated crosslinking experiments also reframe how we think about the long-standing problem of explaining how both PGE1 and isoprenaline elevate cAMP whereas only isoprenaline leads to PKA phosphorylation of glycogen phosphorylase (**Section 1.2.2**). Typically, explanations for this phenomenon focus on sub-cellular localisation of cAMP within cells, with more recent incorporation of the idea that PKA R subunits are anchored alongside ACs. Little consideration has been given to the distribution of the C subunit between different R subunit isoforms either prior to or during elevation of cAMP signalling. One simple explanation for the absence of some downstream effects with PGE1 is that C subunits may be preferentially associated with RII subunits prior to cAMP elevation, such that when PGE1 induces increases in cAMP concentration in proximity of RI subunits, very few C subunit are released since the majority instead associate with anchored RII subunits.

6.3 Future opportunities for exploiting the light-activated crosslinking/R subunit-selective pull down approach

An important near-term goal will be to apply the light-activated crosslinking/R pull down strategy to accurately measure the relative levels of RI-C and RII-C complexes in different cells in the ground state prior to cAMP elevation. This would help determine whether the distribution of C subunits between RI and RII contributes to the inability of PGE1 to trigger the same downstream effects as drugs such as isoprenaline. These measurements will be challenging but should be possible. The measurements will need to account for differences in the pull down efficiency between GST-RIAD and GST-AKAP79 c93 since the RIAD pulls down its cognate R subunit more efficiently (Carlson et al., 2006; Herberg et al., 2000) than the AKAP79 fusion. Secondly, these measurements will need to factor in the inherent capacity of RII-C and RI-C to crosslink with NHS-diazirine. Third they will need to account for the likely better access of NHS-Diazirine to RII-C complexes compared to RI-C complexes, since RII-C is positioned at the cell membrane where the cell-permeable crosslinker first enters the cell. One avenue that we intend to pursue is to compare RI-C vs RII-C crosslinking when NHS-Diazirine is applied after breaking the cells open with a Dounce homogeniser in the absence of detergents. This gentle mechanical shearing technique will expose the intracellular components, while minimizing disruption of the endogenous associations of the holoenzymes, and most importantly not disrupting the holoenzymes themselves.

We examined whether the distribution of the C subunit between RI and RII is altered during or after cAMP elevation. However, we found no evidence for a shift in overall distribution between RI and RII. This leads one to wonder whether a mechanism exists for restraining C subunits within the immediate locale of R subunits following their release. The obvious mechanism to achieve this is through myristoylation of the C subunit. As explained in **Chapter**

5, we have already undertaken XL-MS studies that suggest that indeed anchored RII subunits are specialised for orienting the myristoylated N-terminus of C subunits towards the lipid bilayer. In the future, we also intend to investigate C subunit myristoylation using AKAR4 variants that are targeted to different sub-cellular compartments (Depry, Allen, & Zhang, 2011) in combination with shRNA tools for replacing endogenous C subunits with variants that cannot undergo myristoylation. In particular, it will be interesting to measure compare PKA activity between wild-type and non-myristoylated forms using reporters that target to the cell membrane by virtue of fusion to the C-terminal membrane-targeting sequence of K-Ras (Depry et al., 2011), and the first 10 amino acids of Lyn that target the kinase to cholesterol-rich membrane regions (Depry et al., 2011; Resh, 2013).

6.4 Insights into structure and function of PKA from XL-MS measurements

The use of XL-MS allowed us to firmly establish the location of the RII β D/D in the holoenzyme, which had previously been uncertain due to its absence in the electron density in crystal structures models garnered from x-ray diffraction data. This finding highlights the utility of XL-MS when used in conjunction with traditional structural biology methods such as crystallography. We also used qXL-MS to show that the binding of an AKAP to the holoenzyme induces changes in not only the local interface between the AKAP and the R subunit, but that these interactions are conveyed throughout the molecule, affecting the conformation of the C subunit. The preliminary indication of this study has led us to investigate whether the binding of the AKAP increases the association N-terminus of the C subunit with the membrane.

I have also pioneered XL-MS of homo-oligomeric interlinks using light/heavy oligomeric mixtures. Preliminary experiments GST were very successful overall: 34 of 35 links detected (including 6 dimeric links) were consistent with the crystal structure but one outlier link suggested that the approach could benefit from further pilot experiments. To further test our new method for identifying homo-oligomeric interlinks, I plan to perform test experiments using a protein that can be chemically induced to dimerize. FK506 binding protein (FKBP) is an immunophilin that shows peptidylprolyl *cis/trans* isomerase activity, and functions as a chaperone protein (Kang et al, 2008). Spencer and co-workers discovered that FKBP12 can be induced to dimerize through the addition of the novel ligand FK1012, which contains two immunophilin binding ligands covalently bound to each other (Spencer et al., 1993). These ligands became known as 'dimerizers' (Clackson et al., 1998). This approach was subsequently improved by introducing a point mutation (F36V) into the binding pocket of FKBP and pairing with a novel ligand, AP1903 which operates with a much-improved K_d of 0.094 nM (Clackson et al., 1998). We have obtained a plasmid (gift of Thomas Wandless, Egeler et al., 2011) that will enable us to express and purify FKBP F36V with either light or heavy lys/arg. We will crosslink light/heavy FKBP F36V either with or without the chemical dimerizer AP1903. Homo-oligomeric crosslinks should only appear in the presence of the dimerizer, and identified crosslinks may be referenced against crystal structure PDB ID 1BL4 (**Figure 6.1**). In this way, we can validate our new approach without treating the test protein with urea prior to crosslinking.

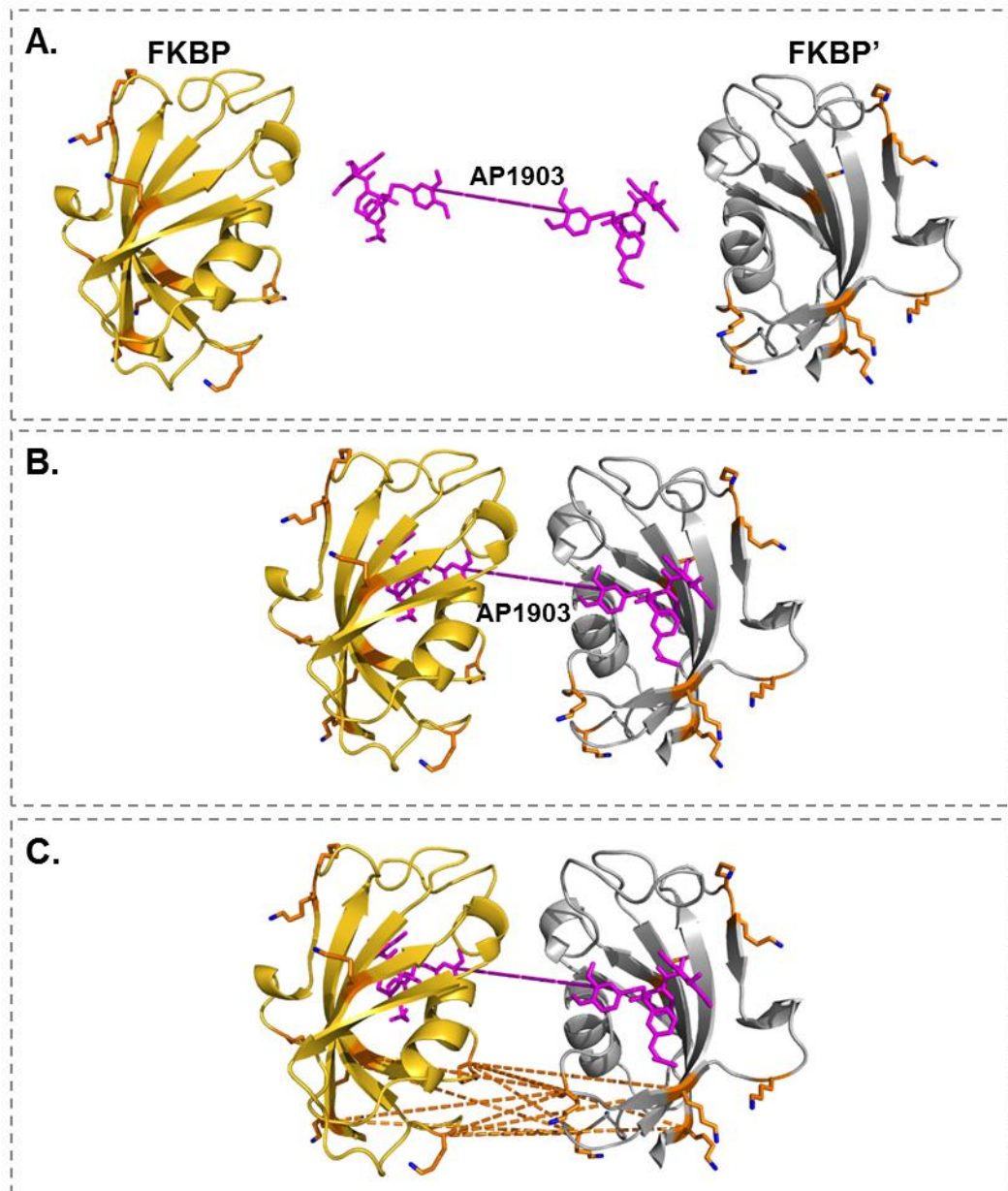


Figure 6.1 FKBP dimerization **A.** The recombinantly expressed F36V-FKBP exists as a monomer in the absence of the ligand. The ligand AP1903 induces binding for the monomers. The dashed line in the model of AP1903 represents the portion of the molecule absent from the crystal structure. **B.** The ligand AP1903 induces dimerization of F36V-FKBP. **C.** Orange dashed lines show the lysine residues within 30Å of each other, which are potential crosslinking sites. (PDB 1BL4, Clackson et al., 1998).

If this approach is confirmed as technically sound, there are many potential applications, both in the context of PKA binding, as well as with other proteins (Ilouz et al., 2012).

6.5 Outlook for homo-oligomeric XL-MS

With respect to father oligomer XL-MS studies of PKA, an important future aim will be to examine the notion that different R subunits fold up into tetramers with C subunits that possess strikingly different quaternary structures. This concept has only emerged recently, triggered by the determination of partial R-C crystal structures in the Taylor lab (Ilouz et al., 2012). It has been posited that key interactions between heterodimers occur between disordered regions (Taylor et al., 2012). XL-MS can potentially help to resolve whether differences in conformation observed in crystal structures are misleading and caused by crystal contacts or whether they do indeed correspond to the conformations observed in solution.

Aside from PKA, XL-MS using light/heavy protein mixtures could also potentially be applied to many other oligomeric protein structures. Potential high-profiles targets include disease-relevant multimeric assemblies like amyloid fibrils; polymeric proteins such as actin and myosin; cage structures such as clathrin/adaptin; and oligomeric receptors such as ion channel receptors for glutamate and GABA.

6.6 Modelling the diffusion and collision rate of C and R subunits at the membrane

Ultimately, one of the future goals of this research is to build a model of the systemic relationship of the proteins and signalling molecules described here. The system we have hypothesized features both a membrane anchored RII-AKAP complex, and a membrane associated myristoylated C subunit, which following activation by cAMP is largely deactivated by association with unoccupied R subunits. The time and distance over which a C subunit can phosphorylate targets before encountering an R subunit is an essential determiner of

total phosphorylation put forth by this model, which requires better kinetic characterization through the application of mathematical modelling. However, the interaction of membrane proteins adds a great deal of complexity on top of the complicated existing models of the cAMP signalling cascade (Heinrich, Neel, & Rapoport, 2002; Rebola et al, 2003; Williamson et al., 2009).

Membrane associated proteins are in constant two-dimensional motion, which is affected by the local composition of the membrane, as well as the anchoring mechanism of the involved proteins and the immediate cellular environment. I will briefly detail some of the obstacles facing the development of an informative model of PKA activity, focusing on the reassociation of C subunits with R subunits at the membrane.

The added emphasis our system places on the control of C subunit diffusion by membrane associated adds a parameter which has not previously been included in mathematical modelling of PKA association and dissociation.

Very broadly, the time necessary for a protein in the cytoplasm to encounter its target differs from the time necessary for the same interaction in the cytoplasm. Batada and colleagues created a simplified model of this interaction which allows for a comparison between membrane anchored and cytoplasmic proteins and compares the expected time necessary for interaction (Batada et al., 2006). For a spherical cell, the expected time for two proteins to interact on the membrane can be represented as $R^2(\log(R/\epsilon)+(\log 2-1+\epsilon/R))/D_1$, while in the cytoplasm the time can be calculated using the formula $R^3/3\epsilon D_2$, where R = the radius of the cell, ϵ = the sum of the radii of the interacting proteins, D_1 is the diffusion coefficient of the cell surface protein, and D_2 is the diffusion rate in the cytoplasm.

These equations show that even with a much greater diffusion rate in the cytoplasm, the R^2 factor of the membrane modelling in comparison to the R^3 of the cytoplasmic model greatly favors interactions on the membrane.

While this simple equation shows the potential spatial and temporal advantages of membrane tethering, it is not suitably complex to describe the membrane associated C-R interaction. While there are no existing models of PKA diffusion in the plane of the membrane, the nature of the interactions allows us to borrow from closely related mechanisms in the GPCR cascade, which has been more extensively modelled, especially the interaction of receptors and G-proteins, which many parallels to our proposed system (Radhakrishnan et al., 2012; Linderman, 2009).

One key component of GPCR modelling is the concept of collision coupling, which encompasses the idea that the two binding partners must first encounter one another by diffusion through the membrane before an interaction can occur (Brinkerhoff, Traynor, & Linderman, 2008)

A robust and experimentally verified model of collision coupling was developed Tian and colleagues to better characterize the collision rate of proteins on the plasma membrane (Tian, Plowman, Parton, Kloog, & Hancock, 2010). They focused on the RAS GTPase K-Ras, which associates with the inner membrane of the via farnesylation and geranylgeranylation, types of anchoring analogous to myristoylation (Konstantinopoulos, Karamouzis, & Papavassiliou, 2007). Tian and coworkers modelled the formation of protein nanoclusters, the behaviour of which is kinetically similar to the multivalent complexes coordinated by AKAPs. This method relies upon the simulation of the Brownian lateral diffusion of particles using the probability distribution of square displacements in conjunction with the experimentally determined diffusion rate of a protein in order to generate a distance moved from a starting position over a given time (Lommerse et al., 2006; Schütz, Schindler, & Schmidt, 1997; Tian et al., 2010).

The lateral diffusion of particles in the model was described using the function:

$$P(r^2, \Delta t) = 1 - \exp\left(-\frac{r^2}{4D\Delta t}\right)$$

$P(r^2, \Delta t)$ = the probability that a protein will be located within an area of radius r after a period of time

r = distance travelled by protein (calculated)

D = diffusion rate (experimentally determined)

Δt = change in time from initiation to measurement

(Tian et al., 2010)

For each member of two populations of proteins, N_1 and N_2 random x and y values are generated to place them within a square which represents the cell membrane. A timepoint is then chosen, and the r value is calculated using the above equation. The direction of travel is determined by the formula $\theta = 2\pi s$, where θ is the direction of travel, and s is a randomly selected value. From these results, the new x and y values of the protein are determined. The position of each of the proteins, as well as the experimentally determined radius of each type of interacting protein is compared to determine where there is an overlap, which generates the calculated number of collisions. This is further used to calculate the rate of collision, using the following formula:

$$k = \frac{MS}{N_1 N_2 \Delta t}$$

k = rate of collision

M = number of collisions

S = Area

N_1 = number of molecules of first protein

N_2 = number of molecules of second protein

(Tian et al., 2010)

While the strength of this model is the need for relatively few experimentally determined inputs, like the copy numbers of the interacting proteins, which I determined for PKA in the course of my investigations, there are a number of confounding factors that limit our ability to adapt this for use with C and R subunit association. The experimentally determined rate of diffusion within the membrane for anchored K-Ras proteins that was used by Tian and colleagues to develop this model was determined using membrane anchored fluorophores and fluorescence recovery after photobleaching (FRAP) (Lommerse et al., 2006). There is no existing experimentally determined diffusion rate for myristoylated C subunits, though a similar approach could be adopted. In addition to which, there are also strong indications in the literature that differential anchoring mechanisms of AKAPs, including myristoylation, palmitoylation restricts the membrane localization and diffusion of the anchored complexes (Delint-Ramirez et al., 2011). The polyvalency of AKAPs would also introduce further variables into the rate of diffusion calculations. However, these variables could be measured experimentally, potentially operating on the assumption that large enough polyvalent complexes are effectively fixed over short changes in time.

Additionally, this model assumes a fixed and experimentally quantifiable number of membrane-associated protein partners. The case presented by the myristoylated C subunit does not fit these parameters. Gaffarogullari and colleagues proposed that phosphorylation at Ser10 and membrane interaction can drive the membrane association of C subunits by inducing the myr-out conformation. This finding was further supported by Bastidas and coworkers, who showed that RII subunits but not RI subunits drive C subunit-membrane attachment (Bastidas et al., 2012), as well as our own qXL-MS data, which indicates a possible shift toward myr-out upon association with and AKAP. All of these models also describe

reversibility in the process, meaning that within the relatively fixed copy number of C subunits, there is a divide between membrane-associated myr-out C subunits, and cytoplasmic myr-in C subunits. There is little understanding of the basal proportion of these two populations in relation to each other, or the potential factors inducing a change in this population. In a similar circumstance, a FRAP-based method was adapted to measure the membrane association of the palmitoylated and myristoylated Src family kinase Lck, with the localization of the protein assessed by differing diffusion rates assigned to cytosolic and membrane associated proteins (Zimmermann et al., 2010). This methodology could be adapted to measure the basal proportion of cytosolic and membrane anchored C subunits, possibly by extending the discriminatory power of the analysis to identify the rates of movement of free cytosolic C subunits, cytosolic PKA tetramers, free membrane-associated C subunits, and membrane associated tetramers.

This is further complicated by the change in molecular radius of the R subunit dimer following the binding of the first C subunit (Batada et al., 2006). This parameter would also be significantly different between anchored and cytoplasmic R subunits, as membrane attachment limits the space for diffusion as well as rotational freedom, which would likely increase the probability of association in the anchored subunits (Batada et al., 2006).

However, the greatest challenge for this type of modelling would be to establish a physiologically informed proportion of cAMP-bound and unbound RII dimers. The binding of cAMP to the RII dimer is both reversible and highly localized, meaning that any effective model would have to take into account the proportion of unavailable RII in a microdomain, potentially dynamically, which would need to be disregarded in calculating the rate of collision. This parameter has not been measured, likely due to the established belief in the field that the approximately even stoichiometry of C:R subunits means that the effect of unoccupied R subunits is negligible.

In order to effectively characterize the interaction of C and R subunits in the plane of the membrane, further work must be done. Experimentally, determination of parameters including rates of diffusion of C and R subunits individually or as members of polyvalent complexes, as well as the proportion of membrane bound C subunit in the total population, and the amount of available unoccupied R subunit must be carried out. Also, the model must be tuned to account for variability in the association of C subunits with the membrane, as well as dynamic availability of R subunits.

6.7 An integrated model for C subunit restraint

Localized cAMP signalling is a mature field with roots in the first half of the twentieth century. Nevertheless, during my doctoral studies, I have made a number of contributions that enable us to extend the overall scheme for understanding how specificity in PKA phosphorylation is achieved within cells. Prior to stimulation, a large excess of R subunits bind and inhibit a relatively small number of C subunits. Typically, membrane-associated RII subunits outnumber RI subunits. Following cAMP elevation in the vicinity of ACs anchored in tandem with RII subunits, C subunits are released from RII. These short-lived C subunits are able to phosphorylate Ser/Thr amino acids within proteins that conform to the consensus PKA recognition motif in their immediate vicinity before they rapidly encounter another (unoccupied) RII subunit. Rapid cycling of C subunits between different anchored RII subunits continue while cAMP is elevated and is sufficient to overcome background dephosphorylation by cellular phosphatases. We can also speculate that membrane insertion of the myristoylated N-terminus of the C subunit prevents it from diffusing out of the plane of the membrane thereby increasing its chances of rapidly encountering another

unoccupied R subunit. It will be very interesting to see how this scheme evolves as more details of cAMP signalling are uncovered in the future.

Chapter 7. References

- Adams, J. A. (2001). Kinetic and catalytic mechanisms of protein kinases. *Chemical Reviews*, 101(8), 2271–2290. <http://doi.org/10.1021/cr000230w>
- Adams, S. R., Harootunian, A. T., Buechler, Y. J., Taylor, S. S., & Tsien, R. Y. (1991). Fluorescence ratio imaging of cyclic AMP in single cells. *Nature*, 349(6311), 694–7. <http://doi.org/10.1038/349694a0>
- Ahmed, H. (2005). Estimation of protein. In *Principles and reactions of protein extraction, purification, and characterization* (pp. 35–37).
- Akimoto, M., Selvaratnam, R., McNicholl, E. T., Verma, G., Taylor, S. S., & Melacini, G. (2013). Signaling through dynamic linkers as revealed by PKA. *Proceedings of the National Academy of Sciences of the United States of America*, 110(35), 14231–6. <http://doi.org/10.1073/pnas.1312644110>
- Altschul, S. F., Gish, W., Miller, W., Myers, E. W., & Lipman, D. J. (1990). Basic local alignment search tool. *Journal of Molecular Biology*, 215(3), 403–10. [http://doi.org/10.1016/S0022-2836\(05\)80360-2](http://doi.org/10.1016/S0022-2836(05)80360-2)
- Andrews, D. L. (2009). Resonance Energy Transfer: Theoretical foundations and developing applications. In *Tutorials in Complex Photonic Media* (pp. 461–499). <http://doi.org/10.1117/3.832717>
- Anjum, R., & Blenis, J. (2008). The RSK family of kinases: emerging roles in cellular signalling. *Nature Reviews. Molecular Cell Biology*, 9(10), 747–58. <http://doi.org/10.1038/nrm2509>
- Bacsikai, B. J., Hochner, B., Mahaut-smith, M., Adams, S. R., Kaang, B., Kandel, E. R., & Tsien, R. Y. (1993). Spatially Resolved Dynamics of cAMP and Protein Kinase A Subunits in Aplysia Sensory Neurons. *Science Report*, 260(January), 222–226. <http://doi.org/10.1126/science.7682336>
- Banerjee, S., & Mazumdar, S. (2012). Electrospray Ionization Mass Spectrometry: A Technique to Access the Information beyond the Molecular Weight of the Analyte. *International Journal of Analytical Chemistry*, 2012, 1–40. <http://doi.org/10.1155/2012/282574>

- Banky, P., Roy, M., Newlon, M. G., Morikis, D., Haste, N. M., Taylor, S. S., & Jennings, P. A. (2003). Related protein - Protein interaction modules present drastically different surface topographies despite A conserved helical platform. *Journal of Molecular Biology*, 330(5), 1117–1129. [http://doi.org/10.1016/S0022-2836\(03\)00552-7](http://doi.org/10.1016/S0022-2836(03)00552-7)
- Bastidas, A. C., Deal, M. S., Steichen, J. M., Keshwani, M. M., Guo, Y., & Taylor, S. S. (2012). Role of N-Terminal myristylation in the structure and regulation of cAMP-dependent protein kinase. *Journal of Molecular Biology*, 422(2), 215–229. <http://doi.org/10.1016/j.jmb.2012.05.021>
- Batada, N. N., Shepp, L. A., Siegmund, D. O., & Levitt, M. (2006). Spatial regulation and the rate of signal transduction activation. *PLoS Computational Biology*, 2(5), 343–349. <http://doi.org/10.1371/journal.pcbi.0020044>
- Bauman, A. L., Soughayer, J., Nguyen, B. T., Willoughby, D., Carnegie, G. K., Wong, W., ... Scott, J. D. (2006). Dynamic Regulation of cAMP Synthesis through Anchored PKA-Adenylyl Cyclase V/VI Complexes. *Molecular Cell*, 23(6), 925–931. <http://doi.org/10.1016/j.molcel.2006.07.025>
- Beavo, J. a, & Brunton, L. L. (2002). Cyclic nucleotide research -- still expanding after half a century. *Nature Reviews. Molecular Cell Biology*, 3(9), 710–8. <http://doi.org/10.1038/nrm911>
- Berman, H. M., Ten Eyck, L. F., Goodsell, D. S., Haste, N. M., Kornev, A., & Taylor, S. S. (2005). The cAMP binding domain: an ancient signaling module. *Proceedings of the National Academy of Sciences of the United States of America*, 102(1), 45–50. <http://doi.org/10.1073/pnas.0408579102>
- Berman, H. M., Westbrook, J., Feng, Z., Gilliland, G., Bhat, T. N., Weissig, H., ... Bourne, P. E. (2000). The Protein Data Bank. *Nucleic Acids Research*, 28(1), 235–242. <http://doi.org/10.1093/nar/28.1.235>
- Bers, D. M. (2002). Cardiac excitation-contraction coupling. *Nature*, 415(6868), 198–205. <http://doi.org/10.1038/415198a>
- Bertherat, J., Horvath, A., Groussin, L., Grabar, S., Boikos, S., Cazabat, L., ... Stratakis, C. A. (2009). Mutations in regulatory subunit type 1A of cyclic adenosine 5'-monophosphate-dependent protein kinase (PRKAR1A): Phenotype analysis in 353 patients and 80 different genotypes. *Journal of Clinical Endocrinology and*

- Metabolism*, 94(6), 2085–2091. <http://doi.org/10.1210/jc.2008-2333>
- Biemann, K. (1990). Sequencing of peptides by tandem mass spectrometry and high-energy collision-induced dissociation. *Methods in Enzymology*, 193(1981), 455–479. [http://doi.org/10.1016/0076-6879\(90\)93433-L](http://doi.org/10.1016/0076-6879(90)93433-L)
- Birnbaumer, L., Pohl, S. L., & Rodbell, M. (1969). Adenyl Cyclase in Fat Cells I. Properties and the effects of adrenocorticotropin and fluoride. *The Journal of Biological Chemistry*, (13), 3468–3476.
- Blencowe, A., & Hayes, W. (2005). Development and application of diazirines in biological and synthetic macromolecular systems. *Soft Matter*, 1, 178–205. <http://doi.org/10.1039/b501989c>
- Bliss, T. V. P., & Collingridge, G. L. (2013). Expression of NMDA receptor-dependent LTP in the hippocampus: bridging the divide. *Molecular Brain*, 6, 5. <http://doi.org/10.1186/1756-6606-6-5>
- Bornhorst, J. A., & Falke, J. J. (2000). Purification of proteins using polyhistidine affinity tags. *Methods in Enzymology*, 326, 245–254. <http://doi.org/10.1097/MPG.0b013e3181a15ae8>.Screening
- Brinkerhoff, C. J., Traynor, J. R., & Linderman, J. J. (2008). Collision coupling, crosstalk, and compartmentalization in G-protein coupled receptor systems: Can a single model explain disparate results? *J Theor Biol.*, 255(3), 278–286. <http://doi.org/10.1016/j.jtbi.2008.08.003>.Collision
- Brunner, J., Senn, H., & Richards, F. M. (1980). 3-Trifluoromethyl-3-phenyldiazirine. A new carbene generating group for photolabeling reagents. *Journal of Biological Chemistry*, 255(8), 3313–3318.
- Brunton, L. L., Hayes, J. S., & Mayer, S. E. (1979). Hormonally specific phosphorylation of cardiac troponin I and activation of glycogen phosphorylase. *Nature*, 280, 78–80.
- Bruystens, J. G. H., Wu, J., Fortezzo, A., Kornev, A. P., Blumenthal, D. K., & Taylor, S. S. (2014). PKA RIa homodimer structure reveals an intermolecular interface with implications for cooperative cAMP binding and carney complex disease. *Structure*, 22(1), 59–69. <http://doi.org/10.1016/j.str.2013.10.012>
- Burns-Hamuro, L. L., Hamuro, Y., Kim, J. S., Sigala, P., Fayos, R., Stranz, D. D., ... Woods, V. L. (2005). Distinct interaction modes of an AKAP bound to two regulatory subunit

isoforms of protein kinase A revealed by amide hydrogen/deuterium exchange. *Protein Science : A Publication of the Protein Society*, 14(12), 2982–2992. <http://doi.org/10.1110/ps.051687305>

Butcher, R. W., & Sutherland, E. W. (1962). Adenosine 3',5'-phosphate in Biological Materials I. Purification and properties of cyclic 3',5'-nucleotide phosphodiesterase and use of this enzyme to characterize adenosine 3',5'-phosphate in human urine. *The Journal of Biological Chemistry*, 237(4), 1244–1250.

Buxton, I. L., & Brunton, L. L. (1983). Compartments of cyclic AMP and protein kinase in mammalian cardiomyocytes. *The Journal of Biological Chemistry*, 258(17), 10233–9.

Cadd, G., & Mcknight, G. S. (1989). Distinct Patterns of CAMP-Dependent Gene Expression in Mouse Brain. *Cell*, 3, 71–79.

Carlson, C. R., Lygren, B., Berge, T., Hoshi, N., Wong, W., Tasken, K., & Scott, J. D. (2006). Delineation of type I protein kinase A-selective signaling events using an RI anchoring disruptor. *Journal of Biological Chemistry*, 281(30), 21535–21545. <http://doi.org/10.1074/jbc.M603223200>

Chen, Y., Harry, A., Li, J., Smit, M. J., Bai, X., Magnusson, R., ... Iyengar, R. (1997). Adenylyl cyclase 6 is selectively regulated by protein kinase A phosphorylation in a region involved in Galphas stimulation. *Proc Natl Acad Sci U S A*, 94(25), 14100–14104. <http://doi.org/Research Support, Non-U.S. Gov't Research Support, U.S. Gov't, P.H.S.>

Cheng, S. H., Rich, D. P., Marshall, J., Gregory, R. J., Welsh, M. J., & Smith, A. E. (1991). Phosphorylation of the R domain by cAMP-dependent protein kinase regulates the CFTR chloride channel. *Cell*, 66(5), 1027–1036. [http://doi.org/10.1016/0092-8674\(91\)90446-6](http://doi.org/10.1016/0092-8674(91)90446-6)

Cheng, X., Phelps, C., & Taylor, S. S. (2001). Differential binding of cAMP-dependent protein kinase regulatory subunit isoforms Ialpha and IIbeta to the catalytic subunit. *The Journal of Biological Chemistry*, 276(6), 4102–4108. <http://doi.org/10.1074/jbc.M006447200>

Clackson, T., Yang, W., Rozamus, L. W., Hatada, M., Amara, J. F., Rollins, C. T., ... Holt, D. A. (1998). Redesigning an FKBP-ligand interface to generate chemical dimerizers with novel specificity. *Proceedings of the National Academy of Sciences of the United States of America*, 95(18), 10437–42. <http://doi.org/10.1073/pnas.95.18.10437>

- Clegg, C. H., Cadd, G. G., & McKnight, G. S. (1988). Genetic characterization of a brain-specific form of the type I regulatory subunit of cAMP-dependent protein kinase. *Proceedings of the National Academy of Sciences of the United States of America*, *85*(11), 3703–7. <http://doi.org/10.1073/pnas.85.11.3703>
- Coghlan, V. M., Perrino, B. A., Howard, M., Langeberg, L. K., Hicks, J. B., Gallatin, W. M., ... Scott, J. D. (1995). Association of Protein Kinase A and Protein Phosphatase 2B with a Common Anchoring Protein. *Science*, *267*(5194), 108–111.
- Colledge, M., Dean, R. a, Scott, G. K., Langeberg, L. K., Huganir, R. L., & Scott, J. D. (2000). Targeting of PKA to glutamate receptors through a MAGUK-AKAP complex. *Neuron*, *27*, 107–119. [http://doi.org/10.1016/S0896-6273\(00\)00013-1](http://doi.org/10.1016/S0896-6273(00)00013-1)
- Colley, D. G., Bustinduy, A. L., Secor, W. E., & King, C. H. (2014). Human schistosomiasis. *The Lancet*, *383*(9936), 2253–2264. [http://doi.org/10.1016/S0140-6736\(13\)61949-2](http://doi.org/10.1016/S0140-6736(13)61949-2)
- Conti, M., & Beavo, J. (2007). Biochemistry and physiology of cyclic nucleotide phosphodiesterases: essential components in cyclic nucleotide signaling. *Annual Review of Biochemistry*, *76*, 481–511. <http://doi.org/10.1146/annurev.biochem.76.060305.150444>
- Cook, W. H., Lipkin, D., & Markham, R. (1957). The formation of a cyclic dianhydrodiadenylic acid (I) by the alkaline degradation of adenosine-5'-triphosphoric acid (II). *Journal of the American Chemical Society*, *79*(13), 3607–3608. <http://doi.org/10.1021/ja01570a086>
- Cooper, D. M. F., & Tabbasum, V. G. (2014). Adenylate cyclase-centred microdomains. *Biochemical Journal*, *462*(2), 199–213. <http://doi.org/10.1042/BJ20140560>
- Corbin, J. D., & Keely, S. L. (1977). Characterization and regulation of heart adenosine 3':5'-monophosphate-dependent protein kinase isozymes. *The Journal of Biological Chemistry*, *252*(3), 910–918.
- Corbin, J. D., Keely, S. L., & Park, C. R. (1975). The distribution and dissociation of cyclic adenosine 3':5'-monophosphate-dependent protein kinases in adipose, cardiac, and other tissues. *J Biol Chem.*, *250*(1), 218–225.
- Corbin, J., Sugden, P., Lincoln, T., & Keely, S. (1977). Compartmentalization Protein Kinase in Heart Tissue. *Journal of Biological Chemistry*, *252*(11), 3854–3861.
- Cori, C. F., & Cori, G. T. (1928). The Mechanism of epinephrine action II The influence of

epinephrine and insulin on the carbohydrate metabolism of rats in the postabsorptive state. *Journal of Biological Chemistry*, 79, 321–341.
<http://doi.org/10.1017/CBO9781107415324.004>

Davoren, P. R., & Sutherland, E. W. (1963). The Cellular Location of Adenyl Cyclase in the Pigeon Erythrocyte. *The Journal of Biological Chemistry*, 238(9), 3016–3023.

de Rooij, J., Zwartkruis, F. J., Verheijen, M. H., Cool, R. H., Nijman, S. M., Wittinghofer, A., & Bos, J. L. (1998). Epac is a Rap1 guanine-nucleotide-exchange factor directly activated by cyclic AMP. *Nature*, 396(6710), 474–477. <http://doi.org/10.1038/24884>

Delange, R. J., Kemp, R. G., Cooper, R. A., & Krebs, E. G. (1968). Activation of skeletal muscle phosphorylase kinase by adenosine triphosphate and adenosine 3',5'-monophosphate. *Biological Chemistry*, (9), 2200–2208.

Delint-Ramirez, I., Willoughby, D., Hammond, G. V. R., Ayling, L. J., & Cooper, D. M. F. (2011). Palmitoylation targets AKAP79 protein to lipid rafts and promotes its regulation of calcium-sensitive adenylyl cyclase type 8. *Journal of Biological Chemistry*, 286(38), 32962–32975. <http://doi.org/10.1074/jbc.M111.243899>

Dell'Acqua, M. L., Faux, M. C., Thorburn, J., Thorburn, A., & Scott, J. D. (1998). Membrane-targeting sequences on AKAP79 bind phosphatidylinositol-4,5-bisphosphate. *EMBO Journal*, 17(8), 2246–2260. <http://doi.org/10.1093/emboj/17.8.2246>

Depry, C., Allen, M. D., & Zhang, J. (2011). Visualization of PKA activity in plasma membrane microdomains. *Molecular bioSystems*, 7(1), 52–58.
<http://doi.org/10.1039/c0mb00079e>

DiPilato, L. M., Cheng, X., & Zhang, J. (2004). Fluorescent indicators of cAMP and Epac activation reveal differential dynamics of cAMP signaling within discrete subcellular compartments. *Proceedings of the National Academy of Sciences of the United States of America*, 101(47), 16513–16518. <http://doi.org/10.1073/pnas.0405973101>

Drummond, G. I., & Perrott-Yee, S. (1961). Enzymatic hydrolysis of adenosine 3',5'-phosphoric acid. *Journal of Biological Chemistry*, 236(4), 1126.

Dunkley, P. R., Jarvie, P. E., & Robinson, P. J. (2008). A rapid Percoll gradient procedure for preparation of synaptosomes. *Nature Protocols*, 3(11), 1718–28.
<http://doi.org/10.1038/nprot.2008.171>

Egeler, E. L., Urner, L. M., Rakhit, R., Liu, C. W., & Wandless, T. J. (2011). Ligand-switchable

- substrates for a ubiquitin-proteasome system. *Journal of Biological Chemistry*, 286(36), 31328–31336. <http://doi.org/10.1074/jbc.M111.264101>
- Er, U., Kazanci, A., Eyriparmak, T., Yigitkanli, K., & Senveli, E. (2007). Melanotic schwannoma. *Journal of Clinical Neuroscience*, 14(7), 676–678. <http://doi.org/10.1016/j.jocn.2006.03.010>
- Eyal, E., Gerzon, S., Potapov, V., Edelman, M., & Sobolev, V. (2005). The limit of accuracy of protein modeling: Influence of crystal packing on protein structure. *Journal of Molecular Biology*, 351(2), 431–442. <http://doi.org/10.1016/j.jmb.2005.05.066>
- Fagan, K. A., Schaack, J., Zweifach, A., & Cooper, D. M. F. (2001). Adenovirus encoded cyclic nucleotide-gated channels: A new methodology for monitoring cAMP in living cells. *FEBS Letters*, 500(1–2), 85–90. [http://doi.org/10.1016/S0014-5793\(01\)02564-9](http://doi.org/10.1016/S0014-5793(01)02564-9)
- Fenn, J. B., Mann, M., Meng, C. K., Wong, S. F., & Whitehouse, C. M. (1989). Electrospray ionization for mass spectrometry of large biomolecules. *Science (New York, N.Y.)*, 246(4926), 64–71. <http://doi.org/10.1126/science.2675315>
- Fischer, E. H., & Krebs, G. (1955). Conversion of phosphorylase b to phosphorylase a in muscle extracts. *Journal of Biological Chemistry*, 216, 121–132.
- Fraser, I. D. C., Cong, M., Kim, J., Rollins, E. N., Daaka, Y., Lefkowitz, R. J., & Scott, J. D. (2000). Assembly of an A kinase-anchoring protein- β 2-adrenergic receptor complex facilitates receptor phosphorylation and signaling. *Current Biology*, 10(7), 409–412. [http://doi.org/10.1016/S0960-9822\(00\)00419-X](http://doi.org/10.1016/S0960-9822(00)00419-X)
- Fraser, L. D. C., Tavalin, S. J., Lester, L. B., Langeberg, L. K., Westphal, A. M., Dean, R. A., ... Scott, J. D. (1998). A novel lipid-anchored A-kinase anchoring protein facilitates cAMP-responsive membrane events. *EMBO Journal*, 17(8), 2261–2272. <http://doi.org/10.1093/emboj/17.8.2261>
- Fushimi, K., Sasaki, S., & Marumo, F. (1997). Phosphorylation of serine 256 is required for cAMP-dependent regulatory exocytosis of the aquaporin-2 water channel. *Journal of Biological Chemistry*, 272(23), 14800–14804. <http://doi.org/10.1074/jbc.272.23.14800>
- Gaffarogullari, E. C., Masterson, L. R., Metcalfe, E. E., Traaseth, N. J., Balatri, E., Musa, M. M., ... Veglia, G. (2011). A myristoyl/phosphoserine switch controls cAMP-dependent protein kinase association to membranes. *Journal of Molecular Biology*, 411(4), 823–836. <http://doi.org/10.1016/j.jmb.2011.06.034>

- Gao, T., Yatani, A., Dell'Acqua, M. L., Sako, H., Green, S. A., Dascal, N., ... Hosey, M. M. (1997). cAMP-dependent regulation of cardiac L-type Ca²⁺ channels requires membrane targeting of PKA and phosphorylation of channel subunits. *Neuron*, *19*(1), 185–196. [http://doi.org/10.1016/S0896-6273\(00\)80358-X](http://doi.org/10.1016/S0896-6273(00)80358-X)
- Gasteiger E., Hoogland C., Gattiker A., Duvaud S., Wilkins M.R., Appel R.D., B. A. (2005). Protein Identification and Analysis Tools on the ExPASy Server. *The Proteomics Protocols Handbook*, 571–607. <http://doi.org/10.1385/1592598900>
- Gilman, A. G. (1995). G proteins and regulation of adenylyl cyclase. *Bioscience Reports*, 182–212. <http://doi.org/10.1007/BF01200143>
- Gold, M. G., Fowler, D. M., Means, C. K., Pawson, C. T., Stephany, J. J., Langeberg, L. K., ... Scott, J. D. (2013). Engineering AKAP-selective regulatory subunits of PKA through structure-based phage selection. *Journal of Biological Chemistry*, *288*, 17111–21.
- Gold, M. G., Lygren, B., Dokurno, P., Hoshi, N., McConnachie, G., Taskén, K., ... Barford, D. (2006). Molecular basis of AKAP specificity for PKA regulatory subunits. *Molecular Cell*, *24*(3), 383–95. <http://doi.org/10.1016/j.molcel.2006.09.006>
- Gold, M. G., Reichow, S. L., O'Neill, S. E., Weisbrod, C. R., Langeberg, L. K., Bruce, J. E., ... Scott, J. D. (2012). AKAP2 anchors PKA with aquaporin-0 to support ocular lens transparency. *EMBO Molecular Medicine*, *4*(1), 15–26. <http://doi.org/10.1002/emmm.201100184>
- Gomez, L. L., Alam, S., Smith, K. E., Horne, E., & Dell'Acqua, M. L. (2002). Regulation of A-kinase anchoring protein 79/150-cAMP-dependent protein kinase postsynaptic targeting by NMDA receptor activation of calcineurin and remodeling of dendritic actin. *J Neurosci*, *22*(16), 7027–7044. <http://doi.org/20026752>
- Götz, F., Roske, Y., Schulz, M. S., Autenrieth, K., Bertinetti, D., Faelber, K., ... Klussmann, E. (2016a). AKAP18:PKA-RII α structure reveals crucial anchor points for recognition of regulatory subunits of PKA. *Biochemical Journal*, 1881–1894. <http://doi.org/10.1042/BCJ20160242>
- Götz, F., Roske, Y., Schulz, M. S., Autenrieth, K., Bertinetti, D., Faelber, K., ... Klussmann, E. (2016b). AKAP18:PKA-RII α structure reveals crucial anchor points for recognition of regulatory subunits of PKA. *Biochemical Journal*, (2016). <http://doi.org/10.1042/BCJ20160242>

- Gräslund, S., Nordlund, P., Weigelt, J., Bray, J., Gileadi, O., Knapp, S., ... Gunsalus, K. C. (2008). Protein production and purification. *Nat Meth*, 5(2), 135–146.
<http://doi.org/10.1038/nmeth.f.202>
- Gray, P. C., Johnson, B. D., Westenbroek, R. E., Hays, L. G., Yates, J. R., Scheuer, T., ... Murphy, B. J. (1998). Primary structure and function of an A kinase anchoring protein associated with calcium channels. *Neuron*, 20(5), 1017–1026.
[http://doi.org/10.1016/S0896-6273\(00\)80482-1](http://doi.org/10.1016/S0896-6273(00)80482-1)
- Gronholm, M., Vossebein, L., Carlson, C. R., Kuja-Panula, J., Teesalu, T., Alfthan, K., ... Carpen, O. (2003). Merlin Links to the cAMP Neuronal Signaling Pathway by Anchoring the RI β Subunit of Protein Kinase A. *Journal of Biological Chemistry*, 278(42), 41167–41172. <http://doi.org/10.1074/jbc.M306149200>
- Guggino, W. B., & Stanton, B. A. (2006). New insights into cystic fibrosis: molecular switches that regulate CFTR. *Nature Reviews Molecular Cell Biology*, 7(June), 426–436.
<http://doi.org/10.1038/nrm1949>
- Haga, T., Haga, K., & Gilman, A. G. (1977). Hydrodynamic properties of the beta-adrenergic receptor and adenylate cyclase from wild type and variant S49 lymphoma cells. *The Journal of Biological Chemistry*, 252(16), 5776–5782.
- Haga, T., Ross, E. M., Anderson, H. J., & Gilman, A. G. (1977). Adenylate cyclase permanently uncoupled from hormone receptors in a novel variant of S49 mouse lymphoma cells. *Proceedings of the National Academy of Sciences of the United States of America*, 74(5), 2016–2020.
- Hanks, S. K., & Hunter, T. (1995). The eukaryotic protein kinase superfamily : kinase (catalytic) domain structure and classification. *The FASEB Journal*, 9(8), 576–596.
- Harper, S., & Speicher, D. W. (2011). Purification of proteins fused to glutathione S-transferase. *Methods in Molecular Biology*, 681, 151–175.
<http://doi.org/10.1007/978-1-60761-913-0>
- Hayes, J. S., Bowling, N., King, K. L., & Boder, G. B. (1982). Incubation and sample preparation Preparation of myocytes Electrophoresis and autoradiography Specific activity of [7-32p] A TP, 714, 136–142.
- Hayes, J. S., Brunton, L. L., Brown, J. H., Reese, J. B., & Mayer, S. E. (1979). Hormonally specific expression of cardiac protein kinase activity. *Proceedings of the National*

Academy of Sciences of the United States of America, 76(4), 1570–4.

<http://doi.org/10.1073/pnas.76.4.1570>

Hayes, J. S., Brunton, L. L., & Mayer, S. E. (1980). Selective activation of particulate cAMP-dependent protein kinase by isoproterenol and prostaglandin E1. *Journal of Biological Chemistry*, 255(11), 5113–5119.

Heinrich, R., Neel, B. G., & Rapoport, T. A. (2002). Mathematical models of protein kinase signal transduction. *Molecular Cell*, 9(5), 957–970. [http://doi.org/10.1016/S1097-2765\(02\)00528-2](http://doi.org/10.1016/S1097-2765(02)00528-2)

Henn, V., Edemir, B., Stefan, E., Wiesner, B., Lorenz, D., Theilig, F., ... Klussmann, E. (2004). Identification of a novel A-kinase anchoring protein 18 isoform and evidence for its role in the vasopressin-induced aquaporin-2 shuttle in renal principal cells. *Journal of Biological Chemistry*, 279(25), 26654–26665. <http://doi.org/10.1074/jbc.M312835200>

Herberg, F. W., Dostmann, W. R., Zorn, M., Davis, S. J., & Taylor, S. S. (1994). Crosstalk between domains in the regulatory subunit of cAMP-dependent protein kinase: influence of amino terminus on cAMP binding and holoenzyme formation. *Biochemistry*, 33(23), 7485–7494. <http://doi.org/10.1021/bi00189a057>

Herberg, F. W., Doyle, M. L., Cox, S., & Taylor, S. S. (1999). Dissection of the nucleotide and metal-phosphate binding sites in cAMP-dependent protein kinase. *Biochemistry*, 38(19), 6352–6360. <http://doi.org/10.1021/bi982672w>

Herberg, F. W., Maleszka, a, Eide, T., Vossebein, L., & Tasken, K. (2000). Analysis of A-kinase anchoring protein (AKAP) interaction with protein kinase A (PKA) regulatory subunits: PKA isoform specificity in AKAP binding. *Journal of Molecular Biology*, 298(2), 329–339. <http://doi.org/10.1006/jmbi.2000.3662>

Herberg, F. W., & Taylor, S. S. (1993). Physiological inhibitors of the catalytic subunit of cAMP-dependent protein kinase: effect of MgATP on protein-protein interactions. *Biochemistry*, 32(50), 14015–22.

Herbst, K. J., Allen, M. D., & Zhang, J. (2011). Spatiotemporally regulated protein kinase A activity is a critical regulator of growth factor-stimulated extracellular signal-regulated kinase signaling in PC12 cells. *Molecular and Cellular Biology*, 31(19), 4063–75. <http://doi.org/10.1128/MCB.05459-11>

Hermanson, G. T. (2013). Chapter 3 - The Reactions of Bioconjugation. *Bioconjugate*

Techniques (Third Edition), 229–258. <http://doi.org/http://dx.doi.org/10.1016/B978-0-12-382239-0.00003-0>

- Hofmann, F., Bechtel, P. J., & Krebs, E. G. (1977). Concentrations of Cyclic AMP-dependent Subunits in Various Tissues*. *The Journal of Biological Chemistry*, 252(4), 1441–1447.
- Hornby, J. A. T., Luo, J. K., Stevens, J. M., Wallace, L. A., Kaplan, W., Armstrong, R. N., & Dirr, H. W. (2000). Equilibrium folding of dimeric class μ glutathione transferases involves a stable monomeric intermediate. *Biochemistry*, 39(40), 12336–12344. <http://doi.org/10.1021/bi000176d>
- Horvath, A., Bertherat, J., Groussin, L., Guillaud-Bataille, M., Tsang, K., Cazabat, L., ... Stratakis, C. A. (2010). Mutations and polymorphisms in the gene encoding regulatory subunit type 1-alpha of protein kinase a (PRKAR1A): An update. *Human Mutation*, 31(4), 369–379. <http://doi.org/10.1002/humu.21178>
- Hoshi, N., Langeberg, L. K., & Scott, J. D. (2005). Distinct enzyme combinations in AKAP signalling complexes permit functional diversity. *Nature Cell Biology*, 7(11), 1066–1073. <http://doi.org/10.1038/ncb1315>
- Houssay, B. A. (1956). Carl F and Gerty T cori. *Biochimica et Biophysica Acta*, 20, 11–14.
- Howlett, A. C., & Gilman, A. G. (1980). Hydrodynamic properties of the regulatory component of adenylate cyclase. *Journal of Biological Chemistry*, 255(7), 2861–2866.
- Hu, T., Wu, D., Chen, J., Ding, J., Jiang, H., & Shen, X. (2008). The catalytic intermediate stabilized by a “down” active site loop for diaminopimelate decarboxylase from *Helicobacter pylori*: Enzymatic characterization with crystal structure analysis. *Journal of Biological Chemistry*, 283(30), 21284–21293. <http://doi.org/10.1074/jbc.M801823200>
- Huang, L. J.-S., Durick, K., Weiner, J. A., Chun, J., & Taylor, S. S. (1997). Identification of a Novel Protein Kinase A Anchoring Protein That Binds Both Type I and Type II Regulatory Subunits. *Journal of Biological Chemistry*, 272(12), 8057–8064. <http://doi.org/10.1074/jbc.272.12.8057>
- Huang, L. J., Durick, K., Weiner, J. A., Chun, J., & Taylor, S. S. (1997). D-AKAP2, a novel protein kinase A anchoring protein with a putative RGS domain. *Proceedings of the National Academy of Sciences of the United States of America*, 94(21), 11184–9. <http://doi.org/10.1073/pnas.94.21.11184>

- Huang, Y. Y., Kandel, E. R., Varshavsky, L., Brandon, E. P., Qi, M., Idzerda, R. L., ... Bourtchouladze, R. (1995). A genetic test of the effects of mutations in PKA on mossy fiber LTP and its relation to spatial and contextual learning. *Cell*, *83*(7), 1211–22.
- Huang, Y. Y., Li, X. C., & Kandel, E. R. (1994). cAMP contributes to mossy fiber LTP by initiating both a covalently mediated early phase and macromolecular synthesis-dependent late phase. *Cell*, *79*(1), 69–79.
- Ilouz, R., Bubis, J., Wu, J., Yim, Y. Y., Deal, M. S., Kornev, A. P., ... Taylor, S. S. (2012). Localization and quaternary structure of the PKA RI β holoenzyme. *Proceedings of the National Academy of Sciences of the United States of America*, *109*(31), 12443–8. <http://doi.org/10.1073/pnas.1209538109>
- Insel, P. A., Maguire, M. E., Gilman, A. G., Bourne, H. R., Coffino, P., & Melmon, K. L. (1976). Beta adrenergic receptors and adenylate cyclase: products of separate genes? *Mol Pharmacol*, *12*(6), 1062–1069.
- Iwami, G., Kawabe, J. I., Ebina, T., Cannon, P. J., Homcy, C. J., & Ishikawa, Y. (1995). Regulation of adenylyl cyclase by protein kinase A. *Journal of Biological Chemistry*. <http://doi.org/10.1074/jbc.270.21.12481>
- Jarnæss, E., Ruppelt, A., Stokka, A. J., Lygren, B., Scott, J. D., & Tasken, K. (2008). Dual specificity A-kinase anchoring proteins (AKAPs) contain an additional binding region that enhances targeting of protein kinase A type I. *Journal of Biological Chemistry*, *283*(48), 33708–33718. <http://doi.org/10.1074/jbc.M804807200>
- Johnson, L. N., & Lewis, R. J. (2001). Structural basis for control by phosphorylation. *Chemical Reviews*, *101*(8), 2209–2242. <http://doi.org/10.1021/cr000225s>
- Jones, B. W., Brunet, S., Gilbert, M. L., Nichols, C. B., Su, T., Westenbroek, R. E., ... McKnight, G. S. (2012). Cardiomyocytes from AKAP7 knockout mice respond normally to adrenergic stimulation. *Proceedings of the National Academy of Sciences*, *109*(42), 17099–17104. <http://doi.org/10.1073/pnas.1215219109>
- Jones, M. N. (1999). Surfactants in membrane solubilisation. *International Journal of Pharmaceutics*, *177*(2), 137–159. [http://doi.org/10.1016/S0378-5173\(98\)00345-7](http://doi.org/10.1016/S0378-5173(98)00345-7)
- Kameyama, K., Lee, H. K., Bear, M. F., & Huganir, R. L. (1998). Involvement of a postsynaptic protein kinase A substrate in the expression of homosynaptic long-term depression. *Neuron*, *21*(5), 1163–1175. [http://doi.org/10.1016/S0896-6273\(00\)80633-9](http://doi.org/10.1016/S0896-6273(00)80633-9)

- Kang, C. B., Hong, Y., Dhe-Paganon, S., & Yoon, H. S. (2008). FKBP family proteins: Immunophilins with versatile biological functions. *NeuroSignals*, *16*(4), 318–325. <http://doi.org/10.1159/000123041>
- Kao, R. S., Abbott, M. J., Louie, A., O'Carroll, D., Lu, W., & Nissenson, R. (2013). Constitutive protein kinase A activity in osteocytes and late osteoblasts produces an anabolic effect on bone. *Bone*, *55*(2), 277–287. <http://doi.org/10.1016/j.bone.2013.04.001>
- Katritch, V., Cherezov, V., & Stevens, R. C. (2013). Structure-Function of the G Protein–Coupled Receptor Superfamily. *Annu. Rev. Pharmacol. Toxicol*, *53*, 531–56. <http://doi.org/10.1146/annurev-pharmtox-032112-135923>
- Katsura, T., Gustafson, C. E., Ausiello, D. A., & Brown, D. (1997). Protein kinase A phosphorylation is involved in regulated exocytosis of aquaporin-2 in transfected LLC-PK1 cells. *The American Journal of Physiology*, *272*(6 Pt 2), F817–F822.
- Kawasaki, H., Springett, G. M., Mochizuki, N., Toki, S., Nakaya, M., Matsuda, M., ... Graybiel, A. M. (1998). A family of cAMP-binding proteins that directly activate Rap1. *Science (New York, N.Y.)*, *282*(5397), 2275–2279. <http://doi.org/10.1126/science.282.5397.2275>
- Keely, S. L. (1979a). Prostaglandin E1 activation of heart cAMP-dependent protein kinase: Apparent dissociation of protein kinase activation from increases in phosphorylase activity and contractile force. *Mol.Pharmacol.*, *15*, 235–245.
- Keely, S. L. (1979b). Prostaglandin E1 Activation of Heart cAMP-dependent Protein Kinase: Apparent Dissociation of Protein Kinase Activation from Increases in Phosphorylase Activity and Contractile Force. *Molecular Pharmacology*, *15*, 235–245.
- Kemp, B. E., Graves, D. J., Benjamini, E., & Krebs, G. (1977). Role of multiple basic residues in determining the substrate specificity of cyclic AMP-dependent protein kinase. *Journal of Biological Chemistry*, *252*, 4888–4894.
- Kemp, B. E., & Pearson, R. B. (1990). Protein kinases recognition sequence motifs. *Trends in Biochemical Science*, *15*(9), 342–346.
- Keravis, T., & Lugnier, C. (2012). Cyclic nucleotide phosphodiesterase (PDE) isozymes as targets of the intracellular signalling network: Benefits of PDE inhibitors in various diseases and perspectives for future therapeutic developments. *British Journal of Pharmacology*, *165*(5), 1288–1305. <http://doi.org/10.1111/j.1476-5381.2011.01729.x>

- Kim, C., Xuong, N.-H., & Taylor, S. S. (2005). Crystal structure of a complex between the catalytic and regulatory (R1 α) subunits of PKA. *Science (New York, N.Y.)*, 307(5710), 690–6. <http://doi.org/10.1126/science.1104607>
- Kirschner, L. S., Carney, J. A., Pack, S. D., Taymans, S. E., Giatzakis, C., Cho, Y. S., ... Stratakis, C. A. (2000). Mutations of the gene encoding the protein kinase A type I- α regulatory subunit in patients with the Carney complex. *Nature Genetics*, 26(1), 89–92. <http://doi.org/10.1038/79238>
- Klainer, L., Chi, Y.-M., Freidberg, S., Rall, T. W., & Sutherland, E. W. (1962). Adenyl Cyclase IV. The effects of neurohormones on the formation of adenosine 3',5'-phosphate by preparations from brain and other tissues. *The Journal of Biological Chemistry*, 237, 1239–1243.
- Klarenbeek, J. B., Goedhart, J., Hink, M. A., Gadella, T. W. J., & Jalink, K. (2011). A mTurquoise-based cAMP sensor for both FLIM and ratiometric read-out has improved dynamic range. *PloS One*, 6(4), e19170. <http://doi.org/10.1371/journal.pone.0019170>
- Klauck, T. M., Faux, M. C., Labudda, K., Langeberg, L. K., Jaken, S., & Scott, J. D. (1996). Coordination of three signaling enzymes by AKAP79, a mammalian scaffold protein. *Science*, 271(5255), 1589–1592. <http://doi.org/10.1126/science.271.5255.1589>
- Knighton, D. R., Zheng, J., Eyck, L. F. Ten, Ashford, V. A., Xuong, N., Taylor, S. S., ... Eyck, L. F. T. E. N. (1991). Crystal Structure of the Catalytic Subunit of Cyclic Adenosine-Monophosphate Protein Kinase. *Science*, 253(5018), 407–414.
- Knighton, D. R., Zheng, J., Ten Eyck, L. F., Xuong, N.-H., Taylor, S. S., & Sowadski, J. M. (1991). Structure of a peptide inhibitor bound to the catalytic subunit of cyclic AMP dependent protein kinase. *Science*, 253(May 1990), 414–420.
- Konstantinopoulos, P. A., Karamouzis, M. V., & Papavassiliou, A. G. (2007). Post-translational modifications and regulation of the RAS superfamily of GTPases as anticancer targets. *Nat Rev Drug Discov*, 6(7), 541–555. <http://doi.org/10.1038/nrd2221>
- Kornev, A. P., Haste, N. M., Taylor, S. S., & Eyck, L. F. Ten. (2006). Surface comparison of active and inactive protein kinases identifies a conserved activation mechanism. *Proceedings of the National Academy of Sciences of the United States of America*, 103(47), 17783–17788. <http://doi.org/10.1073/pnas.0607656103>

- Kornev, A. P., & Taylor, S. S. (2010). Defining the conserved internal architecture of a protein kinase. *Biochimica et Biophysica Acta - Proteins and Proteomics*, 1804(3), 440–444. <http://doi.org/10.1016/j.bbapap.2009.10.017>
- Kornev, A. P., Taylor, S. S., & Ten Eyck, L. F. (2008). A helix scaffold for the assembly of active protein kinases. *Proceedings of the National Academy of Sciences of the United States of America*, 105(38), 14377–82. <http://doi.org/10.1073/pnas.0807988105>
- Kovanich, D., Van Der Heyden, M. A. G., Aye, T. T., Van Veen, T. A. B., Heck, A. J. R., & Scholten, A. (2010). Sphingosine kinase interacting protein is an A-kinase anchoring protein specific for type I cAMP-dependent protein kinase. *ChemBioChem*, 11(7), 963–971. <http://doi.org/10.1002/cbic.201000058>
- Kranias, E. G. (1985). Regulation of Ca²⁺ transport by cyclic 3',5'-AMP-dependent and calcium-calmodulin-dependent phosphorylation of cardiac sarcoplasmic reticulum. *Biochimica et Biophysica Acta*, 844(2), 193–199.
- Krebs, E. G., Graves, D. J., & Fischer, E. H. (1959). Factors affecting the activity of muscle phosphorylase b kinase. *The Journal of Biological Chemistry*, 234, 2867–2873.
- Kresge, N., Simoni, R. D., & Hill, R. L. (2005a). Earl W. Sutherland's Discovery of Cyclic Adenine Monophosphate and the Second Messenger System. *Journal of Biological Chemistry*, 280(42), e39–e39. <http://doi.org/10.1074/jbc.X400012200>
- Kresge, N., Simoni, R. D., & Hill, R. L. (2005b). The Regulation of Adenyl Cyclase by G-protein : the Work. *Biochemistry*, 280(44), 41–43.
- Layland, J., Solaro, R. J., & Shah, A. M. (2005). Regulation of cardiac contractile function by troponin I phosphorylation. *Cardiovascular Research*, 66(1), 12–21. <http://doi.org/10.1016/j.cardiores.2004.12.022>
- Le Gall, T., Romero, P. R., Cortese, M. S., Uversky, V. N., & Dunker, a K. (2007). Intrinsic disorder in the Protein Data Bank. *Journal of Biomolecular Structure & Dynamics*, 24(4), 325–342. <http://doi.org/10.1080/07391102.2007.10507123>
- Lee, H. K., Barbarosie, M., Kameyama, K., Bear, M. F., & Huganir, R. L. (2000). Regulation of distinct AMPA receptor phosphorylation sites during bidirectional synaptic plasticity. *Nature*, 405(6789), 955–959. <http://doi.org/10.1038/35016089>
- Leitner, A., Walzthoeni, T., & Aebersold, R. (2014). Lysine-specific chemical cross-linking of protein complexes and identification of cross-linking sites using LC-MS/MS and the

xQuest/xProphet software pipeline. *Nature Protocols*, 9(1), 120–37.

<http://doi.org/10.1038/nprot.2013.168>

Leitner, A., Walzthoeni, T., Kahraman, A., Herzog, F., Rinner, O., Beck, M., & Aebersold, R. (2010). Probing native protein structures by chemical cross-linking, mass spectrometry, and bioinformatics. *Molecular & Cellular Proteomics : MCP*, 9(8), 1634–49. <http://doi.org/10.1074/mcp.R000001-MCP201>

Li, H., Degenhardt, B., Tobin, D., Yao, Z.-X., Tasken, K., & Papadopoulos, V. (2001). Identification, localization, and function in steroidogenesis of PAP7 - A peripheral-type benzodiazepine receptor - and PKA (R1 α)-associated protein. *Molecular Endocrinology*, 15(12), 2211–2228.

Li, L., Desantiago, J., Chu, G., Kranias, E. G., & Bers, D. M. (2000). Phosphorylation of phospholamban and troponin I in β -adrenergic-induced acceleration of cardiac relaxation. *American Journal of Physiology. Heart and Circulatory Physiology*, 278(3), H769–H779.

Li, Y., Chen, L., Kass, R. S., & Dessauer, C. W. (2012). The A-kinase anchoring protein yotiao facilitates complex formation between adenylyl cyclase type 9 and the IKs potassium channel in heart. *Journal of Biological Chemistry*, 287(35), 29815–29824. <http://doi.org/10.1074/jbc.M112.380568>

Limbird, L. E., & Lefkowitz, R. J. (1977). Resolution of beta-adrenergic receptor binding and adenylyl cyclase activity by gel exclusion chromatography. *The Journal of Biological Chemistry*, 252(2), 799–802.

Linderman, J. J. (2009). Modeling of G-protein-coupled receptor signaling pathways. *Journal of Biological Chemistry*, 284(9), 5427–5431. <http://doi.org/10.1074/jbc.R800028200>

Linglart, A., Fryssira, H., Hiort, O., Holterhus, P. M., Perez De Nanclares, G., Argente, J., ... Silve, C. (2012). PRKAR1A and PDE4D mutations cause acrodysostosis but two distinct syndromes with or without GPCR-signaling hormone resistance. *Journal of Clinical Endocrinology and Metabolism*, 97(12), 2328–2338. <http://doi.org/10.1210/jc.2012-2326>

Linglart, A., Menguy, C., Couvineau, A., Auzan, C., Gunes, Y., Cancel, M., ... Silve, C. (2011). Recurrent PRKAR1A Mutation in Acrodysostosis with Hormone Resistance. *The New England Journal of Medicine*, 364(23), 2218–2226.

- Lipkin, D., Cook, W., & Markam, R. (1959). Adenosine-3', 5'-phosphoric Acid : A Proof of Structure. *Journal of the American Chemical Society*, *81*(23), 6198–6203.
- Lommerse, P. H. M., Vastenhoud, K., Pirinen, N. J., Magee, A. I., Spaik, H. P., & Schmidt, T. (2006). Single-molecule diffusion reveals similar mobility for the Lck, H-ras, and K-ras membrane anchors. *Biophysical Journal*, *91*(3), 1090–1097.
<http://doi.org/10.1529/biophysj.105.079053>
- MacCoss, M. J., Wu, C. C., & Yates, J. R. (2002). Probability based validation of protein identifications using a modified SEQUEST algorithm. *Analytical Chemistry*, *74*(21), 5593–5599. <http://doi.org/10.1021/ac025826t>
- Madhusudan, Akamine, P., Xuong, N.-H., & Taylor, S. S. (2002). Crystal structure of a transition state mimic of the catalytic subunit of cAMP-dependent protein kinase. *Nature Structural Biology*, *9*(4), 273–7. <http://doi.org/10.1038/nsb780>
- Makarov, A. (2000). Electrostatic axially harmonic orbital trapping: A high-performance technique of mass analysis. *Analytical Chemistry*, *72*(6), 1156–1162.
<http://doi.org/10.1021/ac991131p>
- Malbon, C. C., Tao, J., & Wang, H. (2004). AKAPs (A-kinase anchoring proteins) and molecules that compose their G-protein-coupled receptor signalling complexes. *The Biochemical Journal*, *379*(Pt 1), 1–9. <http://doi.org/10.1042/BJ20031648>
- Manning, G., Whyte, D. B., Martinez, R., Hunter, T., & Sudarsanam, S. (2002). The Protein Kinase Complement of the Human Genome. *Science*, *298*(5600), 1912–1934.
<http://doi.org/10.1126/science.1075762>
- Marvil, D. K., & Leisinger, T. (1977). N-Acetylglutamate of Escherichia coli: purification, characterization and molecular properties. *The Journal of Biological Chemistry*, *252*, 3295–3303.
- Marx, S. O., Reiken, S., Hisamatsu, Y., Jayaraman, T., Burkhoff, D., Rosembli, N., & Marks, A. R. (2000). PKA Phosphorylation Dissociates FKBP12.6 from the Calcium Release Channel (Ryanodine Receptor). *Cell*, *101*(4), 365–376. [http://doi.org/10.1016/S0092-8674\(00\)80847-8](http://doi.org/10.1016/S0092-8674(00)80847-8)
- Matic, I., Jaffray, E. G., Oxenham, S. K., Groves, M. J., Barratt, C. L. R., Tauro, S., ... Hay, R. T. (2011). Absolute SILAC-compatible expression strain allows sumo-2 copy number determination in clinical samples. *Journal of Proteome Research*, *10*(10), 4869–4875.

<http://doi.org/10.1021/pr2004715>

- Maurice, D. H., Ke, H., Ahmad, F., Wang, Y., Chung, J., & Manganiello, V. C. (2014). Advances in targeting cyclic nucleotide phosphodiesterases. *Nature Reviews. Drug Discovery*, 13(4), 290–314. <http://doi.org/10.1038/nrd4228>
- McCudden, C. R., Hains, M. D., Kimple, R. J., Siderovski, D. P., & Willard, F. S. (2005). G-protein signaling: Back to the future. *Cellular and Molecular Life Sciences*, 62(5), 551–577. <http://doi.org/10.1007/s00018-004-4462-3>
- McTigue, M. A., Williams, D. R., & Tainer, J. A. (1995). Crystal structures of a schistosomal drug and vaccine target: glutathione S-transferase from *Schistosoma japonica* and its complex with the leading antischistosomal drug praziquantel. *Journal of Molecular Biology*, 246(1), 21–27. <http://doi.org/10.1006/jmbi.1994.0061>
- Means, C. K., Lygren, B., Langeberg, L. K., Jain, A., Dixon, R. E., Vega, A. L., ... Scott, J. D. (2011). An entirely specific type I A-kinase anchoring protein that can sequester two molecules of protein kinase A at mitochondria. *Proceedings of the National Academy of Sciences of the United States of America*, 108(48), E1227-35. <http://doi.org/10.1073/pnas.1107182108>
- Michel, J. J. C., & Scott, J. D. (2002). Akap mediated signal transduction. *Annual Review of Pharmacology and Toxicology*, (42), 235–257.
- Mongillo, M., McSorley, T., Evellin, S., Sood, A., Lissandron, V., Terrin, A., ... Zaccolo, M. (2004). Fluorescence resonance energy transfer-based analysis of cAMP dynamics in live neonatal rat cardiac myocytes reveals distinct functions of compartmentalized phosphodiesterases. *Circulation Research*, 95(1), 67–75. <http://doi.org/10.1161/01.RES.0000134629.84732.11>
- Murad, F., Chi, Y.-M., Rall, T. W., & Sutherland, E. W. (1962). Adenyl Cyclase III. The effect of catecholamines and choline esters on the formation of adenosine 3',5'-phosphate by preparations from cardiac muscle and liver. *The Journal of Biological Chemistry*, 237, 1233–1238.
- Naot, D., Grey, A., Reid, I. R., & Cornish, J. (2005). Lactoferrin--a novel bone growth factor. *Clinical Medicine & Research.*, 3(2), 93–101. <http://doi.org/3/2/93> [pii]
- Neuberger, G., Schneider, G., & Eisenhaber, F. (2007). pkaPS: prediction of protein kinase A phosphorylation sites with the simplified kinase-substrate binding model. *Biology*

Direct, 2, 1. <http://doi.org/10.1186/1745-6150-2-1>

- Newlon, M. G., Roy, M., Morikis, D., Hausken, Z. E., Coghlan, V., Scott, J. D., & Jennings, P. A. (1999). The molecular basis for protein kinase A anchoring revealed by solution NMR. *Nature Structural Biology*, 6(3), 222–7. <http://doi.org/10.1038/6663>
- Nicoll, R. A., & Schmitz, D. (2005). Synaptic plasticity at hippocampal mossy fibre synapses. *Nature Reviews. Neuroscience*, 6(11), 863–76. <http://doi.org/10.1038/nrn1786>
- Northup, J. K., Sternweis, P. C., Smigel, M. D., Schleifer, L. S., Ross, E. M., & Gilman, A. G. (1980). Purification of the regulatory component of adenylate cyclase. *Proceedings of the National Academy of Sciences of the United States of America*, 77(11), 6516–6520. <http://doi.org/10.1073/pnas.77.11.6516>
- Oliveria, S. F., Dell'Acqua, M. L., & Sather, W. A. (2007). AKAP79/150 Anchoring of Calcineurin Controls Neuronal L-Type Ca²⁺ Channel Activity and Nuclear Signaling. *Neuron*, 55(2), 261–275. <http://doi.org/10.1016/j.neuron.2007.06.032>
- Ong, S.-E. (2002). Stable Isotope Labeling by Amino Acids in Cell Culture, SILAC, as a Simple and Accurate Approach to Expression Proteomics. *Molecular & Cellular Proteomics*, 1(5), 376–386. <http://doi.org/10.1074/mcp.M200025-MCP200>
- Pearce, L. R., Komander, D., & Alessi, D. R. (2010). The nuts and bolts of AGC protein kinases. *Nature Reviews. Molecular Cell Biology*, 11(1), 9–22. <http://doi.org/10.1038/nrm2822>
- Piggott, L. a, Bauman, A. L., Scott, J. D., & Dessauer, C. W. (2008). The A-kinase anchoring protein Yotiao binds and regulates adenylyl cyclase in brain. *Proceedings of the National Academy of Sciences of the United States of America*, 105(37), 13835–40. <http://doi.org/10.1073/pnas.0712100105>
- Piston, D. W., & Kremers, G.-J. (2007). Fluorescent protein FRET: the good, the bad and the ugly. *Trends in Biochemical Sciences*, 32(9), 407–414. <http://doi.org/10.1016/j.tibs.2007.08.003>
- Ponsioen, B., Zhao, J., Riedl, J., Zwartkuis, F., van der Krogt, G., Zaccolo, M., ... Jalink, K. (2004). Detecting cAMP-induced Epac activation by fluorescence resonance energy transfer: Epac as a novel cAMP indicator. *EMBO Reports*, 5(12), 1176–1180. <http://doi.org/10.1038/sj.embor.7400290>
- Poppe, H., Rybalkin, S. D., Rehmann, H., Hinds, T. R., Tang, X.-B., Christensen, A. E., ... Butt,

- E. (2008). Cyclic nucleotide analogs as probes of signaling pathways. *Nature Methods*, 5(4), 277–278. <http://doi.org/10.1038/nmeth0408-277>
- Preston, G. W., & Wilson, A. J. (2013). Photo-induced covalent cross-linking for the analysis of biomolecular interactions. *Chemical Society Reviews*, 42(8), 3289–301. <http://doi.org/10.1039/c3cs35459h>
- Putnam, C. D., Hammel, M., Hura, G. L., & Tainer, J. A. (2007). X-ray solution scattering (SAXS) combined with crystallography and computation: defining accurate macromolecular structures, conformations and assemblies in solution. *Quarterly Reviews of Biophysics*, 40(3), 191–285. <http://doi.org/10.1016/j.bpj.2010.12.409>
- Radhakrishnan, K., Halász, Á., McCabe, M. M., Edwards, J. S., & Wilson, B. S. (2012). Mathematical simulation of membrane protein clustering for efficient signal transduction. *Annals of Biomedical Engineering*, 40(11), 2307–2318. <http://doi.org/10.1007/s10439-012-0599-z>
- Radivojac, P., Obradovic, Z., Smith, D. K., Zhu, G., Vucetic, S., Brown, C. J., ... Dunker, A. K. (2004). Protein flexibility and intrinsic disorder. *Protein Sci*, 13(1), 71–80. <http://doi.org/10.1110/ps.03128904.structures>
- Rall, T., & Sutherland, E. W. (1958). Formation of a cyclic adenine ribonucleotide by tissue particles. *Journal of Biological Chemistry*, 232, 1065–1076.
- Rall, T., Sutherland, E. W., & Berthet, J. (1957). The relationship of epinephrine and glucagon to liver phosphorylase IV. Effect of epinephrine and glucagon on the reactivation of phosphorylase in liver homogenates. *Journal of Biological Chemistry*, 224, 463–475. <http://doi.org/10.1007/s13398-014-0173-7.2>
- Rall, T., Sutherland, E. W., & Wosilait, W. D. (1956). The Relationship of epinephrine to liver phosphorylase III. Reactivation of liver phosphorylase in slices and in extracts. *Journal of Biological Chemistry*, 218, 483–495.
- Rall, T. w. (1975). Opening Remarks. In G. I. Drummond, P. Greengard, & G. A. Robinson (Eds.), *Advances in cyclic nucleotide research* (Vol. 5, pp. 1–2). New York: Raven Press.
- Rall, T. W., & Sutherland, E. W. (1962). Adenyl Cyclase II. The enzymatically catalyzed formation of adenosine 3',5'-phosphate and inorganic pyrophosphate from adenosine triphosphate. *The Journal of Biological Chemistry*, 237, 1228–1232.
- Rebola, N., Pinheiro, P. C., Oliveira, C. R., Malva, J. O., & Cunha, R. a. (2003). Subcellular

localization of adenosine A(1) receptors in nerve terminals and synapses of the rat hippocampus. *Brain Research*, 987(1), 49–58.

Reinton, N., Collas, P., Haugen, T. B., Skålhegg, B. S., Hansson, V., Jahnsen, T., & Taskén, K. (2000). Localization of a novel human A-kinase-anchoring protein, hAKAP220, during spermatogenesis. *Developmental Biology*, 223(1), 194–204.

<http://doi.org/10.1006/dbio.2000.9725>

Rich, T. C., & Karpen, J. W. (2002). Review article: Cyclic AMP sensors in living cells: What signals can they actually measure? *Annals of Biomedical Engineering*, 30(8), 1088–1099. <http://doi.org/10.1114/1.1511242>

Rich, T. C., Tse, T. E., Rohan, J. G., Schaack, J., & Karpen, J. W. (2001). In vivo assessment of local phosphodiesterase activity using tailored cyclic nucleotide-gated channels as cAMP sensors. *The Journal of General Physiology*, 118(1), 63–78.

<http://doi.org/10.1085/jgp.118.1.63>

Richie-Jannetta, R., Francis, S. H., & Corbin, J. D. (2003). Dimerization of cGMP-dependent Protein Kinase I β Is Mediated by an Extensive Amino-terminal Leucine Zipper Motif, and Dimerization Modulates Enzyme Function. *Journal of Biological Chemistry*, 278(50), 50070–50079. <http://doi.org/10.1074/jbc.M306796200>

Rinner, O., Seebacher, J., Walzthoeni, T., Mueller, L. N., Beck, M., Schmidt, A., ... Aebersold, R. (2008). Identification of cross-linked peptides from large sequence databases.

Nature Methods, 5(4), 315–8. <http://doi.org/10.1038/nmeth.1192>

Robertson, S. P., Johnson, J. D., Holroyde, M. J., Kraniass, E. G., Potter, J. D., & Solaro, R. J. (1982). The Effect of Troponin I Phosphorylation on the Ca²⁺ -binding of Bovine Cardiac Troponin * Properties of the Ca²⁺ -regulatory Site, 257(1), 260–263.

Rodbell, M. (1994). Signal Transduction : Evolution of an idea, 220–237.

Rodbell, M., Birnbaumer, L., Pohl, S. L., & Krans, H. M. J. (1971). The glucagon-sensitive adenylyl cyclase system in plasma membranes of rat liver V. An obligatory role of guanylyl nucleotides in glucagon action. *Journal of Biological Chemistry*, 246(6), 1877–1882.

Rodbell, M., Krans, H. M. J., Pohl, S. L., & Birnbaumer, L. (1971). The glucagon-sensitive adenylyl cyclase system in plasma membranes of rat liver. IV Effects of guanylyl nucleotides on binding of ¹²⁵I-glucagon. *The Journal of Biological Chemistry*, 246(6), 1872–1876.

- Rodbell, M., Lin, M. C., & Salomon, Y. (1974). Evidence for interdependent action of glucagon and nucleotides on the hepatic adenylate cyclase system. *The Journal of Biological Chemistry*, 249(1), 59–65.
- Roh, E., Yun, C.-Y., Young Yun, J., Park, D., Doo Kim, N., Yeon Hwang, B., ... Kim, Y. (2013). cAMP-binding site of PKA as a molecular target of bisabolangelone against melanocyte-specific hyperpigmented disorder. *The Journal of Investigative Dermatology*, 133(4), 1072–9. <http://doi.org/10.1038/jid.2012.425>
- Ross, E. M., & Gilman, A. G. (1977). Reconstitution of catecholamine-sensitive adenylate cyclase activity : Interaction of solubilized components with receptor-replete membranes. *Proceedings of the National Academy of Sciences of the United States of America*, 74(9), 3715–3719.
- Rufer, A. C., Thiebach, L., Baer, K., Klein, H. W., & Hennig, M. (2005). X-ray structure of glutathione S-transferase from *Schistosoma japonicum* in a new crystal form reveals flexibility of the substrate-binding site. *Acta Crystallographica Section F: Structural Biology and Crystallization Communications*, 61(3), 263–265. <http://doi.org/10.1107/S1744309105004823>
- Ruppelt, A., Mosenden, R., Gronholm, M., Aandahl, E. M., Tobin, D., Carlson, C. R., ... Tasken, K. (2007). Inhibition of T cell activation by cyclic adenosine 5'-monophosphate requires lipid raft targeting of protein kinase A type I by the A-kinase anchoring protein ezrin. *Journal of Immunology*, 179(8), 5159–5168. <http://doi.org/10.4049/jimmunol.179.8.5159>
- Russo, C. J., & Passmore, L. A. (2016). Progress towards an optimal specimen support for electron cryomicroscopy. *Current Opinion in Structural Biology*, 37, 81–89. <http://doi.org/10.1016/j.sbi.2015.12.007>
- Sarkar, D., Erlichman, J., & Rubin, C. S. (1984). Identification of a calmodulin-binding protein that co-purifies with the regulatory subunit of brain protein kinase II. *Journal of Biological Chemistry*, 259(15), 9840–9846.
- Sarma, G. N., Kinderman, F. S., Kim, C., von Daake, S., Chen, L., Wang, B. C., & Taylor, S. S. (2010). Structure of D-AKAP2:PKA RI Complex: Insights into AKAP Specificity and Selectivity. *Structure*, 18(2), 155–166. <http://doi.org/10.1016/j.str.2009.12.012>
- Schneider, C. a, Rasband, W. S., & Eliceiri, K. W. (2012). NIH Image to ImageJ: 25 years of

- image analysis. *Nature Methods*, 9(7), 671–675. <http://doi.org/10.1038/nmeth.2089>
- Schütz, G. J., Schindler, H., & Schmidt, T. (1997). Single-molecule microscopy on model membranes reveals anomalous diffusion. *Biophysical Journal*, 73(2), 1073–1080. [http://doi.org/10.1016/S0006-3495\(97\)78139-6](http://doi.org/10.1016/S0006-3495(97)78139-6)
- Seebacher, J., Mallick, P., Zhang, N., Eddes, J. S., Aebersold, R., & Gelb, M. H. (2006). Protein cross-linking analysis using mass spectrometry, isotope-coded cross-linkers, and integrated computational data processing. *Journal of Proteome Research*, 5(9), 2270–82. <http://doi.org/10.1021/pr060154z>
- Shen, J. X., & Cooper, D. M. (2013). AKAP79, PKC, PKA and PDE4 participate in a Gq-linked muscarinic receptor and adenylyl cyclase 2 cAMP signalling complex. *Biochem J*, 455(1), 47–56. <http://doi.org/10.1042/BJ20130359>
- Skålhegg, B. S., Taskén, K., Hansson, V., Huitfeldt, H. S., Jahnsen, T., Lea, T., ... Tasken, K. (1994). Location of cAMP-Dependent Protein Kinase Type I with the TCR-CD3 Complex. *Science*, 263(5143), 84–87.
- Smith, D. B., & Johnson, K. S. (1988). Single-step purification of polypeptides expressed in *Escherichia coli* as fusions with glutathione S-transferase. *Gene*, 67, 31–40.
- Smith, F. D., Reichow, S. L., Esseltine, J. L., Shi, D., Langeberg, L. K., Scott, J. D., & Gonen, T. (2013). Intrinsic disorder within an AKAP-protein kinase A complex guides local substrate phosphorylation. *eLife*, 2, 1–19. <http://doi.org/10.7554/eLife.01319>
- Snyder, E. M., Colledge, M., Crozier, R. A., Chen, W. S., Scott, J. D., & Bear, M. F. (2005). Role for A Kinase-anchoring Proteins (AKAPS) in Glutamate Receptor Trafficking and Long Term Synaptic Depression. *Journal of Biological Chemistry*, 280(17), 16962–16968. <http://doi.org/10.1038/nmeth.2250>. Digestion
- Solaro, R., Moir, A., & Perry, S. (1976). Phosphorylation of troponin I and the inotropic effect of adrenaline in the perfused rabbit heart. *Nature*, 262, 615–617.
- Songyang, Z., Blechner, S., Hoagland, N., Hoekstra, M. F., Piwnicka-Worms, H., & Cantley, L. C. (1994). Use of an oriented peptide library to determine the optimal substrates of protein kinases. *Current Biology*, 4(11), 973–982. [http://doi.org/10.1016/S0960-9822\(00\)00221-9](http://doi.org/10.1016/S0960-9822(00)00221-9)
- Spencer, D. M., Wandless, T. J., Schreiber, S. L., & Crabtree, G. R. (1993). Controlling signal transduction with synthetic ligands. *Science (New York, N.Y.)*, 262(5136), 1019–1024.

<http://doi.org/10.1126/science.7694365>

Stefan, E., Wiesner, B., Baillie, G. S., Mollajew, R., Henn, V., Lorenz, D., ... Klusmann, E. (2007). Compartmentalization of cAMP-dependent signaling by phosphodiesterase-4D is involved in the regulation of vasopressin-mediated water reabsorption in renal principal cells. *Journal of the American Society of Nephrology : JASN*, 18(1), 199–212. <http://doi.org/10.1681/ASN.2006020132>

Stratakis, C. a, Salpea, P., & Margarita, R. (2015). Carney Complex. In *GeneReviews* (pp. 320–322). <http://doi.org/10.1016/j.athoracsur.2005.07.099>

Sutherland, E., & Rall, T. (1957). The properties of an adenine ribonucleotide produced with cellular particles, ATP, Mg⁺⁺, and epinephrine or glucagon. *Journal of the American Chemical Society*, 79(4), 3608. <http://doi.org/10.1021/ja01570a087>

Sutherland, E. W., & Rall, T. (1958). Fractionation and characterization of a cyclic adenine ribonucleotide formed by tissue particles. *Journal of Biological Chemistry*, 232, 1077–1091.

Sutherland, E. W., & Rall, T. W. (1960). The relation of adenosine-3', 5'-phosphate and phosphorylase to the actions of catecholamines and other hormones. *Pharmacol. Rev.*, 12(3), 265–299. <http://doi.org/VL - 12>

Sutherland, E. W., Rall, T. W., & Menon, T. (1962). Adenyl Cyclase I. Distribution, Preparation, and Properties. *Journal of Biological Chemistry*, 237, 1220–1227.

Sutherland, E. W., & Wosilait, W. D. (1955). Inactivation and activation of liver phosphorylase. *Nature*, 175(4447), 169–170. <http://doi.org/10.1038/175169a0>

Tadaa, M., Inuia, M., Yamadaa, M., Kadomaa, M., Kuzuyaa, T., Abea, H., & Kakiuchi, S. (1983). Effects of phospholamban phosphorylation catalyzed by adenosine 3':5'-monophosphate- and calmodulin-dependent protein kinases on calcium transport ATPase of cardiac sarcoplasmic reticulum. *Journal of Molecular and Cellular Cardiology*, 15(5), 335–346.

Tavalin, S. J., Colledge, M., Hell, J. W., Langeberg, L. K., Huganir, R. L., & Scott, J. D. (2002). Regulation of GluR1 by the A-kinase anchoring protein 79 (AKAP79) signaling complex shares properties with long-term depression. *The Journal of Neuroscience : The Official Journal of the Society for Neuroscience*, 22(8), 3044–3051. <http://doi.org/20026277>

- Taylor, S. S., Ilouz, R., Zhang, P., & Kornev, A. P. (2012). Assembly of allosteric macromolecular switches: lessons from PKA. *Nature Reviews. Molecular Cell Biology*, 13(10), 646–58. <http://doi.org/10.1038/nrm3432>
- Taylor, S. S., & Kornev, A. P. (2011). Protein kinases: Evolution of dynamic regulatory proteins. *Trends in Biochemical Sciences*, 36(2), 65–77. <http://doi.org/10.1016/j.tibs.2010.09.006>
- Taylor, S. S., Zhang, P., Steichen, J. M., Keshwani, M. M., & Kornev, A. P. (2013). PKA: lessons learned after twenty years. *Biochimica et Biophysica Acta*, 1834(7), 1271–8. <http://doi.org/10.1016/j.bbapap.2013.03.007>
- Thermo Scientific. (2013). Extinction coefficients. <http://doi.org/10.1007/s00128-006-1097-5>
- Theurkauf, W. E., & Vallee, R. B. (1982). Molecular Characterization of the CAMP-dependent Protein Kinase Bound to Microtubule-associated Protein. *The Journal of Biological Chemistry*, 257(6), 3284–3290.
- Tian, T., Plowman, S. J., Parton, R. G., Kloog, Y., & Hancock, J. F. (2010). Mathematical modeling of K-Ras nanocluster formation on the plasma membrane. *Biophysical Journal*, 99(2), 534–543. <http://doi.org/10.1016/j.bpj.2010.04.055>
- Tibbs, V. C., Gray, P. C., Catterall, W. A., & Murphy, B. J. (1998). AKAP15 anchors cAMP-dependent protein kinase to brain sodium channels. *Journal of Biological Chemistry*, 273(40), 25783–25788. <http://doi.org/10.1074/jbc.273.40.25783>
- Valenti, G., Procino, G., Tamma, G., Carmosino, M., & Svelto, M. (2005). Minireview: Aquaporin 2 trafficking. *Endocrinology*, 146(12), 5063–5070. <http://doi.org/10.1210/en.2005-0868>
- Vallee, R. B., DiBartolomeis, M. J., & Theurkauf, W. E. (1981). A protein kinase bound to the projection portion of MAP 2 (microtubule-associated protein 2). *Journal of Cell Biology*, 90(3), 568–576. <http://doi.org/10.1083/jcb.90.3.568>
- Walsh, D. A., Perkins, J. P., & Krebs, E. G. (1968). An Adenosine 3',5'-Monophosphate-dependant Protein Kinase from Rabbit Skeletal Muscle. *The Journal of Biological Chemistry*, 243(13), 3763–3774.
- Walzthoeni, T., Claassen, M., Leitner, A., Herzog, F., Bohn, S., Förster, F., ... Aebersold, R. (2012). False discovery rate estimation for cross-linked peptides identified by mass

- spectrometry. *Nature Methods*, 9(9), 901–3. <http://doi.org/10.1038/nmeth.2103>
- Walzthoeni, T., Joachimiak, L. A., Rosenberger, G., Röst, H. L., Malmström, L., Leitner, A., ... Aebbersold, R. (2015). xTract: software for characterizing conformational changes of protein complexes by quantitative cross-linking mass spectrometry. *Nature Methods*, 12(12), 1185–90. <http://doi.org/10.1038/nmeth.3631>
- Webb, B. L., Hirst, S. J., & Giembycz, M. A. (2000). Protein kinase C isoenzymes: a review of their structure, regulation and role in regulating airways smooth muscle tone and mitogenesis. *British Journal of Pharmacology*, 130(7), 1433–52. <http://doi.org/10.1038/sj.bjp.0703452>
- Weisskopf, M. G., Castillo, P. E., Zalutsky, R. A., & Nicoll, R. A. (1994). Mediation of hippocampal mossy fiber long-term potentiation by cyclic AMP. *Science (New York, N.Y.)*, 265(5180), 1878–82.
- Welch, E. J., Jones, B. W., & Scott, J. D. (2010). Networking with AKAPs: context-dependent regulation of anchored enzymes. *Mol Interv*, 10(2), 86–97. <http://doi.org/10.1124/mi.10.2.6>
- Williamson, T., Schwartz, J.-M., Kell, D. B., & Stateva, L. (2009). Deterministic mathematical models of the cAMP pathway in *Saccharomyces cerevisiae*. *BMC Systems Biology*, 3, 70. <http://doi.org/10.1186/1752-0509-3-70>
- Willoughby, D., & Cooper, D. M. F. (2006). Ca²⁺ stimulation of adenylyl cyclase generates dynamic oscillations in cyclic AMP. *Journal of Cell Science*, 119(Pt 5), 828–836. <http://doi.org/10.1242/jcs.02812>
- Willoughby, D., Wong, W., Schaack, J., Scott, J. D., & Cooper, D. M. F. (2006). An anchored PKA and PDE4 complex regulates subplasmalemmal cAMP dynamics. *The EMBO Journal*, 25(10), 2051–2061. <http://doi.org/10.1038/sj.emboj.7601113>
- Wong, S. S., & Jameson, D. M. (2012). Chemistry of Protein and Nucleic Acid Cross-Linking and Conjugation. *!Libro*, 608.
- Wosilait, W. D., & Sutherland, E. W. (1956). The relationship of epinephrine and glucagon to liver phosphorylase II. Enzymatic inactivation of liver phosphorylase. *Journal of Biological Chemistry*, 218, 469–481.
- Xu, R. X., Hassell, A. M., Dana Vanderwall, D., Lambert, M. H., Holmes, W. D., Luther, M. A., ... Nolte, R. T. (2000). Atomic Structure of PDE4: Insights into Phosphodiesterase

Mechanism and Specificity. *Science*, 288(5472), 1822–1825.

<http://doi.org/10.1126/science.288.5472.1822>

Zaccolo, M., De Giorgi, F., Cho, C. Y., Feng, L., Knapp, T., Negulescu, P. a, ... Pozzan, T.

(2000). A genetically encoded, fluorescent indicator for cyclic AMP in living cells.

Nature Cell Biology, 2(1), 25–29. <http://doi.org/10.1038/71345>

Zaccolo, M., & Pozzan, T. (2002a). Discrete microdomains with high concentration of cAMP

in stimulated rat neonatal cardiac myocytes. *Science (New York, N.Y.)*, 295(5560),

1711–1715. <http://doi.org/10.1126/science.1069982>

Zaccolo, M., & Pozzan, T. (2002b). Discrete microdomains with high concentration of cAMP

in stimulated rat neonatal cardiac myocytes. *Science (New York, N.Y.)*, 295(5560),

1711–5. <http://doi.org/10.1126/science.1069982>

Zhang, J., Hupfeld, C. J., Taylor, S. S., Olefsky, J. M., & Tsien, R. Y. (2005). Insulin disrupts

beta-adrenergic signalling to protein kinase A in adipocytes. *Nature*, 437(7058), 569–

573. <http://doi.org/nature04140> [pii]\r10.1038/nature04140

Zhang, J., Ma, Y., Taylor, S. S., & Tsien, R. Y. (2001). Genetically encoded reporters of

protein kinase A activity reveal impact of substrate tethering. *Proceedings of the*

National Academy of Sciences of the United States of America, 98(26), 14997–5002.

<http://doi.org/10.1073/pnas.211566798>

Zhang, P., Smith-Nguyen, E. V., Keshwani, M. M., Deal, M. S., Kornev, A. P., & Taylor, S. S.

(2012a). Structure and allostery of the PKA RII β tetrameric holoenzyme. *Science (New*

York, N.Y.), 335(6069), 712–6. <http://doi.org/10.1126/science.1213979>

Zhang, P., Smith-Nguyen, E. V., Keshwani, M. M., Deal, M. S., Kornev, A. P., & Taylor, S. S.

(2012b). Structure and allostery of the PKA RII β tetrameric holoenzyme. *Science (New*

York, N.Y.), 335(6069), 712–6. <http://doi.org/10.1126/science.1213979>

Zhang, P., Ye, F., Bastidas, A. C., Kornev, A. P., Wu, J., Ginsberg, M. H., & Taylor, S. S. (2015).

An Isoform-Specific Myristylation Switch Targets Type II PKA Holoenzymes to

Membranes. *Structure*, 23(9), 1563–1572. <http://doi.org/10.1016/j.str.2015.07.007>

Zhang, W., Guo, H., Jing, H., Li, Y., Wang, X., Zhang, H., ... Ren, F. (2014). Lactoferrin

stimulates osteoblast differentiation through PKA and p38 pathways independent of

Lactoferrin's receptor LRP1. *Journal of Bone and Mineral Research*, 29(5), 1232–1243.

<http://doi.org/10.1002/jbmr.2116>

- Zheng, J., Knighton, D. R., ten Eyck, L. F., Karlsson, R., Xuong, N., Taylor, S. S., & Sowadski, J. M. (1993). Crystal structure of the catalytic subunit of cAMP-dependent protein kinase complexed with MgATP and peptide inhibitor. *Biochemistry*, *32*(9), 2154–61.
- Zimmermann, L., Paster, W., Weghuber, J., Eckerstorfer, P., Stockinger, H., & Schütz, G. J. (2010). Direct observation and quantitative analysis of Lck exchange between plasma membrane and cytosol in living T cells. *Journal of Biological Chemistry*, *285*(9), 6063–6070. <http://doi.org/10.1074/jbc.M109.025981>

Supplementary data

Supplementary table 1. Raw XL-MS data for RII β -C β crosslinking

Id	Protein 1	Protein 2	Pos1	Pos2	MatchOdds	Xcorr _x	Xcorr _b	WTIC	intsum	Id-Score	FDR
FPSHFSSDLKDLLR-KGTAR-a10-b1	C β	RII β	272	266	10.05	0.4	0.55	0.07	895	49.45	0
RKGKSEVEENGAVEIAR-GQYFGELALVTNKPR-a2-b13	RII β	RII β	335	357	9.82	0.24	0.46	0.1	891	46.95	0
IIHPKTDDQR-LKVVDVIGTK-a5-b2	RII β	RII β	144	285	11.21	0.25	0.4	0.08	777	46.2	0
RKGKSEVEENGAVEIAR-GQYFGELALVTNKPR-a4-b13	RII β	RII β	337	357	10.58	0.24	0.37	0.1	828	45.47	0
LKQIEHTLNEK-ILDKQK-a2-b4	C β	C β	89	83	11.51	0.41	0.29	0.05	815	45.25	0
KGKSEVEENGAVEIAR-GQYFGELALVTNKPR-a3-b13	RII β	RII β	337	357	9.81	0.2	0.39	0.1	870	45.13	0
GKSEVEENGAVEIAR-GQYFGELALVTNKPR-a2-b13	RII β	RII β	337	357	11.2	0.24	0.42	0.08	693	45.12	0
ATEQYYAMKILDK-VMLVKHK-a9-b5	C β	C β	78	72	10.35	0.34	0.45	0.06	714	44.43	0
KMYESFIESLPFLK-IIVKNNAK-a1-b4	RII β	RII β	272	256	8.67	0.23	0.28	0.06	1088	44	0
KGKSEVEENGAVEIAR-ITMKR-a1-b4	RII β	RII β	335	324	9.39	0.27	0.41	0.05	822	43.45	0
KGKSEVEENGAVEIAR-ITMKR-a3-b4	RII β	RII β	337	324	9.39	0.32	0.37	0.05	862	43.41	0
NLLQVDLTKR-IVSGKVR-a9-b5	C β	C β	285	279	11.13	0.45	0.52	0.08	456	43.36	0
IIHPKTDDQR-IIHPKTDDQR-a5-b5	RII β	RII β	144	135	11.49	0.2	0.48	0.07	493	43.03	0
NGVSDIKTHK-AKEDFLR-a7-b2	C β	C β	298	292	11.49	0.3	0.54	0.08	382	42.73	0
KMYESFIESLPFLK-KGTAR-a1-b1	RII β	RII β	272	44	9.52	0.22	0.42	0.05	736	42.2	0
LKVVDVIGTK-ITMKR-a2-b4	RII β	RII β	294	324	9.96	0.32	0.42	0.08	636	41.89	0

KMYESFIESLPFLK-NNAKKR-a1-b4	RIIβ	RIIβ	272	260	8.14	0.25	0.27	0.04	1043	41.6	0
ATEQYYAMKILDK-VVKLK-a9-b3	Cβ	Cβ	78	72	10.71	0.39	0.4	0.07	517	40.88	0
KGKSEVEENGAVEIAR-KGTAR-a3-b1	RIIβ	RIIβ	337	44	8.71	0.21	0.48	0.05	685	40.87	0
RKMYESFIESLPFLK-IIVKNNAK-a2-b4	RIIβ	RIIβ	272	256	10.73	0.24	0.3	0.08	637	40.73	0
FPSHFSSDLKDLLR-AKEDFLR-a10-b2	Cβ	Cβ	272	266	11.49	0.27	0.38	0.07	463	40.68	0
IIHPKTDDQR-KGTAR-a5-b1	RIIβ	RIIβ	144	44	9.94	0.24	0.56	0.06	424	40.51	0
LVKDGEHVIDQGDDGDNFYVIDR-KGTAR-a3-b1	RIIβ	RIIβ	183	44	7.41	0.3	0.33	0.05	949	40.26	0
LKQIEHTLNEKR-ILDKQK-a11-b4	Cβ	Cβ	98	92	9.61	0.35	0.24	0.05	797	40.01	0
KGKSEVEENGAVEIAR-GQYFGELALVTNKPR-a1-b13	RIIβ	RIIβ	335	357	10.84	0.17	0.4	0.08	445	39.45	0
GKSEVEENGAVEIAR-ITMKRK-a2-b4	RIIβ	RIIβ	337	324	9.95	0.24	0.27	0.05	696	39.18	0
RKMYESFIESLPFLK-NNAKK-a2-b4	RIIβ	RIIβ	272	260	9.06	0.23	0.34	0.07	684	38.93	0
KGKSEVEENGAVEIAR-KGTAR-a1-b1	RIIβ	RIIβ	335	44	8.52	0.25	0.29	0.06	816	38.92	0
LKQIEHTLNEKR-AKEDFLR-a2-b2	Cβ	Cβ	89	83	11.25	0.21	0.51	0.06	248	38.7	0
LKVVDVIGTK-KGTAR-a2-b1	RIIβ	RIIβ	294	44	9.21	0.35	0.55	0.07	371	38.35	0
KGSEVESVKEFLAK-NGVSDIKTHK-a9-b7	Cβ	Cβ	22	16	8.34	0.16	0.57	0.07	459	38.18	0
KKTLGTGSFGR-VMLVKHK-a2-b5	Cβ	Cβ	53	47	10.32	0.27	0.58	0.1	189	38.12	0
LKVVDVIGTK-IIVKNNAK-a2-b4	RIIβ	RIIβ	294	256	10.49	0.22	0.29	0.07	539	37.95	0
LKVVDVIGTK-RVKGR-a2-b3	RIIβ	Cβ	294	189	9.61	0.25	0.43	0.06	382	36.35	0
LVKDGEHVIDQGDDGDNFYVIDR-IVSGKVR-a3-b5	RIIβ	Cβ	183	251	8.86	0.23	0.31	0.05	531	34.82	0
RKMYESFIESLPFLK-ILDKQK-a2-b4	RIIβ	Cβ	272	73	8.4	0.28	0.28	0.05	590	34.62	0
KMYESFIESLPFLK-RVKGR-a1-b3	RIIβ	Cβ	272	189	8.27	0.26	0.29	0.05	558	33.91	0

IHPKTDDQR-IIVKNNAK-a5-b4	RII β	RII β	144	256	11.06	0.15	0.5	0.11	180	37.55	0.026
KKTLGTGSFGR-VEAPFIPKFR-a2-b8	C β	C β	53	47	9.55	0.2	0.45	0.08	409	37.47	0.026
HKATEQYYAMKILDKQK-VVKLK-a11-b3	C β	C β	78	72	11.12	0.21	0.3	0.05	437	37.44	0.026
FGNLKNGVSDIKTHK-AKEDFLRK-a12-b2	C β	C β	298	292	11.39	0.27	0.35	0.07	318	37.21	0.026
FGNLKNGVSDIKTHK-AKEDFLR-a12-b2	C β	C β	298	292	10.88	0.19	0.4	0.09	307	37.12	0.026
KKTLGTGSFGR-KVEAPFIPKFR-a2-b9	C β	C β	53	47	11.13	0.22	0.34	0.08	343	36.83	0.026
KMYESFIESLPFLK-NNAKK-a1-b4	RII β	RII β	272	260	11.24	0.33	0.33	0.06	314	36.51	0.026
NGVSDIKTHK-AKEDFLRK-a7-b2	C β	C β	298	292	10.65	0.28	0.46	0.05	227	36.21	0.043
HKATEQYYAMKILDK-LKQIEHTLNEKR-a11-b2	C β	C β	78	72	9.32	0.13	0.43	0.05	421	36.19	0.043
GKSEVEENGAVEIAR-ITMKR-a2-b4	RII β	RII β	337	324	7.85	0.24	0.37	0.05	640	36.19	0.043
ILDKQK-VVKLK-a4-b3	C β	C β	82	76	11.15	0.24	0.29	0.1	332	36.05	0.043
LKQIEHTLNEKR-QKVVK-a2-b2	C β	C β	89	83	10.84	0.19	0.41	0.04	279	36.05	0.043
LKQIEHTLNEKR-ILDKQK-a2-b4	C β	C β	89	83	10.6	0.23	0.45	0.09	220	36.04	0.043
LKQIEHTLNEK-ILDKQKVVK-a2-b6	C β	C β	89	83	9.35	0.25	0.37	0.05	456	35.74	0.043
LKVVDVIGTK-NNAKK-a2-b4	RII β	RII β	294	260	11.05	0.4	0.35	0.06	258	35.65	0.043
KKTLGTGSFGR-KVEAPFIPKFR-a1-b9	C β	C β	52	46	9.5	0.25	0.38	0.08	362	35.1	0.061
LVKDGEHVIDQGDDGDNFYVIDR-IIVKNNAK-a3-b4	RII β	RII β	183	256	7.34	0.28	0.24	0.05	782	35	0.061
HKATEQYYAMKILDK-LKQIEHTLNEK-a11-b2	C β	C β	78	72	9.77	0.21	0.31	0.06	435	34.9	0.069
GQYFGELALVTNKPR-ITMKR-a13-b4	RII β	RII β	366	324	8.29	0.37	0.37	0.07	492	34.79	0.069
NGVSDIKTHKWFATTDWIAIYQR-AKEDFLR-a10-b2	C β	C β	301	295	8.19	0.15	0.34	0.05	572	34.64	0.069

GQYFGELALVTNKPR-KGTAR-a13-b1	RII β	RII β	366	44	7.86	0.32	0.39	0.06	503	34.42	0.069
QIEHTLNEKR-ILDKQK-a9-b4	C β	C β	98	92	11.39	0.38	0.31	0.06	191	34.25	0.069
LKQIEHTLNEKR-ILDKQKVVK-a2-b6	C β	C β	89	83	9.01	0.2	0.34	0.08	422	34.16	0.069
LVKDGEHVIDQGDDGDNFYVIDR-RIIVKNNAK-a3-b5	RII β	RII β	183	256	7.59	0.17	0.2	0.05	746	33.79	0.069
NGVSDIKTHK-KVEAPFIPK-a7-b1	C β	C β	298	292	9.75	0.19	0.47	0.05	191	33.79	0.069
KGSEVESVKEFLAK-AKEDFLR-a9-b2	C β	C β	22	16	10.84	0.26	0.24	0.09	284	33.42	0.069
LKQIEHTLNEK-QKVVK-a2-b2	C β	C β	89	83	11.25	0.26	0.42	0.03	69	33.38	0.072
QIEHTLNEKR-AKEDFLR-a9-b2	C β	C β	98	92	10.14	0.23	0.35	0.05	259	33.34	0.072
RKGKSEVEENGAVEIAR-ITMKR-a4-b4	RII β	RII β	337	324	8.84	0.27	0.27	0.04	493	33.1	0.072
RKGKSEVEENGAVEIAR-ITMKR-a2-b4	RII β	RII β	335	324	7.55	0.23	0.24	0.04	650	32.73	0.072
HKATEQYYAMKILDK-VVKLK-a11-b3	C β	C β	78	72	9.36	0.15	0.41	0.17	160	32.69	0.072
HKATEQYYAMK-KKTLGTGSFGR-a2-b2	C β	C β	69	63	8.45	0.14	0.34	0.05	438	32.69	0.072
HKATEQYYAMKILDKQK-AKEDFLR-a11-b2	C β	C β	78	72	9.32	0.09	0.3	0.1	351	32.64	0.072
LVKDGEHVIDQGDDGDNFYVIDR-IIHPKTDDQR-a3-b5	RII β	RII β	183	135	9.84	0.2	0.25	0.07	357	32.57	0.072
KWENPPPSNAGLEDFER-KVEAPFIPK-a1-b1	C β	C β	35	29	8	0.23	0.35	0.06	390	31.72	0.072
ATEQYYAMKILDK-LKQIEHTLNEKR-a9-b2	C β	C β	78	72	6.75	0.22	0.25	0.04	651	31.56	0.072
MYESFIESLPFLKSLEFSER-KGTAR-a13-b1	RII β	RII β	285	44	8.29	0.22	0.34	0.05	378	31.48	0.072
KGKSEVEENGAVEIAR-NNAKK-a3-b4	RII β	RII β	337	260	8.26	0.2	0.25	0.04	466	31.08	0.079
ATEQYYAMKILDK-LKQIEHTLNEKR-a9-b11	C β	C β	78	72	8.52	0.18	0.31	0.03	381	31.06	0.079

FPSHFSSDLKDLLR-IVSGKVR-a10-b5	Cβ	Cβ	272	266	9.29	0.15	0.38	0.16	122	30.91	0.079
KMYESFIESLPFLK-NNAKKR-a1-b5	RIIβ	RIIβ	272	261	8.61	0.24	0.24	0.05	415	30.9	0.079
KWENPPPSNAGLEDFER-NGVSDIKTHK-a1-b7	Cβ	Cβ	35	29	7.47	0.17	0.26	0.06	510	30.77	0.079
AKEDFLR-RVKGR-a2-b3	Cβ	Cβ	29	23	8.99	0.23	0.31	0.07	266	30.56	0.079
KVEAPFIPK-AKEDFLR-a1-b2	Cβ	Cβ	315	309	8.1	0.26	0.37	0.05	300	30.51	0.079
ATEQYYAMKILDK-LKQIEHTLNEK-a9-b2	Cβ	Cβ	78	72	8.14	0.2	0.21	0.04	458	29.82	0.091
ATEQYYAMKILDK-QIEHTLNEKR-a9-b9	Cβ	Cβ	78	72	7.3	0.23	0.18	0.05	564	29.68	0.101
AKEDFLRK-RVKGR-a2-b3	Cβ	Cβ	29	23	9.14	0.17	0.31	0.04	232	29.63	0.101
ATEQYYAMKILDK-RVKGR-a9-b3	Cβ	Cβ	78	72	7.86	0.18	0.31	0.04	353	29.39	0.106
KWENPPPSNAGLEDFER-AKEDFLR-a1-b2	Cβ	Cβ	35	29	7.64	0.14	0.28	0.06	376	29.07	0.106
FGNLKNGVSDIKTHK-KGSEVESVKEFLAK-a12-b9	Cβ	Cβ	298	292	8.51	0.21	0.23	0.07	310	28.68	0.106
KMYESFIESLPFLK-LKVVDVIGTK-a1-b2	RIIβ	RIIβ	272	285	6.84	0.11	0.27	0.03	485	28.64	0.106
DLKPENLLIDHQGYIQVTDGFAKR-AKEDFLR-a24-b2	Cβ	Cβ	195	189	6.69	0.16	0.19	0.04	564	28.33	0.106
KMYESFIESLPFLKSLEFSER-KGTAR-a14-b1	RIIβ	RIIβ	285	44	7.86	0.22	0.32	0.06	231	27.76	0.106
LKQIEHTLNEKR-RVKGR-a2-b3	Cβ	Cβ	89	83	8.07	0.12	0.3	0.03	260	27.69	0.106
KWENPPPSNAGLEDFER-IVSGKVR-a1-b5	Cβ	Cβ	35	29	7.92	0.24	0.19	0.04	384	27.65	0.106
QIEHTLNEKR-VVKLK-a9-b3	Cβ	Cβ	98	92	10.01	0.29	0.25	0.04	72	27.61	0.106
LKQIEHTLNEKR-ILDKQKVVK-a2-b4	Cβ	Cβ	89	83	7.07	0.16	0.3	0.05	337	27.54	0.106
RFGNLKNGVSDIKTHK-AKEDFLR-a13-b2	Cβ	Cβ	298	292	8.21	0.2	0.2	0.06	315	27.51	0.106
LEYSFKDNSNLYMMEYVPGGEMFSHLR-ILDKQK-a6-b4	Cβ	Cβ	117	111	7.45	0.13	0.3	0.03	309	27.34	0.106

KWENPPPSNAGLEDFER- ATEQYYAMKILDKQK-a1-b13	Cβ	Cβ	35	29	7.75	0.18	0.25	0.05	291	26.82	0.106
KWENPPPSNAGLEDFER- LKQIEHTLNEKR-a1-b11	Cβ	Cβ	35	29	7.94	0.15	0.23	0.05	278	26.52	0.106
HKATEQYYAMKILDK- LKQIEHTLNEKR-a11-b11	Cβ	Cβ	78	72	6.93	0.09	0.27	0.05	336	26.39	0.106
KMYESFIESLPFLK-RIIVKNNAK-a1- b5	RIIβ	RIIβ	272	256	7.99	0.2	0.19	0.03	253	25.21	0.121
ATEQYYAMKILDKQK- LKQIEHTLNEKR-a9-b2	Cβ	Cβ	78	72	7.2	0.14	0.21	0.04	309	25.18	0.121
KWENPPPSNAGLEDFER- LKQIEHTLNEKR-a1-b2	Cβ	Cβ	35	29	7.05	0.17	0.31	0.04	205	25.17	0.121
FGNLKNGVSDIKTHK- NLLQVDLTKR-a5-b9	Cβ	Cβ	291	285	6.96	0.12	0.22	0.1	289	25.16	0.121
FPSHFSSDLKDLLRNLQVDLTKR- IVSGKVR-a10-b5	Cβ	Cβ	272	266	8.2	0.13	0.17	0.12	197	25.13	0.121
NLLQVDLTKRFGNLK- NGVSDIKTHK-a9-b7	Cβ	Cβ	285	279	7.01	0.14	0.26	0.07	222	24.68	0.129
LKQIEHTLNEK-RVKGR-a2-b3	Cβ	Cβ	89	83	8.17	0.2	0.16	0.02	226	24.35	0.129
ATEQYYAMKILDK-QKVVKLK-a9- b5	Cβ	Cβ	78	72	7.54	0.22	0.25	0.04	129	23.59	0.154
KWENPPPSNAGLEDFER- QIEHTLNEKR-a1-b9	Cβ	Cβ	35	29	6.6	0.1	0.17	0.05	321	23.45	0.154
ATEQYYAMKILDKQK- NGVSDIKTHK-a13-b7	Cβ	Cβ	82	76	6.58	0.17	0.22	0.07	224	22.86	0.154
HKATEQYYAMKILDK- QIEHTLNEKR-a11-b9	Cβ	Cβ	78	72	6.83	0.13	0.27	0.02	159	22.67	0.16
RKMYESFIESLPFLKSLEFSER- KGTAR-a15-b1	RIIβ	RIIβ	285	44	5.48	0.14	0.13	0.03	440	22.27	0.16
HKATEQYYAMKILDKQK- QIEHTLNEKR-a11-b9	Cβ	Cβ	78	72	6.27	0.08	0.28	0.03	178	22.07	0.164
HKATEQYYAMKILDKQK- LKQIEHTLNEKR-a11-b2	Cβ	Cβ	78	72	6.1	0.15	0.23	0.02	219	21.62	0.164
RKMYESFIESLPFLKSLEFSER- IIVKNNAK-a15-b4	RIIβ	RIIβ	285	256	6.03	0.15	0.11	0.03	360	21.54	0.164

NLDPEQMSQVLDAMFEKLVK- IIHPKTDDQR-a17-b5	RIIβ	RIIβ	180	135	7.3	0.17	0.06	0.06	247	21.33	0.164
LKQIEHTLNEKR-AKEDFLR-a11-b2	Cβ	Cβ	98	92	6.46	0.18	0.12	0.06	260	21.26	0.164
ATEQYYAMKILDKQK-VVKLK-a9- b3	Cβ	Cβ	78	72	7.77	0.15	0.2	0.02	45	20.99	0.164
LKQIEHTLNEKR-HKATEQYYAMK- a2-b2	Cβ	Cβ	89	83	5.94	0.11	0.23	0.02	211	20.88	0.164
NGVSDIKTHK-QIEHTLNEKR-a7-b9	Cβ	Cβ	298	292	6.92	0.23	0.23	0.02	70	20.68	0.164
QIEHTLNEKR-ILDKQKVVK-a9-b4	Cβ	Cβ	98	92	7	0.21	0.16	0.03	132	20.34	0.164
KWENPPPSNAGLEDFER- KKTGLTGSFGR-a1-b2	Cβ	Cβ	35	29	6.16	0.14	0.23	0.02	141	20.14	0.164
LKVVDVIGTK-VVKLK-a2-b3	RIIβ	Cβ	294	78	9.49	0.32	0.37	0.05	284	33.24	0.167
GQYFGELALVTNKPRAASAHAI GT VK-LKQIEHTLNEKR-a13-b11	RIIβ	Cβ	366	89	5.02	0.26	0.13	0.06	785	28.11	0.2
GQYFGELALVTNKPR- FGNLKNGVSDIK-a13-b5	RIIβ	Cβ	366	282	7.39	0.22	0.15	0.04	333	24.94	0.2
GQYFGELALVTNKPRAASAHAI GT VK-LKQIEHTLNEKR-a13-b2	RIIβ	Cβ	366	80	4.85	0.16	0.1	0.03	669	24.65	0.2
LKQIEHTLNEK-LKVVDVIGTK-a2- b2	Cβ	RIIβ	89	83	7.48	0.19	0.2	0.03	147	22.52	0.2

Supplementary table 2. Raw XL-MS data for RII β -C β -AKAP18 α crosslinking

Id	Protein 1	Protein 2	Pos1	Pos2	MatchOdds	Xcorr _x	Xcorr _b	WTIC	intsum	Id-Score	FDR
LKQIEHTLNEK-ILDKQK-a2-b4	C β	C β	83	76	11.51	0.43	0.29	0.06	0.52	50.16	0
GKSEVEENGAVEIAR-GQYFGELALVTNKPR-a2-b13	RII β	RII β	328	357	11.17	0.19	0.38	0.07	0	45.44	0
RKGKSEVEENGAVEIAR-GQYFGELALVTNKPR-a2-b13	RII β	RII β	326	357	9.81	0.24	0.38	0.09	0	44.79	0
KMYESFIESLPFLK-NNAKKR-a1-b4	RII β	RII β	263	260	8.18	0.3	0.28	0.05	0.4	44.5	0
IIHPKTDDQR-LKVVDVIGTK-a5-b2	RII β	RII β	135	285	10.77	0.24	0.49	0.06	0	44.42	0
FPSHFSSDLKDLLR-KGTAR-a10-b1	C β	RII β	266	44	10.62	0.41	0.26	0.06	0.48	44.41	0
NLLQVDLTKR-IVSGKVR-a9-b5	C β	C β	279	254	11.34	0.31	0.63	0.09	0.63	42.61	0
KMYESFIESLPFLK-IIVKNNAK-a1-b4	RII β	RII β	263	256	8.25	0.27	0.23	0.05	0	42.35	0
HKATEQYYAMKILDKQK-VVCLK-a11-b3	C β	C β	72	81	11.49	0.18	0.32	0.05	0.76	42.24	0
NGVSDIKTHK-AKEDFLR-a7-b2	C β	C β	292	23	11.43	0.27	0.45	0.08	0	41.27	0
KGKSEVEENGAVEIAR-ITMKR-a1-b4	RII β	RII β	326	324	9.4	0.28	0.33	0.06	0.94	41.25	0
ILDKQK-VVCLK-a4-b3	C β	C β	76	81	11.5	0.34	0.51	0.1	0.88	41.17	0
KGKSEVEENGAVEIAR-ITMKR-a3-b4	RII β	RII β	328	324	9.3	0.29	0.26	0.07	0.94	41.05	0
KGSEVESVKEFLAK-NGVSDIKTHK-a9-b7	C β	C β	16	292	9.78	0.22	0.58	0.08	0.57	40.47	0
KKTLGTGSFGR-VEAPFIPKFR-a2-b8	C β	C β	47	317	10.85	0.26	0.44	0.07	0.92	40.23	0
LKQIEHTLNEKR-ILDKQK-a11-b4	C β	C β	92	76	10.06	0.41	0.32	0.05	0	40.07	0
LKQIEHTLNEK-AKEDFLR-a2-b2	C β	C β	83	23	11.48	0.24	0.46	0.08	0.6	38.43	0
KKTLGTGSFGR-VMLVKHK-a2-b5	C β	C β	47	61	11.51	0.3	0.47	0.1	0	38.36	0
AKEDFLRK-RVKGR-a2-b3	C β	C β	23	192	10.22	0.23	0.44	0.05	0.52	37.98	0

LKVVDVIGTK-KGTAR-a2-b1	RIIβ	RIIβ	285	44	8.83	0.26	0.57	0.07	0	37.96	0
LVKDGEHVIDQGDDGDNFYVIDR-KGTAR-a3-b1	RIIβ	RIIβ	174	44	8.37	0.3	0.33	0.06	0	37.89	0
ATEQYYAMKILDK-VMLVKHK-a9-b5	Cβ	Cβ	72	61	10.08	0.26	0.27	0.06	0.56	37.59	0
LKQIEHTLNEKR-AKEDFLR-a11-b2	Cβ	Cβ	92	23	10.53	0.25	0.4	0.06	0	37.04	0
LVKDGEHVIDQGDDGDNFYVIDR-IIVKNNAK-a3-b4	RIIβ	RIIβ	174	256	7.33	0.15	0.24	0.04	0.22	36.73	0.026
KMYESFIESLPFLK-KGTAR-a1-b1	RIIβ	RIIβ	263	44	8.18	0.31	0.28	0.04	0	36.55	0.026
LKQIEHTLNEKR-ILDKQKVVK-a2-b6	Cβ	Cβ	83	78	10.41	0.18	0.35	0.05	0.88	36.5	0.026
KVEAPFIPKFR-AKEDFLR-a9-b2	Cβ	Cβ	317	23	10.5	0.2	0.35	0.07	0.36	36.29	0.03
IHPKTDDQR-KGTAR-a5-b1	RIIβ	RIIβ	135	44	9.85	0.22	0.39	0.06	0.46	35.89	0.03
LKVVDVIGTK-NNAKK-a2-b4	RIIβ	RIIβ	285	260	11.34	0.41	0.32	0.06	0	35.82	0.03
HKATEQYYAMKILDK-LKQIEHTLNEKR-a11-b2	Cβ	Cβ	72	83	9.49	0.17	0.34	0.06	0.43	35.37	0.03
LVKDGEHVIDQGDDGDNFYVIDR-IVSGKVR-a3-b5	RIIβ	Cβ	174	254	7.92	0.26	0.3	0.06	0.17	34.9	0
LKVVDVIGTK-IIVKNNAK-a2-b4	RIIβ	RIIβ	285	256	9.96	0.3	0.27	0.06	0	34.62	0.03
HKATEQYYAMKILDK-LKQIEHTLNEKR-a11-b11	Cβ	Cβ	72	92	10.14	0.18	0.26	0.05	0.32	34.59	0.03
HKATEQYYAMKILDKQK-AKEDFLR-a11-b2	Cβ	Cβ	72	23	9.89	0.22	0.29	0.1	0.68	34.29	0.03
HKATEQYYAMK-AKEDFLR-a2-b2	Cβ	Cβ	63	23	10.24	0.32	0.36	0.07	0	33.97	0.03
KGSEVESVKEFLAK-AKEDFLR-a9-b2	Cβ	Cβ	16	23	10.6	0.26	0.3	0.09	0.7	33.9	0.03
LVKDGEHVIDQGDDGDNFYVIDR-IHPKTDDQR-a3-b5	RIIβ	RIIβ	174	135	9.75	0.25	0.21	0.08	0	33.36	0.03
AKEDFLR-VMLVKHK-a2-b5	Cβ	Cβ	23	61	9.62	0.22	0.43	0.05	0	33.36	0.03
IHPKTDDQR-IIVKNNAK-a5-b4	RIIβ	RIIβ	135	256	11.05	0.26	0.29	0.1	0	33.19	0.03
HKATEQYYAMK-ILDKQK-a2-b4	Cβ	Cβ	63	76	10.9	0.21	0.3	0.15	0	32.97	0.03

VMLVKHK-ILDKQK-a5-b4	Cβ	Cβ	61	76	10.94	0.29	0.23	0.11	0	32.54	0.03
GQYFGELALVTNKPR-KGTAR-a13-b1	RIIβ	RIIβ	357	44	7.85	0.38	0.33	0.07	0	32.41	0.035
KKTLGTGSFGR-KVEAPFIPKFR-a1-b9	Cβ	Cβ	46	317	8.97	0.22	0.32	0.08	0.79	32.41	0.035
NGVSDIKTHK-KVEAPFIPK-a7-b1	Cβ	Cβ	292	309	10.15	0.32	0.37	0.05	0	32.36	0.035
KWENPPPSNAGLEDFER-NGVSDIKTHK-a1-b7	Cβ	Cβ	29	292	8.77	0.31	0.34	0.07	0.31	32.19	0.035
KWENPPPSNAGLEDFER-ILDKQK-a1-b4	Cβ	Cβ	29	76	9.67	0.21	0.19	0.04	0	32.07	0.035
DLKPENLLIDHQGYIQVTDGFGFAKR-AKEDFLR-a24-b2	Cβ	Cβ	189	23	7.01	0.12	0.33	0.04	0.29	32.03	0.035
FGNLKNGVSDIK-AKEDFLR-a5-b2	Cβ	Cβ	285	23	8.15	0.25	0.24	0.05	0	31.84	0.035
LKQIEHTLNEKR-ILDKQKVVK-a11-b6	Cβ	Cβ	92	78	10.47	0.19	0.23	0.05	0.75	31.51	0.035
LKVVDVIGTK-VVKLK-a2-b3	RIIβ	Cβ	285	81	9.23	0.29	0.3	0.05	0	31.35	0
KWENPPPSNAGLEDFER-KVEAPFIPK-a1-b1	Cβ	Cβ	29	309	8.88	0.17	0.31	0.05	0.42	30.72	0.035
LKQIEHTLNEKR-HKATEQYYAMK-a2-b2	Cβ	Cβ	83	63	9.08	0.14	0.29	0.05	0.4	30.52	0.035
QIEHTLNEKR-VVKLK-a9-b3	Cβ	Cβ	92	81	11.18	0.29	0.28	0.02	0	29.73	0.035
KVEAPFIPK-AKEDFLR-a1-b2	Cβ	Cβ	309	23	8.01	0.29	0.33	0.05	0	29.51	0.035
LKQIEHTLNEKR-HKATEQYYAMK-a11-b2	Cβ	Cβ	92	63	7.58	0.2	0.26	0.04	0	29.29	0.035
LKVVDVIGTK-ITMKR-a2-b4	RIIβ	RIIβ	285	324	8.93	0.2	0.26	0.05	0	28.93	0.035
NLLQVDLTKRFGNLK-NGVSDIKTHK-a9-b7	Cβ	Cβ	279	292	7.21	0.14	0.32	0.08	0.91	27.85	0.041
KMYESFIESLPFLKSLEFSER-KGTAR-a14-b1	RIIβ	RIIβ	276	44	8.17	0.17	0.27	0.05	0.36	27.07	0.041
NGVSDIKTHK-EFLAKAK-a7-b5	Cβ	Cβ	292	21	6.72	0.23	0.34	0.06	0.72	26.75	0.041
KWENPPPSNAGLEDFER-LKQIEHTLNEKR-a1-b11	Cβ	Cβ	29	92	7.13	0.19	0.26	0.06	0.28	26.43	0.041

NGVSDIKTHK-QIEHTLNEKR-a7-b9	C β	C β	292	92	8.38	0.2	0.28	0.03	0.7	26.17	0.041
HKATEQYYAMKILDKQK- KWENPPPSNAGLEDFER-a11-b1	C β	C β	72	29	8.17	0.18	0.19	0.05	0.51	25.99	0.041
KMYESFIESLPFLK-LKVVDVIGTK- a1-b2	RII β	RII β AKAP1	263	285	5.9	0.16	0.15	0.05	0.48	25.77	0.051
FGNLKNGVSDIK-ICEKDR-a5-b4	C β	8	285	15	6.68	0.23	0.11	0.05	0.86	24.44	0.25
ATEQYYAMKILDKQK- NGVSDIKTHK-a13-b7	C β	C β	76	292	8	0.13	0.17	0.07	0.94	24.39	0.077
QIEHTLNEKR-VMLVKHK-a9-b5	C β	C β	92	61	8.06	0.13	0.25	0.04	0	24	0.077
KWENPPPSNAGLEDFER- LKQIEHTLNEKR-a1-b2	C β	C β	29	83	6.84	0.22	0.15	0.06	0	23.73	0.086
FGNLKNGVSDIKTHK- KGSEVESVKEFLAK-a5-b9	C β	C β	285	16	7.49	0.17	0.23	0.03	0.54	23.66	0.094
KGSEVESVKEFLAKAK-ILDKQK-a9- b4	C β	C β	16	76	7.69	0.16	0.15	0.03	0.89	22.35	0.109
KWENPPPSNAGLEDFER- HKATEQYYAMK-a1-b2	C β	C β	29	63	6.53	0.1	0.16	0.05	0.24	22.01	0.117
ATEQYYAMKILDKQK- NGVSDIKTHK-a9-b7	C β	C β	72	292	6.42	0.11	0.18	0.07	0.38	21.23	0.125
AVQQYLEETQNKKQPGEKNSTKA EEGDR-KMYESFIESLPFLK-a22-b1	AKAP1 8	RII β	61	263	3.9	0.11	0.15	0.04	0	21.07	0.4
ATEQYYAMKILDK-EFLAKAK-a9-b5	C β	C β	72	21	6.43	0.11	0.31	0.02	0	20.79	0.14
FGNLKNGVSDIKTHK- NLLQVDLTKR-a5-b9	C β	C β	285	279	5.69	0.12	0.17	0.1	0.65	20.68	0.147
KTLGTGSFGRVMLVK-ILDKQK-a1- b4	C β	C β	47	76	7.75	0.14	0.2	0.01	0.77	20.65	0.147

Supplementary table 3. Raw data for XL-MS of RI β -C β crosslinking

Id	Protein 1	Protein2	Pos 1	Pos2	Match Odds	Xcorr x	Xcorr b	WTI C	intsum	delta S	Id-Score	FDR
DYKXTALAK-TDLKLWGIDR-a3-b4	RI β	RI β	121	220	10.29	0.27	0.58	0.07	757	0	47.87	0
AATVKAK-LEKEENR-a5-b3	RI β	RI β	214	57	11.45	0.42	0.55	0.1	517	0	45.8	0
DYKTMALAK-TDLKLWGIDR-a3-b4	RI β	RI β	121	220	10.29	0.18	0.46	0.06	784	0	45.37	0
DYKXTALAK-ILDKQK-a3-b4	RI β	C β	121	76	11.49	0.45	0.48	0.08	518	0	44.22	0
DYKXTALAK-AATVKAK-a3-b5	RI β	RI β	121	214	10.94	0.34	0.53	0.06	481	0	43.29	0
TXTALAKAISK-TDLKLWGIDR-a7-b4	RI β	RI β	128	220	9.73	0.22	0.45	0.07	712	0.87	43.19	0
KVEAPFIPK-AKEDFLR-a1-b2	C β	C β	309	23	10.89	0.25	0.46	0.09	535	0	42.69	0
AKEDFLR-AKEDFLR-a2-b2	C β	C β	23	23	11.48	0.21	0.49	0.07	367	0	41.14	0
TXTALAKAISK-DYKXTALAK-a7-b3	RI β	RI β	128	121	10.16	0.19	0.44	0.07	573	0.87	41	0
EHFEKLEKEENR-AATVKAK-a5-b5	RI β	RI β	54	214	11.26	0.49	0.37	0.06	426	0.55	39.67	0
AKEDFLR-VXLVKHK-a2-b5	C β	C β	23	61	9.85	0.3	0.55	0.07	379	0.34	39.51	0
LKQIEHTLNEK-ILDKQKVVK-a2-b6	C β	C β	83	78	10.92	0.3	0.38	0.09	437	0.89	39.32	0
KVEAPFIPKFR-VXLVKHK-a9-b5	C β	C β	317	61	11.43	0.32	0.34	0.08	426	0.66	39.29	0
AATVKAK-AKEDFLR-a5-b2	RI β	C β	214	23	11.14	0.35	0.33	0.08	453	0	39.02	0
LKQIEHTLNEK-VXLVKHK-a2-b5	C β	C β	83	61	11.16	0.17	0.42	0.05	372	0.57	38.82	0
LKQIEHTLNEKR-ILDKQK-a11-b4	C β	C β	92	76	11.02	0.44	0.29	0.07	486	0.28	38.65	0
NGVSDIKTHK-AKEDFLR-a7-b2	C β	C β	292	23	9.41	0.2	0.51	0.09	384	0	37.99	0
AATVKAK-ILDKQK-a5-b4	RI β	C β	214	76	11.04	0.43	0.36	0.07	361	0	37.88	0
VXLVKHK-ILDKQK-a5-b4	C β	C β	61	76	11.51	0.49	0.38	0.07	271	0	37.75	0
LEKEENR-LEKEENR-a3-b3	RI β	RI β	57	57	10.78	0.29	0.42	0.07	326	0	37.67	0
NLLQVDLTKR-IVSGKVR-a9-b5	C β	C β	279	254	9.81	0.21	0.53	0.09	297	0.89	37.61	0
FLREHFEKLEK-AATVKAK-a8-b5	RI β	RI β	54	214	10.64	0.37	0.16	0.07	611	0.6	37.29	0

LKQIEHTLNEK-ILDKQK-a2-b4	C β	C β	83	76	11.43	0.32	0.41	0.16	179	0	37.23	0
HKATEQYYAXK-ILDKQK-a2-b4	C β	C β	63	76	11.07	0.28	0.37	0.15	273	0.62	37.22	0
EHFEKLEKEENR-DYKXTALAK-a8-b3	R1 β	R1 β	57	121	10.02	0.22	0.34	0.08	474	0	36.99	0
EHFEKLEKEENR-DYKXTALAK-a5-b3	R1 β	R1 β	54	121	9.58	0.23	0.4	0.07	453	0.55	36.95	0
KVEAPFIPKFR-AKEDFLR-a9-b2	C β	C β	317	23	10.94	0.24	0.33	0.09	354	0.66	36.79	0
KKTLGTGSFGR-VXLVKHK-a2-b5	C β	C β	47	61	10.99	0.23	0.36	0.09	319	0	36.76	0
TXALAKAISK-LEKEENR-a7-b3	R1 β	R1 β	128	57	10.08	0.46	0.49	0.07	245	0.51	36.75	0
EHFEKLEKEENR-LEKEENR-a8-b3	R1 β	R1 β	57	57	11.41	0.22	0.37	0.06	270	0.88	36.69	0
HKATEQYYAXK-KKTLGTGSFGR-a2-b2	C β	C β	63	47	10.67	0.21	0.39	0.06	300	0.64	36.12	0
KKTLGTGSFGR-VEAPFIPKFR-a2-b8	C β	C β	47	317	10.01	0.19	0.28	0.07	498	0.83	36.1	0
VSILESLEKWER-KXYEEFLSK-a9-b1	R1 β	R1 β	259	242	9.75	0.27	0.29	0.1	469	0	35.92	0
VSILESLEKWER-KMYEEFLSK-a9-b1	R1 β	R1 β	259	242	9.63	0.29	0.3	0.1	472	0.25	35.86	0
KXYEEFLSK-AATVKAK-a1-b5	R1 β	R1 β	242	214	10.77	0.31	0.29	0.07	380	0	35.85	0
EHFEKLEKEENR-TXALAKAISK-a5-b7	R1 β	R1 β	54	128	10.65	0.23	0.42	0.08	236	0.64	35.74	0
NLLQVDLTR-AATVKAK-a9-b5	C β	R1 β	279	214	9.52	0.39	0.37	0.1	361	0	35.46	0
ATEQYYAXKILDK-VXLVKHK-a9-b5	C β	C β	72	61	8.79	0.19	0.27	0.06	577	0.27	34.75	0
EHFEKLEKEENR-LEKEENR-a5-b3	R1 β	R1 β	54	57	11.32	0.24	0.27	0.06	287	0.79	34.72	0
ILDKQKVVK-VXLVKHK-a6-b5	C β	C β	78	61	9.87	0.27	0.38	0.06	293	0	34.32	0
LEKEENR-AKTDLK-a3-b2	R1 β	R1 β	57	216	9.14	0.34	0.39	0.09	322	0.85	34.09	0
NGVSDIKTHK-AKEDFLRK-a7-b2	C β	C β	292	23	10.43	0.28	0.36	0.09	213	0.7	33.9	0
EHFEKLEKEENR-KXYEEFLSK-a5-b1	R1 β	R1 β	54	242	9.99	0.13	0.39	0.05	269	0.59	33.86	0
AKEDFLR-ILDKQK-a2-b4	C β	C β	23	76	9.32	0.19	0.36	0.09	322	0.75	33.57	0
LKQIEHTLNEKR-VXLVKHK-a2-b5	C β	C β	83	61	9.91	0.18	0.26	0.07	371	0.47	33.04	0
AATVKAK-AATVKAK-a5-b5	R1 β	R1 β	214	214	11.5	0.35	0.33	0.05	97	0	32.98	0
DLKPENLLIDHQGYIQVDFGFAKR-KVEAPFIPK-a24-b1	C β	C β	189	309	7.26	0.2	0.21	0.06	720	0	32.96	0

TXTALAKAISK-TXTALAKAISK-a7-b7	RIβ	RIβ	128	128	11.42	0.21	0.25	0.05	204	0.46	32.62	0
EHFEKLEKEENR-KXYEEFLSK-a8-b1	RIβ	RIβ	57	242	9.62	0.19	0.29	0.05	345	0	32.31	0
TXTALAKAISK-KVIPKDYK-a7-b5	RIβ	RIβ	128	118	9.53	0.21	0.33	0.06	281	0.38	32.06	0
LKQIEHTLNEKR-VXLVKHK-a11-b5	Cβ	Cβ	92	61	9.9	0.15	0.26	0.05	334	0.34	32.04	0
LEKEENRQILAR-AATVKAK-a3-b5	RIβ	RIβ	57	214	9.89	0.26	0.3	0.13	212	0.29	31.99	0
VMLVKHK-ILDKQK-a5-b4	Cβ	Cβ	61	76	9.17	0.26	0.34	0.13	234	0.66	31.81	0
LKQIEHTLNEKR-AATVKAK-a2-b5	Cβ	RIβ	83	214	10.45	0.25	0.2	0.09	282	0	31.8	0.07
VRFP SHFSSDLKDLLR-AATVKAK-a12-b5	Cβ	RIβ	266	214	8.73	0.22	0.32	0.05	362	0.37	31.71	7
FPSHFSSDLKDLLR-IVSGKVR-a10-b5	Cβ	Cβ	266	254	9.39	0.13	0.39	0.19	119	0.64	31.68	0
LKQIEHTLNEKR-ILDKQKVVK-a2-b6	Cβ	Cβ	83	78	8.93	0.2	0.2	0.07	468	0	31.58	0
KVEAPFIPKFR-AATVKAK-a9-b5	Cβ	RIβ	317	214	8.43	0.3	0.32	0.06	348	0.67	31.07	7
LKQIEHTLNEK-AKEDFLR-a2-b2	Cβ	Cβ	83	23	9.6	0.2	0.35	0.06	180	0.62	30.97	0
TXTALAKAISK-AATVKAK-a7-b5	RIβ	RIβ	128	214	9.44	0.34	0.26	0.07	287	0.56	30.94	0
TXTALAKAISK-EHFEKLEK-a7-b5	RIβ	RIβ	128	54	9.53	0.2	0.37	0.06	160	0.13	30.87	0
ILDKQKVVK-VXLVKHK-a4-b5	Cβ	Cβ	76	61	8.24	0.2	0.39	0.06	280	0	30.79	0
AATVKAK-IVSGKVR-a5-b5	RIβ	Cβ	214	254	9.61	0.37	0.35	0.09	124	0	30.68	7
QIEHTLNEKR-ILDKQK-a9-b4	Cβ	Cβ	92	76	9.09	0.24	0.34	0.07	220	0	30.64	0
EHFEKLEKEENR-AATVKAK-a8-b5	RIβ	RIβ	57	214	10.81	0.27	0.31	0.04	74	0.69	30.38	0
LKQIEHTLNEKR-HKATEQYYAXK-a2-b2	Cβ	Cβ	83	63	8.98	0.19	0.18	0.05	423	0.68	30.33	0
KKTLGTGSFGR-VMLVKHK-a2-b5	Cβ	Cβ	47	61	9.57	0.29	0.27	0.1	194	0.81	30.18	0
HKATEQYYAXK-VXLVKHK-a2-b5	Cβ	Cβ	63	61	11.23	0.24	0.19	0.04	151	0.64	30.16	0
EHFEKLEKEENR-IVSGKVR-a5-b5	RIβ	Cβ	54	254	9.99	0.22	0.26	0.15	122	0	29.95	7
LKQIEHTLNEKR-VMLVKHK-a2-b5	Cβ	Cβ	83	61	9.28	0.17	0.26	0.08	245	0.68	29.68	0

KKTLGTGSFGR-KVEAPFIPKFR-a2-b9	Cβ	Cβ	47	317	8.06	0.14	0.35	0.06	291	0.69	29.6	0
DYKXTALAK-QIEHTLNEKR-a3-b9	Riβ	Cβ	121	92	7.21	0.19	0.42	0.05	290	0	29.58	0.07
FPSHFSSDLKDLLR-AATVKAK-a10-b5	Cβ	Riβ	266	214	9.08	0.26	0.29	0.09	177	0.76	29.17	0.07
KWENPPPSNAGLEDFER-AKEDFLR-a1-b2	Cβ	Cβ	29	23	8.47	0.18	0.25	0.07	323	0	29.06	0
EHFEKLEK-AATVKAK-a5-b5	Riβ	Riβ	54	214	10.65	0.28	0.27	0.03	64	0.2	29.05	0
EHFEKLEKEENR-TXTALAKAISK-a8-b7	Riβ	Riβ	57	128	8.03	0.11	0.3	0.04	325	0.81	28.89	0
AKEDFLR-VMLVKHK-a2-b5	Cβ	Cβ	23	61	7.99	0.15	0.37	0.04	239	0	28.8	0
FGNLKNGVSDIK-NLLQVDLTKR-a5-b9	Cβ	Cβ	285	279	8.8	0.19	0.28	0.12	199	0.45	28.77	0
LKQIEHTLNEKR-ILDKQK-a2-b4	Cβ	Cβ	83	76	9.94	0.22	0.15	0.12	212	0.42	28.72	0
KVEAPFIPK-VXLVKHK-a1-b5	Cβ	Cβ	309	61	8.31	0.16	0.39	0.06	164	0.28	28.69	0
LKQIEHTLNEK-AATVKAK-a2-b5	Cβ	Riβ	83	214	8.89	0.16	0.3	0.09	161	0	28.29	0.07
TDLKLWGIDRDSYR-IVSGBVU-a4-b5	Riβ	Cβ	220	254	7.66	0.12	0.29	0.04	345	0.59	28.22	0.07
FLREHFEKLEK-TDLKLWGIDR-a8-b4	Riβ	Riβ	54	220	7.61	0.2	0.17	0.04	443	0.66	27.65	0
KMYEEFLSK-AATVKAK-a1-b5	Riβ	Riβ	242	214	7.8	0.11	0.32	0.05	220	0	27.13	0
LEYSFKDNSNLYXVXEYVPGGEXFSHLR-AKEDFLR-a6-b2	Cβ	Cβ	111	23	6.75	0.12	0.26	0.03	418	0.4	27.08	0
AATVKAK-AKTDLK-a5-b2	Riβ	Riβ	214	216	8.67	0.26	0.25	0.06	178	0.95	26.93	0
QKSNSQCDSHDEEISPTPPNPVVK-LKQIEHTLNEK-a2-b2	Riβ	Cβ	68	83	5.71	0.11	0.18	0.05	605	0.33	26.83	0.1
LKQIEHTLNEKR-TXTALAKAISK-a11-b7	Cβ	Riβ	92	128	8	0.15	0.24	0.05	259	0.46	26.56	0.1
QIEHTLNEKR-VXLVKHK-a9-b5	Cβ	Cβ	92	61	9.83	0.26	0.2	0.03	107	0	26.5	0
QIEHTLNEKR-AKEDFLR-a9-b2	Cβ	Cβ	92	23	7.03	0.16	0.35	0.06	195	0	25.98	0
DLKPENLLIDHQGYIQVDFGFAKR-AKEDFLR-a24-b2	Cβ	Cβ	189	23	5.74	0.19	0.25	0.04	444	0.18	25.74	0
HKATEQYYAMK-AATVKAK-a2-b5	Cβ	Riβ	63	214	7.9	0.21	0.21	0.08	224	0	25.62	0.1

HKATEQYYAXK-QIEHTLNEKR-a2-b9	Cβ	Cβ	63	92	8.77	0.22	0.24	0.04	113	0	25.52	0
HKATEQYYAXK-LEKEENR-a2-b3	Cβ	RIβ	63	57	8.56	0.21	0.21	0.05	152	0.79	25.33	0.1
QIEHTLNEKR-ILDKQKVVK-a9-b4	Cβ	Cβ	92	76	7.82	0.28	0.28	0.04	133	0.82	24.91	0
NGVSDIKTHK-KVEAPFIK-a7-b1	Cβ	Cβ	292	309	6.43	0.14	0.35	0.04	214	0.93	24.91	0
HKATEQYYAXK-AATVKAK-a2-b5	Cβ	RIβ	63	214	7.43	0.19	0.25	0.08	181	0.62	24.69	0.1
FPSHFSSDLKDLLR-EHFEKLEKEENR-a10-b8	Cβ	RIβ	266	57	7.07	0.13	0.31	0.03	160	0	24.23	0.1
TDLKLWGIDR-EHFEKLEK-a4-b5	RIβ	RIβ	220	54	6.54	0.18	0.28	0.04	232	0	23.95	0
TDLKLWGIDRDSYR-TXTALAKAISK-a4-b7	RIβ	RIβ	220	128	7.25	0.18	0.22	0.08	192	0.38	23.91	0
LKQIEHTLNEKR-NGVSDIKTHK-a11-b7	Cβ	Cβ	92	292	7.68	0.15	0.15	0.06	244	0.58	23.83	0
VSITEBCGBEFCEF-IVSGKVR-a6-b5	Cβ	Cβ	342	254	7.9	0.19	0.15	0.18	116	0.59	23.73	0.1
AATVKAK-VIPKDYK-a5-b4	RIβ	RIβ	214	118	7.04	0.22	0.3	0.04	126	0	23.68	0
LEYSFKDNSNLYXVXEYVPGGEXFSHLR R-AKEDFLR-a6-b2	Cβ	Cβ	111	23	5.67	0.11	0.2	0.03	416	0.31	23.6	0
KVIPKDYK-AATVKAK-a5-b5	RIβ	RIβ	118	214	7.3	0.18	0.21	0.06	188	0	23.6	0
CVKLDRPRFER-AATVKAK-a3-b5	RIβ	RIβ	347	214	7.35	0.18	0.18	0.11	164	0	23.08	0
HKATEQYYAXKILDK-LKQIEHTLNEK-a11-b2	Cβ	Cβ	72	83	5.95	0.09	0.21	0.03	336	0.82	22.87	0
NGVSDIKTHK-QIEHTLNEKR-a7-b9	Cβ	Cβ	292	92	7.15	0.2	0.3	0.05	68	0.65	22.84	0
TXTALAKAISK-QIEHTLNEKR-a7-b9	RIβ	Cβ	128	92	7.21	0.21	0.25	0.04	126	0.83	22.79	0.12 5
VSITEBCGBEFCEF-IVSGKVR-a9-b5	Cβ	Cβ	345	254	7.25	0.2	0.16	0.18	117	0.33	22.68	0.12 5
HKATEQYYAXKILDK-LKQIEHTLNEKR-a11-b2	Cβ	Cβ	72	83	5.63	0.13	0.21	0.04	346	0.33	22.66	0
LKQIEHTLNEKR-QIEHTLNEKR-a2-b9	Cβ	Cβ	83	92	6.79	0.11	0.29	0.04	126	0.27	22.62	0
RFGNLKNGVSDIK-TXTALAKAISK-a6-b7	Cβ	RIβ	285	128	6.91	0.25	0.18	0.08	187	0	22.5	0.12 5
TMTALAKAISK-TDLKLWGIDR-a7-b4	RIβ	RIβ	128	220	6.67	0.27	0.11	0.05	314	0	22.42	0

EHFEKLEKEENR-IVSGKVR-a8-b5	RIβ	Cβ	57	254	7.04	0.1	0.2	0.12	117	0	22.04	0.12	5
LKQIEHTLNEKR-QIEHTLNEKR-a11-b9	Cβ	Cβ	92	92	6.7	0.13	0.28	0.02	130	0.51	21.98	0	0
GPLKCVKLDPRP-VIPKDYK-a4-b4	RIβ	RIβ	344	118	7.25	0.2	0.1	0.13	181	0.51	21.81	0	0
EHFEKLEKEENR-AKTDLK-a8-b2	RIβ	RIβ	57	216	6.83	0.2	0.21	0.05	148	0	21.76	0	0
KKTLGTGSFGR-QIEHTLNEKR-a2-b9	Cβ	Cβ	47	92	6.4	0.12	0.29	0.04	105	0.9	21.54	0	0
QIEHTLNEKR-VMLVKHK-a9-b5	Cβ	Cβ	92	61	6.97	0.15	0.19	0.05	146	0	21.45	0	0
TXTALAKAISK-VXLVKHK-a7-b5	RIβ	Cβ	128	61	5.8	0.21	0.23	0.04	220	0.62	21.43	0.14	3
AATVKAK-VXLVKHK-a5-b5	RIβ	Cβ	214	61	6.64	0.16	0.21	0.05	152	0	21.38	0.14	3
ATEQYYAXKILDKQK-VSITEKCGK-a13-b6	Cβ	Cβ	76	342	5.88	0.19	0.22	0.07	202	0.22	21.29	0	0
VMLVKHKATEQYYAXK-KGSEVESVK-a5-b1	Cβ	Cβ	61	8	5.6	0.12	0.14	0.04	354	0.89	21.16	0	0
RKXYEEFLSK-RKXYEEFLSK-a2-b2	RIβ	RIβ	242	242	7.75	0.17	0.08	0.02	180	0.89	20.96	0	0
GPLGSMGNTAIKKGSEVESVK-AATVKAK-a14-b5	Cβ	RIβ	8	214	6.28	0.15	0.19	0.12	138	0.29	20.93	0.14	3
LKQIEHTLNEKR-ILDKQKVVK-a2-b4	Cβ	Cβ	83	76	6.4	0.13	0.18	0.03	212	0	20.92	0	0
QIEHTLNEKR-AATVKAK-a9-b5	Cβ	RIβ	92	214	7.15	0.2	0.26	0.02	17	0	20.72	0.14	3
GPLKCVKLDPRP-VIPKDYK-a7-b4	RIβ	RIβ	347	118	6.61	0.21	0.1	0.12	184	0.67	20.65	0	0
HKATEQYYAXK-KKTLGTGSFGR-a2-b1	Cβ	Cβ	63	46	5.89	0.1	0.28	0.03	130	0.51	20.5	0	0
RKXYEEFLSK-AATVKAK-a2-b5	RIβ	RIβ	242	214	5.97	0.2	0.19	0.06	187	0.6	20.43	0	0
QIEHTLNEKR-IVSGKVR-a9-b5	Cβ	Cβ	92	254	6.34	0.18	0.19	0.08	124	0	20.18	0	0

Supplementary table 4. Raw data for qXL-MS crosslinking of RII β -C β -AKAP18

Protein1	Protein2	Pos1	Pos2	log2ratio	pvalue	neglog10pvalue	sum_score	significance
RII β	RII β	285	324	-2.4282	1.3E-09	8.88081	38.7848	TRUE
C β	RII β	266	44	-1.536	0.00258	2.58808	36.4216	FALSE
RII β	RII β	263	44	-1.37	1.6E-05	4.80054	36.5995	TRUE
RII β	RII β	285	44	-1.2368	1.3E-06	5.88446	77.828	TRUE
RII β	RII β	357	44	-1.1126	0.00012	3.93306	78.1822	TRUE
C β	RII β	192	263	-1.0959	0.01206	1.91859	36.968	FALSE
RII β	RII β	174	44	-0.6546	0.00032	3.49408	231.375	FALSE
C β	C β	192	23	-0.6525	1.7E-05	4.78338	149.516	FALSE
C β	RII β	81	285	-0.6463	0.0016	2.79604	36.4954	FALSE
RII β	RII β	326	357	-0.6081	0.05244	1.2803	174.681	FALSE
RII β	RII β	256	263	-0.5473	0.06269	1.20284	214.947	FALSE
RII β	RII β	256	285	-0.4331	0.00022	3.64989	37.7278	FALSE
RII β	RII β	260	263	-0.4264	0.043	1.36655	303.276	FALSE
RII β	RII β	260	285	-0.4076	0.03576	1.44657	39.0669	FALSE
RII β	RII β	135	256	-0.3897	0.03582	1.44583	35.4036	FALSE
C β	C β	254	279	-0.3623	0.02188	1.65987	77.6777	FALSE
C β	C β	23	309	-0.3316	0.00206	2.68664	39.7457	FALSE
RII β	RII β	324	326	-0.3156	0.23174	0.635	119.8	FALSE
C β	RII β	254	174	-0.2855	0.00662	2.179	116.074	FALSE
C β	C β	47	61	-0.2009	0.35244	0.45291	39.2205	FALSE
RII β	RII β	174	256	-0.1672	0.40362	0.39403	65.7572	FALSE
RII β	RII β	324	328	-0.1448	0.43816	0.35837	219.372	FALSE
C β	C β	23	92	-0.0326	0.69412	0.15857	38.2498	FALSE
C β	C β	76	81	-0.0286	0.92618	0.0333	78.0941	FALSE

Cβ	Cβ	292	309	0.02517	0.86738	0.06179	36.4836	FALSE
Cβ	Cβ	317	47	0.04106	0.5802	0.23642	135.574	FALSE
Cβ	Cβ	292	29	0.0681	0.76764	0.11484	74.1333	FALSE
RIIβ	RIIβ	135	285	0.07632	0.67778	0.16891	49.8773	FALSE
Cβ	Cβ	317	46	0.10541	0.17398	0.75951	142.698	FALSE
Cβ	Cβ	81	92	0.17582	0.13028	0.88513	75.4148	FALSE
Cβ	Cβ	23	292	0.229	0.15416	0.81203	299.741	FALSE
Cβ	Cβ	23	61	0.25118	0.37134	0.43023	36.2009	FALSE
Cβ	Cβ	292	92	0.26208	0.37174	0.42976	35.5508	FALSE
Cβ	Cβ	76	92	0.3279	0.0004	3.39427	151.278	FALSE
Cβ	Cβ	78	83	0.33558	0.04468	1.34986	70.1781	FALSE
RIIβ	RIIβ	328	357	0.3364	0.00016	3.79414	239.669	FALSE
RIIβ	RIIβ	135	174	0.3603	0.00058	3.23609	81.1807	FALSE
Cβ	Cβ	72	92	0.48768	0.08412	1.07511	52.207	FALSE
Cβ	Cβ	29	76	0.55822	0.12362	0.9079	46.0249	FALSE
Cβ	Cβ	61	72	0.61983	0.04856	1.31369	69.2276	FALSE
Cβ	Cβ	72	81	0.69929	0.0199	1.70112	229.697	FALSE
Cβ	Cβ	76	83	0.71535	4.1E-06	5.38987	147.904	FALSE
Cβ	Cβ	23	83	0.93902	0.00022	3.65263	129.596	FALSE
Cβ	Cβ	72	83	0.97129	0.01142	1.94241	246.353	FALSE
Cβ	Cβ	16	292	1.08597	1.3E-06	5.89942	151.592	TRUE

Supplementary table 5. Raw data for XL-MS for light/heavy GST crosslinking

Id	Protein1	Protein2	Pos1	Pos2	Match		Xcorr _x	Xcorr _b	WTIC	intsum	deltaS	Id-Score	FDR
					Odds								
IKGLVQPTR-IKGLVQPTR-a2-b2	GST	GST	10	10	11.5		0.23	0.37	0.05	583	0	42.32	0
VDFLSBLPEMLB-IKGLVQPTR-a6-b2	GST SILAC	GST	124	10	9.49		0.21	0.43	0.08	676	0	41.48	0
IAYSKDFETLK-IKGLVQPTR-a5-b2	GST	GST	112	10	11.46		0.21	0.42	0.09	374	0	39.82	0
IBGLVQPTU-IKGLVQPTR-a2-b2	GST SILAC	GST	10	10	9.76		0.29	0.34	0.07	601	0	38.81	0
DFETLBVDFLSB-IBGLVQPTU-a6-b2	GST SILAC	GST SILAC	118	10	9.18		0.22	0.39	0.07	547	0	37.72	0
LLLEYLEEKYEHLIER-IEAIPQIDKYLK-a9-b9	GST	GST	26	190	10.77		0.27	0.43	0.13	257	0.67	37.21	0
VDFLSKLPEMLK-IKGLVQPTR-a6-b2	GST	GST	124	10	10.55		0.23	0.39	0.08	342	0.63	36.87	0
VDFLSKLPEMLK-IAYSKDFETLK-a6-b5	GST	GST	124	112	9.62		0.22	0.34	0.07	519	0.19	36.87	0
BFELGLEFPNLPYYIDGDVB-IBGLVQPTU-a1-b2	GST SILAC	GST SILAC	44	10	8.91		0.17	0.34	0.05	500	0.39	34.79	0
DFETLKVDFLSKLPEMLK-IKGLVQPTR-a6-b2	GST	GST	118	10	8.72		0.15	0.27	0.07	554	0.5	34.21	0
VDFLSBLPEMLB-IAYSDFETLB-a6-b5	GST SILAC	GST SILAC	124	112	8.36		0.23	0.28	0.06	555	0	33.74	0
LLLEYLEEBYEEHLYEU-IEAIPQIDBYLB-a9-b9	GST SILAC	GST SILAC	26	190	10.96		0.22	0.29	0.15	190	0	33.68	0
NKKFELGLEFPNLPYYIDGDVK-IKGLVQPTR-a3-b2	GST	GST	44	10	8.51		0.13	0.34	0.08	430	0	33.21	0
DFETLKVDFLSKLPEMLK-IKGLVQPTR-a12-b2	GST	GST	124	10	9.99		0.21	0.36	0.06	157	0.47	31.44	0
IAYSDFETLB-IAYSKDFETLK-a5-b5	GST SILAC	GST	112	112	9.93		0.07	0.25	0.07	245	0	30.45	0
IKGLVQPTR-YLKSSK-a2-b3	GST	GST	10	193	8.26		0.16	0.29	0.04	377	0	30.25	0

DFETLKVDFLSK-IKGLVQPTR-a6-b2	GST	GST	118	10	6.75	0.21	0.26	0.05	547	0.6	29.94	0
IEAIPQIDBYLB-IBGLVQPTU-a9-b2	GST SILAC	GST SILAC	190	10	9.08	0.14	0.32	0.08	210	0	29.84	0
IEAIPQIDKYLK-YLBSSB-a9-b3	GST	GST SILAC	190	193	8.73	0.3	0.31	0.08	222	0.94	29.6	0
IEAIPQIDKYLK-KRIEIPQIDK-a9-b1	GST	GST	190	180	7.34	0.16	0.23	0.07	467	0	29.11	0
IEAIPQIDKYLK-IKGLVQPTR-a9-b2	GST	GST	190	10	8.75	0.25	0.24	0.08	268	0.28	28.86	0
NKKFELGLEFPNLPYYIDGDVK-IKGLVQPTR-a2-b2	GST	GST	43	10	7.87	0.11	0.32	0.06	293	0	28.75	0
IEAIPQIDKYLKSSK-IKGLVQPTR-a9-b2	GST	GST	190	10	7.77	0.14	0.34	0.08	243	0	28.47	0
NBBFELGLEFPNLPYYIDGDVB-IBGLVQPTU-a2-b2	GST SILAC	GST SILAC	43	10	6.99	0.16	0.31	0.04	342	0.07	27.51	0
IAYSBDFFETLB-IBGLVQPTU-a5-b2	GST SILAC	GST SILAC	112	10	6.98	0.14	0.32	0.11	222	0	26.37	0
DFETLBVDFLSBLPEMLB-IBGLVQPTU-a12-b2	GST SILAC	GST SILAC	124	10	7.17	0.14	0.28	0.04	251	0	25.61	0
IEAIPQIDBYLB-YLKSSK-a9-b3	GST SILAC	GST	190	193	8.32	0.19	0.17	0.07	157	0.93	24.25	0
RIEIPQIDKYLK-IKGLVQPTR-a10-b2	GST	GST	190	10	7.25	0.06	0.18	0.04	286	0.88	24	0
KRIEIPQIDK-YLKSSK-a1-b3	GST	GST	180	193	7.88	0.21	0.31	0.02	44	0.72	23.76	0
YIADKHNMLGGCPKER-IBGLVQPTU-a14-b2	GST	GST SILAC	86	10	7.07	0.13	0.22	0.04	198	0.61	23.19	0
NBBFELGLEFPNLPYYIDGDVB-IBGLVQPTU-a3-b2	GST SILAC	GST SILAC	44	10	5.19	0.16	0.22	0.03	401	0.2	23.01	0
LLLEYLEEKYEEHLYER-DEGDKWR-a9-b5	GST	GST	26	39	6.85	0.19	0.17	0.08	209	0.93	22.32	0
LLLEYLEEBYEEHLYEU-DEGDBWU-a9-b5	GST SILAC	GST SILAC	26	39	7.56	0.23	0.14	0.09	128	0.42	22.02	0
DFETLBVDFLSBLPEMLB-IKGLVQPTR-a12-b2	GST SILAC	GST	124	10	5.7	0.13	0.21	0.05	267	0	21.41	0

IEAIPQIDBYLBSSB- IBGLVQPTU-a9-b2	GST SILAC	GSTSILAC	190	10	4.82	0.15	0.13	0.03	384	0	20.01	0
IEAIPQIDBYLB- a9-b2	GST SILAC	GST	190	10	6.66	0.13	0.15	0.05	147	0	20.01	0

In memory of Gregory Hutko